RESEARCH & DEVELOPMENT

Performance Improvement from Deep Layers of Subgrade Stabilization

Vincent O. Ogunro, PhD, principal Investigator
Miguel A. Pando, PhD, Kay Researcher
Rajaram Janardhanam, PhD, Key Researcher
Arezou Eslaminejad, Graduate Research Assistant
Yogesh Y. Parkhi, Graduate Research Assistant
Brian J. Weyer, Graduate Research Assistant

Department of Civil and Environmental Engineering

University of North Carolina at Charlotte

9201 University City Boulevard

Charlotte, NC 28223

NCDOT Project 2009-03

FHWA/NC/2009-03

January 2015

Performance Improvement from Deep Layers of Subgrade Stabilization

FINAL REPORT

North Carolina Department of Transportation
(Research Project No. FHWA/NC 2009-03)

Submitted by

Vincent O. Ogunro, Ph.D.
Principal Investigator

Miguel A. Pando, Ph.D.
Key Researcher

Rajaram Janardhanam, Ph.D.
Key Researcher

Arezou Eslaminejad
Graduate Research Assistant

Yogesh Y. Parkhi
Graduate Research Assistant

Brian J. Weyer
Graduate Research Assistant

UNC CHARLOTTE

Department of Civil & Environmental Engineering
The University of North Carolina at Charlotte
9201 University City Blvd
Charlotte, NC 28223

January 30, 2015

Technical Report Documentation Page

1. Report No. FHWA/NC/2009-03	2. Government Accession No.	3. Recipient's Catalog No.
4. Title and Subtitle Performance Improvement from Deep Layers of Subgrade Stabilization		5. Report Date January 2015 6. Performing Organization Code
7. Author (s): Vincent Ogunro, Miguel Pando, Rajaram Janardhanam Arezou Eslaminejad, Yogesh Y. Parkhi, and Brian J. Weyer.		8. Performing Organization Report No.
9. Performing Organization Name and Address University of North Carolina at Charlotte 9201 University Boulevard Charlotte, NC 28223		10. Work Unit No. (TRAIS) 11. Contract or Grant No.
12. Sponsoring Agency Name and Address North Carolina Department of Transportation Research and Analysis Group 1 South Wilmington Street Raleigh, North Carolina 27601		13. Type of Report and Period Covered August 16, 2008 – Aug 15, 2012 14. Sponsoring Agency Code 2009-03
15. Supplementary Notes		

16. Abstract

NCDOT routinely and successfully stabilizes subgrades of pavements constructed west of Interstate-95. The depth of the stabilized subgrade has been typically limited to 178 mm (7 in.) or 200 mm (8 in.) depending on whether cement or lime stabilization is needed. The subgrade stabilization practices has resulted in excellent, uniform, and cost effective subgrade support. With the recent advances in earthwork equipment, new cost competitive equipment is capable of performing deep subgrade stabilization to approximately double the current thickness, e.g. to about 406 mm (16 in.). This research project investigated the potential pavement performance improvement of deep layers of subgrade stabilization (to about 406 mm) compared to the current NCDOT subgrade stabilization practice (up to 200 mm). The motivation is to maximize the benefits of deep layers of subgrade stabilization, by quantifying the potential performance improvement of deeper subgrade stabilization over the current NCDOT practice. Performance improvements of deep layers of subgrade stabilization were evaluated using data collected at a test site of lime and cement stabilized sections constructed for this study. The test sections are laid out starting with the first control section, followed by 2 deep layers of subgrade stabilization and ending with the second control test section. The control test sections were designed and constructed to the current NCDOT practice, while deep layers of subgrade stabilization are composed of chemically stabilized layers approximately 1.5 and 2 times the stabilized depth of the current NCDOT practice. Dynamic Cone Penetrometer (DCP) and Falling Weight Deflectometer (FWD) data were collected at the site and used to evaluate the performance improvement from the deep layers of subgrade stabilization sections. Results from this study suggest that using deep layers of subgrade stabilization will result in improved performance and also could be cost effective given the decreased thickness of the asphalt pavement layer as well as in terms of life-cycle cost given the potential of a longer pavement life

17. Key Words Performance, Deep Layers, Subgrade Stabilization, Finite Element, FWD, Chemically Stabilized test sections	18. Distribution Statement		
19. Security Classif. (of this report) Unclassified	20. Security Classif. (of this page) Unclassified	21. No. of Pages 281	22. Price

Form DOT F 1700.7 (8-72) **Reproduction of completed page authorized**

DISCLAIMER

The contents of this report reflect the views of the authors and not necessarily the views of the University. The authors are responsible for the facts and the accuracy of the data presented herein. The contents do not necessarily reflect the official views or policies of either the North Carolina Department of Transportation or the Federal Highway Administration at the time of publication. This report does not constitute a standard, specification, or regulation.

ACKNOWLEDGEMENTS

We would like to thank North Carolina Department of Transportation and the Federal Highway Administration for sponsoring this project, and providing personnel for part of the field studies and traffic control. Our Steering and Implementation Committee consisted of Judith Corley-Lay, Ph.D., P.E. (Chair), Jack E. Cowert, P.E., Mehdi Haeri, Tom Hearne, P.E., Lamar Sylvester, P.E., Clark Morrison, Ph.D., P.E., James (Jim) Phillips, P.E., Njoroge W. Wainaina, P.E., Moy Biswas, Ph.D., P.E., Ron Hancock, P.E., Chris Peoples, P.E., Kevin Sebold, C. K. Su, Eric Conner, Jonathan Miller, P.E., and Mustan Kadibhai, P.E.. We are appreciative of their support and guidance towards the success of this project. The research team is grateful for the guidance and patience of the committee. We would like to thank the Charlotte Department of Transportation for providing data of an instrumented site to validate our numerical model. The research team is grateful to NCDOT Pavement unit especially Judith Corley-Lay, Clark Morrison and Josh Holland, for their significant contributions to this study.

EXECUTIVE SUMMARY

NCDOT routinely and successfully stabilizes subgrades of pavements constructed west of Interstate-95. The depth of the stabilized subgrade has been typically limited to 178 mm (7 in.) or 200 mm (8 in.) depending on whether cement or lime stabilization is needed. The subgrade stabilization practices has resulted in excellent, uniform, and cost effective subgrade support. With the recent advances in earthwork equipment, new cost competitive equipment is capable of performing deep subgrade stabilization to approximately double the current thickness, e.g. to about 406 mm (16 in.). This research project investigated the potential pavement performance improvement of deep layers of subgrade stabilization (to about 406 mm) compared to the current NCDOT subgrade stabilization practice (up to 200 mm). The motivation is to maximize the benefits of deep layers of subgrade stabilization, by quantifying the potential performance improvement of deeper subgrade stabilization over the current NCDOT practice

A framework was developed to predict the equivalency among the different pavement structures. In essence, the framework is based on using numerical methods to predict pavement responses at critical locations in pavement. For this studies, the pavement responses were calculated using multilayer elastic linear analysis program (EVERSTRESS©) and a finite element numerical model (Abaqus). A viscoelastic, non-linear 3D finite element with stress-dependent soil model was implemented to adequately simulate responses of pavement under moving axle load. Then the calculated responses were used in current pavement performance models to predict the number of load repetitions to failure. Equivalent pavement sections were established when the number of load repetitions for the reduced HMA layer thickness of deep subgrade stabilization pavement and that of the standard NCDOT pavement were equal.

Performance improvements of deep layers of subgrade stabilization were evaluated using data collected at a test site of lime and cement stabilized sections constructed for this study. The test sections are laid out starting with the first control section, followed by 2 deep layers of subgrade stabilization and ending with the second control test section. The control test sections were designed and constructed to the current specification of NCDOT, while deep layers of subgrade stabilization are composed of chemically stabilized layers approximately 1.5 and 2 times the stabilized depth of the control test section. Dynamic Cone Penetrometer (DCP) and Falling Weight Deflectometer (FWD) data were collected at the site and used to evaluate the performance improvement from the deep layers.

The results of this study will be useful to frame recommendations to modify current pavement and subgrade design practices by Pavement Management Unit and the Geotechnical Engineering Unit. Since this results have cost and maintenance implications, pavement construction and maintenance units can also use the research product. Results from this study suggest that using deep layers of subgrade stabilization will result in improved performance and also could be cost effective given the decreased thickness of the asphalt pavement layer as well as in terms of life-cycle cost given the potential of a longer pavement life.

TABLE OF CONTENTS

LIST OF FIGURES

LIST OF TABLES

CHAPTER 1 INTRODUCTION

1.1 Background

The benefits of subgrade stabilization are well recognized by engineers. Stabilization is primarily implemented to improve the strength and stiffness of subgrades and accelerate construction. Subgrade stabilization eliminates lost time by providing dry and strong construction foundation in cases where otherwise the construction project could have been slowed or temporarily stopped, which often translates into economic savings. In the past, this approach was used to provide durable foundation for construction equipment without necessarily considering the stabilized subgrade in the structural value of the treated road system. However, many highway agencies now consider the stabilized subgrade as structural layers to take advantage of their improved strength/stiffness and durability.

Conventional subgrade stabilization techniques in one lift are normally limited to depths less than 304.8 mm (12 in.). However, historically, stabilized subgrades with depths greater than 304.8 mm (12 in.) that were treated in one lift, and with conventional construction methods were found to be inadequate. For example, in 1966, the Oklahoma DOT developed a technique (the ripping technique) of subgrade stabilization to a depth of 609.6 mm (24 in.), with the objective of controlling the problems associated with swelling clay soils. In 1968, S. J. Groves and Sons, a company in Springfield, Illinois collaborated with Professor Marshall R. Thompson of Civil Engineering Department, University of Illinois, Urbana, Illinois developed a deep-plow construction technique to stabilize subgrade for Interstate-180 near Hennepin, Illinois to depths of up to 609.6 mm (24 in.). As the need for accelerated pavement construction and highways with long term performance benefits grew, coupled with frequent rights-of-way through terrains of unsuitable subgrade, DOTs have renewed interest in deep subgrade stabilization to reduce construction cost and increase life of the pavement system. With the recent development of new equipment's capable of subgrade stabilization to depths of 406 mm (16 in.) to 610 mm (24 in.) in one lift, deep subgrade stabilization has successfully been implemented in ALDOT, GADOT, KYDOT, OklaDOT and IDOT.

1.2 Research Needed

NCDOT routinely and successfully stabilizes subgrades of pavements constructed west of Interstate-95. However, the depth of the stabilized subgrade has been typically limited to 178 mm (7 in.) or 200 mm (8 in.) depending on whether it is using cement or lime stabilization, respectively. With the recent advances in earthwork equipment, new cost competitive equipment is capable of performing subgrade stabilization to approximately double the current thickness, e.g. about 406mm (16 in.) are available. The benefits of deep subgrade stabilization layers to NCDOT, can be expected in reduction in asphalt concrete layer thicknesses and the associated reduction in initial construction costs, and/or better long-term performance resulting in lower maintenance and rehabilitation costs which have not yet been investigated nor quantified.

Between 2001 and 2006, NCDOT on average, stabilized over 233 lane kilometers (145 lane miles) each year. In 2006, the average bidding costs of lime and lime stabilization were \$163.00/MT and \$2.40/m^2, respectively. While for the same period, the average bidding costs for PG64-22 binder and B25.0C asphalt concrete were \$498.36/MT and \$43.33/MT, respectively. Therefore, a 25 mm reduction in B25.0C asphalt concrete for every 100 mm increase of stabilized subgrade would result in substantial construction cost savings to the state. With the increasing cost of asphalt binder and asphalt concrete (with the price of crude oil now over \$100 per barrel), the up-front cost savings from reducing hot mix asphalt (HMA) layer thickness is expected to be significant. Further, savings are also expected from the reduction in the frequency, amount of pavement maintenance and from expected delays in pavement rehabilitation. According to the National Asphalt Pavement Association (NAPA), asphalt pavement consists of approximately 95% sand, stone and gravel bound by 5% of asphalt cement, a product of crude oil. In the past few years crude oil prices have increased to over \$100 per barrel; with these current prices, construction costs of pavement will eventually be impacted. As mentioned earlier, various transportation departments have successfully used deep subgrade stabilization techniques and reduced the thickness of surface asphalt layer.

Practice of deep subgrade stabilization in the United States has been few and limited to address site-specific subgrade improvement issues. If deep subgrade stabilization is routinely practice, the resulting potential benefits when a pavement is designed to have the same life span as the current standard subgrade stabilization are: a stronger structural foundation platform, potential reduction in asphalt layer thickness which may result in reduced construction costs, and decrease in maintenance cost. With the intention to verify the benefits associated from increasing the depth of the treated layer, namely deep subgrade stabilization, there is a need for conducting quality controlled laboratory and field tests to produce data that can be used for back calculations to determine parameters that can be used in pavement design. As a result NCDOT embarked on this research to quantify the benefits associated with deep subgrade stabilization methods based on NC conditions including subgrade type, construction means and methods, material and construction cost, etc. The expected benefits are reduction in asphalt layer thickness as well as in initial construction costs.

1.3 Objectives

The overarching goal of this research is to investigate the potential structural performance and value of deep subgrade stabilization with the objective of incorporating the improved and thicker stabilized subgrade as a structural layer of the pavement system. The issue is whether the gain in thick stabilized subgrade layer performance results in significant reduction of the asphalt concrete thickness, and whether the reduction in asphalt concrete layer thickness results in direct savings in initial construction costs without compromising the long-term performance of the pavement system. More specific objectives of this project include:

(1) to determine analytically and/or numerically the equivalent pavement sections for the deep stabilized subgrade sections,

(2) to compare the initial costs of construction and expected life of alternative pavement layer systems,

(3) to monitor the changes in material engineering properties and field performance of the constructed alternative pavement layer systems over time,

(4) to optimize the pavement layer system of the equivalent pavement sections determined analytically/numerically by back calculation of pavement response from field and laboratory data, and to make

recommendations on the most effective use of deep subgrade stabilization based on cost benefit analysis of the constructed test sections.

1.4 Scope and Research Strategy

To achieve the overall goal and specific objectives stated above, the research project was structured into three phases. In Phase I, an extensive literature review was conducted to assess the current state of practice of chemical stabilization of highway subgrades and to collect relevant information on lessons-learned from deep stabilization case histories. In this phase, a survey of all the state transportation agencies in the United States was designed and conducted to document past and current experiences of deep subgrade stabilization practices. The research team developed and assessed the framework for determining the equivalent pavement sections using a multilayer linear analysis program (EVERSTRESS, WSDOT 2005) and a finite element program (Abaqus FE, Hibbit et al. 2005). The equivalent pavement analysis framework was based on the responses (strains) determined from these programs for the bottom-up fatigue cracking and subgrade rutting distresses.

Phase II required laboratory and field experiments which were developed to collect, classify, and determine the engineering properties of representative samples of the test sections. The experimental program was carefully formulated to collect laboratory data to predict field behavior, and for validating in-situ test results of test sections. For Phase II, in partnership with NCDOT, test sections were constructed at one of NCDOT’s projects to study the performance of deep subgrade stabilization. Two test sites, comprising of four test sections each, were constructed and instrumented for lime and cement chemical stabilization, respectively.

In Phase III, comparative performance analysis of standard stabilized subgrade and deep subgrade stabilization sections were performed and validated using in-situ test data. Cost comparison of equivalent test sections was conducted to assess whether initial construction savings accrued from deep subgrade stabilization. The data and results obtained from the test sections were used to assess performance of the deep subgrade stabilization in Phase III. In this phase, the numbers of load repetition to failure for the control test sections (standard NCDOT pavement design structure for the test site) were used to determine the equivalent asphalt concrete layer thicknesses for the deep subgrade stabilization test sections. Cost savings was assessed by comparing reduced cost from reduced asphalt concrete layer thickness and additional construction cost of deep stabilization.

1.5 Organization of Report

The literature review and the survey of DOTs current/past deep subgrade practices are presented in Chapter 2. In Chapter 3, the framework for determining the equivalent pavement sections using a multilayer linear analysis program (EVERSTRESS) and a finite element program (Abaqus) is developed and evaluated. The equivalent pavement analysis framework is based on the responses (strains) determined from these programs for the bottom-up fatigue cracking and subgrade rutting distresses. Chapter 4 details the tasks of selecting test sites, sample collection and experimentation including laboratory tests of subgrade soils and stabilized soils. Laboratory testing of samples collected during field stabilization operation and in-situ testing (Dynamic Cone Penetration – DCP and Falling Weight Deflectometer – FWD) are presented in Chapter 5. In Chapter 6, pavement responses are predicted numerically for the test sections using Abaqus FE model and EVERSTRESS multilayer linear analysis program. A parametric study is performed to analyze the behavior of the pavement structure for various thicknesses of subgrade layers. This chapter concludes with a possible reduction in HMA layer thickness for a range of stabilized layer based on the traffic load-related failure criteria. Chapter 7 assesses cost implications of deep subgrade stabilization using data from this project. In Chapter 8, conclusions were drawn, recommendations made, implementation proposed, and potential complementary future research proposed.

CHAPTER 2 LITERATURE AND STATE OF PRACTICE

2.1 Background

Chemical stabilization is a widely used technique of fine-grained subgrade soils which can result in significant improvement of the engineering properties of the soils. Chemical stabilization of subgrade involves the treatment of soils with additives such as a lime, cement, fly ash, cement kiln dust, and combination of these products. As a strong construction platform and for construction expediency, chemical subgrade stabilization of weak subgrade has gained wide acceptance in roadway operation. However, no universal acceptance or consensus of chemically stabilized subgrade as a structural layer contributing to load distributions and bearing capacity in a pavement has been found. This could be due to several factors such as the complex additive – soil interactions, degree of weathering, soil heterogeneity and presence of organics, as stabilized engineering properties is due to the degree and quality of reaction (Little, 2012); limited study with the objective to directly correlate laboratory and field performance (Hopkins et al., 1995); lack of defined structural and performance characteristics, and testing protocol to the requirements of MEPGD (Little, 1999).

Some Departments of Transportation (DOTs) have successively incorporated stabilized subgrade as a structural layer in their pavement design. In a table of layer coefficients (ai) used to determine structural number (SN) for cement stabilized subgrades (ACI, 2009) which will be presented later in this chapter, the compressive strength requirement and layer coefficient values vary significantly among the DOTs. In an effort to build on the benefits from subgrade stabilization and the availability of new equipment capable of deeper subgrade stabilization in one lift, few DOTs (ALDOT, GADOT, KYDOT, OklaDOT and IDOT) are venturing in deep subgrade stabilization to improve long-term performance and possibly reduce flexible pavement cost (construction and maintenance). Several challenges still remain to be overcome for deep subgrade stabilization to be incorporated as a routine pavement structural layer.

Since cementiously stabilized subgrade layers structural characteristics and performance models have not been implemented in MEPGD (NCHRP 04-36, project report has just been completed but not yet released to the public), DOTs rely on SN (a product of layer coefficient and thickness) of layers in their design. To achieve the required SN of a pavement to meet specific design characteristics, the layer thicknesses or the layer coefficients or both can be adjusted. This highlights the significance of accurate assessment of the SN of stabilized subgrade layer. This is also particularly challenging because of the several factors of subgrade stabilization influencing structural and performance characteristics. The added challenges of field implementation and quality control of deep subgrade stabilization underscore the importance of this study. The following sections of this chapter present literatures on laboratory characteristics of subgrade stabilization, field operation and quality control of stabilization, effect of subgrade stabilization on structure strength improvement both in the laboratory and the field, and summary of survey result of subgrade stabilization practices of DOTs. Though several other additives possess the pozzolanic characteristics required to form cementiously stabilized subgrade, detailed discussion is limited to lime and cement stabilization, the two chemical additives currently used by North Carolina DOT and that were used for the field test sections evaluated in the study.

2.2 Lime Stabilization

Lime stabilized subgrade provides low-cost means of soil improvement since low amount of chemical additive contents is required. When implemented appropriately, it eliminates undercuts and removal/replacement of inferior soils. Many engineering properties of natural subgrade are positively enhanced including soil workability by reducing soil plasticity index. The process forms a quick weather-resistant work platform and provides excellent pavement support for construction equipment. For most DOTs, it is typical to use lime contents ranging from 4-7% by weight. Ingles and Metcalf (1973) stated that a general rule of thumb for lime stabilization is to use 1% lime by weight for every 10% of clay. Since few roadway soils have clay contents exceeding 80%, lime contents in subgrade stabilization rarely exceed 8%. Stabilization provides extended performance over the life span of the pavement through pozzolanic effect. It is well established that lime stabilization is not a recent phenomenon, by the 1950s it was widely used to stabilize heavy clays in Texas (Vorobieff and Murphy, 2003). Fine grained soils with a minimum of 25% passing the #200 sieve (0.075 mm) and a PI greater than 10 are ideal candidates for lime stabilization (National Lime Association, 2004), this same criteria are used by NCDOT.

2.2.1 Lime-Soil Stabilization Mechanisms

The initial interaction between lime and soil causes a rapid reduction in plasticity, and initiation of texture transformation of the clay minerals. The texture is modified from fine grained soils into a friable, granular structure, thus improving its workability and ease of compaction. The level of improvement and strength increase is based on three factors: the type and amount of clay, the increase in pH due to the addition of lime, and the amount of silica and alumina present (Castel and Arulanandan, 1979). The mechanics responsible for reactions necessary for strength gain include cation exchange, flocculation and agglomeration phases. Carbonation is another process that may occur in the field. This reversion process is disadvantageous to soil stabilization. Summary of the processes are presented in the subsections that follow.

a. Cation Exchange

Cation exchange or “Molecular Crowding” occurs immediately when clay minerals are mixed with calcium based compounds. As these compounds are found in hydrated lime or quicklime, excess calcium ions are released and absorbed on the surface of clay particles to replace the cations adjacent to the clay lattice (Rogers and Glendinning, 2000). Molecular crowding according due to absorption of calcium hydroxide in place of calcium cation according to some researchers (Little, 1999). During this reaction weaker monovalent cations (Na+ and K+) are replaced with excess stronger multivalent cations (Ca++). The general order of cation replacement associated with soils (Thompson, 1964) is shown in the Lyotropic series (Equation 2.1).

$$Na^{+} < K^{+} < Ca^{++} < Mg^{++} \tag{2. 1}$$

b. Flocculation and Agglomeration

Expansive clay minerals have a diffuse double layer that causes it to swell when the mineral comes in contact with water. This attribute is commonly found in Montmorillonite, Kaolinite and Illite, the common clay minerals in soils. After the cation exchange has taken place, the thickness of the double diffuse layer reduces and there is a greater attraction among clay particles. As the particles begin to stick and clump together, the texture improves and the shear resistance of the increases. While the particles are bonding together, the nature of the texture is transforming from a fine grained soil in to a friable, granular material (Rogers and Glendinning, 2000, Thompson, 1964).

c. Pozzolanic Reaction

The pozzolanic reaction is the phase of mineralogy where full stabilization has been attained. Silica and alumina from clay mix with lime to generate the following cementitious compounds (Rogers and Glendinning, 2000):

$$Ca^{++} + OH^{-} + \text{soluble clay silica} = \text{calcium silicate hydrate (CSH)} \tag{2.2}$$

$$Ca^{++} + OH^{-} + \text{soluble clay alumina} = \text{calcium aluminate hydrate (CAH)} \tag{2.3}$$

These cementitious agents are responsible for major strength increase in soil lime mixtures (Thompson, 1964). Possible sources of silica and alumina include clay minerals, quartz, feldspars, mica, crystalline minerals, and amorphous minerals (National Research Council, 1987).

As the soil is stabilizing with the required amount of lime, the pH value dramatically increases from its original state to a pH of 12.4 which is equivalent to the pH value of lime slurry. Once the pozzolanic reaction is developed, it remains as long as calcium is present. Over the life span of the pavement, the pH of the subgrade fluctuates between and 12.3-12.5 and the foundation slowly but continuously gain strength.

d. Carbonation

Lime carbonation is an undesirable process that occurs when calcium oxide (lime) and carbon dioxide from the atmosphere react to form calcium carbonate and magnesium carbonate. These compounds are weaker forms of the cementitious agents resulting in strength reduction. It also occurs on construction sites near industrial parks, where the carbon dioxide content in the air may be high. In these cases, the amount of carbon dioxide content in rain water may increase significantly (George, et al., 1992, Thompson, 1964). This detrimental process can be avoided with expedited construction sequences that avoid prolonged exposure of stabilized layers to air and rainfall (Mallela, et al., 2004). Though disadvantageous to subgrade stabilization of most soils, Graves and Eades (1987) and Little et al. (1996) have shown that carbonation reaction is beneficial in the long-term of calcareous aggregate stabilization.

2.2.2 Types of Lime

Lime is prepared by heating natural limestone until carbon dioxide is no longer present. The most common types of lime used for stabilization are quick lime, hydrated lime, and occasionally dolomitic lime. Overview of quick lime, hydrated lime and Slurry will be presented in the following subsection. Table 2.1 presents chemical and physical properties of typical commercial lime (quicklime and hydrated lime).

Table 2.1: Properties of Commercial Limes – Quicklime and Hydrated Lime (NLA, 1988)

Quicklime				
Constituent	High Calcium Range, % [a]		Dolomitic Range, % [a]	
CaO	92.25 - 98.00		55.50 - 57.50	
MgO	0.30 - 2.50		37.60 - 40.80	
SiO_2	0.20 - 1.50		0.10 - 1.50	
Fe_2O_3	0.10 - 0.40		0.05 - 0.40	
Al_2O_3	0.10 - 0.50		0.05 - 0.50	
H_2O	0.10 - 0.90		0.10 - 0.90	
CO_2	0.40 - 1.50		0.40 - 1.50	
Specific Gravity	3.2 – 3.4		3.2 - 3.4	
Specific Heat at 100°F (38°C)	0.19 BTU/lb	442 J/kg	0.21 BTU/lb	488 J/kg
Bulk Density, pebble lime	55 - 60 lb/ft^3	880 - 960 kg/m^3	55 - 60 lb/ft^3	880 - 960 kg/m^3

Hydrated Lime				
Principal Constituent	High Calcium $Ca(OH)_2$		Dolomitic (Monohydrated) $Ca(OH)_2 \cdot MgO$	
Specific Gravity	2.3 - 2.4		2.7 - 2.9	
Specific Heat at 100°F (38°C)	0.29 BTU/lb	674 J/kg	0.29 BTU/lb	674 J/kg
Bulk Density	25 - 35 lb/ft^3	400 - 560 kg/m^3	25 - 35 lb/ft^3	400 - 560 kg/m^3

[a] Percentage by weight.

a. Quicklime (CaO)

Quicklime is created by transforming calcium carbonate ($CaCO_3$) in to calcium oxide (CaO). This occurs when carbon dioxide is released by heating natural limestone, resulting in a powdered form of lime (O'Connor and Parsons, 2006). When quicklime is mixed with water, it releases heat through an exothermic reaction; the equation for the chemical reaction is displayed in Equation 4.

$$CaO + H_2O \rightarrow Ca(OH)_2 + heat \tag{2.4}$$

Quicklime is a concentrated form of lime; therefore smaller amounts can be used for stabilization as opposed to other lime types. Due to the higher concentrations of quicklime, particles are large and heavy which prevents them from moving, thus, reducing the potential for dust blowing around the site (O'Connor and Parsons, 2006). It is also used for drying saturated soils. Amounts ranging from 1-4% by weight can prepare a wet site for construction within hours of the initial spreading (National Lime Association, 2004).

b. Hydrated Lime ($Ca(OH)_2$)

Hydrated lime, also referred to as slaked lime, is generated from an exothermic reaction when quicklime and water are combined together to produce a loose and dry powder (O'Connor and Parsons, 2006). This form has a smaller concentration of lime, when compared to quicklime, therefore greater amounts are required for stabilization. Hydrated lime is a safer product to work with because this form of lime does not create an exothermic reaction when it comes in contact with water.

c. Lime Slurry

Lime slurry is a method where water is mixed with hydrated lime or quicklime to form slurry. After the slurry has been made, it can be spread on the site or injected into the subgrade. This is an ideal application in areas where dust is a major problem and during summer months, slurry applications pre-wet the soil and minimizes drying action. It also permits better distribution, and better desirable environmental dust free application.

2.2.3 Lime Content

Maintenance of high pH is required for pozzolanic reaction and continued long-term strength improvement. Determining the optimum lime percentage for each soil type is important to verify the amount that will yield the maximum strength.

a. Establishing the Lime Content

The optimum lime content can be determined from a combination of two procedures. The first phase is a pH test, developed by Eades and Grim (1966). This method dictates that soil samples should be tested at a range of lime contents, typically 2-7% lime by soil weight. The soil lime slurry that provides a pH of 12.4 is the minimum lime content necessary to achieve stabilization. Full stabilization is not achieved until the ion exchange has been completed. This occurs when the pH has reached a steady value of at least 12.4 (Rogers and Glendinning, 2000).

The Eades and Grim pH test provides a minimum guideline for the lime content suitable to provide complete stabilization. It is common to follow this procedure with a series of unconfined compression tests to verify the amount of lime that will provide the maximum strength. These samples are tested at different percentages of lime by dry weight of soil (i.e. 4%, 6%, and 8%). The percentage that results in the maximum strength is considered to be the optimum lime content.

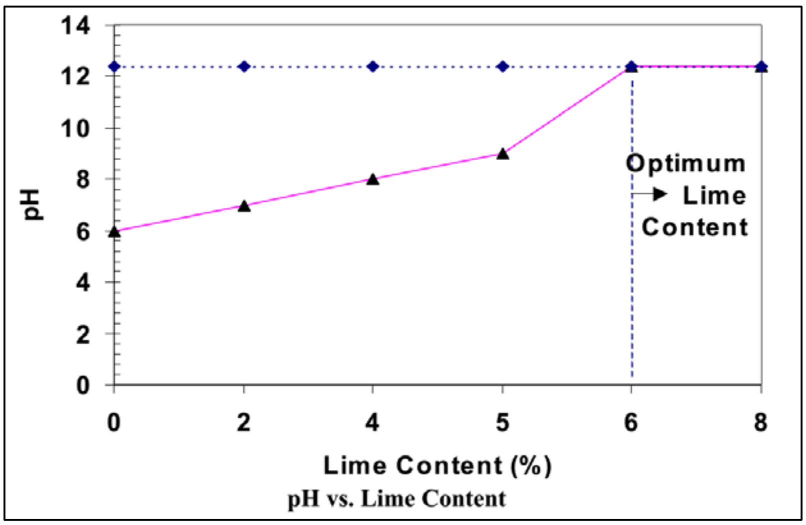

Figure 2.1 pH vs. Lime Content (INDOT, 2008)

It is important to verify the lime content that yields the highest strength, due to the fact that it is likely for soils to decrease in unconfined compressive strengths as the lime contents increase past optimum.

The decrease in strength is a result of excess use of lime that leads to soil deterioration. Soil deterioration occurs from calcium leaching due to excess lime (Kitazume, et al., 2003). As will be presented in later section of this chapter on moisture density curves, increasing the lime content reduces the maximum dry density. After the optimum amount has been exceeded the strength decreases due to the decrease in maximum dry unit weight (Bell, 1996). There are cases where strengths increased with increasing lime contents, or they achieved a plateau with increasing lime content.

Bell (1996) studied three minerals, kaolinite, montmorillionite and quartz, and their reactions with lime. Samples were prepared at 2, 4, 6, 8, and 10% lime and tested at 1, 3, 7, 14, and 28 days for each of the soils types in order to determine the optimum lime content. Montmorillionite rapidly achieved maximum strength at a lime content of 4%, after optimum was achieved it drastically reduced. Initial rapid strength gain is commonly associated with soils containing montmorillionite. Kaolinite reached maximum strength between 4% and 6%, exhibited fluctuation in strengths past the optimum lime content. There was no normal trend for kaolinite. Quartz reached maximum strength between 4% and 8%, after 4% lime content, strengths remained at a constant level. El-Rawi and Al-Samadi (1995), two other researchers who studied the same topic, evaluated three silty clays varying in color. The maximum strengths, resulting from 6% lime, were 399.91 kPa (58 psi), 599.87 kPa (87 psi) and 1199.73 kPa (174 psi). Slight fluctuations occurred past optimum as the lime contents increased up to 10%. When an adequate lime content is not used in stabilization long term pozzolanic reaction, which only occurs if pH is equal or greater than 12.4, is not maintained.

b. Reverse Effects

Stabilization is a permanent transformation of clay minerals. However, if the right amount of lime is not applied to the soil the process can reverse after an extended period of time. This was noticed in an experimental study conducted by Lund and Ramsey (1958) in Nebraska, where glacial clays were treated with lime contents ranging from 3 to 10 percent. The section treated with 3% lime displayed decreasing plasticity indexes. However, when the section was tested 7 years after construction the plasticity indexes began to increase and the volumetric change increased from 19.15 to 27.36. The sections stabilized with 6% and 10% lime, preformed as expected with a low plasticity index. After 10 years the plasticity index was 10 for both sections. The increasing changes in soil properties show that the benefits once obtained from the lime treatment can be reversed in the future if sufficient lime content is not used from the start.

2.2.4 Mellow Period

Mellowing is defined as the elapsed time between the addition of lime and water to the soil and the final compaction of the mixture (Sweeney, et al., 1988). This period ranges between 24-72 hours, and while the reaction occurs, larger clay clods are broken down so they can be properly compacted. This provides a better mix and uniformity of the stabilized layer. If mellowing occurs for longer spans of time it can often be detrimental to the stabilized layer (Holt et al., 2000). An extended period of mellowing may result in the consumption of the lime and eventual reversal of benefits of stabilization.

During this phase of construction, lime stabilization has an advantage over cement stabilization since after the soil has set for a time it can still be remixed prior to compaction. Remixing of the soil is advantageous for lime stabilization because it re-homogenizes the lime mixture. Whereas for cement stabilization re-compaction of newly formed cementitious bonds that have just been created would be destroyed and would result in a weaker layer.

2.2.5 Moisture Density Relationship

Compaction is a method by which a given mass of soil is reduced in volume by momentary applications of energy, thus increasing its shear strength and decreasing its compressibility and permeability (Daita, et al., 2005). At standard compaction energy of 600 kN-m/m^3 (12400 ft-lb/ft^3) soil particles achieve their closest packing to reach maximum density at optimum moisture content. At this compaction rate soil samples are near their highest strengths (Prusinski and Bhattacharja, 1999). For natural soils and soil lime mixtures, it is important to establish the optimum moisture content and the maximum dry unit weight before compressive strength tests are performed. This ensures the maximum strength will be attained. The intent of the test is to find the optimum amount of moisture to add to the soil that will yield the maximum dry unit weight.

For natural soils, optimum moisture contents vary based up on the mineralogical composition of the soil type. Granular soils composed of sandy materials tend to have lower optimum moisture contents, while silty and clayey materials have higher optimum moisture contents. When soil-lime samples are being prepared for strength testing, it is necessary to perform an individual moisture density test for each lime content specified. Figure 2.2

illustrates the normal or expected trend of compaction curves with lime. As the lime content increases the curve continues to shift downwards and to the right.

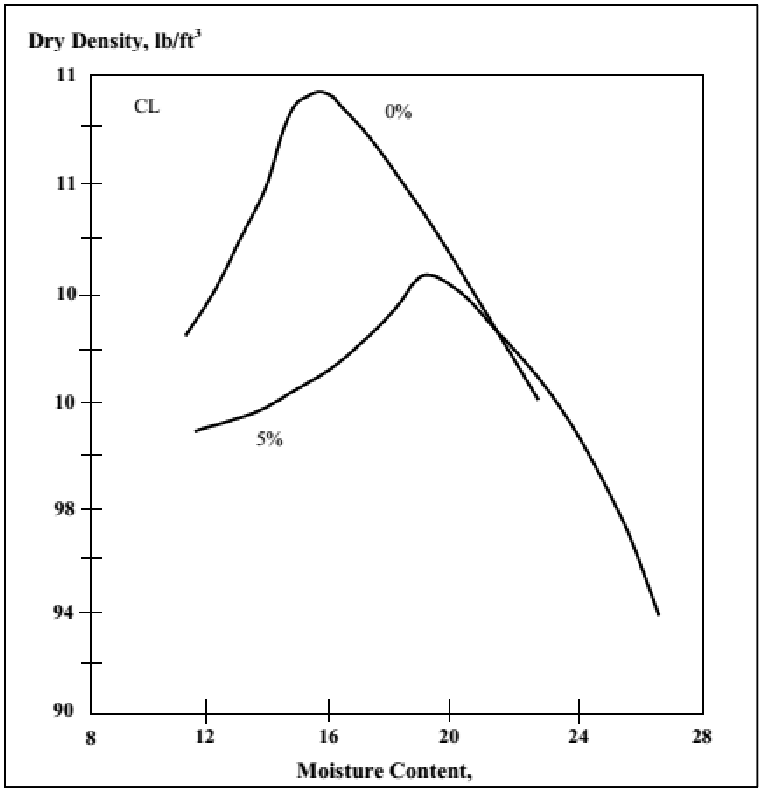

Figure 2.2 Shift in the moisture-density relationship of a soil, as a result of adding lime (Little, 1995)

The shift in the location of the optimum from natural soils is a result of two processes. The first process is the increase in moisture content. As the lime content increases so does the availability of calcium oxide (CaO). Heckel (1997) referred to a previous study by Herrin and Mitchell (1961) which stated “An increase in the percentage of CaO would increase the amount of H_2O needed to form $Ca(OH)_2$”. This statement explains that the moisture content increases as the lime content increases in order to supply the demand for water to form new chemical reactions.

The second process is the reduction in the maximum dry density. It indicates that the ending product of the soil is different from the parent material (Daita, et al., 2005). After treatment have been completed, the transition results in the cementation of particles into a loose structure. The cementation that develops at contact points between edge to face points of adjacent clay particles offers greater resistance to the soil, thus resulting in an expected lower density at a given compaction effort (Sweeney, et al., 1988).

The increase in moisture and the decrease in dry density vary upon the soil composition and the quantity of lime added to the soil. As mentioned before, with higher lime contents the change is more drastic. As presented in Table 2.2 for 5 soil types. Among 4 of the 5 soil types, an average of 5.75% lime increased the optimum moisture content by 2.83% and decreased the maximum dry density by 1.0 kN/m^3 (6.4 pcf). The fifth soil type, quartz, had the smallest decrease in maximum dry density at .094 kN/m^3 (0.6 pcf) while the optimum moisture content increased by 4 %. The main difference between quartz and the other soil types was the level of activity. Quartz had a lower level of activity than kaolinite or montmorillonite, which may have affected the initial rate of reaction of lime with the soil (Bell, 1996).

Table 2.2: Density Moisture Relation with Lime

Soil Classification	% Clay	Lime Content (%)	OMC (%)	MDD kN/m^3 (pcf)	Citation
CL-ML	11	0	13.1	17.8 (113.4)	Solanki et al., 2009
		3	14.7	17.1 (108.7)	
		6	15.9	16.8 (107.2)	
		9	16.5	16.6 (105.9)	
Expansive Clay	33	0	20.5	16.1 (102.6)	Nalbantoglu, 2006
		3	21.25	15.7 (99.9)	
		5	21.3	15.4 (98.3)	
		7	22.5	15.4 (98.2)	
Kaolinite	94	0	29.5	13.7 (87.4)	Bell, 1996
		6	31.0	12.7 (81.1)	
Montmorillonite	76	0	20.0	12.6 (80.5)	
		4	25.0	11.3 (71.8)	
Quartz	68	0	28.5	13.8 (88.0)	
		6	32.0	13.7 (87.4)	

Even though it is expected for soils to act in the manner shown above, it does not always occur. Some soils react differently, for instance the optimum moisture content may decrease as opposed to increasing while the maximum dry density increases instead of decreasing.

2.2.6 Curing

Primary strength gains occur during the first 7 days. At this point, initial reactions taking place are most active after the soil, water and lime has been mixed (Bell, 1996). The rate of effectiveness for the pozzolanic reaction, an important characteristic of strength gain, is time and temperature dependent. The pozzolanic effect is responsible for the long term strength development that occurs in lime stabilization. To observe development in strength over time, stabilized samples are cured around 25°C±4° for different durations.

Bell (1996) studied the duration effects at a constant temperature for Upper Boulder Clay and Tea Laminated Clay. In the study, the researcher examined the strength of lime stabilized samples at different moisture contents and lime contents. Trials of samples were mixed at 2, 4 and 6% lime with 10, 20 and 30% moisture content, and cured at 20°C for 0, 7, 14 and 28 days. At the optimum moisture content and wet of optimum, compressive strengths increased over the course of the study. Strengths of stabilized samples prepared dry of optimum initially increased, then followed by a decrease. Insufficient amounts of water led to inadequate compaction, and are rapidly used through the hydration process which led to an early gain of maximum strength.

Construction of soil subgrade stabilization normally occurs during the summer months, when ground and air temperatures are warm and optimal results can be achieved. At these temperatures, samples replicate ideal conditions of strengths developed in the field.

a. Accelerated Curing

Accelerated curing is a technique used to expedite quality control of roadway construction. With the ability of knowing long term strengths in short time frames, state agencies can save time and money by opening highways earlier and moving on to future projects. The protocol set by the National Lime Association (2004) recommends lime stabilized samples to be cured at a temperature of 40°C for 7 days. Higher temperatures accelerate the pozzolanic reactions and reduce the curing period required for strength development (Rao and Shivananda, 2005). Samples cured under these conditions have been considered to provide strengths equivalent to 28 day strengths, however the duration of strength may differ based on soil variation. When comparing strength versus rising temperature shown in Figure 2.3, the investigators indicate that curing samples at 50° C provides at least twice the strength of curing samples at room temperature (25°C). When accelerated curing is used, temperatures above 49°C should be avoided in accordance with ASTM D 5102 (2009). Temperatures at 49°C and higher are not typically encountered in the field, therefore the data obtained from lab samples would be deemed unreliable.

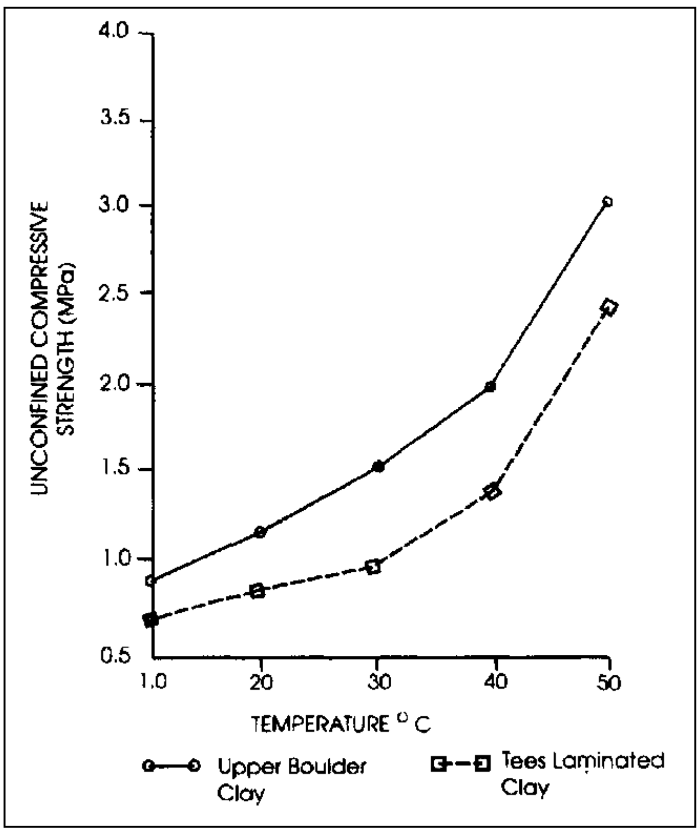

Figure 2.3 Influence of curing temperature on strength development (Bell, 1996)

2.2.7 Strength Parameters

Unconfined Compression tests are the most common, economical and reliable means for obtaining maximum undrained shear strength for fine grained soils. They are also used to evaluate the effectiveness of lime stabilization. In order for a soil type to be successfully stabilized, there must be a gain of at least 344.75 kPa (50 psi) from its natural strength (Little and Nair, 2009).

Soil composition, soil processing, lime content and curing temperature are parameters that can influence pozzolanic reaction and strength gain of lime stabilized soils (Mooney, et al., 2010). The amount of strength gain based on the addition of lime, depends on chemical and physical conditions. The strength increase between the natural soil state and the stabilized state can be influenced by: the type and amount of clay, the increase of pH in addition to lime due to particle dissociation, and the amount of silica and alumina present for cementing agents (Castel and Arulanandan, 1979). Strength gain occurs rapidly within the first 7 days and can be attributed to the quantity of lime, curing temperature, and the curing duration period (Bell, 1996).

a. Clay Type and Content

The level of reactivity is dependent upon the amount of pozzolans created during the chemical reaction. Soils with a high level of activity react better with lime and ultimately resulting in more efficient chemical reactions. This varies for each soil type and it is dependent on the amount and type of clay in the soil composition. Soils with high plasticity, containing montmorillonite, are more reactive and initially achieve higher strengths compared to soils containing lower levels of activity, such as kaolinite.

In a study performed by Bell (1996), the author noted that expansive clays rapidly increase in unconfined compressive strength with small percentages of lime during initial stages of curing. A maximum strength of 799.82 kPa (116 psi) for montmorillonite was achieved with 4% lime at 1,3,14, and 28 days. This strength was attained at each of the days listed previously. The other minerals studied, kaolinite and fine quartz required longer durations of curing to achieve remarkably increased strengths (Bell, 1996). Kaolinite attained a maximum strength of 999.78 kPa (145 psi) at 28 days, and at 21 days fine quartz attained a maximum strength of 4998.88 kPa (725 psi). In this study, the author studied the influence of lime addition on the three major minerals (kaolinite, montmorrillonite and fine-grained quartz) in clays soils.

For natural soils, the strength value is not as consistent considering that clay content is in soils composed of different minerals and are are significantly different than single mineral clay type. Table 2.3 shows a range in strengths based on clay content compiled from two studies with similar classifications. Although these soil classifications are similar, they were extracted from different locations which would have significantly impacted their clay mineral composition and result in different reaction processes.

Table 2.3: Unconfined Compressive Strength Variation due to Clay Content

AASHTO Classification	% Clay	% Lime	Curing Duration (Days)	Unconfined Strength kPa (psi)	Citation
A-6	8	6	6	620.6 (90)	Mooney & Toohey, 2010
A-6	28	6	6	1172.2 (170)	Mooney & Toohey, 2010
A-6	45	6	7	599.9 (87)	El-Rawi & Al- Samadi, 1995
A-7-6	29	6	6	827.4 (120)	Mooney & Toohey, 2010
A-7-6	29	6	6	551.6 (80)	Mooney & Toohey, 2010
A-7-6	55	6	7	1199.7 (174)	El-Rawi & Al- Samadi, 1995
A-7-6	69	6	7	399.9 (58)	El-Rawi & Al- Samadi, 1995

2.2.8 Resilient Modulus

Resilient modulus is a laboratory test that can be used to assess the behavioral response of granular materials or stabilized subgrade under cyclic/repetitive loading. The dynamic stiffness values of pavement layer systems are measured by the resilient modulus test or the cyclic triaxial testing. Cylindrical specimens are subjected to a different low confining stresses, with pulse applications of cyclic axial loads. The constant confining stresses of the specimen represent the lateral stresses caused by overburden pressures and applied wheel loads (George, 2004). Deviatoric stresses are additional stresses created when traffic is permitted on the roadway. The resilient modulus test is an attempt to simulate actual field conditions, providing different stress states to represent vehicle loading over pavements and subgrades.

The soil specimen endures a lengthy process of preparation and testing. Disturbed samples can be made by either static or dynamic compaction and must meet a target moisture content and compaction density. The test begins with a conditioning phase of 1000 cycles, and continues into the recorded test which is composed of 15 sequences. Each sequence consists of 100 cycles. The specimen is constantly confined at stresses of 41.37

kPa (6 psi), 27.58 kPa (4 psi), and 13.79 kPa (2 psi). Additional stresses of 68.95 kPa (10 psi), 55.16 kPa (8 psi), 41.37 kPa (6 psi), 22.58 kPa (4 psi), and 13.79 kPa (2 psi) are applied cyclically at each confining stress state, through the Haversine load pulse for 0.1 second duration and 0.9 second rest period. Upon completion of the cyclic phase, the option for quick shear is available to determine the ultimate strength of the soil after testing. After the full test has been completed, 15 points are plotted on a full log scaled graph and presented in a summary table. These points are the resilient modulus at the different confining and deviatoric stresses. The resilient modulus value is expressed as the ratio of applied deviator stress and the resilient axial strain recovered after removal of the deviator stress (Hopkins, 2004).

Resilient modulus is the main component for designing pavement thickness in mechanistic empirical design guideline (MEPDG). Due to the complexity and the time required for the test, many state agencies use typical values or values determined from empirical relations as opposed to performing laboratory tests. Table 2.4 lists a set of values for each soil type for Resilient Modulus, specified from NCHRP (2004).

Multiple relationships have been derived relating resilient modulus values to results obtained through unconfined compression (UC), California bearing ratio (CBR), falling weight deflectometer (FWD), dynamic cone pentrometer (DCP) and other soil properties. Different versions of the relationships between relating resilient modulus and standard soil property test methods are listed in Table 2.5. Modulus values may also be predicted by indirect correlations to standard tests listed previously or from back calculations of deflection results of strength data. The essential problem of using empirical relations for determining resilient modulus values is that it assigns set values for each soil type. The models do not account for the change in the resilient modulus as the stress and strain conditions change (Hopkins, 2004).

The molding water content for resilient modulus samples is one of the most important parameters in obtaining ideal values. The slightest change in the wrong direction can result in a drastic change of values. Resilient modulus samples perform best at their most ideal conditions when they are made dry of optimum moisture content. Two studies conducted by Puppala et al. (1996) and Achampong et al. (1997) resulted in similar conclusion after testing multiple samples. Achampong et al. (1997) tested resilient modulus samples on CL and CH samples at 2% dry of optimum, at optimum and 2% wet of optimum and compared the results. At a deviatoric stress of 13.79 kPa (2 psi), the resilient modulus values were 65,600 kPa (9515 psi), 62,000 kPa (8992psi) and 48,300 kPa (7005 psi). As the moisture content increases the modulus decreases. The highest strength of the sample was achieved at 65,600 kPa (9515 psi) when the sample was dry of optimum moisture content. The resilient modulus value at 2 % wet of optimum was only about 73% of the value at 2 % dry of optimum.

2.2.9 Resilient Modulus with Lime

Limited research has been conducted on resilient modulus associated with lime stabilization. From the few studies conducted it has been noted that the stiffness parameters of fine grained soils greatly improved with small contents of lime treatment. The addition of lime increases the strength of the soil, thus considerably increasing the resistance to permanent deformation or rutting (Puppala, et al., 1996).

In a study conducted by Solanki, Khoury and Zaman (2009), soil from Oklahoma classified as a CL-ML was tested at 0, 3, 6 and 9 % lime. The method used to observe the effect of the additive was to select one sequence and evaluate the resilient modulus at each percentage of lime. At a confining pressure of 41.37 kPa (6 psi) and load of 24.82 kPa (3.6 psi), the resilient modulus increased indicating production of more cementious compounds in the sample. The results matched well with other researchers, such as Achampong et al. (1997) who evaluated increasing lime and cement contents at different moisture contents of CL and CH soil samples. Other additives used in Solanki et al. (2009) study were coal Fly ash (CFA) and cement kiln dust (CKD). Figure 2.4 presents the graphical results of the resilient modulus versus the contents of lime and other additives for one such test. At 3 % lime, there was a 459 % increase from natural soils, however the changes among the lime content were minimal compare to CFA and CKD.

Table 2.4: Typical Resilient Modulus Values for Subgrade Materials (NCHRP, 2004)

Material Classification	**M_R Range kPa (psi)**	**Typical M_R kPa (psi)**
A-1-a	244,773 - 289,590 (35,500 - 42,000)	275,800 (40,000)
A-1-b	241,325 - 275,800 (35,000 - 40,000)	262,010 (38,000)
A-2-4	193,060 - 258,563 (28,000 - 37,500)	220,640 (32,000)
A-2-5	165,480 - 227,535 (24,000 - 33,000)	193,060 (28,000)
A-2-6	148,243 - 213,745 (21,500 - 31,000)	179,270 (26,000)
A-2-7	148,243 - 258,563 (21,500 - 28,000)	227,535 (24,000)
A-3	168928 - 244,773 (24,000 - 35,500)	199,955 (29,000)
A-4	148,243 - 199,955 (21,500 - 29,000)	227,535 (24,000)
A-5	117,215 - 175823 (17,000 -25,500)	137,000 (20,000)
A-6	93,083 - 165,480 (13,500 - 24,000)	117,215 (17,000)
A-7-5	55,160 - 120,663 (8,000 - 17,500)	82,740 (12,000)
A-7-6	34,475 - 93,082 (5,000 - 13,500)	55,160 (8,000)
CH	34,475 - 93,082 (5,000 - 13,500)	55,160 (8,000)
MH	55,160 - 120,663 (8,000 - 17,500)	79,293 (11,500)
CL	93,083 - 165,480 (13,500 - 24,000)	117,215 (17,000)
ML	117,215 - 175823 (17,000 -25,500)	137,000 (20,000)
SW	193,060 - 258,563 (28,000 - 37,500)	220,640 (32,000)
SP	165,480 - 227,535 (24,000 - 33,000)	193,060 (28,000)
SW - SC	148,243 - 213,745 (21,500 - 31,000)	175823 (25,500)
SW - SM	165,480 - 227,535 (24,000 - 33,000)	193,060 (28,000)
SP - SC	148,243 - 213,745 (21,500 - 31,000)	175823 (25,500)
SP - SM	165,480 - 227,535 (24,000 - 33,000)	193,060 (28,000)
SC	148,243 - 258,563 (21,500 - 28,000)	227,535 (24,000)
SM	193,060 - 258,563 (28,000 - 37,500)	220,640 (32,000)
GW	272353 - 289590 (39,500 - 42,000)	282695 (41,000)
GP	241,325 - 275,800 (35,000 - 40,000)	262,010 (38,000)
GW - GC	193,060 - 275,800 (28,000 - 40,000)	237876 (34,500)
GW - GM	244,773 - 279,248 (35,500 - 40,500)	265,457 (38,500)
GP - GC	193,060 - 268,905 (28,000 - 39,000)	234430 (34,000)
GP - GM	213,745 - 275,800 (31,000 - 40,000)	248220 (36,000)
GC	165,480 - 258,563 (24,000 - 37,500)	213,745 (31,000)
GM	227,535 - 289,590 (33,000 - 42,000)	265,457 (38,500)

Table 2.5: Models Relating Soil Properties to Resilient Modulus

Strength/Index Property	Model	Comments	Agency/Origin
CBR	M_R(psi)= 1500(CBR)	CBR= California Bearing Ratio	Corps of Engineers
CBR	M_R(psi)= $3166(CBR)^a$	CBR= California Bearing Ratio a= .4779707	Georgia DOT
R value	M_R(psi)=A + B (R value)	R value = Stabilometer value, lbs A = 772 B = 369 to 555	Asphalt Institute
R value	M_R(psi)= 3500 + 125 (R value)	R values	Colorado Dept. of Highways
Soil Properties	M_R(psi)= 37.431 - .4566(PI)- .6719(w_c)- .1424(P_{200})+ .179(σ_3)- .3248(σ_d)+ 36.722(CH)+ 17.097(MH)	PI=Plasticity Index,% P200= percent passing 200 sieve σ_3= confining stress, psi σ_d= deviator stress, psi 1 for CH soil, 0 otherwise 1 for MH soil, 0 otherwise	Highyway Research Information Service
Soil Properties	M_R(ksi)=(a'+b'σ_d)/σ_d	a'= 318.2 + .337(q_u) +(.73%Clay) +2.26(PI)- .915(γ_s)- 2.19(S) - .304(P_{200}) b'= 2.10+.00039(1/a)+.104(q_u) +.09(LL) -.10 (P_{200}) qu= unconfined compressive strength, psi 1/a=intial tangent modulus of UC test, psi LL= liquid limit,% S= degree of saturation γ_s= dry density, pcf	n/a
Soil Properties	M_R= 34280 - 359 S% 325 σ_d+ 263 σ_3 + 96 PI + 107 P_{200}		Wyoming Soils
Soil Properties	M_R(MPa)=16.75((LL/$w_c\gamma_{dr}$)$^{2.06}$ + (P_{200}/100)$^{-.59}$)		Mississippi Soils

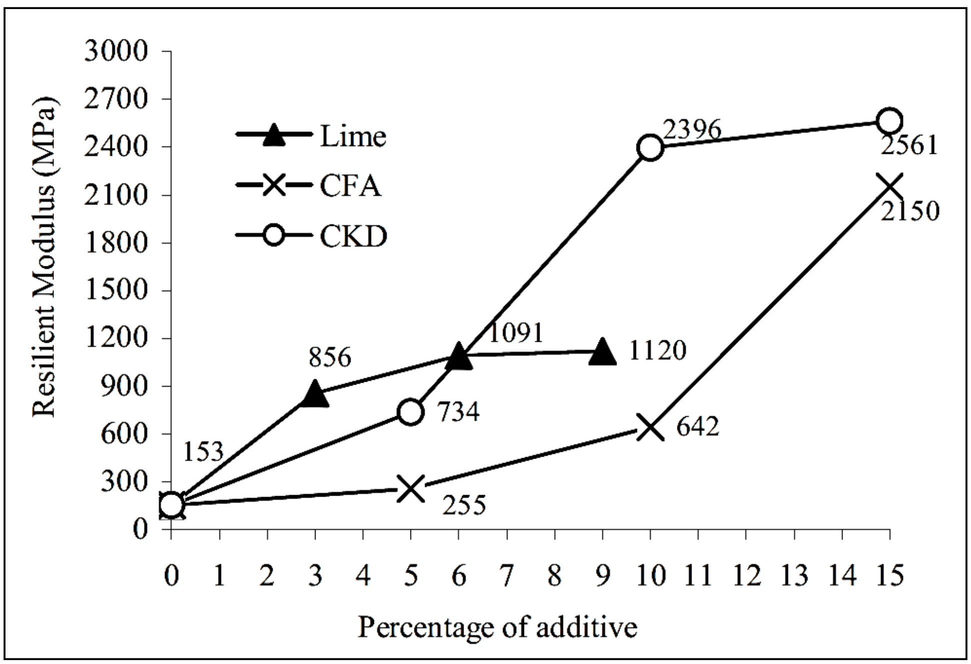

Figure 2.4 Resilient Modulus at different lime contents (Solanki, et al. 2009)

2.3 Cement Stabilization

The first street in the United State known to have been stabilized using soil cement was constructed in Sarasota, FL in 1915 using a mixture of shells, sand and Portland cement. As of 2009, there were approximately 125,000 miles of soil cement stabilized roadways in the United States (ACI 2009). Soil cement is used for stabilization in many applications including recycled pavements, highway construction projects, airport runways and tarmacs. Almost all soil types are suitable for soil cement stabilization excluding highly plastic soils, organic soils, heavily sulfated soil and poorly reacting sandy soils. Granular soils with fines content between 5%-35% passing the No. 200 sieve produce the best results for soil cement stabilization. Soils of this grain size distribution have proven to be easy to pulverize and require a lower amount of cement. The most common types of Portland cement used in soil cement stabilization are ASTM C150 Type I and II or ASTM C1157 Type GU or MS (ACI 2009).

Using cement in granular soils for stabilization creates pozzolanic reactions similar to those found in concrete. The coarse particles of material are cemented together at contact points. By increasing the compaction of the soil particles, more contact points are formed creating a stronger bond. There are five major factors that influence the degree of stabilization including the nature of the soil, the percentage of cement used in mixing, moisture content at compaction, the density obtained during compaction and the conditions present during the curing period (Puffer 1981).

2.3.1 Cement Soil Stabilization Mechanisms

The mechanisms of cement soil stabilization are akin to those of lime soil stabilization involving a cation exchange or molecular crowding initially followed by flocculation or aggregation and finally hydration reactions due to complex pozzolanic actions resulting in soil strength increase. Schoute (1999) detailed the stages of chemical reactions occurring during cement treated soils as:

$$\underset{\text{(tricalcium silicate)}}{2(3CaO.SiO_2)} + \underset{\text{(water)}}{6H_2O} \rightarrow \underset{\text{(calcium silicate hydrate)}}{3CaO.2SiO_2.3H_2O} + \underset{\text{(calcium hydroxide)}}{3Ca(OH)_2} \quad (2.5)$$

$$2(2CaO.SiO_2) + 4H_2O \rightarrow 3CaO.2SiO_2.3H_2O + Ca(OH)_2 \quad (2.6)$$

(bicalcium silicate) (water) (calcium silicate hydrate) (calcium hydroxide)

$$2CaO.Al_2O_3 + 2H_2O + Ca(OH)_2 \rightarrow 3CaO.Al_2O_3.Ca(OH)_2.12H_2O \quad (2.7)$$

(tricalcium aluminate) (water) (calcium hydroxide) (tretracalcium aluminate hydrate)

The reaction processes in equations 2.5 – 2.7 are similar to those of concrete, except that cement paste in soil are not filling voids in the aggregates in soils but the gels (CSH and CAH) are cementiously binding soil particles/gains at their points of contact. Strength arises from the cement-clay hydrated gel surrounded by zone of flocculated clay, pasted together by a secondary contact cementation (Schoute, 1999).

2.3.2 Cement Content

Though ACI (2009) provides initial estimates of the cement content requirements for various soil types, each client/organization uses different criteria to determine acceptable mix proportions. The criteria include, but are not limited to, adequate strength and durability (wetting and drying or cycles of freezing and thawing). The United States Army Corps of Engineers (USACE) durability requirements (Table 2.6) and minimum compressive strength values (Table 2.7) for a cement stabilized pavement layer (USACE, 1994) appear to have been adopted by many DOTs for use in establishing the cement cements for different soil types.

Table 2.6: USACE Proposed Durability Requirements for Cement Stabilized Subgrade

Type of soil stabilized	Maximum allowable weight loss after 12 wetting-and-drying or freezing-and-thawing cycles, % of initial specimen weight
Granular, *PI* < 10	11
Granular, *PI* > 10	8
Silt	8
Clays	6

Table 2.7: USACE Minimum UCS Requirements for Cement Stabilized Subgrade

Stabilized soil layer	Minimum unconfined compressive strength at 7 days, psi	
	Flexible pavement	Rigid pavement
Base course	750	500
Subbase course, select material or subgrade	250	200

2.3.3 Strength Parameters

Most other factors and characteristics observed in lime subgrade stabilization are found with cement stabilized soils. However, Miller (2000) found that the addition of quick lime during stabilization increased the unconfined compressive strength (UCS) of the samples rather slowly compared to CKD. Cement or CKD stabilized soil gains most of its strength in 7-14 days of curing. To reach its maximum strength, lime treated soils may need from 28 days to 1 year of time (Miller 2000). This is attributable to the slow pozzolanic action in lime stabilization while quick hydration of the hydrates occur in cement stabilize soils. Hence, cement should be mix, placed and compacted quickly to avoid disruption of the hydration process. Considering that cement stabilized subgrade generally exhibits higher UCS versus lime (ACI 2009), resilient modulus test as presently conserved tends not to be appropriate because of the high stiffness of the mixture.

2.3.4 Flexural and Indirect Stresses

MEPDG recommends that flexural tensile stresses in stabilized layer should be resisted to prevented fatigue cracks (AASHTO, 2004). These fatigue cracks initiated by the repeated loading of traffic are considered the main failure mode in stabilized soils according to Lav et al. (2006). Though CKD stabilization enhances the indirect tensile characteristics and modulus of rupture of the soil samples, it was not as effective in improving the samples fatigue performance (Solanki and Zaman, 2014). Using best fit curves to correlate all their data points, Solanki and Zaman (2014) propose that modulus of rupture (MR) be 41% of the UCS.

2.4 Field Cementiously Stabilized Subgrades

2.4.1 Stabilization Construction Process

a. Lime

The most widely used methods of lime application are dry and slurry methods. In the dry application method, a truck places dry lime directly on top of the subgrade to be stabilized. A rotary mixer then mixes the dry lime with the subgrade soil in multiple passes to ensure the lime is thoroughly mixed. As the soil and lime are mixed, water is added for dust control and to assist in the chemical reactions that occur (Smith 2008). This method was used in a Georgia DOT study of lime subgrade stabilization using pelletized quicklime. The slurry method involves mixing hydrated lime prior to application. Lime is mixed in a spreader truck with water to a predetermined concentration. The lime is spread across the subgrade soil at a predetermined rate and mixed using a rotary mixer. Due to the slurry form, water does not need to be added during the initial mixing process. After the lime is thoroughly mixed, compaction of the mixture is completed by a vibratory sheep’s-foot roller, flat steel roller or rubber-tire roller, depending on the compaction specifications. The mixture can be compacted in multiple lifts, or it can be compacted in one lift depending on the thicknesses of the stabilized subgrade. In a Georgia DOT study, only the first 7 inches of soil-lime mixture were compacted while the rest was windrowed into the adjacent lane. Compaction was completed using a vibratory sheep’s-foot roller and a rubber-tire roller. After compaction was completed, the remaining 7 inches of soil were returned and compacted in the same manner. A mellowing period (or hydration period) of 2 to 7 days follows compaction. During the curing period, a coat of asphaltic binder may be applied directly after compaction to assist in moisture retention or water can be sprayed at intervals to assist in the hydration.

b. Cement

The construction process for soil cement stabilized layers is the same as when using pelletized quicklime. Dry cement is placed on top of the subgrade soil using a spreader truck at a given rate. A rotary mixer is then utilized with a water truck to mix the soil and cement (ACI 2009). After the mixing has occurred, a vibratory sheep's-foot roller and flat steel roller are used to compact the layer to a specified density. The layer is then cured for a minimum of ten days before the base or surface layers are applied.

2.4.2 Quality Control Testing (Unconfined Compressive Strength)

Unconfined compressive strength (UCS) testing is the most widely used reference for stabilized soil strength. Samples are collected in the field after mixing and before compaction of the treated layer This UCS testing can be used to determine the proportion of cement required to achieve a given compressive strength value (ACI 2009).

2.4.3 Dynamic Cone Penetration Testing

The dynamic cone penetrometer is a very versatile piece of equipment frequently used in pavement testing. DCP is used for a number of tasks including: assessing the compaction quality of subbases and subgrades in roadways, identifying thickness values of bases, subbases and subgrade soils, and help monitor strength development of stabilized soils. Chen et al. (2005) developed correlations between layer elastic modulus values (E) and DCP testing. 198 FWD and DCP tests were completed on various types of highways in the state of Texas. Using the MODULUS backcalculation program, FWD data was used to determine a modulus value for the base course and subgrade soil layers of the pavement structures. Two widely used correlations were used to develop moduli values from DCP testing. First, the correlations by Webster et al. (1992) relate the penetration index (PI; mm/blow) to the CBR value. The equation is presented below as Equation 2.8. Other commonly used correlations are summarized in Table 2.8.

$$\text{CBR} = \frac{292}{PI^{1.12}} \tag{2.8}$$

The results from using the developed correlation were compared to those from the correlation developed by Powell et al. (1984). Figure 2.5 shows the comparison between the two correlations. At lower moduli values the correlations are very similar though as the values get larger, there is a noticeable variance.

Table 2.8: Modulus Values Estimation from the California Bearing Ration (CBR) and Penetration Index (PI)

E (MPa)	E (ksi)	Citation
$10.34 * CBR$	$1500 * CBR$	AASHTO (1993)[1]
$17.58 * CBR^{0.64}$	$2550 * CBR^{0.64}$	Powell et al., (1984).
$664.67 * PI^{-0.7168}$	$96.468 * PI^{-0.7168}$	Chen et al. (2005)[2]
$537.76 * PI^{-0.6645}$	$78.05 * PI^{-0.6645}$	Chen et al. (2005)[3]

[1] Provides a rough estimate as the constant of correlation ranged from 750 - 3,000 and also limited to only fine-grained soils with a soaked CBR value of 10 or less (Chen et al. 2005).

[2] Derived from combination of Webster et al. (1992) and Powell et al. (1984)

[3] After applying "mean shift outlier model" by Sanford Weisberg (1985) to remove the outliers from the data set.

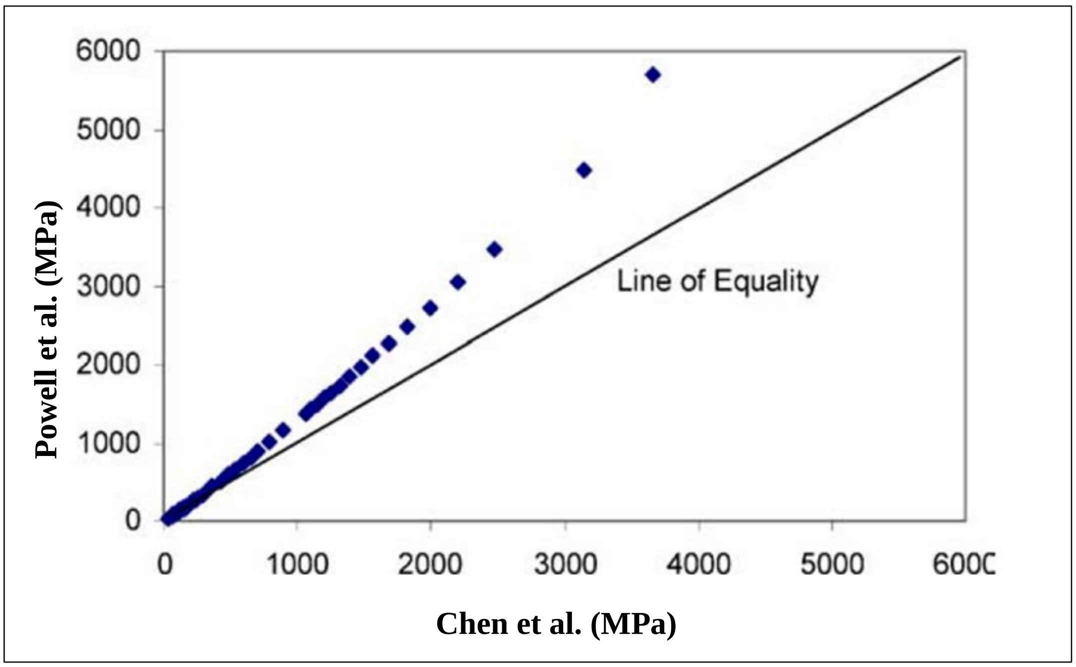

Figure 2.5 Comparison of modulus values estimated from DCP data based on Chen and Powell models (Chen et al. 2005)

In a study by Miller (2000), DCP was used in testing four different stabilized subbase sections in Ada, Oklahoma, each stabilized with a different agent. Three of the test sections were stabilized with cement kiln dust (CKD) from different manufacturers and one was stabilized with granular quick lime. Each section was stabilized to a depth of eight inches. DCP testing was completed 28 and 56 days after construction was complete at ten different locations throughout the entire test area. Three DCP tests were conducted at each of the ten locations. The purpose of performing DCP testing was to verify the behavior found in the unconfined compressive strength samples and to verify the depth of each stabilized layer. Reported penetration index values were averaged along the entire depth of eight inches. Figure 2.7 presents the 56 day DCP profiles from all ten test locations. The results shown represent typical DCP profiles. Notice the change around 200 mm in each test, as this corresponds to the 8 inch depth of the stabilized layer in each section. These results verified the unconfined compressive strength results for this project.

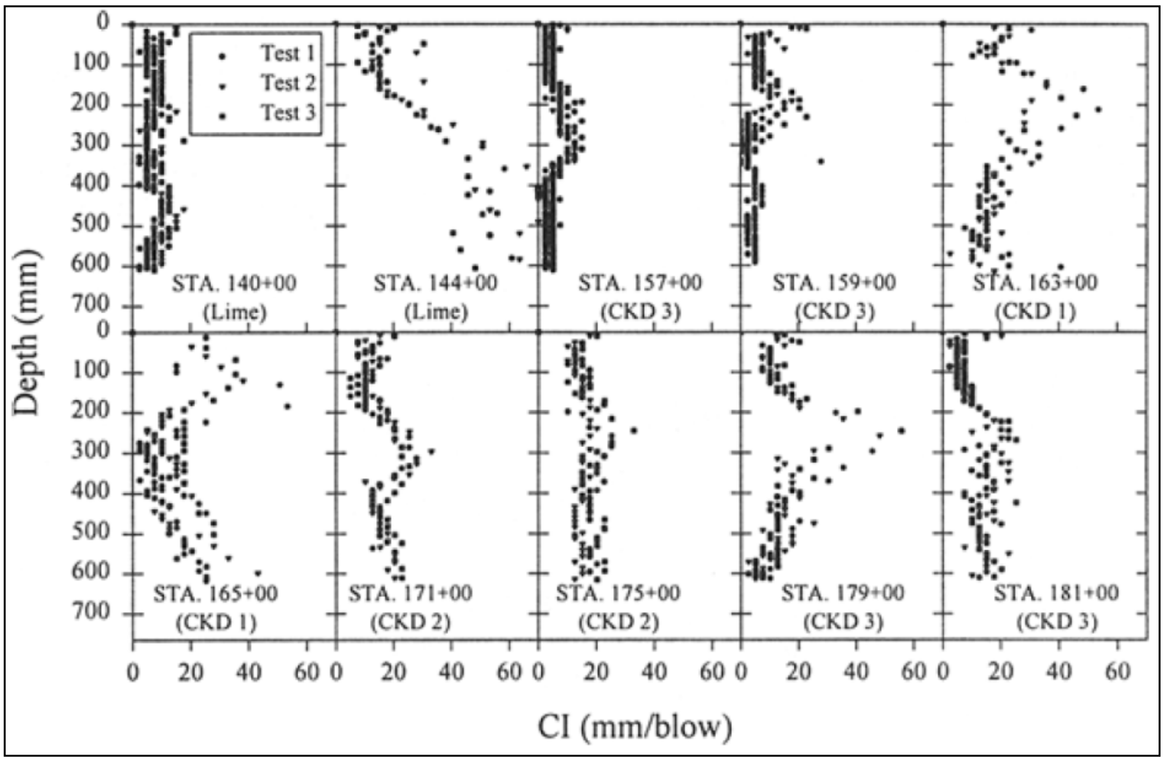

Figure 2.6 DCP profiles of stabilized subbase layers (Miller 2000)

McElvaney and Djatnika (1991) also developed correlations to relate the unconfined compressive strength of three different soil types to DCP penetration index. The three different types of soil tested are clay, silty clay and sandy clay.

2.4.4 Falling Weight Deflectometer (FWD) Testing

Falling Weight Deflectometer (FWD) Testing has become a pavement engineering industry standard for determining the stiffness of a pavement structure. The FWD is a non-destructive testing tool that applies an impulse load to a 300 mm circular plate in contact with the pavement surface (Appea and Al-Qadi 2000). The load is meant to simulate dynamic loading of traffic. Geophones placed at approximately 0 mm, 203 mm (8 in), 305 mm (12 in), 457 mm (18 in), 406 mm (24 in), 609 mm (36 in) and 812 mm (48 in) record the deflection of the pavement surface during the loading process. The response from the impulse load is taken as a realistic pavement response of traffic loading. Using the deflection data from testing, calculations can be performed in two different manners to calculate the modulus of each layer in the pavement structure: backcalculation and forwardcalculation. Backcalculation is the most widely used method for determining the modulus values for each layer in a pavement structure. FWD backcalculation data can assist in determining the effect of stabilization techniques. It is also widely used in correlation with the subgrade design resilient modulus for input in the AASHTO flexible pavement design procedure.

Appea and Al-Qadi (2000) used FWD testing to determine the strength contribution from geotextile and geogrid reinforced aggregate bases in multiple pavement structures. The purpose of this study was to determine if the intrusion of fine material from the subgrade layer was weakening the aggregate base layer. Nine test sections were constructed; three were control sections with no reinforcement in the aggregate base, three were reinforced with geotextile and three were reinforced with geogrid. The test sections were broken up into three groups based on the aggregate base layers being 100 mm, 150 mm, and 200 mm thick. Using the ELMOD backcalculation program the moduli values for each layer were calculated. It was found that the base layer moduli values in the control sections were weaker than those using geotextile and geogrid reinforcement. Over a period of 5 years, a 33 percent decrease in strength was found in the non-stabilized control sections when compared to the geosynthetic stabilized sections. It was proven through excavation of the test sections that intrusion of fine material from the subgrade into the aggregate base was present. By using FWD testing, Appea and Al-Qadi (2000) were able to validate the effectiveness of a geosynthetic as a separator between the aggregate base and subgrade layers of a pavement structure.

In a study by Russell and Hossain (2000) nine subgrade sections of Kansas DOT projects were tested. Resilient modulus samples were extracted from Shelby tubes and tested in accordance with AASHTO T 274-82 “Standard Method of Test for Resilient Modulus of Subgrade Soils” with some slight modifications in the conditioning phase. FWD testing was completed on each test section in the outer wheel path of travel. Three drops were completed at most test intervals with target loads of 27kN (6,069 lbs) for the first drop and 40kN (8,992 lbs) for the second and third drops. In this study both EVERCALC 4.0 and DARWin 2.01 were used for backcalculation. It was found that data from EVERCALC and DARWin were very similar for soils that had slightly nonlinear characteristics (Russell and Hossain 2000). The average correction factor to convert backcalculated modulus values to design resilient modulus values was found to be 0.33 which is in line with the factor used by AASHTO in the flexible pavement design guide. Other studies have found that the factor of 0.33 is not accurate for all cases. Mooney et al. (2000) tested a general aviation airport runway using pavement pressuremeter, FWD and triaxial testing. Backcalculation was completed using the Strategic Highway Research Program, MODULUS. The calculated values were found to be 3-7 times larger than the values determined from pressuremeter and triaxial testing. Nazzal and Mohammad (2010) completed similar testing as Russell and Hossain (2000) and found that the ratio of E_{FWD}/M_r was larger with weaker subgrade soils.

A new analysis method has been developed to determine layered elastic moduli values from load-deflection data called forwardcalculation. This new method of analysis differs from backcalculation in that it calculates modulus values directly from load-deflection data through close-form equations rather than through an iterative process used by backcalculation programs. Forwardcalculation also uses a variability ratio between the subgrade and bound surface moduli to determine the modulus of intermediate layers.

Using the new forwardcalculation procedure, Stubstad et al. (2005) evaluated the data in the FHWA pre-1998 Long Term Pavement Performance (LTPP) database. After evaluation was complete it was found that most comparisons were favorable. 300 FWD points were used to make comparisons between forwardcalculation and backcalculation of subgrade moduli. Table 2.6 shows the results and comparison of the median, average, standard deviation and nationwide variability of materials (COV) of these 300 points. The standard deviation and median of the forward calculated values are much lower than the backcalculated values. The standard deviation of the backcalculated data from the LTPP database was larger than the median value which is unfeasible. This confirms that some of the backcalculated moduli values in the database are too high. Forwardcalculation is not recommended for pavement structures consisting of more than three layers as the closed-form equations only provide modulus values for three layers.

Table 2.9: LTPP Database Comparison of Back and Forward Calculation Results

Statistic	Forwardcalculated Subgrade	Backcalculated Subgrade
Median (MPa)	129	236
Average (MPa)	150	320
Std. dev. (MPa)	68	493
COV (%)	46	154

2.5 Numerical modeling and Viscoelastic HMA behavior

Many researchers have used finite element method to simulate pavement response under vehicle loading. A study by Elseifi, et al. (2006) showed that elastic FE model underpredicts pavement response to vehicular loading at intermediate and high temperatures, and overpredicts pavement response at low temperatures. Also, elastic FE model fails to simulate permanent deformation or relaxation behavior of HMA materials. The authors recommended that incorporating non-linear material properties by considering effect of time and temperature improves FE model pavement responses predictive capability. Further, friction model to define layer interaction properties and simulating dynamic vehicle loading considerably improves accuracy of FE results.

Hadi and Bohinayake (2003) used ABAQUS/STANDARD to simulate pavement response located in South Callington, Australia. The behavior of new asphalt layer is considered to be linear elastic and k-theta (k-θ) model is used to describe non-linear behavior of granular materials. Though (k-θ) model better reproduces traffic loads on granular materials, the analysis found that static loading with linear material properties produced higher deflection at the top of subgrade than dynamic moving load with non-linear pavement material properties (Hadi and Bodhinayake, 2003).

Using the dynamic wheel load data determine with a computer program COMPAS, the dynamic response and permanent deformation at the pavement surface was calculated using three-dimensional finite element program ABAQUS (Mikhail and Mamlouk, 1998). The study considers HMA layer as viscoelastic material. The behavior of granular base and subgrade layer is assumed to elastoplastic represented by Drucker-Prager model. It is observed that the number of load repetitions to failure for thick pavements was approximately 63% and 14% greater than that for thin and medium-thickness pavements respectively (Mikhail and Mamlouk, 1998).

Mulungye et al. (2007) studied effect of transportation truck on flexible pavement with thin HMA layer and soft peat soil subgrade. Various factors like tire pressure, wheel load, and axle configuration were taken into consideration. The pavement response under moving load at different tire pressures is modeled using finite element software ANSYS/ED. A pavement model was analyzed separately in longitudinal and transverse planes. In longitudinal plane, the viscoelastic surface layer gives better strain prediction than linear material properties when compared with in-situ measured data. Whereas, lateral strain prediction in surface layer with linear material characteristics is slightly better than viscoelastic surface layer (Mulungye et al., 2007). Moreover the load repetitions to fatigue failure of pavement increase by 90% on average when tire pressure increases from 50psi to 70psi. This percent increase is almost 50% when tire pressure increases from 70 psi to 90psi, and 90psi to 110psi.

Elseifi et. al. (2006) used laboratory determined material properties into three-dimensional finite element model to predict pavement responses to vehicular loading at different speeds and temperatures. The non-linear material properties of HMA layer are obtained by performing indirect creep compliance test. A generalized Kelvin model was used to describe isotropic viscoelastic behavior of HMA layer. The material constants from the model were obtained by conducting a non-linear regression on experimental data. The FE model response was found to be in good agreement with field-measured pavement response. The average error of 15% was found in predicting transverse and longitudinal strain and 11% error in vertical stress prediction.

Yoo and Al-Qadi (2006) discussed different loading methods used in simulating moving load in finite element analysis. One of the methods is trapezoidal loading amplitude method. In this method, a uniform step load is applied to the first set of elements and same step load is applied to the next set with a distance corresponding to simulated speed. The main drawback of this theory is, at a given time, all elements under the loading influential area are loaded in similar trapezoidal manner. In reality, tire pressure varies non-uniformly and applies different loading amplitudes during the entrance and exit of tire. The authors considered these factors and developed a new continuous loading amplitude method. The method applies different loading amplitudes on different loading elements.

Yoo et al. (2006) also considered factors like pavement interface layer condition, surface shear forces to evaluate pavement response. To simulate interface layer friction effect, different constitutive models like simple friction model and elastic stick-slip model were considered. Detailed discussion about these models is presented elsewhere. According to this study, FE analysis of flexible pavement with fully bonded interface layers underestimated the measured strain and gives incorrect results at some of the interfaces when compared with field response. Therefore, it is not considered in this study. Analyzing different friction models and comparing the results with experimental data, it is observed more practical in predicting pavement responses to dual tire while the simple friction model with coefficient of friction as 1 predicts better pavement responses to wide-base tire (Yoo, et al., 2006). The elastic stick-slip model defines the maximum allowable shear stress - elastic stick, or the permissible deformation – elastic slip, at which relative movement occurs at the interface. Also, the effect of shear forces on the pavement response is not significant because of their low values. Similar observation has been made by Siddharthan et al. (2002). But, inclusion of shear stress improves the strain predictability of FE model at different layers of a pavement closer to field response. The study concluded that continuous loading amplitude method along with non-uniform tire pressure, appropriate layer interface properties depending upon the tire configuration and inclusion of surface shear pressure significantly improve stress-strain prediction of FE model (Yoo et al., 2006).

The trapezoidal impulsive loading amplitude method used to simulate moving load in FE model use quasi-static approach. A quasi-static analysis is used ‘if loading is cyclic and of frequency less than roughly one-quarter the structure’s lowest natural frequency of vibration’ (Cook, et al., 1989). Dynamic analysis differs from quasi-static analysis due to the fact that first takes mass effect into consideration while second neglects it. Considering wheel load as static is oversimplified assumption and gives erroneous results. In reality, the pavement is subjected to moving vehicular load which is time dependent and therefore frequency dependent. Low vehicle speeds means longer loading time and vice-a-versa. For flexible pavements, the natural frequency lies in between 6 to 12Hz. According to Gillespie et al. ‘truck loading frequency is about 4.5Hz at 58km/h and 6.5Hz at 82km/h’ (Gillespie, 1993). Therefore, in cases where vehicle loading frequency is close or lies in range of pavement natural frequency, it is important to consider dynamic effects of system.

According to a study by Cebon (1986), dynamic analysis increases the fatigue damage of pavement by four times and rutting damage by at least 40%. Even for smooth pavement, dynamic analysis of a pavement increases its response by 10% to 15% (Cebon, 1986). Crisman and Facchin (2005) performed the dynamic analysis of pavement with viscoelastic material properties. The dynamic analysis of a pavement, neglecting damping, gave 3% less surface deflection than static analysis for a vehicle speed of 72km/hr whereas 8% decrease is found for a vehicle speed 108km/hr. The introduction of damping coefficient for asphalt concrete reduced the surface deflection by 5-15% as the loading time decreases. Also, dynamic analysis with damping of all layers has significant effect on a pavement response (Crisman and Facchin, 2005).

Yoo and Al-Qadi (2006) incorporated inertia and damping effects of transient dynamic load in flexible pavement analysis and compared the results with quasi-static analysis. Elastic and inelastic material properties of different layers were obtained by FWD and indirect creep compliance test respectively. The dynamic loads were modeled in ABAQUS using DLOAD subroutine. The vehicle dynamic load reduces flexible pavements service life and increases rutting damage. It is observed that peak stresses and strains at different layers in dynamic analysis are always greater than quasi-static analysis at all temperatures. The maximum difference in both cases are 39% in the tensile strain at the bottom of HMA layer, 25% in the compressive strain at the top of subgrade and 10% in the longitudinal strain (Al-Qadi, et al., 2008).

2.5 Interaction between Pavement Layers

The layer interface properties are dependent upon layer materials, traffic loading, time, and temperature. The surrounding temperature also affects the interface strength. It is observed that interface strength and reaction modulus decreases with increase in temperature and increases with increase in normal stress. Also, material characteristics like gradation of aggregates present in asphalt mix and binder content influences the interface shear strength. It is noticed that coarse gradations provide more shear resistance than fine gradations.

The layer interaction significantly affects pavement responses to vehicular loading. Generally, stresses and strains are calculated at layer interfaces to determine failure of pavement system. Inadequate bond between pavement layers may lead to slippage and separation of layers. This results into potholes, cracking at the pavement surface, and ultimately reduces pavement life. By ensuring proper bond between the layers, one can reduce the cost of maintenance and rehabilitation.

A flexible pavement rehabilitation project on I-40 in Tennessee, milled 2in of existing pavement surface and reconstructed with polymer modified base course followed by a surface course. The hot-mix overlay melted the asphalt contained left in the grooved, milled pavement. The melted asphalt led to a strong bond between the placed mixture and underlying pavement. In layered elastic theory, stress-strain compatibility is assumed between all layers. Many researchers considered the interface between layers to be fully bonded with no gaps. Yin et al. (2007) did finite element analysis of flexible pavement under dynamic moving load. In finite element model, the bond between HMA and underlying layer is assumed to be perfect bond with no slippage. The assumption is generally more applicable to hot-mix asphalt layers, since the possibility of slippage is greater at the subbase/subgrade interface.

Elseifi et al. (2006) used Coulomb friction model with a friction angle of 45^0 to simulate the field response of Virginia Smart Road. The FE results are in good agreement with measured response. For vehicle speed of 8kmph, an error of less than 5% is observed between measured and predicted longitudinal strain at the bottom of viscoelastic HMA layer. Whereas approximately 15% error is observed in predicting longitudinal and transverse strains at the bottom of wearing surface at vehicle speed of 24.1kmph.

Yoo (2007) studied the effect of dynamic moving load on flexible pavement response. A simple friction model with friction coefficient varying from 0.2 to 1.0 is used to define layer interface condition. A strain comparison has been done at the bottom of HMA layer for different friction coefficients. The study found that effect of coefficient of friction is reduced as the depth increased. For wide base tire configuration, coefficient of friction 1 gives the pavement response closest to field measurements. In case of dual tires, approximately 25% error is observed in transverse strain with coefficient of friction 1 whereas error is approximately in between 26-43% when coefficient of friction varies from 0.2-0.7. While in case of longitudinal strain, the percentage errors are very close to each other for different coefficient of frictions.

In this study, stress-strain distribution in a pavement structure with layer interaction defined by simple friction model and full-bond condition is studied.

In summary, finite element model of a pavement with suitable model dimensions, appropriate boundary conditions, and layer interactions; inclusion of appropriate material properties by considering effect of time and temperature, tire-pavement stress distribution, and vehicle characteristics can be used effectively to determine potential distress.

2.8 Deep Subgrade Stabilization

Deep plow stabilization for lime has been primarily used to control swelling soils, expedite construction, and construct unsurfaced haul roads (Thompson, 1972). In the past, this practice was not commonly utilized due to lack of equipment capable of handling this construction. The majority of mixers and rippers were not able to pulverize soils adequate at and beyond a depth of 0.30 meters (12 inches). For situations where deep stabilization were required, it was normally conducted in several lifts. Some percentage of lime was applied and mixed to the top layer, than soil from the bottom layer is churned to the top for chemical treatment. A different method for deep stabilization is excavating and relocating soils from the surface, treating the bottom layer and continuing stabilization in lifts until the desired grade level is reached.

For this study, layers stabilized at depths beyond 0.18 or 0.20 meters (7 or 8 inches) are considered to be deep stabilized layers for lime and cement stabilized soils, respectively. These typical depths for North Carolina DOT standard subgrade stabilization are used as basis for this research.

2.8.1 Survey of Deep Layers of Subgrade Stabilization Practices in the United States

Hopkins et al. (2004) conducted a soil stabilization survey for pavement design throughout the United States. Information was obtained on chemical additives, stabilization methods, chemical contents for stabilization, and soil criteria for stabilization. However there was no mention of standard stabilization depths for each chemical additive.

In March 2010, a survey of deep layers of subgrade stabilization was sent to state transportation agencies through the AASHTO Pavement Materials Committee (Appendix A.1). The purpose of the survey was to determine if other states were practicing deep layers of subgrade stabilization or experimented with the idea. If they do, whether the deep layers get structural credits in determining the thickness of flexible pavement during design? Of the fifty states, thirty five states responded to the survey (Figure 2.7). With the aid of the survey performed by Hopkins et al. (2004), it was discovered that Idaho, Illinois, New York, Pennsylvania, Texas, Utah, and Wyoming also use lime stabilization. Unfortunately no additional data was obtained about the details of their stabilization.

Sixteen of the states use cement stabilization to improve the subgrades. The following states perform cement stabilized subgrade to depth of 7 inches or greater: Minnesota, Nebraska, New Mexico, Louisiana, Georgia, North Carolina Kentucky, Ohio, and Pennsylvania (Figure 2.8). Sixteen states provided information on their lime contents, and standard depth of stabilization for the additive (Figure 2.9). Twelve of these states conduct subgrade stabilization to depth of eight (8) inches and more, while only Alabama, California, and Ohio are currently practicing deep layer of subgrade stabilization. Other states such as Arkansas, Arizona, Georgia, and Kentucky have the capability of performing deep subgrade stabilization if the project requires it.

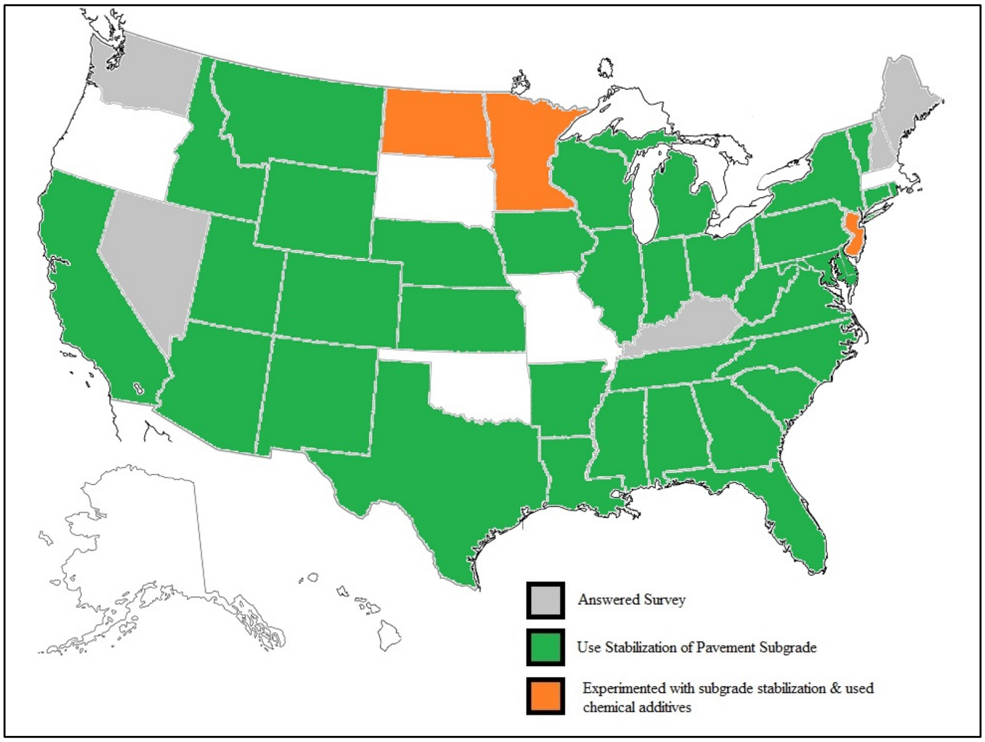

Figure 2.7 Survey response map of states utilizing/performing soil stabilization of pavement subgrade and/or experimented with chemically stabilized subgrade

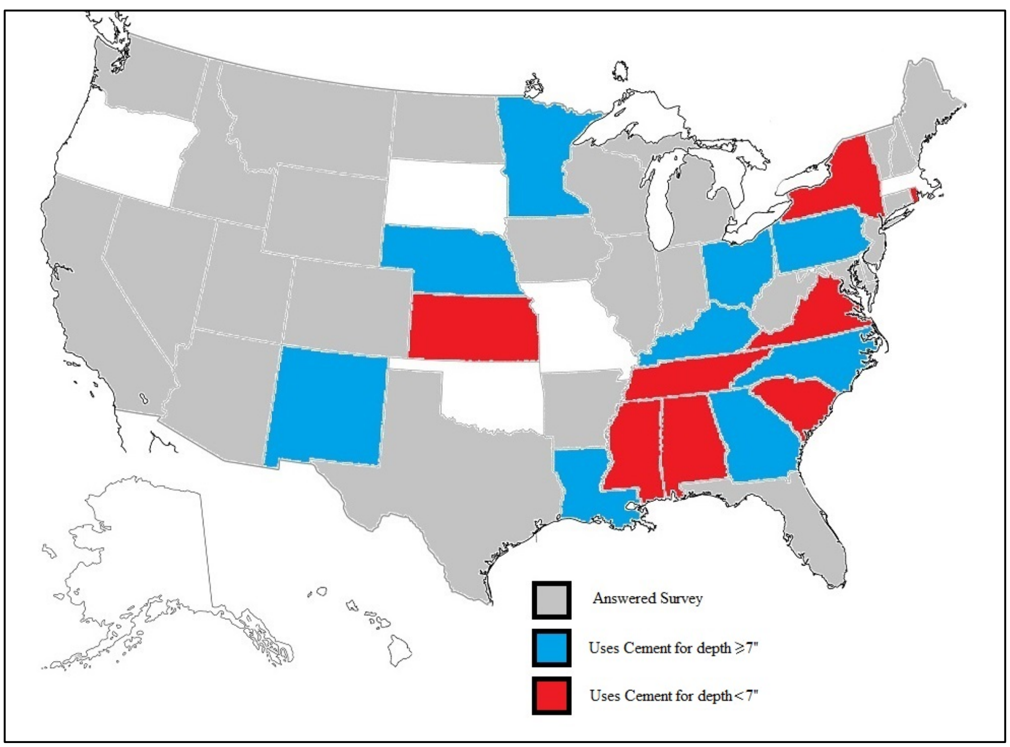

Figure 2.8 Map showing states using chemical additive of cement in subgrade stabilization

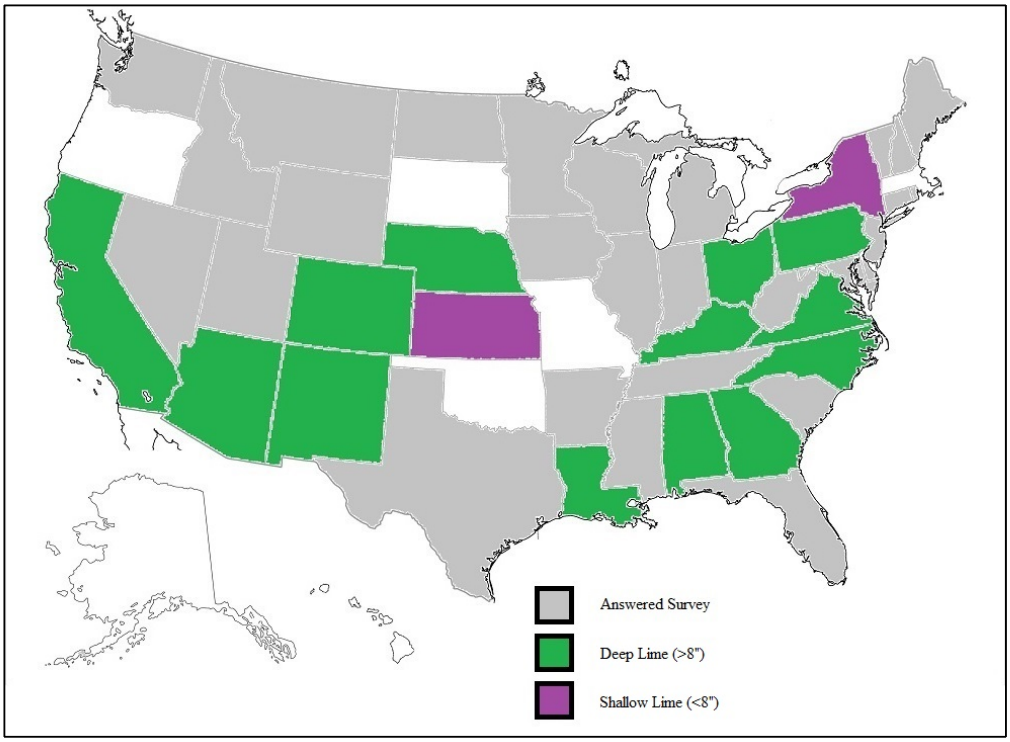

Figure 2.9 States using chemical lime in subgrade stabilization

2.8.2 Past vs. Current Methods of Deep Subgrade Stabilization Practices

In the past, deep layers of subgrade stabilization practices were limited by availability of equipment. Mechanical equipment was limited to mixing shallow depths, therefore if deep stabilization was required, multiple lifts of the layer must be performed. More recent applications conducted by the USACE (1994) and New York Transportation Department (2008) used multiple lifts, sometimes with multiple increments of the application rates. The advantages of this method was that the operator had a better control of the chemical additive distribution and density compaction of the layers. However, such construction practices can be time consuming and expensive.

With the advances in new equipment, subgrades can be stabilized to as much as twice the depth limit of the practices. Attempts to perform stabilization to deep layers had been made in the past. The method consisted of plows and rippers capable of mixing up to 90 cm (3ft) been attached to a tractor to stabilize the soils. These procedures documented by Thompson (1972) were attempted in the Oklahoma and in the Illinois procedures of deep stabilization with lime. Subgrade stabilization at greater depth can now be achieved and compacted in one lift, as opposed to multiple lifts. The field test sites for this study were implemented using this construction process. The advantages of deep stabilization with one lift are the expedited time in construction and cost savings. In addition to the cost of new equipment to stabilize to greater depths, there is the challenge of controlling the distribution of lime throughout the layer, and of monitoring compaction effectiveness at the bottom of the layer.

CHAPTER 3 FRAMEWORK FOR PREDICTION OF EQUIVALENT PAVEMENT SECTIONS

3.1 Introduction

As indicated in Chapter 1, the main goal of this project was to investigate the benefits, in terms of potential cost savings and structural performance, of pavement sections that include deep subgrade stabilization. Justification for carrying out such a study was provided in Chapter 2, where a summary of the literature review was presented, that highlighted the positive experience reported in the literature with deep subgrade stabilization. Chapter 2 further justifies this study by presenting results of the survey which summarized the state of practice at the time of the start of this project. Before presenting the experimental work component (Phase II), this chapter describes the proposed framework used to compare pavement sections with different depths and treatment conditions of subgrade stabilization.

Specifically, this chapter describes the framework developed to predict the equivalency among the different pavement sections that were investigated in this study. In essence, the framework is based on using numerical methods to predict the overall pavement performance of the different pavement designs considered, and then the number of load repetitions to failure was estimated for a range of pavement sections using current pavement performance models. When the number of load repetitions of reduced hot-mix asphalt (HMA) layer thicknesses of pavements with deep subgrade layer stabilization are equal to those estimated for the standard NCDOT pavement structure, then equivalent pavement sections are said to be established.

This chapter is divided into three main sections: (i) overview of the proposed framework; (ii) background on material characterization and simplified models often used in pavement analyses; and (iii) a more detailed description of the numerical approach used for the equivalency framework.

3.2 General overview of the Proposed Equivalency Framework

As will be described in the Phase II section of this report, this study involved comparing two pavement sections containing deep subgrade stabilization to a control pavement section that includes a commonly used NCDOT standard subgrade stabilization depth (lime subgrade stabilization of 200 mm (8 inches)). These three pavement sections are shown schematically in Figure 3.1. All three pavement sections used the same materials including the underlying untreated subgrade foundation. The thickness of the subgrade stabilization layer was the main difference between the three sections. The chemical additive type and application rate was the same in all sections. Similarly, the ABC base and top HMA layers were also the same for all three pavement sections in Figure 3.1.

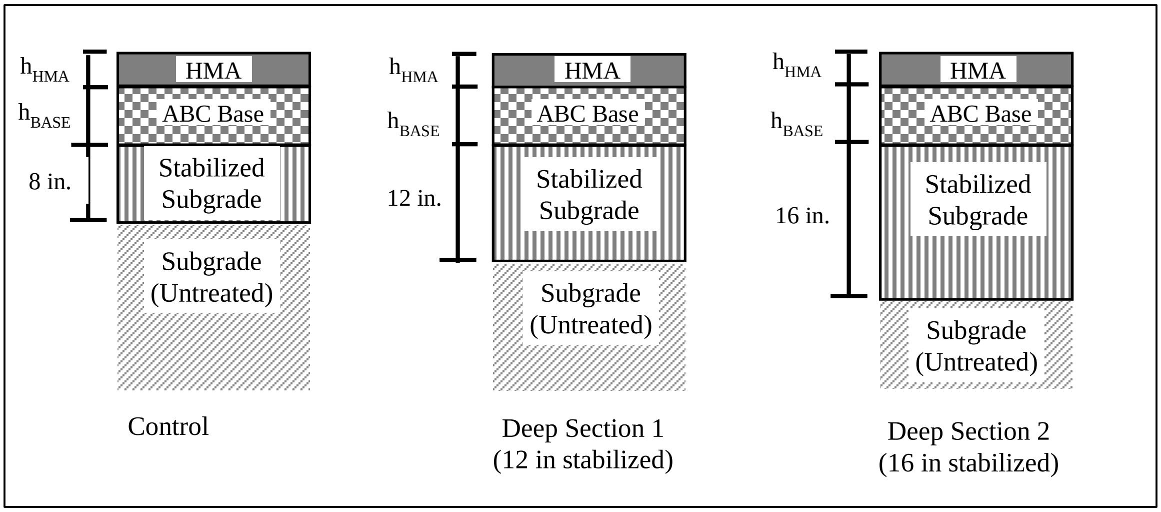

Figure 3.1 Schematic illustrating the 3 pavement sections considered in this study

The main approach used to assess equivalency was based on computing the number of axle-load applications to reach a certain failure state (N_f). This number of axle-load applications (N_f) was computed for the three sections shown in Figure 3.1 but varying the thicknesses of the HMA layer (h_{HMA}). The relationship between N_f and HMA thickness (h_{HMA}) was obtained for the three sections for a failure condition. This type of relationship is shown schematically in Figure 3.2. This figure is generated using a current distress prediction equation (number of axle-load repetitions (N_f)) but with pavement responses estimated using two main methods as described later in this chapter. For example, if we assume the control pavement section containing NCDOT standard subgrade stabilization depth is to achieve a prescribed failure condition in 6 x 10^6 axle-load repetitions the equivalent HMA thicknesses for the 3 sections would be 180, 172, and 165 mm (7.09, 6.85, and 6.60 in.) for the Control, Deep Section 1, and Deep Section 2 pavement sections, respectively. This difference in HMA thickness can be used for performance comparison purposes. Further details are presented later in the chapter.

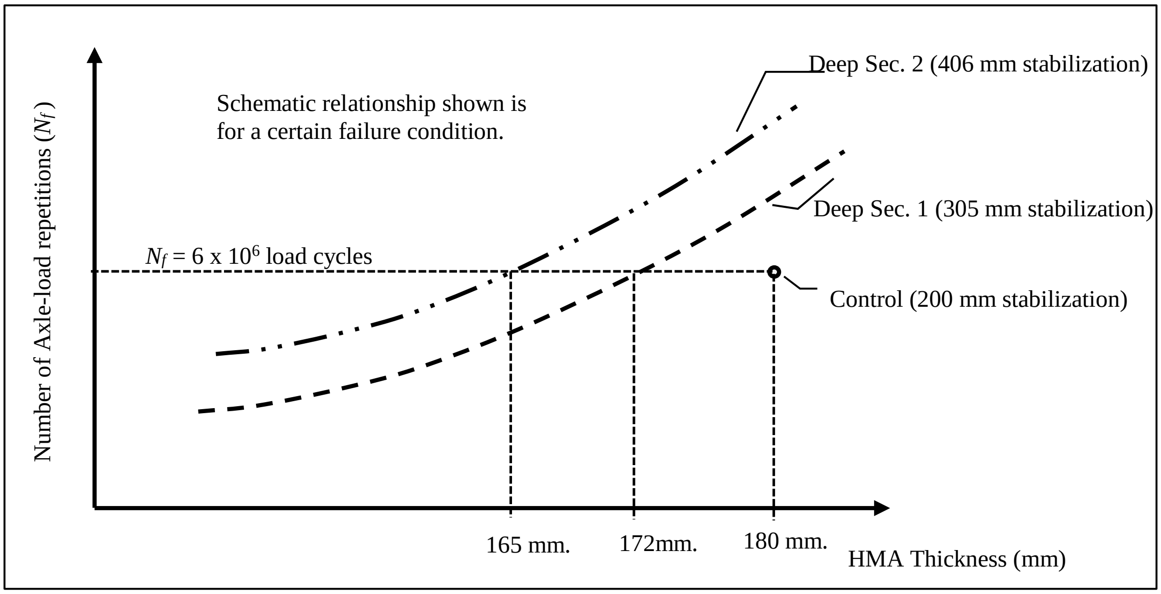

Figure 3.2 Schematic showing equivalency framework used in this study

3.3 Background on Material and Pavement Analyses Tools Used

3.3.1 Definitions Related to Pavement Sections Considered

In this study, 4-layer flexible pavement systems were considered as previously shown in Figure 3.1. Each section had a hot-mix asphalt (HMA) layer at the top, followed by an aggregate base layer, underlain by a stabilized subgrade (subbase layer), and the untreated subgrade layer was located at the bottom of the pavement structure. Obviously, materials of a pavement structure are not homogenous, thus possess diverse engineering properties and to appropriately predict their characteristic responses requires different material mechanical models. In the following subsections, the materials of a pavement structure are discussed and applicable mechanical models for characterizing their responses are presented.

3.3.1.1 Hot Mix Asphalt (HMA)

HMA is a time, temperature, and stress dependent material. At low temperature and high loading frequency it behaves more like elastic material whereas at high temperature and low loading frequency their response is more viscous. An asphalt concrete mixture exhibits elastic, plastic, visco-elastic, and visco-plastic response under repetitive loading (Perl et al. 1983; Uzan 2005; Uzan and Levenberg 2007). To simplify the complicated material behavior of HMA, many researchers have successfully applied the theory of linear viscoelasticity (LVE) to describe the behavior of HMA (Applied Research Associates, ARA 2004). The following sections provide a brief overview of linear viscoelasticity and the associated material parameters.

a. Linear Viscoelasticity

Linear viscoelastic theory is used to model time-dependent material behavior which is applicable to predict HMA behavior under small strains. Under the application of load, resistance to shear flow is the definitive characteristic of viscous material (Yun, 2008). The longer the loading time is, the larger the deformation of viscoelastic material. Moreover, temperature variation during the year significantly influences the resilient modulus of HMA layer which in turn affects the stress-strain response. In summary, viscoelastic material exhibits time and temperature dependent behavior.

Typical constitutive relationship between stress and strain for linear viscoelastic materials is given by Equation 3.1 and 3.2.

$$\sigma = \int_0^t E(t-\tau)\frac{d\varepsilon}{d\tau}d\tau \tag{3.1}$$

and

$$\varepsilon = \int_0^t D(t-\tau)\frac{d\sigma}{d\tau}d\tau \tag{3.2}$$

Where:

$E(t)$ = relaxation modulus;

$D(t)$ = creep compliance; and,

τ = integration variable.

For a particular temperature, within linear viscoelastic range, $E(t)$ and $D(t)$ are functions of time alone. $E(t)$ and $D(t)$ are also referred to as unit response functions. These responses are determined by performing experiments in linear viscoelastic range. The unit response functions, $E(t)$ and $D(t)$ are not easy to obtain experimentally in time domain. The long loading time needed to determine time dependent material properties may damage the specimen during the experiment and lead to erroneous results. Also, in time domain, it is difficult to obtain relaxation modulus or creep compliance of the material at short loading times. Therefore, the complex modulus (E^*) modeling of HMA is commonly used to derive the important parameters required to study the behavior of a linear viscoelastic material in frequency domain.

b. Complex Modulus, Dynamic Modulus and Phase Angle

Complex modulus (E^*) is obtained when viscoelastic material is subjected to sinusoidal loading in the frequency domain. Mathematically, complex modulus is defined as the ratio of amplitude of sinusoidal stress at any given time and frequency, to amplitude of sinusoidal strain at the same time and frequency (Liao, 2007).

Complex modulus consists of two parts: storage modulus (E') representing elastic part, and loss modulus (E'') representing the viscous part. In complex number, E^* is denoted as:

$$E^* = E' + iE'' \tag{3.3}$$

This can also be represented graphically as shown in Figure 3.3.

The dynamic modulus is the absolute value of the complex modulus, defined as the ratio of peak stress to peak strain.

$$\text{Dynamic modulus, } \left|E^*\right| = \frac{\sigma_0}{\varepsilon_0} \tag{3.4}$$

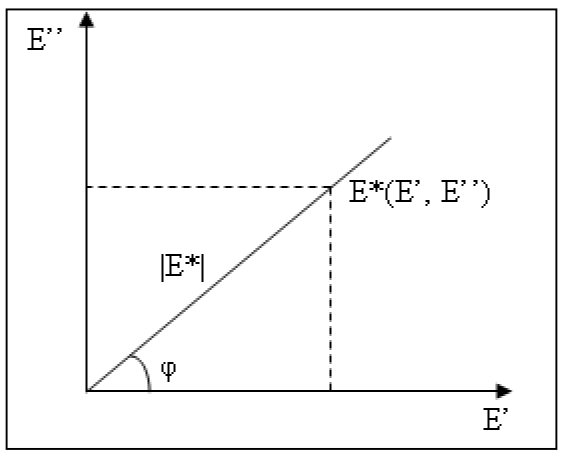

Figure 3.3 Graphical representation of Complex Modulus

Due to the nature of viscoelastic materials, there is a time lag between sinusoidal stress and sinusoidal strain, referred to as phase angle (φ). Figure 3.3 depicts that a material is purely elastic if $\varphi=0^0$, and the material response is purely viscous if $\varphi=90^0$. Between these extremes, material becomes more and more viscous with increase in phase angle. Therefore, the storage modulus (E') and loss modulus (E'') are interdependent. This interdependency is achieved with the master curve if one of the quantity must be known. In MEPDG, the dynamic modulus values at different frequencies are used to develop the master curve. To define viscoelastic behavior of material, dynamic modulus test is performed at different loading frequencies and temperatures. Generally, to obtain time or frequency dependent properties of linear viscoelastic material, time-temperature superposition (t-TS) principle can be used.

c. Time-Temperature Superposition Principle for Linear Viscoelastic Materials

Materials using t-TS principle are also referred to as thermorheologically-simple materials. According to t-TS principle, the response of linear viscoelastic materials at high temperature is identical to that of low loading frequency, and behavior of material at low temperature is similar to that of high loading frequency. The significance of using this principle in laboratory testing is that long time behavior of material a can be predicted by its behavior at high temperature. Also, material response at low temperature can be found out by performing experiments at high loading frequency. This helps to reduce the testing time significantly by performing experiments only for a narrow range of loading frequencies and temperatures (Liao, 2007).

The time-temperature superposition principle helps to combine effect of time and temperature into a single parameter, called reduced time or frequency (Equation 3.5). A single master curve is obtained by shifting dynamic modulus data of material obtained at different temperatures to a reference temperature. The horizontal distance required to superimpose a curve to reference temperature is log of time-temperature shift factor (α_T) (Equation 3.6). A single master curve representing dynamic modulus at different temperatures and frequency is a function of sigmoidal coefficients and reduced frequency as given in Equation 3.7.

The reduced frequency is given by,

$$f_R = f \times a_T \tag{3.5}$$

Where

f_R = reduced frequency in Hz;

f = frequency in Hz; and,

a_T = time-temperature shift factor that can be computed as follows:

$$\log a_T = \alpha_1 T^2 + \alpha_2 T + \alpha_3 \tag{3.6}$$

Where:

$\alpha_1, \alpha_2,$ and α_3 = shift function coefficients; and,

T = temperature.

From the above discussions, the dynamic modulus can be computed using the following expression:

$$\left|E^*\right| = a + \frac{b}{1 + \frac{1}{\exp^{d+e(\log f_R)}}} \tag{3.7}$$

Where,

$a, b, d,$ and ℓ = sigmoidal coefficients;

A typical master curve and time-temperature shift factor function is presented in Figures 3.4 and 3.5, respectively.

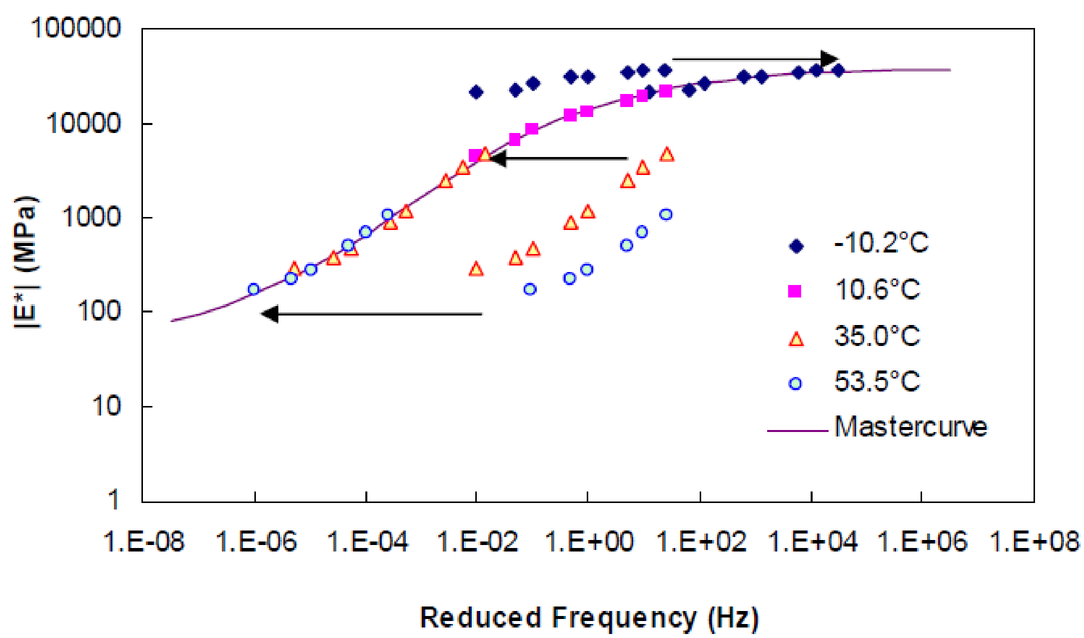

Figure 3.4 Dynamic Modulus Mastercurve (ref. temperature of 10°C) (Yun, 2008)

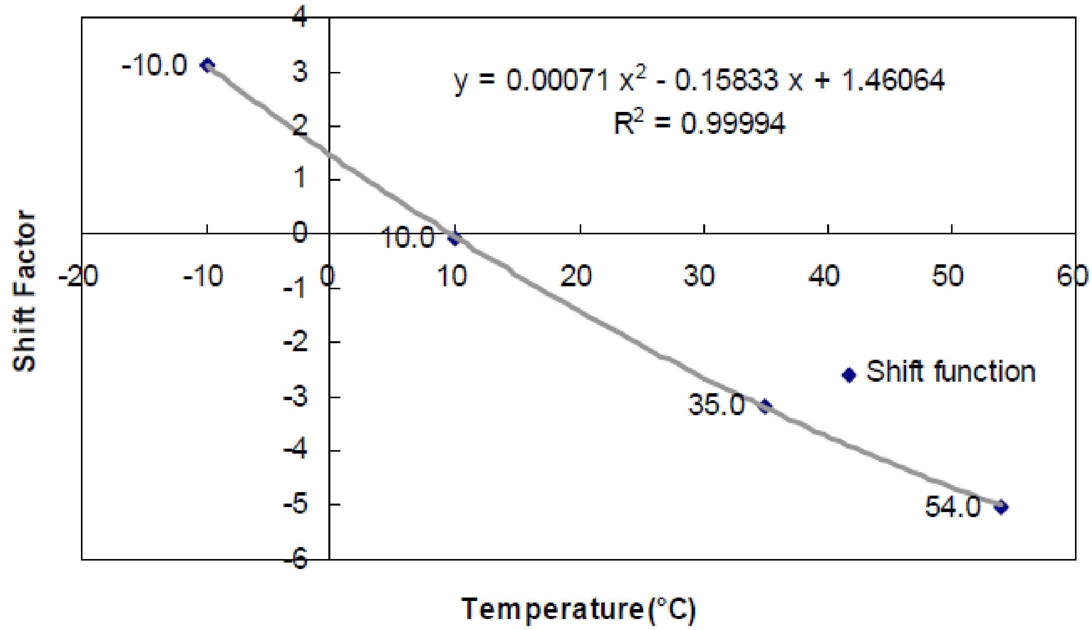

Figure 3.5 Shift Factor Function (reference temperature of 10°C) (Yun, 2008)

Similar mastercurves and shift factors were developed by Kim et al. (2005) for typical North Carolina asphalt concrete mixes. The data from Kim et al. (2005) were used to estimate the linear viscoelastic parameters of the asphalt concrete mixes used in the Abaqus finite element numerical modeling of this project. Detail of the Abaqus FE numerical model used to determine pavement responses is presented in Appendix A.

3.3.1.2 Aggregate Base, Stabilized Subbase and Subgrade Soil Characterization

The aggregate base and subgrade soils are typically unbound granular materials and therefore, do not behave linear elastically under repetitive vehicular loading. Many research studies have documented the behavior of aggregate material and subgrade soil as being non-linear and stress dependent behavior under dynamic loading (Uzan 1985; and Sweere 1990). Generally, unbound aggregates and sometime bound stabilized fine-grained soils used in base and subbase layers, respectively, exhibit non-linear stress-hardening behavior. In contrast, unbound fine-grained subgrade soils can exhibit a non-linear stress-softening behavior (Tutumluer and Kim, 2006). The mechanical behavior and properties of unbound granular materials are significantly affected by their stress state.

Though the response of granular and lightly bound soils is known to be more complex and poorly understood, within the mechanistic-empirical pavement design guide (MEPDG) model (NCHRP 1-37A, 2004) it is conveniently characterized by recoverable (resilient) and plastic strains. The resilient modulus (M_R), is defined as the elastic modulus based on the recoverable strain under repeated loads which can be expressed mathematically as follows:

$$M_R = \sigma_d / \varepsilon_R \tag{3.8}$$

Where,

σ_d = the deviatoric stress; and,

ε_R = the recoverable strain.

In resilient modulus tests, a soil specimen is subjected to dynamic loading in a way which is similar to vehicular loading experienced by the pavement. Specifically, the test uses a haversine stress pulse with a 0.1 second of loading followed by a 0.9 second of unloading which is applied on a soil specimen in order to simulate moving loads. The test is performed at different confining and deviatoric stress levels to simulate different depth within the pavement structure and also different levels of traffic loads.

In standard resilient modulus tests, a static confining stress is applied on a specimen using triaxial pressure chamber; and fixed count of pulsed axial deviator stress is applied though an actuator. The vertical and lateral displacement is measured with the help of sensors attached on the specimen. With the help of laboratory test results, mathematical models have been developed relating resilient modulus as a function of one or more stress variables. A more general expression for resilient modulus as a function of stress state is given below.

$$M_R = K_1 \left[f(\sigma) \right]^{K_2} \tag{3.9}$$

Where,

K_1, K_2 = regression coefficients obtained from laboratory tests; and

σ = applied stress.

Hicks and Monismith (1971) proposed a model known as the K-θ model to capture non-linear stress dependent behavior of granular materials. The authors expressed the resilient modulus as a function of the bulk modulus as follows:

$$M_R = K_1(\theta)^{K_2} \tag{3.10}$$

Where,

K_1, K_2 = regression values obtained from triaxial test

θ = bulk stress = $\theta = \sigma_1 + \sigma_2 + \sigma_3 = \sigma_1 + 2\sigma_3 = \sigma_d + 3\sigma_3$

Though the K-θ model is widely used for its simplicity, it does not consider the effect of shear behavior sufficiently (Kim, 2007). According to Brown and Pappin (1981), the K-θ model does not take care of volumetric strains, so it is advisable to use the model for a limited stress range when confining pressure is less than deviator stress. Uzan (1985) proposed the following equation to capture this stress dependency of the modulus:

$$M_R = K_1\left(\frac{\theta}{p_0}\right)^{K_2}\left(\frac{\sigma_d}{p_0}\right)^{K_3} \tag{3.11}$$

Where,

θ = bulk stress;

p_0 = unit pressure;

$K_1, K_2,$ and K_3 = regression constants; and,

σ_d = deviator stress.

For MEPDG (NCHRP, 2004), the resilient modulus is determined using a more generalized constitutive equation that combines both the hardening effect of the bulk stress and the softening effect of the shear stress level (See Eq. 3.12). An increase in bulk stress θ produces a stiffening effect, thus the exponent k2 corresponding to bulk stress term should be positive, while the exponent k3 of shear stress term should be negative as it describes softening behavior (Kim, 2007).

$$M_R = k_1 p_a \left(\frac{\theta}{p_a}\right)^{k_2} \left(\frac{\tau_{oct}}{p_a}+1\right)^{k_3} \tag{3.12}$$

Where,

θ = bulk stress = $\sigma_1+\sigma_2+\sigma_3$;

σ_1 = major principal stress;

σ_2 = σ_3 for resilient modulus test on cylindrical specimen;

σ_3 = minor principal stress;

$\tau_{oct} = \frac{1}{3}\sqrt{(\sigma_1-\sigma_2)^2+(\sigma_1-\sigma_3)^2+(\sigma_2-\sigma_3)^2}$ octahedral shear stress;

p_a = atmospheric pressure; and,

$k_1, k_2,$ and k_3 = regression constants.

NCDOT currently analyzes resilient modulus tests using a form of the K-θ model presented in Equation 3.13 to capture the stress dependency of the parameter.

$$M_R = K_1(\sigma_c)^{K_2}(\sigma_d)^{K_5} \tag{3.13}$$

Where,

σ_c = σ_3 confining pressure;

σ_d = $\sigma_1-\sigma_3$ deviator stress (cyclic stress); and,

k_1, k_2, and k_5 = regression constants.

In Chapter 4, resilient modulus tests of some representative samples of the stabilized subgrade and untreated subgrade were conducted for the lime test sections at the NCDOT materials laboratory in Raleigh, NC. The results were evaluated using Equation 3.13 in accordance with NCDOT practices. For the aggregate base material used in this study, no laboratory experimental tests were conducted to measure its engineering properties. However, the modulus values of the base, stabilized subgrade and the untreated subgrade layers were measured non-destructively with the Falling Weight Deflectometer (FWD). For the numerical analyses performed in this study did not consider stress sensitive behavior of the base, stabilized subgrade and untreated subgrade layers.

3.4 Numerical Approach Used for the Equivalency Framework

Repetitive vehicle load on pavement surface leads to the development of stresses at different layers of a pavement. Pavement's life is inversely proportional to the amount of distress developed from the responses of these layers to the stresses. Accumulation of the distresses within different layers results in pavement failure. Some of the common asphalt concrete pavement distresses are top-down fatigue cracks, bottom-up fatigue cracks, rutting, and thermal cracks. In this study, bottom-up fatigue cracks and rutting at the subgrade layer are considered for analysis of pavement failure.

Various theories and mathematic models have been proposed to determine stresses, strains and deflections at different layers of a pavement. Two approaches were used in this study: the layered elastic theory and finite element method (FEM). Resulting from layered elastic theory, several software's such as Kenpave, Elsym5, EVERSTESS 5.0, BISAR 3.0 are available to compute stresses, strains and deflections in a pavement system. The theory assumes that each layer is represented as homogeneous, isotropic, linearly elastic solids or the subgrade layer has stress dependent modulus. While a static, uniformly distributed, circular loading is assumed to be applied on pavement surfaces. Also, stress-strain compatibility at all pavement interfaces is assumed. FEM on the other hand is a widely used numerical method for solving engineering problems with complex geometries, loading conditions, and various material properties. The method is useful in analyzing problems for which analytical solution is very hard or impossible to obtain. If the system under analysis is modeled aptly with appropriate material model and, proper loading and boundary conditions were utilized then the FEM results in a solution close to the exact solution. In FEM, the system to be analyzed is divided into number of small elements through a discretization process. Each element is connected directly or indirectly to other elements through common nodes, boundary conditions, or surface interactions (Hua, 2000). Material properties are assigned to each element which are then combined to obtain global equations. Material properties along with boundary conditions describe the behavior of the entire structure. The load is applied on the nodes of elements and by solving the system of simultaneous algebraic equations, nodal displacements are calculated. From nodal displacements, using stress-strain constitutive relationship, moments, shear forces, and stresses are determined. Following which the results are analyzed. When necessary, mesh refinement is done to increase the level of accuracy (Desai, 1979, Loulizi, et al., 2006).

EVESTRESS and ABAQUS are used based on their successful application in previous research studies (Huang, 1995, Liao, 2007, Yoo, 2008) where they have been reported as being used successfully for the analysis of pavements. The following subsections describe in more details these two main software's used for this study.

3.4.1 EVERSTRESS Software

This software was developed by the Washington State Department of Transportation (WSDOT) as an extension to the WESLEA layered elastic analysis software originally developed by the Waterways Experiment Station, U.S. Army Corps of Engineers. EVERSTRESS can analyze pavement structures containing up to five layers and can consider stress sensitive characteristics of unbound pavement materials (Sivaneswaran, et al., 1999). The frictional contact between different layers can be specified as either unbonded or fully bonded. In this study, the version EVESTRESS© 5.0 was used for layered elastic analysis of pavement under a static circular loading.

EVERSTRESS 5.0 is a plane-strain software package that assumes axisymmetric conditions in the lateral directions for simplicity. Plane-strain conditions are assumed and evaluated using the effective radius to model tire loading. EVERSTRESS allows for the user to define up to a 5 layer pavement system. The program allows for up to 20 loads to be applied to the pavement system. The program is limited to 50 evaluation points which translate to 10 loading points consisting of 5 loading points each in x and y directions and 5 evaluation locations in the z direction below each loading. Other limitations to using a plane-strain software like EVERSTRESS, include only circular tire contact areas, and static loading conditions.

3.4.2 Finite Element Analyses using ABAQUS

In this study, the general-purpose finite element program ABAQUS was used for pavement analyses. This selection was based on its successful application in previous pavement research studies (Huang, 1995, Liao, 2007, Yoo, 2008). The specific versions used were Abaqus/CAE 6.10 and 6.11.

3.4.3 Comparison between EVERSTRESS and ABAQUS

A comparative study was conducted between EVERSTRESS© 5.0 and finite element software Abaqus/CAE 6.10 based on elastic theory approach. A single static load was applied on a 4-layer flexible pavement with different thicknesses of lime stabilized subgrade as shown in Figure 3.6.

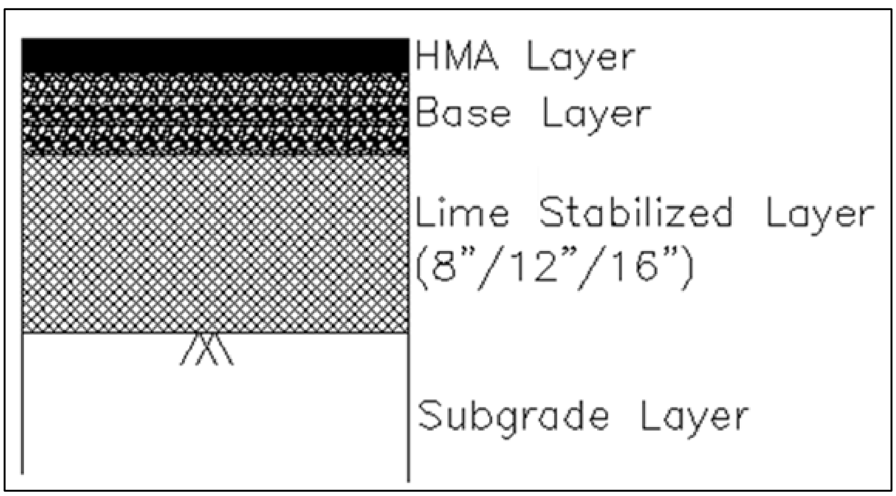

Figure 3.6 Layer Flexible Pavement System used in comparison study

In this comparative study, the lime stabilized subgrade was treated as the structural subbase layer. A tire load of 40.03 kN (9000 Ib) applying a uniform pressure of 689.5 kPa (100 psi) on a circular load area was modeled. The pavement response was calculated for different thicknesses of HMA and stabilized subgrade or subbase layer. The following subsections present material input parameters.

3.4.3.1 Material Data Units

In this analysis, the material properties for all the layers (HMA, base aggregate, stabilized subgrade and untreated subgrade) are assumed to be stress insensitive linear elastic. The values of material properties and thicknesses of the pavement layers used in both EVERSTRESS and Abaqus FE modeling are summarized in Table 3.1.

Table 3.1: Material Properties of Different Layers

Pavement Layer	Thickness, mm (in.)	Density, kg/m^3 (pcf)	Modulus E, MPa (ksi)	ν
HMA	180 (7.09)	2403 (150)	3103 (450)	0.35
Base	200 (8.00)	2082 (130)	207 (30)	0.35
Subbase	200 (8) – 406 (16)	1762 (110)	143.7 (20.84)	0.35
Subgrade	Large - infinite	1682 (105)	14	0.45

Where,

E = modulus of elasticity; and,

ν = Poisson's ratio.

3.4.3.2 Asphalt Pavement System Modeling

The material parameters of layers used for both EVESTRESS and ABAQUS are kept constant and equal to the values presented in Table 3.1. The thicknesses of the surface (HMA) and stabilized subgrade (subbase) layers are varied from 165 mm to 180 mm (6.50 inches to 7.10 inches), and from 200 mm to 400 mm (8 in. to 16 in.), respectively. The thicknesses of the base and subgrade layers are maintained constant at 200 mm (8 in.) and infinite (assumed), respectively in both methods.

The 3-D finite element model developed using ABAQUS/CAE 6.11 has dimensions 2720 mm by 2720 mm (107 in. by 107 in.). The side boundary of the model is approximately 20 times the tire radius in order to minimize edge effects. The subgrade layer, which implicitly is assumed to be infinite, is modeled in ABAQUS to be 3800 mm

(150 in.) thick, which is almost 5 times the cumulative thickness of the overlaying pavement structure (surface, base and subbase layers). As the loading is axisymmetric and pavement model is symmetric about X and Y-axis, only one-quarter of the pavement cross-sections are modeled to reduce the computational time required to run the analysis as well as memory storage needed for the analysis.

The boundary conditions at the bottom of subgrade is fixed, i.e. its motion is constrained horizontally as well as vertically. Also, the horizontal displacement perpendicular to boundaries of the pavement model and along the line of symmetry is constrained. The pavement layer interfaces are tied to each other in order to maintain the same interaction condition as EVERSTRESS. The model is discretized with 8-node linear brick reduced integration elements (C3D8R). The FE mesh includes fine mesh near the loading area where the stress gradient is high and coarse mesh away from it. The FE model is presented in Figure 3.7.

The response to be analyzed is tensile strain at the bottom of HMA layer and vertical compressive strain at the top of subgrade layer causing fatigue and rutting failure respectively. Distribution of tensile strain and vertical displacement at different layers of pavement are shown in Figure 3.8 and 3.9, respectively. It is seen that under the application of static, uniform load the maximum tensile strain in HMA layer is at the bottom, and the maximum compressive strain is at the top; while vertical displacement decreases along the depth of a pavement. In the subgrade, maximum vertical displacement is observed at the top and under the center of loading area.

Some values of the critical responses - tensile strains at the bottom of the HMA and vertical strain at the top of the subgrade layers - determined by ABAQUS and EVERSTRESS are presented in Table 3.2. From Tables 3.2(a) and 3.2(b), it can be observed that the values of tensile strains at the bottom of HMA layers are not significantly difference, it appears that the values decrease with increase in subbase layer thickness. As pavement layers are tied to each other, increase in subbase thickness increases the strength of the pavement structure which consequently contributes to strain reduction at the bottom of HMA layer.

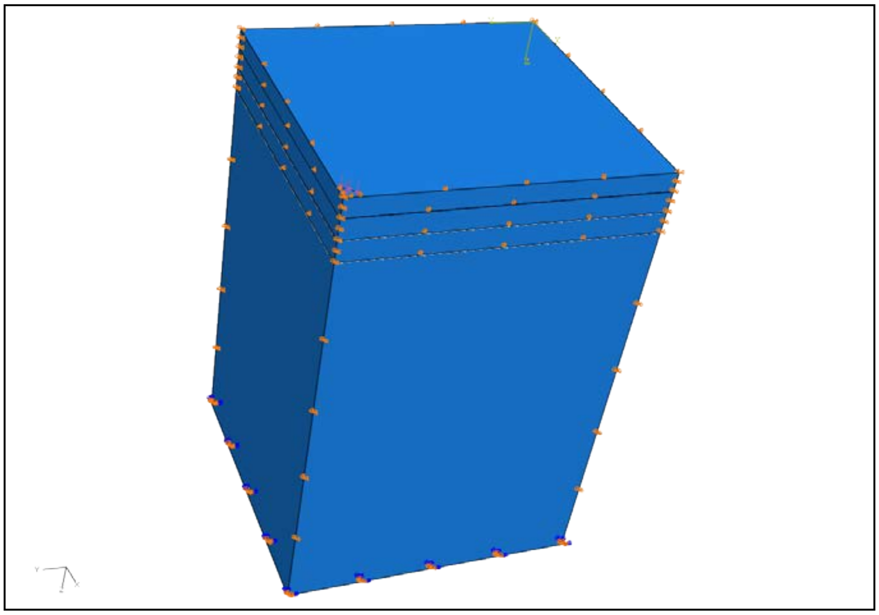

Figure 3.7 FE Model of 4-Layer Flexible Pavement

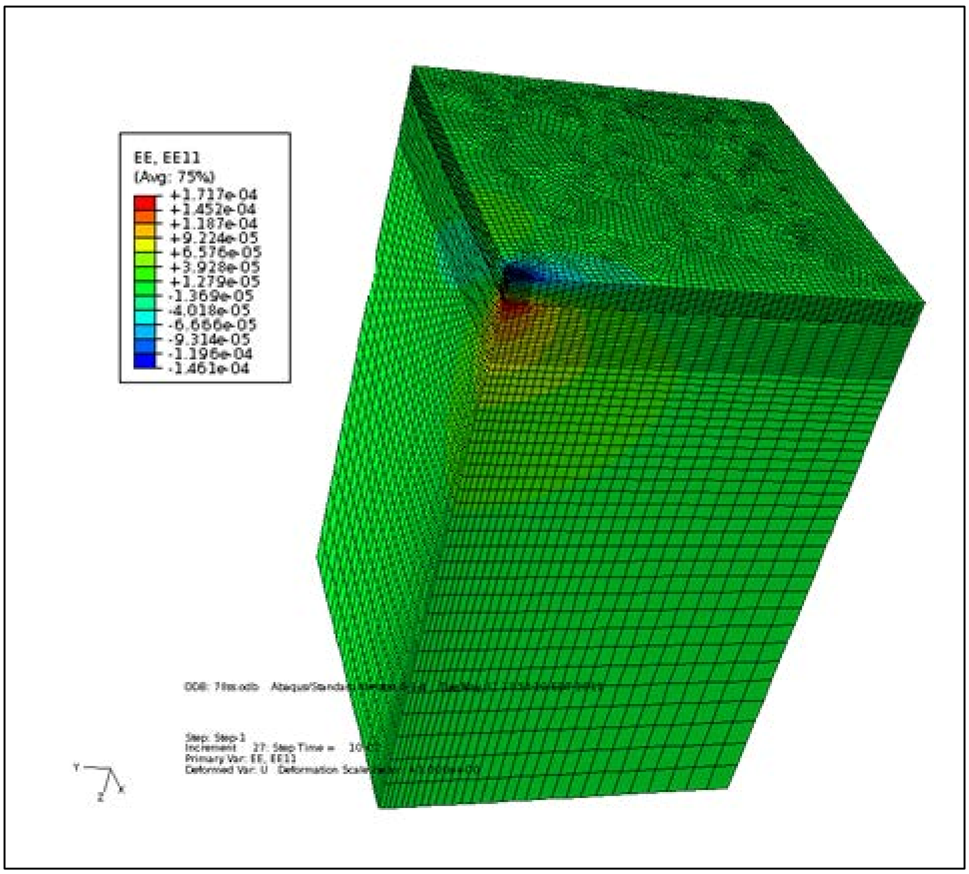

Figure 3.8 Variation of Tensile Strain (FE11) in Pavement System

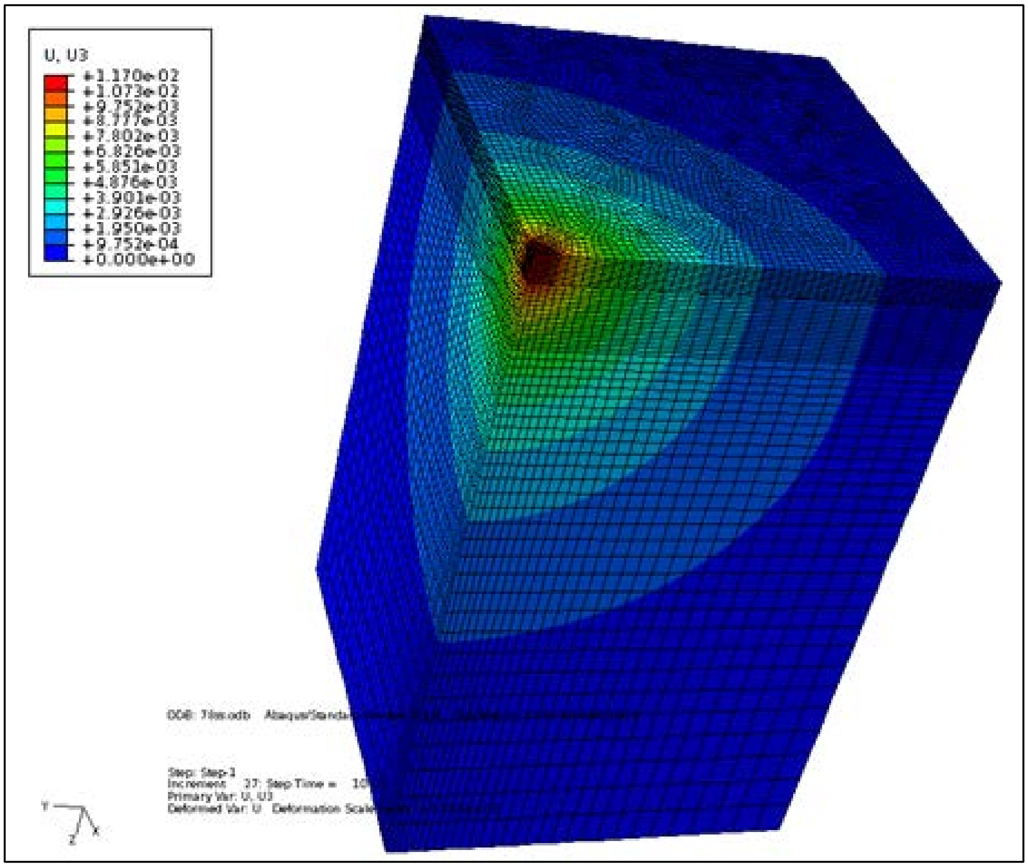

Figure 3.9 Variation of Vertical Displacement (U3) in Pacement System

Table 3.2: Comparison of Tensile Strains at the Bottom of HMA Layer

(a) EVERSTRESS

HMA (in)	Stabilized Layer Thickness (in)		
	8	12	16
7.09	2.066E-04	2.043E-04	2.027E-04
6.75	2.191E-04	2.166E-04	2.150E-04
6.5	2.289E-04	2.263E-04	2.246E-04

(b) ABAQUS

HMA (in)	Stabilized Layer Thickness (in)		
	8	12	16
7.09	1.616E-04	1.605E-04	1.598E-04
6.75	1.718E-04	1.706E-04	1.699E-04
6.5	1.798E-04	1.786E-04	1.779E-04

Strain values obtained from EVERSTRESS are observed to be greater than those from ABAQUS. For subbase and subgrade, EVERSTRESS determines stress compatible moduli iteratively, which is far lower than the moduli obtained from the resilient modulus tests; whereas ABAQUS assumes constant modulus outside the limiting data. As layer interfaces are fully bonded to each other, decrease in modulus reduces the strength of the entire pavement structure. Therefore, strain calculated from EVERSTRESS is greater than that obtained from ABAQUS. It is observed that tensile strain calculated by EVERSTRESS is approximately 27% higher than from ABAQUS.

3.4.4 Equivalency Framework for Predicting Pavement Distress/Failure

Pavement distress/failure will provide the relationship between the critical pavement response and the allowable number of load applications before failure (Wang and Al-Qadi, 2011). Two types of failure modes that occur in a pavement system are rutting and fatigue cracking. Pavement damage models used in predicting failure in pavement systems are empirical-mechanistic models that calculate the deformation and fatigue cracking in the pavement systems (AASHTO, 2008). The results obtained from this analysis will be used to determine the performance of the pavement under heavy loading conditions.

3.4.4.1 Number of Load Repetitions (Nf) related cracking of HMA layer

Alligator cracking and longitudinal cracking are two types of wheel load related cracking in HMA pavement systems. According to AASHTO (2008), alligator cracking initiates at the bottom of the HMA layer and then propagate to the surface of the pavement as a result of cumulative increase in traffic loads, while longitudinal cracks initiate at the surface of the HMA and propagate to the bottom of the layer. These two types of fatigue cracking can be referred to as bottom-up and top-bottom failures. The general formula used here to predict load related bottom-up cracking (alligator) in HMA according to AASHTO (2008) is as follows:

$$N_{f-HMA} = k_{f1}\,(C)(C_H)\beta_{f1}(\varepsilon_t)^{\beta_{f2}k_{f2}}\,(E_{HMA})^{\beta_{f3}k_{f3}} \qquad (3.14)$$

Where,

N_{f-HMA} = the allowable number of axle-load applications for a flexible pavement and HMA overlays;

ε_t = the tensile strain at critical locations and calculated by the structural response model (in/in);

E_{HMA} = the dynamic modulus of the HMA measured in compression (psi);

$k_{f1}k_{f2}k_{f3}$ = the global field calibration parameters ($k_{f1} = 0.007566$, $k_{f2} = -3.9492$ and $k_{f3} = -1.281$);

$\beta_{f1}\beta_{f1}\beta_{f1}$ = the local or mixture specific field calibration constants (values set to 1.0 for global calibration effort); and,

C = 10^M and C_H is the thickness correction term which is dependent on the type of cracking.

The parameter M, needed to compute the value of C, is estimated using the following expression:

$$M = 4.84\left(\frac{V_{be}}{V_a+V_{be}} - 0.69\right) \tag{3.15}$$

Where,

V_{be} = effective asphalt content by volume (%); and,

V_a = the percent air voids in the HMA mixture.

For this study, the HMA considered had a V_{be} = 13% and a V_a = 4% which corresponds to an HMA surface layer with a 83.3mm (3.28 in.) thickness. The values of V_{be} = 10.8% and V_a = 4%, were used for an HMA intermediate layer of 106.7 mm (4.20 in.) thickness.

Since the analysis here is limited to bottom-up cracking, the thickness correction factor (C_H) is presented in Equation 3.16:

$$C_H = \frac{1}{0.000398 + \frac{0.003602}{1+e^{(11.02-3.49h_{HMA})}}} \tag{3.16}$$

Where,

h_{HMA} = the total HMA thickness in inches.

The number of load repetitions required to cause bottom-up failure was calculated using the above mathematical model (Equations 3.14 -3.16). The estimated values of load repetitions to failure using the strain responses are summarized in Table 3.3 for the three thicknesses of stabilized subgrade considered.

Table 3.3: Number of Load Repetitions for Bottom-Up Fatigue Failure

(a) Everstress Analysis

HMA mm (in)	Stabilized Layer Thickness mm (in)		
	200 (8)	305 (12)	406 (16)
180 (7.09)	7.279E+07	7.608E+07	7.848E+07
171 (6.75)	5.772E+07	6.039E+07	6.219E+07
165 (6.5)	4.856E+07	5.080E+07	5.233E+07

(b) Abaqus FE Models

HMA mm (in)	Stabilized Layer Thickness mm (in)		
	200 (8)	305 (12)	406 (16)
180 (7.09)	1.920E+08	1.973E+08	2.007E+08
171 (6.75)	1.508E+08	1.550E+08	1.576E+08
165 (6.5)	1.260E+08	1.294E+08	1.314E+08

3.4.4.2 Estimating Equivalent HMA Thicknesses of the Deep Subgrade Stabilization Layers

Considering that the load-related fatigue failures are more conservative and produce lower percentage increase in load repetitions with increase in deep subgrade stabilized layer thickness, the equivalent HMA thicknesses of deep subgrade stabilization layers are limited to bottom-up fatigue failure. The predicted load repetitions to failure (Nf) of the HMA thicknesses for the control (NCDOT standard) and deep subgrade stabilization layers are plotted against the HMA thicknesses (Figures 3.10 and 3.11). The best fit lines for the trends produced an exponential relationship as a function of the HMA thickness, as presented in Equation 3.17:

$$N_f = k_1 \exp(k_2 h_{HMA}) \tag{3.17}$$

Where,

k_1 and k_2 = best fit constants, with the corresponding constant values for each subgrade stabilization layer presented in Table 3.4.

Table 3.4: Constant of the Best Fit Exponential Relationship for the N_f Values

Stabilization Layer Thickness (inches)	Constant Values			
	EVERSTRESS		ABAQUS	
	k_1	k_2	k_1	k_2
8	5.63E+05	0.6859	1.22E+06	0.7141
12	5.95E+05	0.6842	1.24E+06	0.7145
16	6.04E+05	0.6866	1.24E+06	0.7178

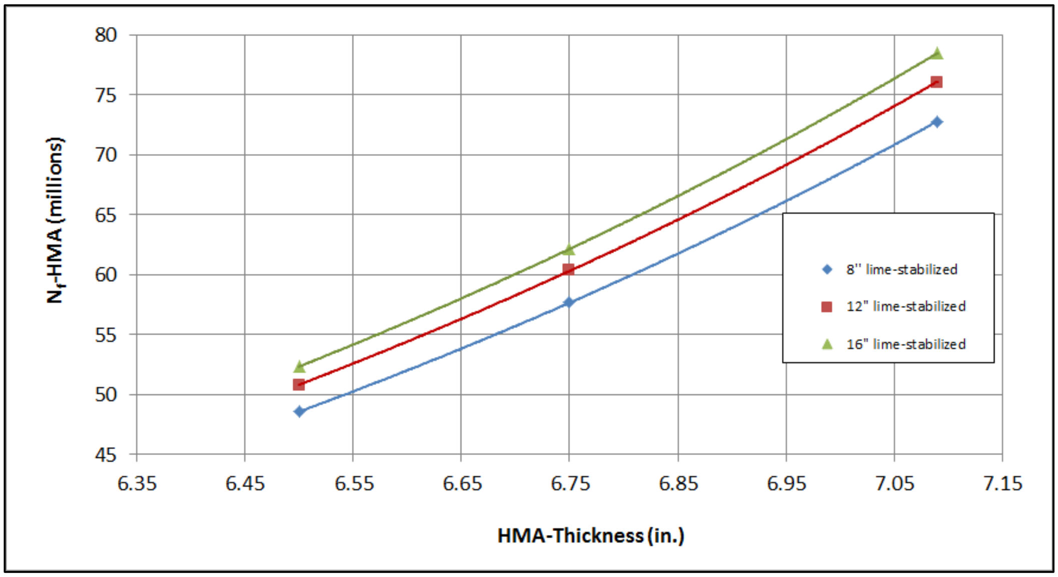

Figure 3.10 Load Repetition for Bottom-Up Cracking versus HMA thickness for Different Subgrade Stabilization Layers (EVESTRESS predicted strain responses)

Since the controlling number of load repetitions to failure is governed by the standard NCDOT pavement section (including 8 inches of stabilized subgrade layer and 7.09 inches of HMA), the HMA thickness of deep subgrade stabilization resulting in the same load repetitions to failure is estimated and presented in Table 3.5 as the equivalent pavement section.

This approach provides a framework for estimating the equivalent HMA thicknesses for the deep subgrade stabilization layer based on a selected type of failure mode. A more global approach involves using a combined damaged ratio to estimate overall performance of each pavement section. However, significant laboratory and field data beyond the scope of this project is required to achieve this

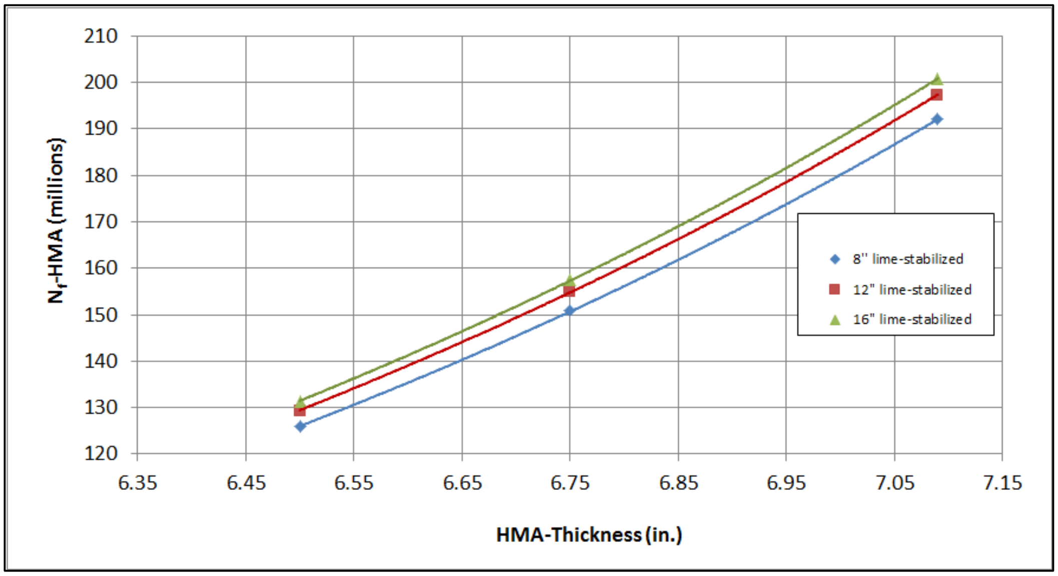

Figure 3.11 Load Repetition for Bottom-Up Cracking versus HMA thickness for Different Subgrade Stabilization Layers (ABAQUS predicted strain responses)

Table 3.5: Equivalent Pavement Sections in HMA Thickness (inches)

Stabilization Layer Thickness (inches)	Response Model	
	EVERSTRESS	ABAQUS
8	7.09	7.09
12	7.02	7.05
16	6.98	7.03

3.4.4.3 Limitations of EVERSTRESS and ABAQUS F.E. Elastic Model

In practice, the layered elastic analysis approach is a simplified approach for pavement analysis. The pavement response is dependent on many factors such as vehicle speed, material properties of different layers, and surrounding temperature. FE method gives more accurate results than layered elastic analysis by simulating dynamic loading conditions, providing non-linear material properties, and defining infinite number of boundary conditions (Logan, 1992). Also, from literature review, it is verified that FE analysis is more rigorous and gives better approximation of field measured data. The major drawbacks of layered elastic theory are summarized below:

(1) It assumes material behavior as linearly elastic. In reality, in flexible pavements, the hot-mix asphalt (HMA) layer behaves visco-elastically. A viscoelastic material possesses both the elastic property of a solid and the viscous behavior of a liquid depending on the operating temperature and loading rate.

(2) Vehicle loading is assumed to be static, circular and uniformly distributed but in reality, the loading is dynamic, non-circular with varying pressure.

(3) Effects of vehicle speed and environmental factors such as temperature have not taken into consideration. According to Loulizi et al. (2006), layered elastic theory overpredicts pavement responses to vehicular loading at low and intermediate temperatures whereas it underestimates pavement responses at high temperatures.

(4) Assumes material to be weightless neglecting inertia effect which affects pavement response.

3.5 Summary of Chapter

In this chapter, the approach used for estimating equivalent section for pavement having deep subgrade stabilization was presented. The controlling factor is the load repetitions to failure of control pavement section containing NCDOT standard subgrade stabilization depth. From the results of the example presented in Table 3.5 in Section 3.4.4 above, the HMA thickness required to achieve equivalent section reduces as the thickness of stabilized subgrade increases. Though HMA thickness reduction is small, it should be noted that this analysis is based on elastic model and material properties. We have demonstrated that HMA and pavement geomaterials exhibit nonlinear behaviors. For the performance analysis in Chapter 6, a more rigorous numerical model of viscoelastic FE model of asphalt pavement under moving wheel load was implemented. The details of the FE implementation in Abaqus including viscoelastic material properties, pavement layer interaction, and loading method are presented in Appendix A.2. The results of the numerical model were validated using data from field measurement. The model response predictions closely match the field measure values.

CHAPTER 4 LABORATORY CHARACTERIZATION AND GEOTECHNICAL TESTING OF TEST SITE SOIL

4.1 Project Site Selection and Soil Sampling

4.1.1 Project Site and Test Section Layout

The project site is located on the NC Highway 16 Bypass near Denver in Lincoln County, North Carolina. This location is part of the NCDOT TIP R-2206CA project. The constructed test sections begin approximately one mile north of the intersection of NC-150 in the right-hand on northbound lane starting at about latitude 35.569125°N and longitude 81.076938°W and ending at about latitude 35.577383°N and longitude 81.074657°W. Figure 4.1a presents an aerial view of the site indicating the location and close proximity of the two, constructed test sections. The lime stabilized section is between stations 246+07 & 256+64, while the cement-section is between stations 257+17 & 266+90 (Figure 4.1b).

This site was chosen because it provides adequate length to build several test sections of over 200 m in length and for the proximity of both lime and cement sections which ensure the test sections will be subjected to equivalent traffic loads and acceptable local climatic/environmental conditions.

4.1.2 Soil Sampling

The goal is to collect sufficient disturbed and undisturbed samples to well characterize the subgrade and the stabilized layer of the test sections. Cognizant of the fact that the road stations of the constructed test sections might differ from the proposed stations, the test sections were subdivided into approximately 53 m (175 ft) sampling intervals. Sampling plan and procedure was submitted to NCDOT prior to commerce sampling. The sample collection process started with marking and staking out sampling stations prior to collecting the soil. Soil samples were collected from the midpoint of each subsection with the stations of the sampling locations duly recorded.

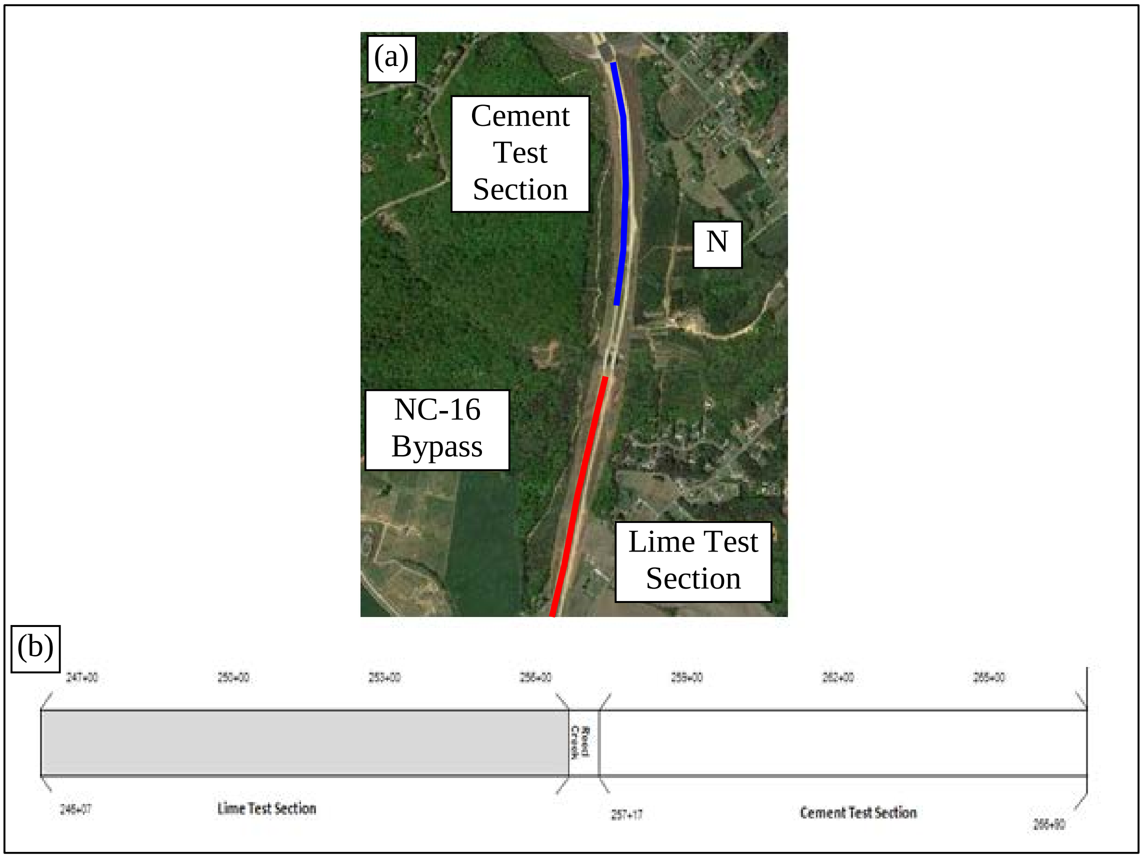

Figure 4.1 (a) Aerial view of NC-16 project site, (b) Test sites layout along the North Bound lane of the NC-16 (TIP R-2206CA)

Disturbed soil samples were collected from the stabilization layer, while both undisturbed and disturbed soil samples were collected from the subgrade layer. The disturbed samples were collected with the assistance of the contractor while NCDOT drilling team from NCDOT geotechnical unit from Harrisburg, NC collected the undisturbed samples. Each stabilized layer sample was collected within the depth ranges corresponding to the test section’s stabilized layer thickness; the subgrade samples were collected at depth below the proposed stabilized layers. The two undisturbed samples collected from each sampling location were sealed in the Shelby tubes with wax at both ends and then packed in specially constructed holders to minimize handling issues during transportation to UNC Charlotte (Figure II.2). A total of 64 30-gallon drums of disturbed soil samples (32 drums from lime stabilization section of which 16 from the stabilized layer and subgrade; and similarly 32 drums from cement stabilization section) and 59 Shelby tubes of undisturbed samples (30 samples from subgrade of lime section and 29 from the cement section).

Figure 4.2 Waxing Shelby tube samples in the holder device

Micaceous clays were observed in the field during soil sampling particularly in the lime stabilized section. The distinct flakes of mica were evident throughout the section. The site is mainly composed of saprolitic soils. The in-situ soils clearly exhibit the granitic texture and fabric of the of parent rock. Although the subgrade layer of the site is Piedmont residual soil, there were evidences of pockets of mixture sandy soils in the soils within the stabilized layers. Also, locations with sand pockets in the subgrade presented sample recovery problem during undisturbed sampling. When sample recovery problems were encountered, a plunger tube was used to attempt a whole collection. This approach worked in some locations; while others locations were too sandy to obtain a sample, therefore instead of 64 shelby tubes of undisturbed samples only 59 samples were successfully collected.

4.2 Laboratory Characterization of Lime Test Site Soils

Index and engineering properties of soil samples collected from the stabilized subgrade layer (subbase layer) and subgrade layer were performed, with the exception of resilient modulus, in the Geotechnical Research Lab at the University of North Carolina at Charlotte. The Resilient Modulus tests were performed at the NC DOT Materials Testing Unit in Raleigh, North Carolina. Soil samples collected at one selected location from each test section were treated with chemical additives and tested for their geotechnical properties. For convenience and coherence, the result of laboratory experiments will be presented and treated separately under lime stabilized and cement stabilized test sections.

4.2.1 Laboratory Test of Lime Section Soils

Illustration of the lime test sections, the start and end of the as-built stations of each test section and the sample locations (G, H, N and O) of soils treated with chemical lime additives in the laboratory are presented in Figure 4.3. Samples collected at test location G fall within the lime stabilized test section 1 (the approach 8-inch standard depth lime stabilized subgrade "control" test section), location H falls within the lime stabilized test section 2 (12 inch-deep lime stabilized subgrade test section), location N is within the lime stabilized test section 3 (16 inch-deep lime stabilized subgrade test section), and location O lays within the lime stabilized test section 4 (the exiting 8-inch standard deep lime stabilized subgrade "control" test section).

4.2.2 Soil Classification

The index properties of the untreated soils within the stabilization and subgrade layer are summarized in Tables 4.1 and 4.2. These tables present key index properties such as percent fines, liquid limit, plastic limit, plasticity index and specific gravity in addition to depth and station of sampling. Each table is followed with the grain size distribution curves of the selected locations for which soil samples were treated in the laboratory with lime additives and engineering properties determined (Figures 4.4 and 4.5). Classifications based on the Unified Soil Classification System (USCS) and the American Association State Highway and Transportation Officials (AASHTO) are summarized in Table 4.3 for the soils of the stabilized layer and subgrade layer. A majority of the soils can be classified as silty sand (SM) for both layers. Soils at selected sampling locations G, H, and N can be classified as silty sands, while at location O as inorganic silt.

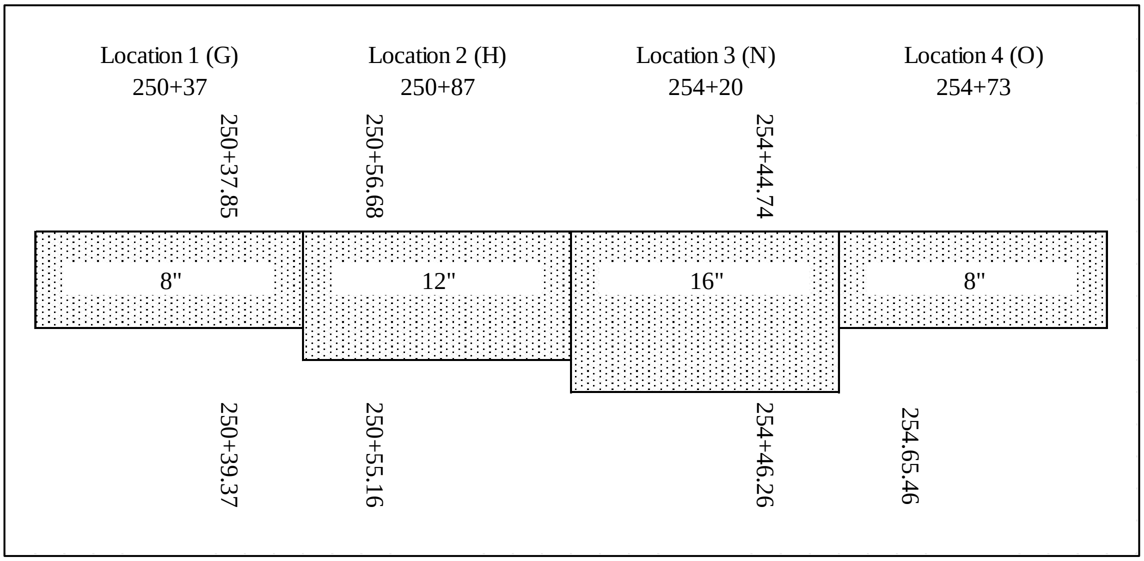

Figure 4.3 Selected lime sampling locations for lab engineering properties tests

Table 4.1: Soil Characterization for Stabilization Layer

Test Section	Sample Location	Station	% Fines	LL	PI	G_S	USCS	AASHTO
Lime 1 (8-inch)	A	247+27	43.37	35	9.2	2.75	**SM**	**A-4**
	B	247+80	36.26	32.5	7.7	2.72	**SM**	**A-4**
	C	248+33	34.54	33.5	3	2.77	**SM**	**A-2-4**
	D	248+87	40.97	31.5	3.6	2.71	**SM**	**A-4**
	E	249+40	57.97	55.5	24.3	2.74	**MH**	**A-7-5**
	F	249+93	37.15	42	6	2.76	**SM**	**A-5**
	G	250+37	35.73	29.5	1.7	2.67	**SM**	**A-2-4**
Lime 2 (12-inch)	H	250+87	48.63	41	4.8	2.71	**SM**	**A-5**
	I	251+53	52.23	40	11.3	2.7	**ML**	**A-6**
	J	252+06	31.07	37.5	10.8	2.72	**SM**	**A-2-4/A-2-6**
Lime 3 (16-inch)	K	252+60	16.6	35	8.3	2.69	**SM**	**A-2-4/A-4**
	L	253+13	50.97	34.5	6.2	2.69	**SC**	**A-4**
	M	253+66	40.86	34.5	10.8	2.7	**SC/SM**	**A-4**
	N	254+20	41.14	39	10.1	2.73	**SM**	**A-4**
Lime 4 (8-inch)	O	254+73	70.05	52	18.3	2.75	**MH**	**A-7-6**
	P	255+26	35.34	37	14.1	2.74	**SC**	**A-2-6**

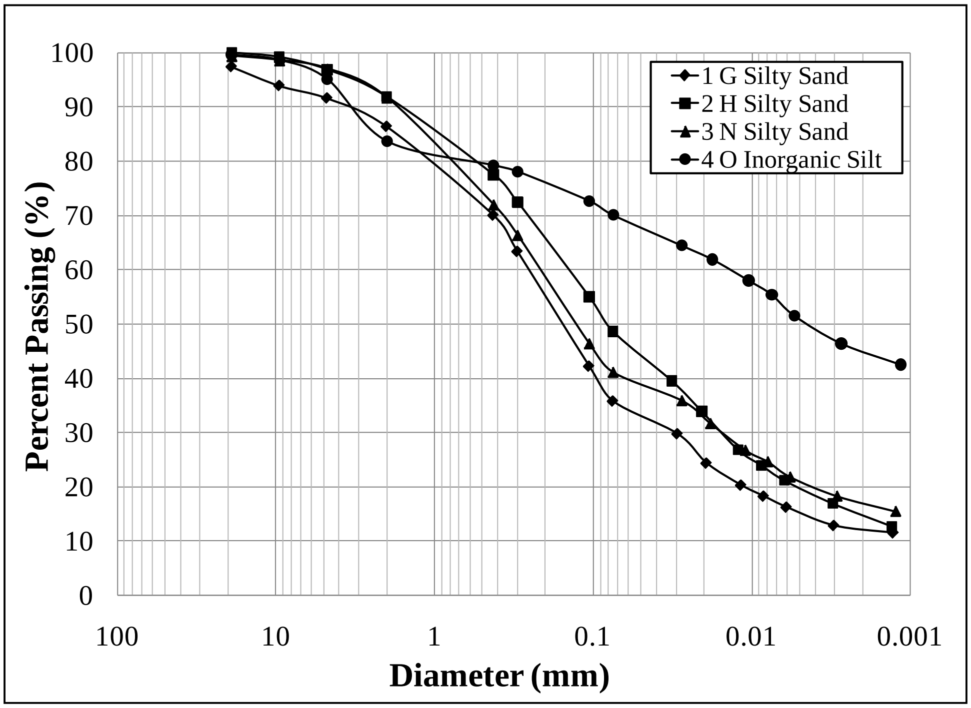

Figure 4.4 Grain size distribution of sampling locations of soils tested in the laboratory treated with lime additives

Table 4.2: Soil Characterization for Subgrade Layer

Test Section	Sample Location	Station	% Fines	LL	PI	G_S	USCS	AASHTO
Lime 1 (8-inch)	A	247+27	45.2	34.5	3.9	2.83	**SM**	**A-4/A-2-4**
	B	247+80	46.19	37.5	9.1	2.82	**SM**	**A-4**
	C	248+33	32.4	31.5	3.2	2.7	**SM**	**A-2-4**
	D	248+87	35.84	31.5	1.3	2.72	**SM**	**A-2-4**
	E	249+40	57.06	52	15.9	2.76	**MH**	**A-7-5**
	F	249+93	60.33	45	0.6	2.78	**ML**	**A-5/A-2-5**
	G	250+37	31.98	34	1	2.74	**SM**	**A-2-4**
Lime 2 (12-inch)	H	250+87	34.96	41	0.6	2.74	**SM**	**A-2-5**
	I	251+53	48.72	41	3.1	2.72	**SM**	**A-5/A-2-5**
	J	252+06	41.26	36	5.3	2.77	**SM**	**A-4**
Lime 3 (16-inch)	K	252+60	35.13	36.5	3.9	2.78	**SM**	**A-2-4**
	L	253+13	24.76	30.5	0.5	2.7	**SM**	**A-2-4**
	M	253+66	49.79	40	7.7	2.79	**ML**	**A-4/A-5**
	N	254+20	43.38	45	17.5	2.72	**SM**	**A-7-6**
Lime 4 (8-inch)	O	254+73	56.44	45	12	2.99	**ML**	**A-7-5**
	P	255+26	32.19	32.5	0	2.88	**SM**	**A-2-4**

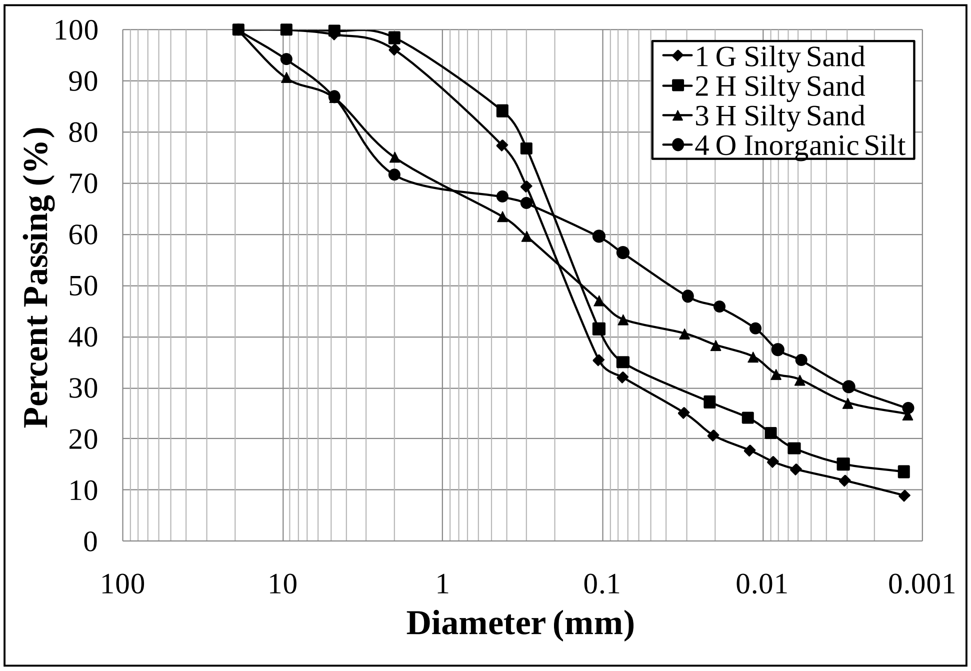

Figure 4.5 Grain size distribution for subgrade of selected sampling locations for geotechnical properties testing

Table 4.3: Soil Classification for Natural Soils of Stabilization and Subgrade Layer

Layer		Stabilization		Subgrade	
Location	**Station**	**USCS**	**AASHTO**	**USCS**	**AASHTO**
A	247+27	SM	A-4	SM	A-4/A-2-4
B	247+80	SM	A-4	SM	A-4
C	248+33	SM	A-2-4	SM	A-2-4
D	248+87	SM	A-4	SM	A-2-4
E	249+40	MH	A-7-5	MH	A-7-5
F	249+93	SM	A-5	ML	A-5/A-2-5
G	250+37	SM	A-2-4	SM	A-2-4
H	250+87	SM	A-5	SM	A-2-5
I	251+53	ML	A-6	SM	A-5/A-2-5
J	252+06	SM	A-2-4/A-2-6	SM	A-4
K	252+60	SM	A-2-4/A-4	SM	A-2-4
L	253+13	SC	A-4	SM	A-2-4
M	253+66	SC/SM	A-4	ML	A-4/A-5
N	254+20	SM	A-4	SM	A-7-6
O	254+73	MH	A-7-6	ML	A-7-5
P	255+26	SC	A-2-6	SM	A-2-4

Soils with greater than 25% fines (passing the No. 200 sieve, 0.075 mm) and a plasticity index of higher than 10 are suitable candidates for lime stabilization (National Lime Association, 2004). Based on these 2 criteria, soils from 7 of the sampled locations

(E, I, J, M, N, O, P) met both requirements, soils from 8 of the sampled locations (A, B, C, D, F, G, H, L) met one of the requirements while location K did not meet any of the requirements (Table 4.4). The presence of random sand pockets in the soil of the stabilized layer could have resulted in the majority of the soil being classified as silty sands (SM). Although soil classification was used preliminarily to select a chemical additive and determine the suitability of a soil for lime stabilization, the final selection as lime stabilized soils was validated through unconfined compressive strength gain.

4.2.3 Establishing Minimum Lime Contents Required for Stabilization

The minimum optimum lime content required for soil stabilization is determined using the Eades and Grim (1966) pH test. 20 g soil sample passing through the No. 40 sieve is placed in a tightly capped bottle and mixed with 0, 3, 4, 5, 6, and 7% lime of dry weight of the soil in accordance with ASTM D6276 – 99a (2006). The results of the minimum lime contents required for stabilization of the soil samples are presented in Table 4.4. The values affixed with an asterisk(*) are soils that did not reach a pH value of 12.4 after thirty seconds of shaking every ten minutes for an hour; however a pH value of 12.3 was reached. Figure 4.6 presents the plot of pH values versus lime contents for the soil samples from instrumented locations. The pH values of the untreated soils are about 5.2. Lime contents used for the Eades and Grim tests were limited to 7% as beyond this value, lime stabilization is uneconomical and rarely used soil improvement.

From the results of minimum required lime contents and soil classifications (Table 4.4), only 3% lime contents is required for silty sands (SM) reached a pH of 12.4. The only exception is the SM soil samples from station 252+60 which did not meet any National Lime Association criteria. In order to elevate the pH of this soil slurry, higher lime content (6%) was necessary to fully react with the soil. For the other classifications, such as ML, MH or SC, lime contents greater than 3% were required to initiate stabilization process.

Table 4.4: Minimum Required Lime Content and Soil Classification of Soils

Location	% Fines	Eades and Grim	USCS
A	43.4	3	SM
B	36.3	3	SM
C	34.5	3	SM
D	41.0	3	SM
E	58.0	6	MH
F	37.2	3	SM
G	35.7	3	SM
H	48.6	-	SM
I	52.2	6*	ML
J	31.1	3	SM
K	16.6	6	SM
L	51.0	7*	SC
M	40.9	6*	SC/SM
N	41.1	3	SM
O	70.1	4	MH
P	35.3	3	SC

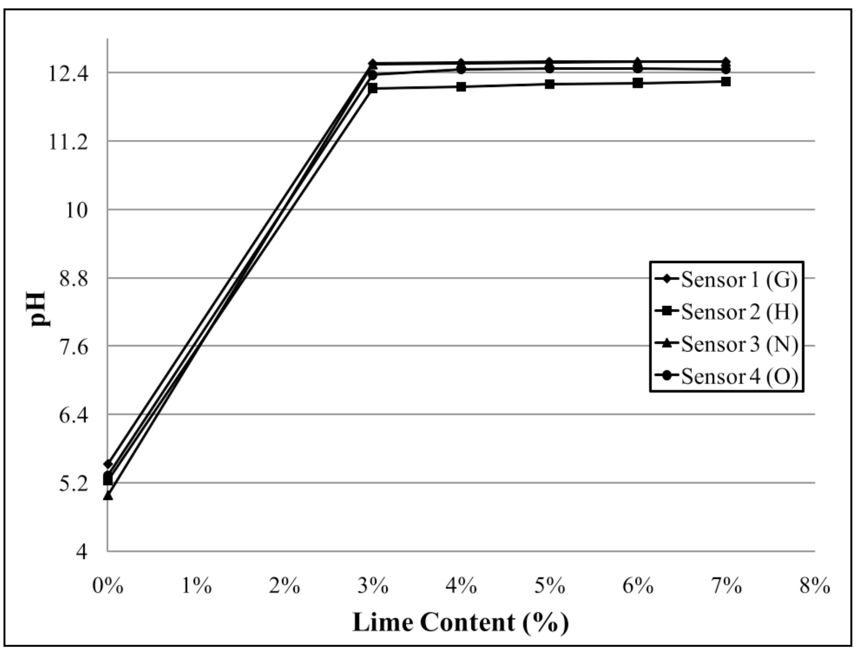

Figure 4.6 pH versus lime content

4.2.4 Moisture – Dry Density Relationships

a. Moisture – Dry Density Relationships of Untreated Soils

Standard Proctor moisture - dry density tests were performed for all the untreated soil samples collected from the stabilized and subgrade layers in accordance with ASTM D698 (2000). A compaction effort of 600 kN-m/m^3 (12,400 ft-lb$_f$/ft^3) was applied to each sample. The results of optimum moisture contents and maximum dry densities of the soils from the stabilized and subgrade layers are presented in Table 4.5. Figures 4.7 and 4.8 present the moisture – dry density curves of the soil samples from the selected locations G, H, N, and O.

From the results presented in Table 4.5 above, soils with high plasticity (examples of samples from stations 249+40, 249+93, 250+87, and 254+73) correlated well with high optimum moisture contents and low maximum dry densities, and vice versa which conform well with the findings of Daita, et al. (2005). This trend was also noticed for most of the soils in the subgrade layer. Most high plasticity soils of this research were classified as inorganic silts and clayey sands.

Table 4.5: Density Moisture Results

Layer	Stabilizied Layer			Subgrade Layer		
Section	% Fines	Optimum Moisture Content %	Maximum Dry Density kN/m^3 (pcf)	% Fines	Optimum Moisture Content %	Maximum Dry Density kN/m^3 (pcf)
A	43.4	17	16.9 (107.5)	45.2	19.5	16.0 (102)
B	36.3	18	16.9 (107.4)	46.19	19.8	16.1 (102.6)
C	34.5	19.5	15.8 (100.5)	32.4	19.5	15.9 (101.3)
D	41.0	20	16.5 (104.8)	35.84	21.5	15.5 (98.5)
E	58.0	26.5	14.3 (90.8)	57.06	25	14.8 (93.9)
F	37.2	25.5	14.6 (92.8)	60.33	26.5	13.9 (88.2)
G	35.7	20	16.0 (101.7)	31.98	21	15.1 (96.2)
H	48.6	24	14.3 (91.3)	34.96	22.4	14.8 (94.2)
I	52.2	24	15.4 (98.3)	48.72	22.5	14.7 (93.7)
J	31.1	20	16.1 (102.2)	41.26	21	15.6 (99.1)
K	16.6	21	16.1 (102.4)	35.13	19.5	15.8 (100.4)
L	51.0	21	15.8 (100.5)	24.76	22	15.4 (98.2)
M	40.9	20	16.3 (103.7)	49.79	22.5	15.4 (98.3)
N	41.1	19.5	15.9 (101.4)	43.38	21.5	15.5 (98.4)
O	70.1	35	13.1 (83.7)	56.44	30	13.7 (87.4)
P	35.3	16	17.2 (109.2)	32.19	22.5	15.4 (98)

b. Moisture – Dry Density Relationships of Lime Treated Soils

After the determination of optimum moisture content for the subgrade soils, a series of moisture density tests were performed on stabilized layer soils treated with different lime contents. These series of tests were performed for samples collected from G, H, N, and O locations. The compaction tests were performed immediately after mixing and after a 24-hour mellowing period for samples treated with 3 - 9% of lime contents. The moisture – dry density relations of all the lime treated soils are plotted in Figures 4.7 through 4.12.

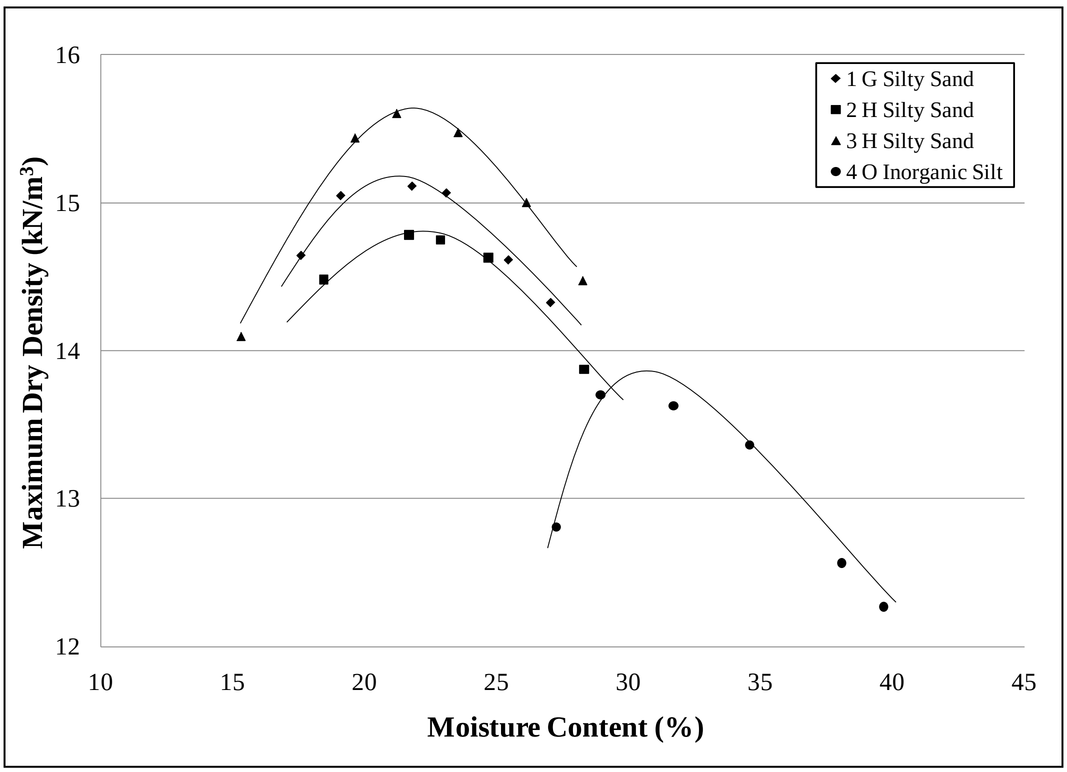

Figure 4.7 Moisture-Dry Density Curves of subgrade layer from the selected locations G, H, N, and O

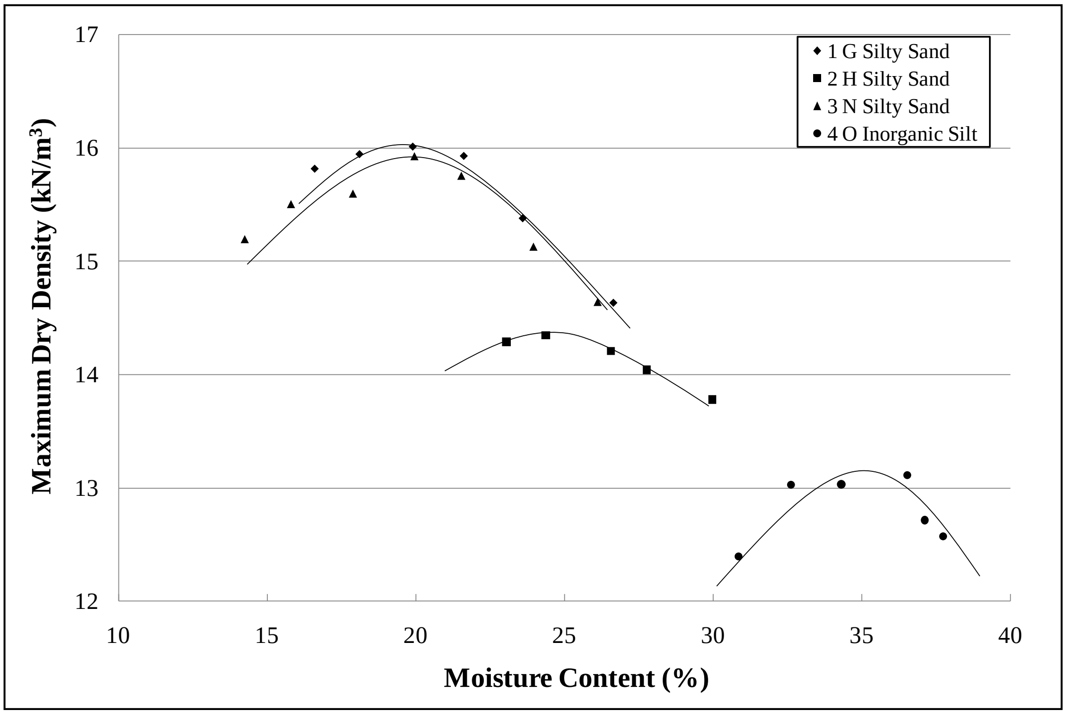

Figure 4.8 Moisture-Dry Density Curves of untreated soils of the stabilized layer from the selected locations G, H, N, and O

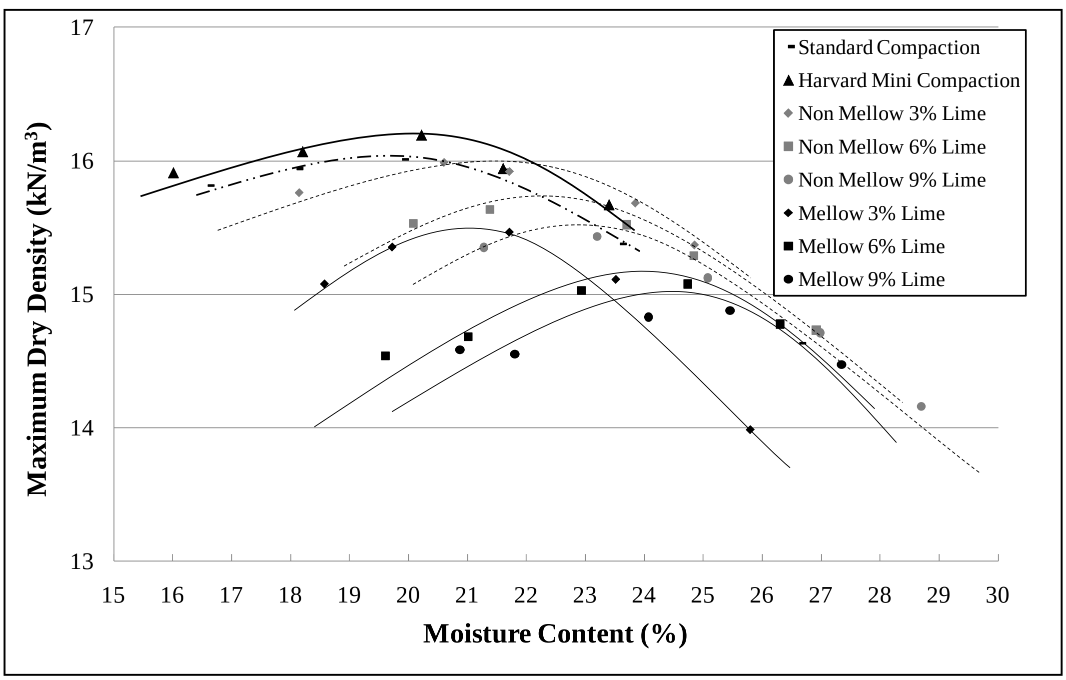

Figure 4.9 Lime Test Section 1 (Location G) Density – Dry Moisture Curve at different lime contents

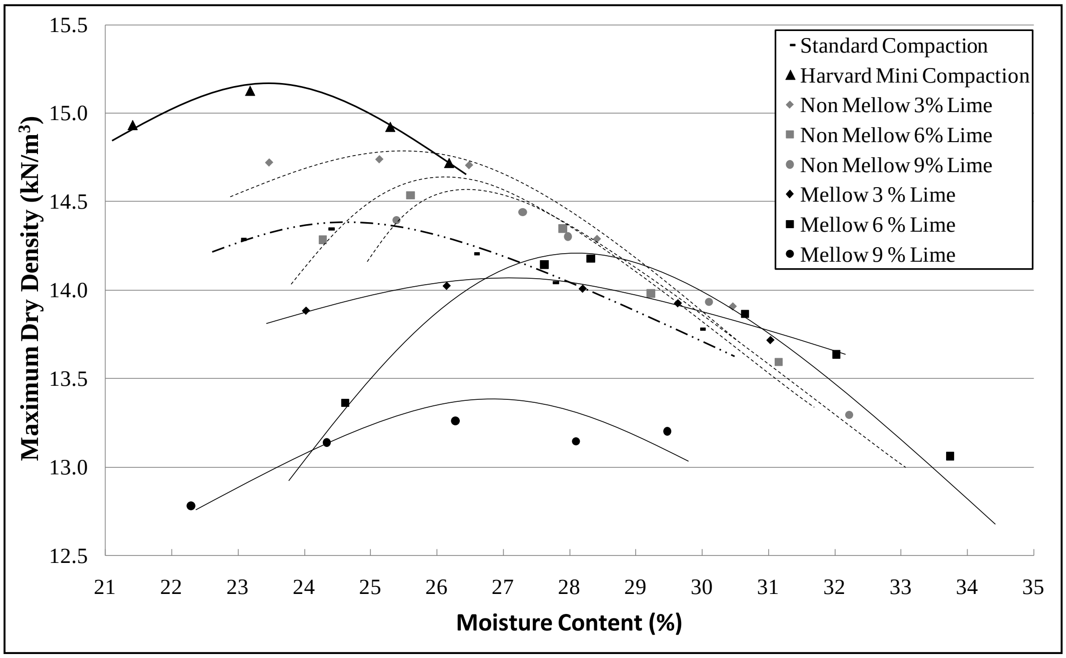

Figure 4.10 Lime Test Section 2 (Location H) Density – Dry Moisture Curve at different lime contents

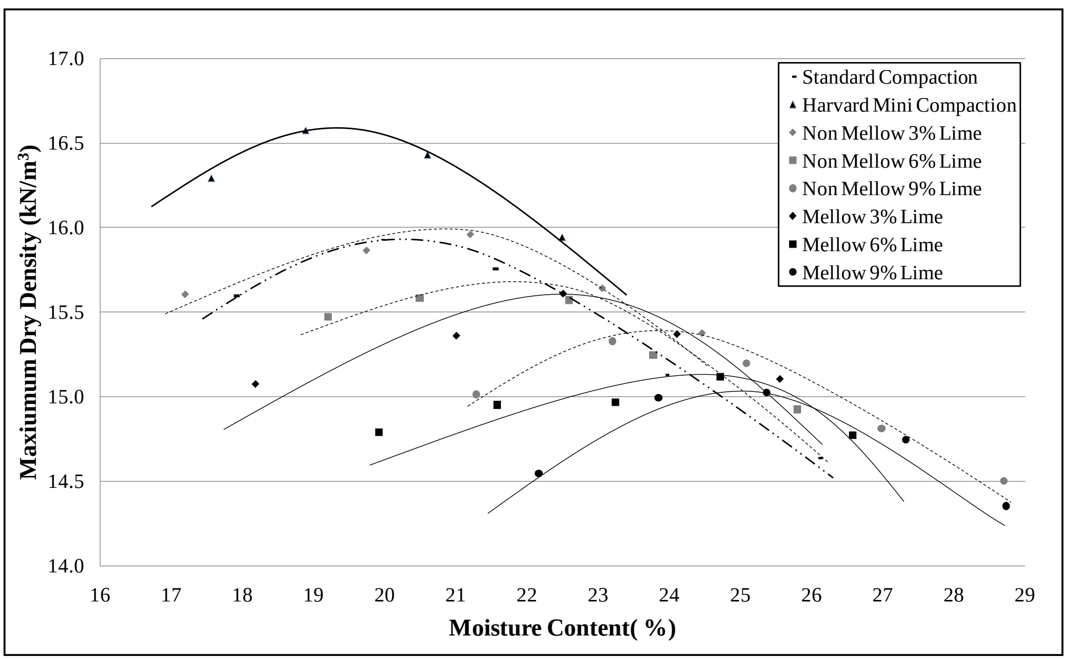

Figure 4.11 Lime Test Section 3 (Location N) Density – Dry Moisture Curve at different lime contents

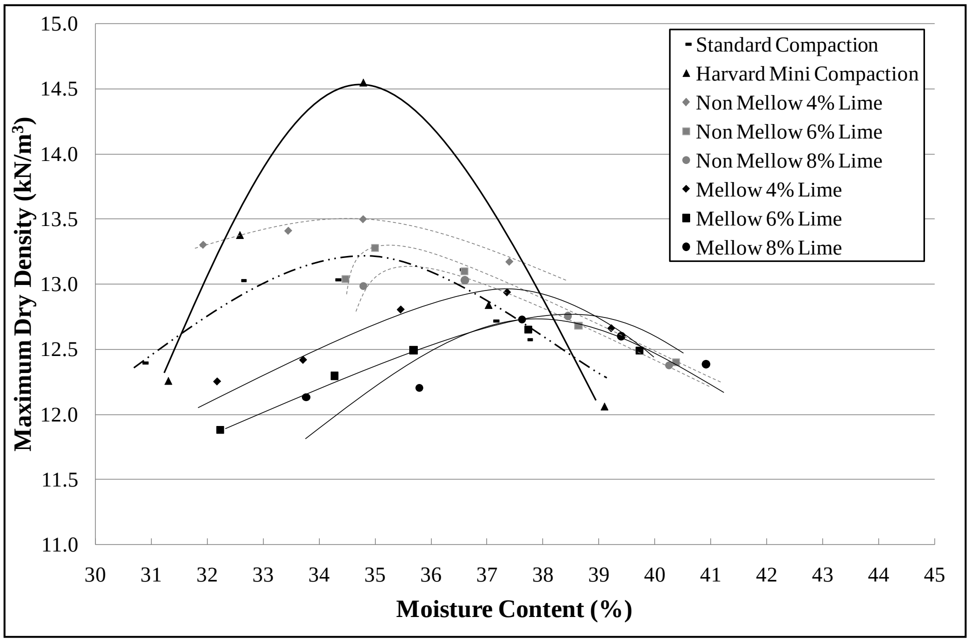

Figure 4.12 Lime Test Section 4 (Location O) Density – Dry Moisture Curve at different lime contents

Moisture density curves for lime treated soils were plotted for the four instrumented locations selected as representative of the test sections. Each location was evaluated with three lime contents to investigate their effects on moisture content and maximum dry density. During the flocculation and agglomeration phase of lime stabilization, the soil structure and texture begin to change as soon as the reactions begin to take place. As lime reacts with fine grained soils they begin to floc to each other and form larger clods, becoming more granular in shape, which may have varying effects on the moisture-density relationships of the stabilized soils. With the addition of lime, more water is consumed through an exothermic reaction and the optimum moisture content increases.

Figures 4.9 through 4.12 present the moisture-density curves of lime stabilized soils from the stabilized layer of selected test locations. At locations 1 (G) and 3 (N) representative of the test sections 1 and 3, the moisture density-curve exhibited standard patterns of increasing optimum moisture contents and decreasing maximum dry densities, upon the addition of more lime. When the soils were mellowed at higher lime contents the optimum moisture content further increased and the maximum dry densities decreased. The mellowing period provided more opportunity for the reactive fines in the soil to fully react with lime. It also provided the opportunity for a complete reaction with the lime, an exothermic process that requires more water than the non-mellowing condition. As a consequence mellowing required more water to reach the maximum dry unit weight, thus resulting in increase in the optimum moisture content. Whereas in the non mellowed condition, the reaction process might be often incomplete, thus resulting in lower optimum moisture content when compared to the mellowed condition. The addition of lime increases the workability of the soils and reduces the slope of the moisture-density curve from the natural state. Thus resulting in a curve that is more leveled out in agreement with the observations from Kavak and Akyarh (2007).

The moisture-density curves did not follow the typical trends for samples from selected locations 2 (H) and 4 (O). For non-mellowed condition, location 2 (H) exhibited typical trends; however, after mellowing, the optimum moisture content for the 6% lime content is higher (wetter) while the optimum moisture content for 9% is lower (drier) when compared with density-moisture content relationship for the soil at 3% lime content. According to Daita et al. (2005) when the optimum moisture contents decrease, this is a sign of soil changing to a coarser particle distribution, and when the optimum moisture content increases then soils are changing to a finer particle distribution. Based on the work of Daita et al. (2005), soil from location 2 (H) appeared to become finer with the addition of 6% lime, however with 9% lime the soil appears to aggregate to a more coarse particle distribution. The optimum moisture content decreased from 28.5% to 26.5% when the lime content was increased from 6% to 9% lime content. Although the experimental studies by Daita et al. (2005) were performed with lime kiln dust; the chemical compositions and reaction processes are still equivalent to those of lime.

Unlike silty sands, when lime is added to inorganic silt collected from location 4 (O) the textural transformation begins immediately from a platy material to granular structure. The particles of inorganic silt soils similar to those samples from instrumented location 4 (O) became finer as time passed with the addition of lime according to Bell and Coulthard (1990). The non mellowed samples generally have higher maximum dry densities and lower optimum moisture contents that the corresponding mellowed samples of the same lime content. For mellowed and non-mellowed conditions, the moisture-density curves present decreasing maximum dry densities at slightly increasing (but may be considered constant) optimum moisture content as the lime contents increased. Since the increase in optimum moisture content is insignificant as lime content increases, the change in optimum moisture is negligible for non mellowed or mellowed samples as lime contents increase. This behavior is similar to the findings of Consoli et al. (2009) for the moisture-density relationship of sandy lean clay soil where the optimum moisture content remained constant as the lime contents increased from 3% to 11% lime. However, no explanations were offered on mechanism or phenomenon controlling the trend of constant optimum moisture content by the authors.

4.3 Geotechnical Engineering Strength of Lime treated and untreated Test site soils

The aims of this engineering characterization of the soil samples are to establish baseline of the stiffness and strength values of the untreated soil, and to determine the lime content required to achieve NCDOT target strength/stiffness value for stabilized soils. UCS is the engineering parameter commonly used to evaluate the strength of treated and untreated soil material. It is a simple, easy, quick and adequately reliable strength parameter based of the failure strength of the sample to assess quality of stabilized soil. Resilient modulus (M_r) is the stiffness parameter currently used in pavement design and performance evaluation. It is main input parameter of treated and untreated soils for predicting pavement responses under different traffic loading condition. For this project, the geotechnical engineering tests conducted on lime treated and untreated soil samples are limited to unconfined compression strength (UCS) and resilient modulus (M_r).

4.3.1 Unconfined Compression Tests

4.3.1.1 Lime Content Strength Verification

Once the optimum moisture contents were established at various lime contents, specimens for unconfined compression strength determination were made at the various lime contents to determine the lime contents required to achieve the minimum NCDOT target UCS value of 414 kPa (60 psi) for lime stabilized soils. Field molding moisture contents are very difficult to maintain in the field due to the heterogeneity of soil and the always variable atmospheric conditions at different sites. In order to ensure complete hydration of process of the chemical additives, stabilized layers are typically mixed and compacted at wet of optimum moisture contents during field stabilization process. For these reasons, the effect of molding moisture contents at optimum and at 2% wet of optimum on the UCS were assessed for the different soil samples treated to lime contents in the rage 0% - 9% of the soil dry mass (Figure 4.13). However for practical and economic reasons, the basis for selecting the lime content for the soils includes (1) archiving the target minimum UCS value of 414 kPa (60 psi) recommended by NCDOT for lime stabilization and (2) verifying that lime stabilization is appropriate by ensuring the stabilized samples gain at least 344.75 kPa (50 psi) from their untreated state (Little and Nair, 2009).

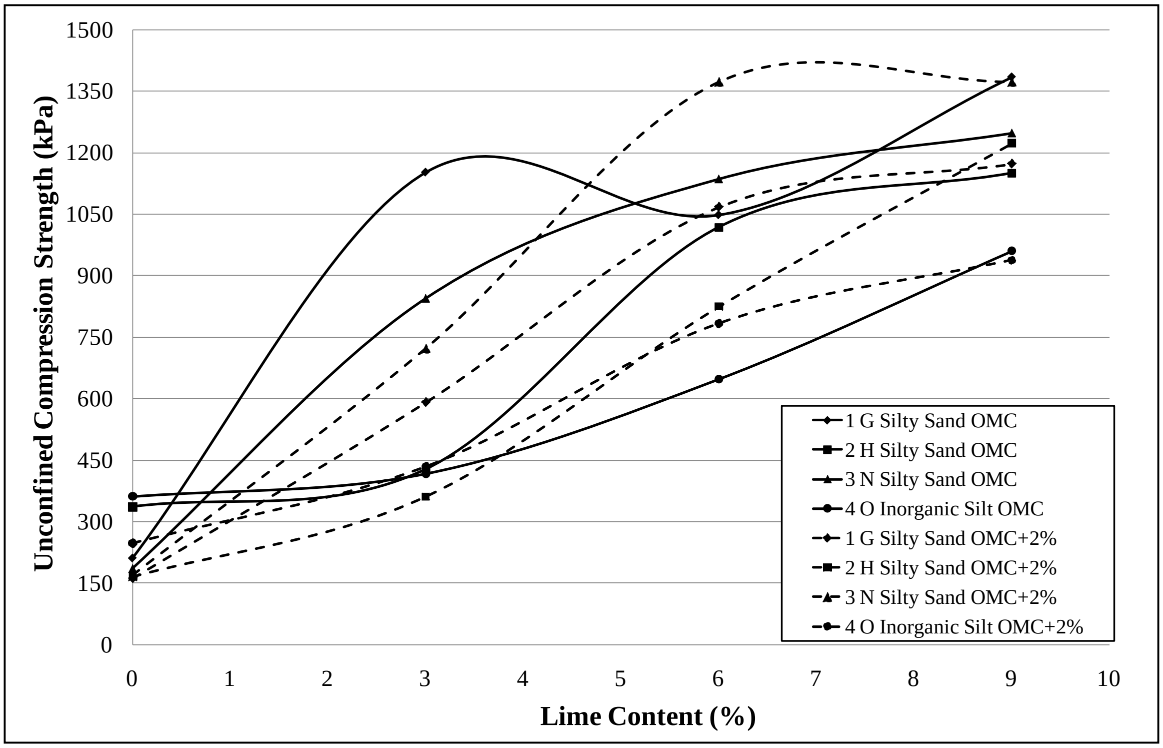

Figure 4.13 UCS for different Lime Contents at OMC and OMC +2%

UC samples were prepared at different lime contents to evaluate the effect of the lime level on unconfined compressive strength. Since only one drum of soil sample was collected at each selected location and to ensure adequate materials are available for the suite of planned tests, Harvard miniature samples were used as a means to conserve soil. Soil samples were made at optimum moisture contents and at 2% wet of optimum moisture content, in accordance with the recommendations of many researchers to accommodate extra moisture needed for the hydration process during the curing period (Bell, 1996, Mateos and Davidson, 1963, Ozier and Moore, 1976).

However because of the size of the Harvard Miniature, moisture contents were harder to maintain and control throughout sample preparation. Figures 4.13 depicted the strengths as the lime contents increase. Except for instrumented location 1(G) for which the unconfined compression (UC) decreased from 1151.47 kPa (167 psi) at 3% lime to 1048.04 kPa (152 psi) at 6% lime, the unconfined compression strength of all other samples generally increased with increasing lime content when compacted at the optimum moisture content. The strengths of all the samples consistently increased when compacted at 2% wet of optimum moisture content.

In Figure 4.13 the unconfined compression value for the sample compacted at optimum moisture content from instrumented location 1 (G) fluctuated as the lime contents increased. The strength decreased from 3% lime to 6% lime, and then increased again with 9% lime. This was the only instance where there was a fluctuation, generally as the lime content was increased the strength increased as well. It is possible that the unconfined strength value at 6% lime is an outlier, and should not be considered for this study. Fluctuations in unconfined compression strength may also occur due to non-uniform distributions of lime in the soil mixture (Bell, 1996). This is possible considering the small size of the Harvard miniature samples.

For the same soil sample at instrumented location 1(G), the unconfined compression strength at 9% lime was lower in soil samples compacted at optimum moisture plus 2% than the samples compacted at optimum moisture content. There was a difference of 207 kPa (30 psi) between the unconfined compressive strength values of the two moisture contents at 9% lime. This is contrary to the expectation that insufficient amounts of water can result in maximum strength being attained early in the curing process when the water is consumed resulting in peak strengths that are lower than when there are generally sufficient amounts of water.

It is common for fine grained soils to be stabilized between 4-6% lime, anything more is considered uneconomical. Also, for the lab analysis, the strength gained at 6% lime content meets NCDOT lime stabilization strength requirement of 414 kPa (60 psi) minimum UCS value and the strength gain of at least 344.75 kPa (50 psi) over their untreated state stipulation by Little and Nair (2009). Since minimum lime contents for most of the soils is 3%, it can be argued that 6% lime content is sufficient to achieve long term durability of soil stabilization.

4.3.1.2 Unconfined Compression Strength (UCS)

A series of unconfined compression tests were conducted at two lime contents (6% and estimated field application rate). The 6% lime content is estimated from lab results presented in Figure 4.13 while, the field application rates were the estimated rates of lime contents used in the field. The field rates were back calculated based on the specific gravity, moisture content, maximum dry density and the lime rate of 15kg/cm^2 applied by the contractor. Table 4.6 presents the results of the strength for selected sampling stations, along with the parameters used during mixing. Figures 4.14 and 4.15 illustrate the effects of curing duration on strength gain. An additional 2% of moisture was added during the mix process to ensure complete for hydration of the lime.

Table 4.6: Unconfined Compressive Strength Data

Instrumented Location	**Research Lime Content**	**Moisture Content**	**Natural Soil kPa (psi)**	**3 Day kPa (psi)**	**7 Day kPa (psi)**
1 (G)	6%	26%	110.8 (16.1)	659.2 (95.6)	1126.6 (163.4)
2 (H)	6%	30%	185.7 (26.9)	838.4 (121.6)	1041.8 (151.1)
3 (N)	6%	27%	153.5 (22.27)	625.4 (90.7)	857.7 (124.4)
4 (O)	6%	40%	126.2 (18.30)	531.6 (77.1)	607.4 (88.1)
Instrumented Location	**Field Lime Content**	**Moisture Content**	**Natural Soil kPa (psi)**	**3 Day kPa (psi)**	**7 Day kPa (psi)**
1 (G)	4.6%	25.5%	110.8 (16.1)	547.5 (79.4)	991.5 (143.8)
2 (H)	5.1%	30%	185.7 (26.9)	892.9 (129.5)	1232.1 (178.7)
3 (N)	4.6%	25%	153.5 (22.27)	608.1 (88.2)	1059.1 (153.6)
4 (O)	5.6%	39.5%	126.2 (18.30)	408.2 (59.2)	504.0 (73.1)

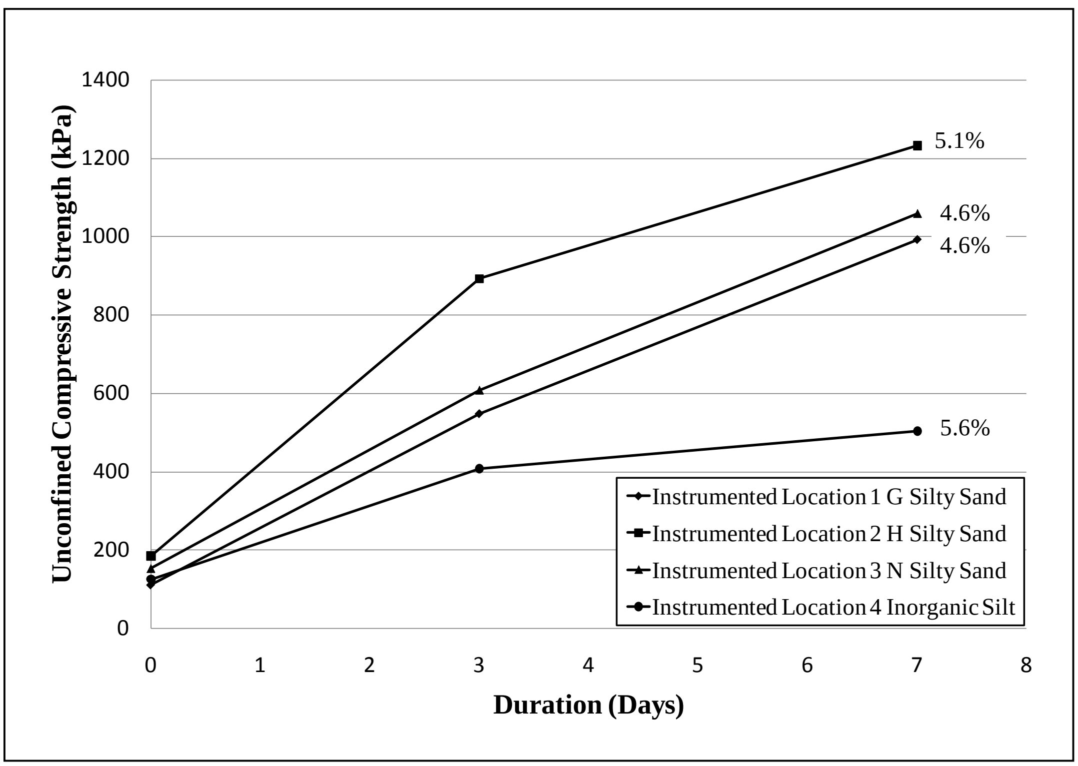

Figure 4.14 UC Strength from field Lime Content

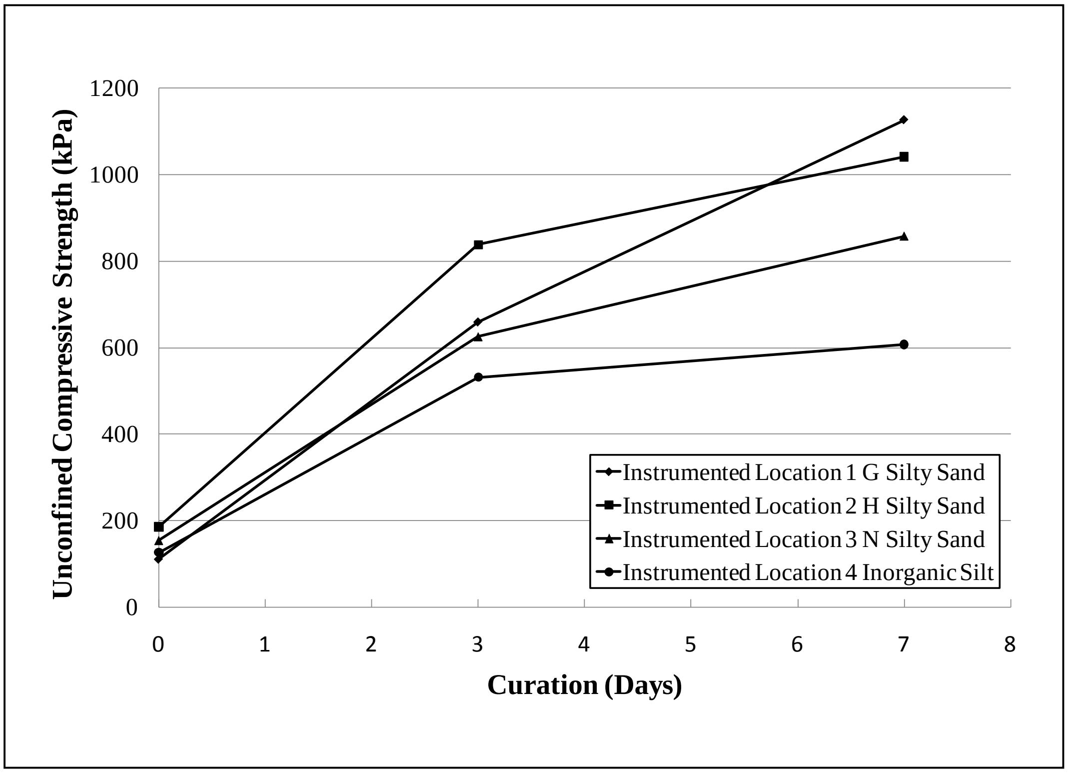

Figure 4.15 UC Strength at 6% Lime Content

Unconfined compression samples were prepared in a controlled environment to produce similar conditions that occur in the field. The moisture contents obtained from the mellowing phase of the moisture-density curve were used to make these samples. This was chosen because lime stabilized soils were mellowed in the field before they were compacted. The *State of the Art Report* on lime stabilization stated that moisture density relationships are always changing, and it is important to use the proper curve to obtain the best results (National Research Council, 1987).

The most notable increases in strength occurred during the initial stages of the curing, when the cementitious processes were most active and strength gain was initiated. This happened within the first seven days of final compaction. The moisture in the stabilized sample is critical for the influence of strength gain, since it controls the hydration process. As previously mentioned, it was recommended to use moisture slightly wetter than the optimum to achieve maximum strengths. Any amount less than optimum, lime could rapidly consume moisture and maximum strengths may not be developed in a shorter period when all the lime has not had time to react which could weaken the stabilization over time (Bell, 1996).

Figures 4.14 and 4.15 illustrated the increase in strengths of soil stabilization with lime mixed at field rates and 6% research content. At 7 day curing, strengths for soil stabilization at instrumented locations 1 (G) and 4 (O) displayed opposite behavior to locations 2 (H) and 3(N) for the 6% lime concentration compared to the field lime concentration. As the lime contents are decreased slightly, the strengths for locations 1 (G) and 4 (O) decreased, however it increased for locations 2 (H) and 3 (N). Locations 2 (H) and 3 (N) have a fine contents of 48.6% and 41.1%, and a liquid limit of 41 and 39, which were higher than these of location 1 (G). The maximum strength gain is clearly dependant on obtaining the accurate optimum lime content and several engineering properties of the soil.

Instrumented location 1 (G) displayed a continuing increase in strength beyond 7 days for both lime contents. Instrumented locations 2 (H) and 3 (N) continued to increase past 7 days with field lime contents, however for 6% lime content they show signs of remaining constant past 7 days. Instrumented location 4 (O), classified as the inorganic silt, had the least strength gain of the four soils for both lime contents. The maximum strength was reached at 7 days and then began to steady past that. Once the maximum was reached and the strengths showed signs of steadiness, they will continue to gain strength over time, however the rate of strength gain will not be as rapid as what occurred at the early curing days.

Based on the work of Little and Nair (2009), lime stabilization is appropriate if stabilized samples gain at least 344.75 kPa (50 psi) from their untreated state during long term reactions. Figures 4.16 and 4.17 present the strength of the untreated soil, and the strength gained from stabilization for the 6% (research) and field lime contents. The darker shade of grey represents the strength of soil in the untreated state, and the lighter grey represents the strength gain from the addition of lime. All soils qualified as being successfully stabilized for the field and 6% (research) lime contents. These results validate the index properties from soil classification for selecting lime as a stabilizing agent for these soil types at the beginning of the research. Since there was a substantial strength gain of at least 481.3 kPa (69psi) for instrumented location 4 (O), and these locations are considered to have lime reactive soils that can produce quality paving materials (National Research Council, 1987, Thompson, 2005). The values reached at 7 days of curing also fell within the North Carolina Department of Transportation standards, where the preferred strength of stabilized soil samples was a maximum of 1723.75 kPa (250 psi).

As previously presented in Section 5.2 (Eades and Grim pH) samples from instrumented location 3 (H) did not reach a pH of 12.4 after an hour. Therefore no minimum lime content was established for this location. However, Figures 4.16 and 4.17 show that with lime contents of 5-6% the soil at this location is a candidate for lime stabilization. In fact the field lime content of 5.1% produced lime stabilization stronger than the 3 other instrumented locations. This location produced the second highest strength gain for the 6% research lime content. The strength gain can be attributed to the extra time provided during the mellowing period for the pH to elevate to 12.4 and the pozzolanic reaction induced between soil and lime after sufficient time has occurred.

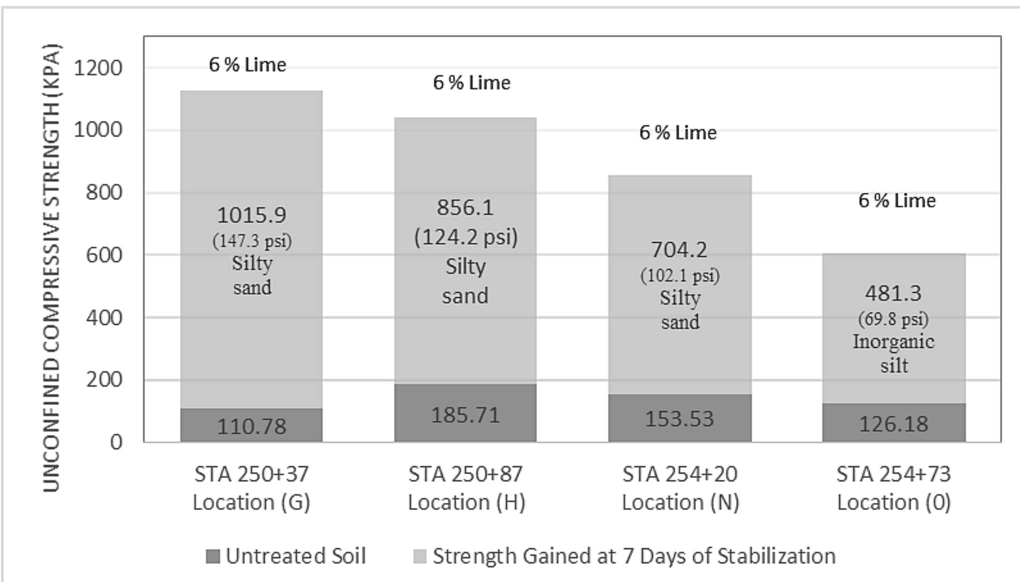

Figure 4.16 UC Strength Gain from 6% Lime Content

4.3.2 Resilient Modulus Tests

Resilient Modulus tests were prepared and performed at the Geotechnical Materials and Testing Unit in Raleigh, North Carolina. Two specimens were tested for each sampling stations. Table 4.7 – 4.10 summarize the results of resilient modulus tests on undisturbed soils from the subgrade layer extracted from Shelby tubes collected during field testing. Lime stabilized samples were mixed at field lime contents (1 (G)-4.6%, 2 (H)-5.1%, 3 (N)-4.6%, and 4 (O)-5.6%). By using the field lime application rates, the results of the resilient modulus can be used to validate the field/nondestructive test (FWD) as well as data for the numerical modeling of the pavement response. Tables 4.11 – 4.14 summarize the results of resilient modulus tests on soils and lime stabilized soils of the stabilized layer at selected sampling stations. The percent increase by treating the soils with lime are provided in the last column. In Table 23, the percent increase by treating the soil sample collected at instrumented location 1 (G) with lime over the untreated soil value ranges from 86 to 149%. In Table 24, the percent gain from treating the soil sample collected at instrumented location 2 (H) with lime over the untreated soil value ranges from 364 to 868%. In Table 25, the percent gain from treating the soil sample collected at instrumented location 3 (N) with lime over the untreated soil value ranges from 164 to 305%. In Table 26, the percent gain from treating the soil sample collected at instrumented location 4 (O) with lime over the untreated soil value ranges from 100 to 173%. Resilient modulus samples for the stabilized soils were compacted to 95% ± 1%, in accordance with NCDOT standard practices.

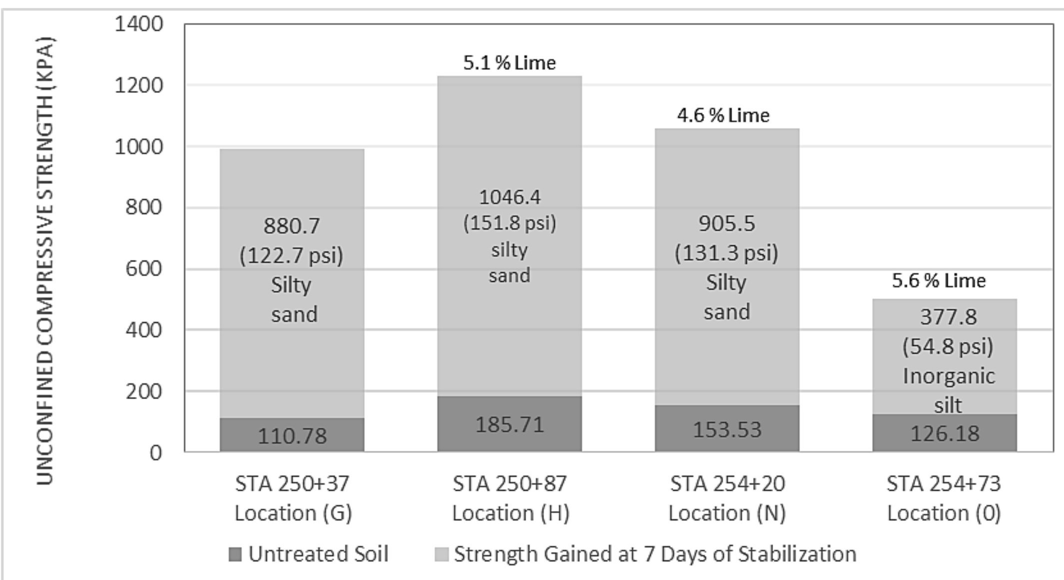

Figure 4.17 UC Strength Gain from Field Lime Contents

The stress sensitive relationships of the resilient modulus (Mr) of the untreated soil and lime treated soil samples are presented in the tables as well. If more than one sample was performed for the untreated or treated soils, then the percentage increase as determined based on the mean values. The resilient modulus (Mr) in kPa (psi) of both the treated and untreated soils are adequately represented with stress softening and stress dependent relationships of the form presented in Equation 5.1.

$$M_r = k_1 \sigma_d^{k_2} \sigma_c^{k_3} \tag{4.1}$$

Where,

k_1, k_2, and k_3 = constraints derived from the experimental data;

σ_d = the deviatoric cyclic stress (kPa or psi); and,

σ_c = the confining stress (kpa or psi).

Resilient modulus is not based on the failure of strength of the sample but the elastic stiffness of a sample which constitutes critical data for pavement design. Tables 4.7 through 4.14 present the resilient modulus data obtained from the tests performed at the NC DOT Materials and Testing Unit, for untreated soils and soil-lime mixture samples. Due to the time constraints and the long sample preparation, only one sample for each instrumented location was tested except in cases where the compaction density and moisture content requirements were not met. In cases where density and moisture content were not met in the first trial the specimens were still test and the data was still used for comparison purposes. Resilient modulus samples were only tested using the field lime content applications rates.

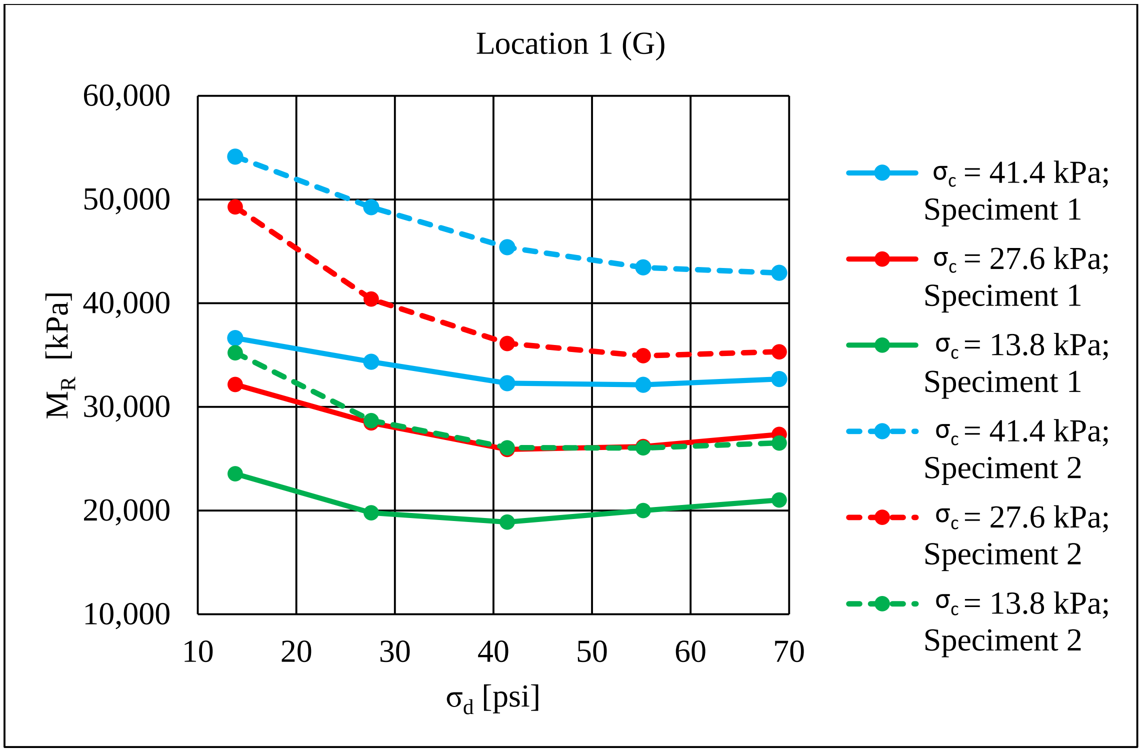

Figure 4.18 Resilient Modulus of Subgrade Layer for Location 1

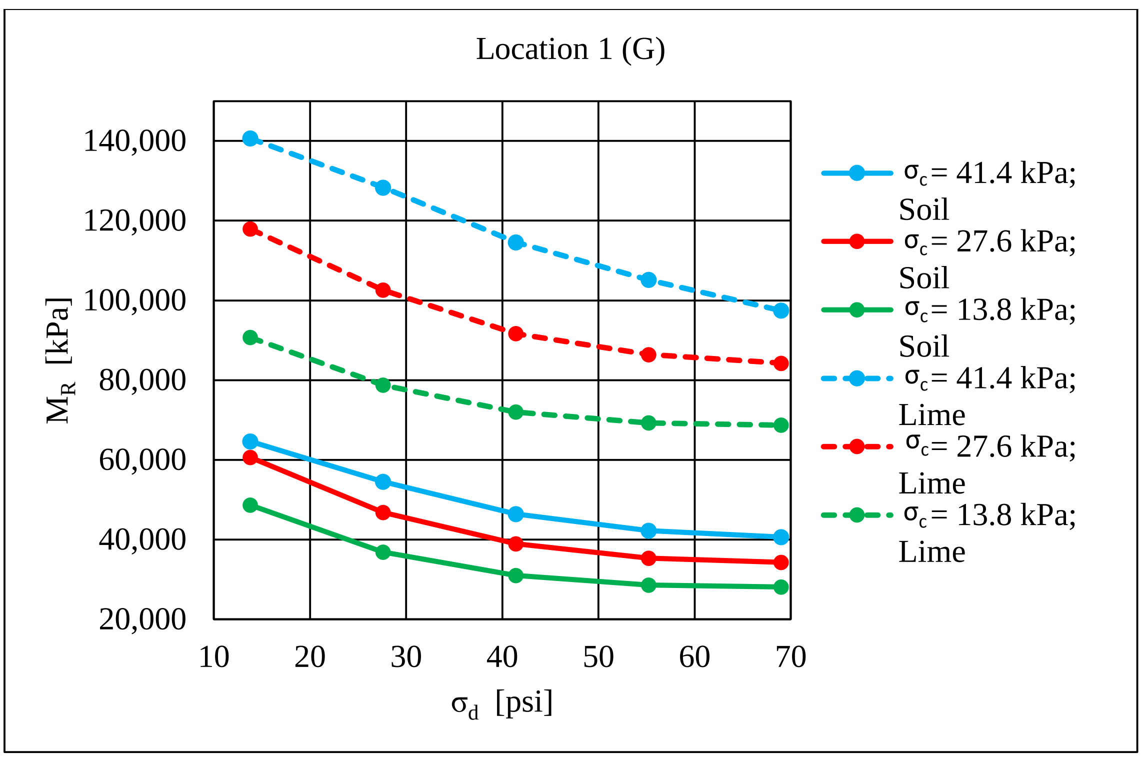

Figure 4.19 Resilient Modulus of Untreated and Lime Stabilized Soil for Location 1

Table 4.7: Resilient Modulus Data for Each Location

Sampling Location		$M_r = k_1(\sigma_c)^{k_2}(\sigma_d)^{k_3}$								
		Subgrade Layer			Subgrade Stabilization Layer					
					Natural Soil			Treated Soil		
		k_1	k_2	k_3	k_1	k_2	k_3	k_1	k_2	k_3
G	Trial 1	2,535	-0.09238	0.44454	14,549	-0.30351	0.18391	11,581	-0.21567	0.38925
	Trial 2	4,008	-0.18725	0.46014	-	-	-	-	-	-
H	Trial 1	2,157	-0.09958	0.52727	14,549	-0.30351	0.18391	25,110	-0.05130	0.20166
	Trial 2	2,988	-0.22895	0.47060	-	-	-	19,622	-0.02593	0.24509
N	Trial 1	13,867	-0.23220	0.25310	14,549	-0.30351	0.18391	22,329	-0.19631	0.17607
	Trial 2	18,413	-0.18103	0.21596	6,312	-0.32986	0.38086	-	-	-
O	Trial 1	8,800	-0.24039	0.31202	13,338	-0.15960	0.14351	22,024	0.00280	0.19100
	Trial 2	7,128	-0.09927	0.34285	-	-	-	-	-	-

Unlike the results of samples prepared for the unconfined compression samples, resilient modulus did not increase when samples are prepared slightly wet of optimum or at optimum moisture contents. Since this test is a measure of stiffness, resilient modulus tests are performed on samples prepared at dry of optimum. Achampong et al. (1977) tested resilient modulus samples at 2% dry of optimum, optimum and 2% wet of optimum and noticed that modulus values decrease as moisture contents increase. The author's also stated that as the deviatoric stress increases the resilient modulus value decrease. The findings of Achampong et al. (1977) are confirmed by the data from samples from instrumented locations tested for this research. Instrumented locations 2 (H) and 3 (N) displayed increasing resilient modulus values as the moisture contents decreased, and all locations displayed decreasing resilient modulus values as the deviator stresses increased. Puppala et al. (1996) also found the relationship between moisture content and resilient modulus as well as a correlation between confining stress and resilient modulus. As the confining stress increases so does the resilient modulus (Puppala, et al., 1996). When the samples are tightly confined they produce stronger values of stiffness. However, as the confining stress reduces the particles are not tightly packed together, allowing them to move. As the particles are able to move the samples loses its stiffness and the resilient modulus value decreases. These observations are supported by data obtained from the instrumented locations. The last column in Tables 4.11 through 4.14 contains the percentage gain in resilient modulus of the lime stabilized samples. The addition of lime resulted in 100% gain of resilient modulus values at a minimum. In some instances such as instrumented location 2 (H) the addition of lime led to a gain of over 800% in resilient modulus at deviator stresses of 41.6 kPa (6psi) or greater. This is in agreement with the findings of Solanki et al. (2009) which indicated that the presence of lime provides a large increase in resilient modulus values. The complete of the plots resilient modulus of untreated soils and lime stabilized soils can be found in the Appendix B.

For unconfined compression tests, silty sands were consistently stronger than the inorganic silt. However for resilient modulus, the results were opposite. In its untreated state the resilient modulus of the inorganic silt is about 34,475 kPa (5000 psi) higher than the strongest sandy silt. Some of the main differences between the two soil types were the percent fines; the inorganic silt had 70% passing through the #200 sieve and a liquid limit of 52. Increased fines content and the texture of the soil may have been better for absorbing impulse loads than for coarser soil structure, since fine particles are less likely to move easily during repetitive loading. With the addition of lime to soils from instrumented locations 2 (H) and 4 (O), samples yielded similar results which are also the highest resilient modulus of the four values. Instrumented locations 1 (G) yielded some of the highest unconfined compressive strengths however it produced the lowest resilient modulus values. It is worth noting that instrumented location 1(G) had the least amount of fines passing the #200 sieve, 35.7%.

Due to the expensive instruments and technical expertise required to perform resilient modulus tests in the laboratory, different correlations have been developed to predict values based on other simple and easily performed test. A well known correlation developed by Thompson (2010), was based on a series of unconfined compression tests and corresponding resilient modulus tests. The main issue with this type of correlations is that it is not soil specific, and are generally generated to cover all soil types. Correlations such as these tend to work better for some soils but not others. As presented in Table 5, the Mechanistic Empirical Design Guideline (MEPDG) recommends that the resilient modulus values for silty sands range from 165,480 to 258,653 kPa (24,000 to 37,500 psi). However the resilient modulus values for silty sands from this research range from 13,790 to 68,950 kPa (2,000 to 10,000 psi) in Tables 23-25. The values listed in the MEPDG over predicted by at least 200% the resilient modulus values obtained in the lab data for silty sands samples tested in this project. For inorganic silt, the MEPDG recommended a range from 55,160 to 120,663 kPa (8,000 to 17,500 psi). The lab results fit within this range, these values are presented in Table 26. This demonstrates that correlations work better for some types of soils better than others.

Correlations are formatted to generally yield conservative values. According to Mooney et al. (2010), Thompson's equation underestimates resilient modulus values by 20-50% at a confining pressure of 13.79 kPa (2 psi), and 50-80% at a confining pressure of 27.58 kPa (4 psi). Mooney and Toohey (2010) developed two correlations at confining pressures of 13.79 kpa (2 psi) and 27.58 kPa (4 psi) and a deviator stress of 41.37 kPa (6 psi). They plotted their results against Thompson's relation to assess the validity of his correlation. They verified that Thompson's relations were considerably conservative for both confining stresses.

It should be mentioned that resilient modulus is a measure of stiffness of soil or stabilized soil at small strains, while unconfined compression is the measure of unconfined compressive failure strength of the soil sample. The range of the unconfined compression is measured at large strains and is incompatible to the resilient modulus parameter. Therefore the resilient modulus and unconfined compression values are incompatible and not within the same range of stress strain paths.

4.4 Laboratory Characterization of Cement Test Site Soils

Samples collected from cement stabilized test sections were characterized and tested in the Laboratory for index tests of index and engineering properties. Because cement stabilized soils generally possess high stiffness values, indirect tensile tests (IDT) rather than the resilient modulus tests were performed on the treated samples.

4.4.1 Laboratory Test of Cement Section Soils

The cement test sections are schematically illustrated in Figure 4.20. The start and end of the as-built stations of each test section are shown in the Figure. Disturbed samples used for index characterization of the test site soils and for moisture – density test were collected from 16 different locations. Soil samples used for UCS and the IDT tests were collected from stations 260+11, 264+06.5 and 264+59 i.e. sampling locations U, BB and CC, respectively. Sampling locations U, BB and CC are situated in test sections C1, C3 and C4, respectively.

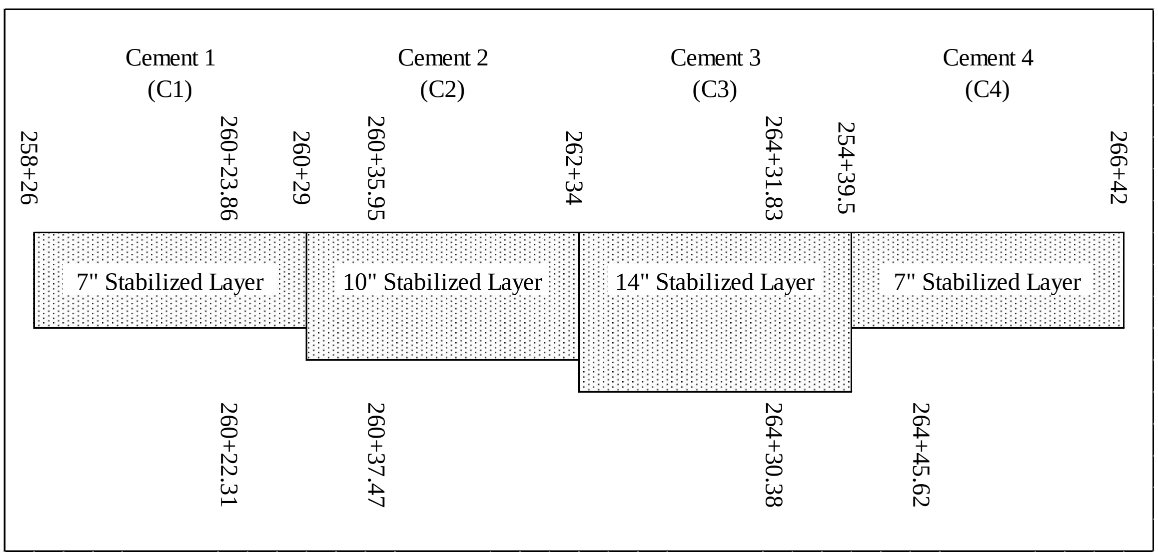

Figure 4.20 Schematic illustration of the cement test sections.

4.4.2. Soil Classification

The index properties of the untreated soils from the cement test sections are presented in Tables 4.8 and 4.9. Classifications based on the Unified Soil Classification System (USCS) and the American Association State Highway and Transportation Officials

(AASHTO) are summarized in Table 4.8 for the soils of the stabilized and subgrade layer. A majority of the soils can be classified as silty sand (SM) for both layers. Table 4.9 present key index properties such as liquid limit, plasticity index, and specific gravity. The grain size distribution curves of the subgrade soil from the selected sampling locations are presented in Figure 4.21. The engineering properties of soils from these 3 sampling locations will be presented later.

Table 4.8: Soil Characterization of Cement Test Sections

Layer		Stabilization		Subgrade	
Location	Station	USCS	AASHTO	USCS	AASHTO
Q	258+23	SM	A-2-4	SM	A-2-4/A-4
R	258+69	SM	A-2-4	SM	A-2-4
S	259+15	SM	A-2-4/A-4	SM	A-4
T	259+61	SM	A-2-4	SM	A-4/A-2-4
U	260+11	SM	A-4/A-2-4	SM	A-4/A-2-4
V	260+67	ML	A-5/A-2-5	ML	A-7/A-7-6
W	261+23	SM	A-4/A-2-4	SM	A-4
X	261+79	SM	A-4/A-2-4	SM	A-2-4
Y	262+35.5	SM	A-4/A-2-4	SM	A-4/A-2-4
Z	262+92.5	SM	A-4/A-2-4	SM	A-4/A-2-4
AA	263+49.5	SM	A-4/A-2-4	SM	A-2-4
BB	264+06.5	SM	A-4	SM	A-2-4
CC	264+59	SM	A-1-b/A-2-4	SM	A-4/A-2-4
DD	265+05	SM	A-4	SM	A-4
EE	265+50	ML	A-4	SM	A-2-4
FF	265+96	SM	A-2-4/A-4	SM	A-2-4/A-4

Table 4.9: Index Properties of Soils from the Cement Test Sections

Layer		Stabilization				Subgrade			
Location	Station	USCS	LL	PI	G_s	USCS	LL	PI	G_s
Q	258+23	SM	31	1.1	2.64	SM	26.3	5.7	2.69
R	258+69	SM	33.9	4.1	2.70	SM	31.9	2.1	2.76
S	259+15	SM	37.9	7.6	2.71	SM	28.1	6.9	2.68
T	259+61	SM	30.5	0.6	2.72	SM	29.3	3.7	2.68
U	260+11	SM	37.8	3.7	2.74	SM	32.7	2.3	2.71
V	260+67	ML	42	3.9	2.74	ML	28.1	13.9	2.70
W	261+23	SM	29.4	4.5	2.62	SM	28.7	5.3	2.68
X	261+79	SM	32.5	3.8	2.68	SM	25.0	2.0	2.68
Y	262+35.5	SM	31.8	0.3	2.68	SM	30.0	4.0	2.71
Z	262+92.5	SM	36	3.7	2.76	SM	31.2	1.8	2.70
AA	263+49.5	SM	35.2	2.2	2.64	SM	28.1	1.9	2.71
BB	264+06.5	SM	33	8.8	2.72	SM	27.6	1.4	2.77
CC	264+59	SM	32.4	1.8	2.69	SM	32.8	1.2	2.73
DD	265+05	SM	34	5.2	2.65	SM	25.2	5.8	2.69
EE	265+50	ML	34.5	8.0	2.62	SM	28.6	3.4	2.73
FF	265+96	SM	35.8	6.6	2.77	SM	27.5	6.5	2.73

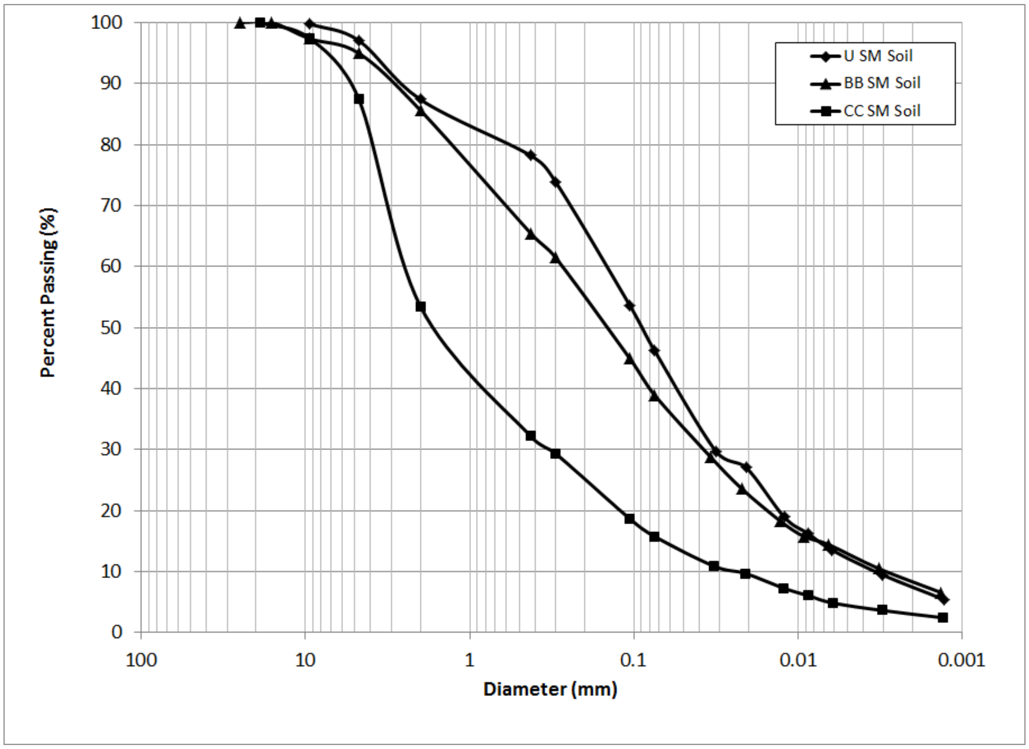

Figure 4.21 Grain size distribution of sampling locations of soils tested in the laboratory treated with cement additives

4.4.3 Moisture – Dry Density Relationships of Cement Test Section Soils

a. Moisture – Dry Density Relationships of Untreated Soils

The results of the Standard Proctor moisture - dry density tests performed in accordance with ASTM D698 (2000) on all the untreated soil samples collected from the stabilized and subgrade layers of cement stabilized test sections are presented in Table 4.10. A compaction effort of 600 kN-m/m^3 (12,400 ft-lb$_f$/ft^3) was applied to each sample. The results of optimum moisture contents of the soils are presented in the Table 4.10.

Table 4.10: Density Moisture Results of Cement Test Section Soils

Sampling Location	Subgrade Soil		Stabilized layer Soil	
	OMC (%)	γ_{maxd} (pcf	OMC (%)	γ_{maxd} (pcf)
Q	14.5	113.5	15.0	109.8
R	13.5	109.8	14.5	111.6
S	19.0	99.2	17.5	104
T	20.0	101.5	17.6	101
U	20.0	102.5	18.8	102
V	18.8	92.1	18.4	95.6
W	16.5	105.7	14.0	109.5
X	14.5	109.1	14.0	110.4
Y	20.5	98.2	17.0	103.5
Z	16.5	106.4	18.8	90.0
AA	16.5	104.2	17.0	108.8
BB	13.5	114.8	13.4	110.8
CC	16.0	106.8	16.8	103.6
DD	21.0	103.0	17.8	107.5
EE	19.5	106.1	17.0	108.8
FF	15.0	103.6	18.5	111.6

4.5 Geotechnical Engineering Strength of Cement treated and untreated Test site soils

4.5.1 Unconfined Compression Tests

Once the optimum moisture content at the target cement content was established, unconfined compression test specimens were prepared. The field application rate of 25 kg/m^2 for a layer of 180 mm was used to estimate the cement content used in the laboratory. Specimens were prepared at wet of OMC (OMC+2%), placed in Ziploc bag with moist sponge and cured in an environmental control chamber for 7 and 14 days at 23°C. The strength gained by the cement stabilized soils over the subgrade soils are presented in

Figure 4.22. Though the treated soils gained substantial strengths when treated with cement additives, the 7-day UCS values of the specimens were less than the NCDOT specified minimum 7-day value of 1378.95 kPa (200 psi) for cement stabilized soils.

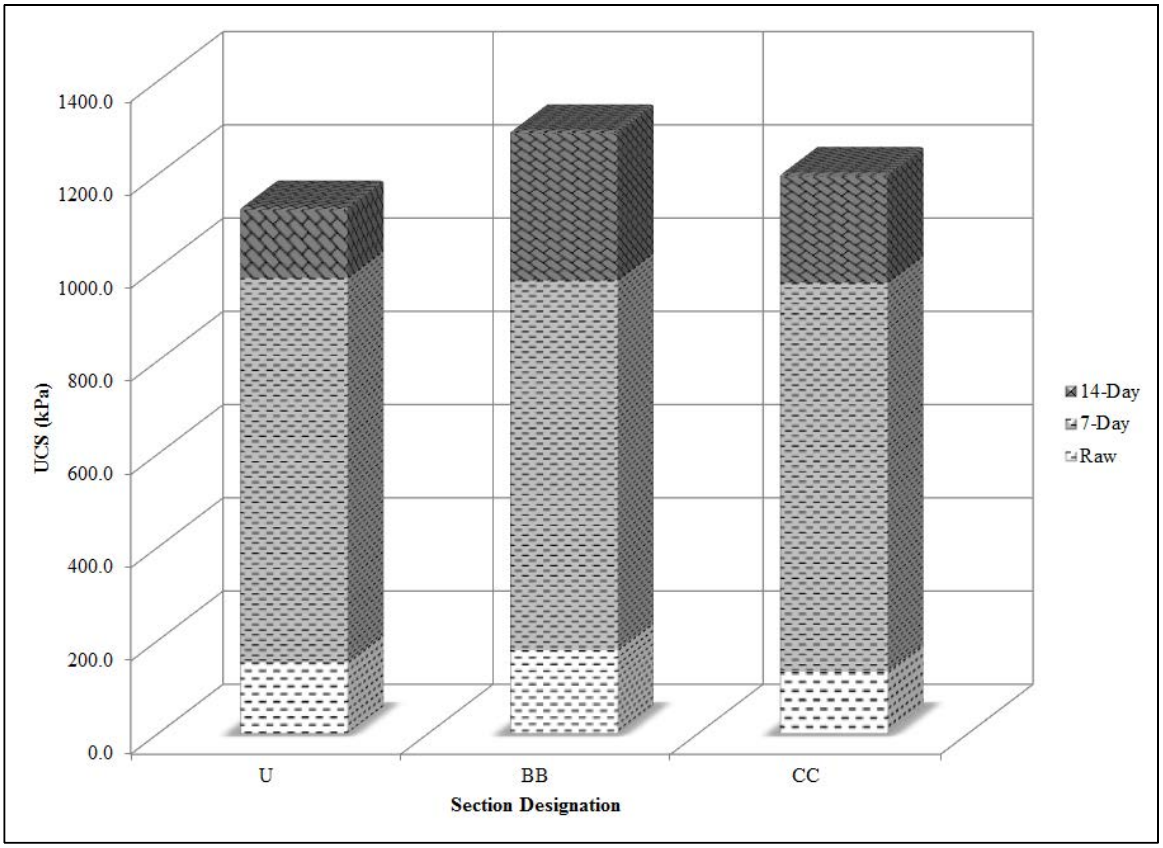

Figure 4.22 UCS values of the subgrade soils and the cement treated soils.

4.5.2 Indirect Tensile Tests

Resilient modulus tests are often performed on lime treated soil samples to measure the stiffness of the stabilized soil under simulated traffic loading. However, cement stabilized soils exhibit higher stiffness values than lime stabilized soils. Under axially applied repeated traffic loads, cement stabilized soils would not deform sufficiently for resilient modulus measurement. Therefore, static indirect tensile tests in accordance to ASTM D6931 were performed on soil specimens treated with cement. The results are presented in Figure 4.23. Attempt to measure the dynamic IDT was unsuccessful.

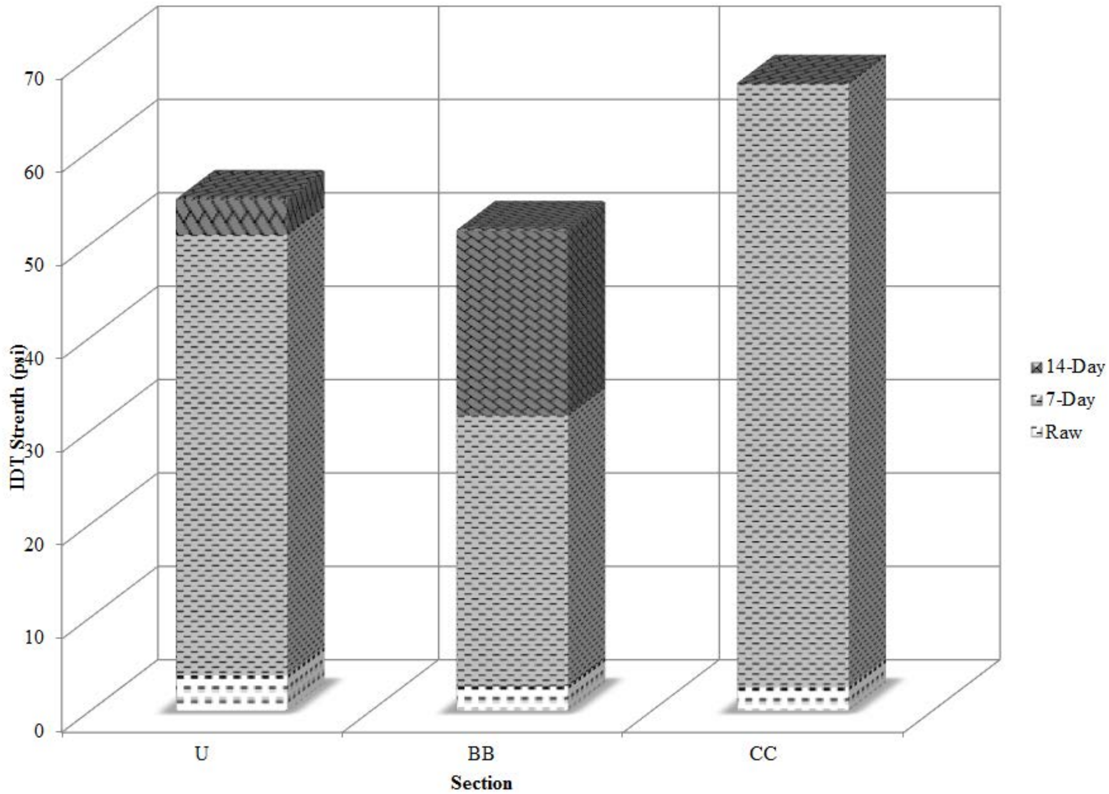

Figure 4.23 IDT values of the subgrade soils and cement treated soil specimens

4.6 Summary

This research was undertaken to evaluate the original soil properties for future stabilized subgrade and subgrade layers, as well as to determine their effectiveness of lime stabilized candidate. To recall, soils exhibiting poor qualities requiring alterations are successfully stabilized when natural soils gain at least 344.75 kPa (50 psi) in strength. Stabilization effects take place when the soil lime mix reaches a pH of 12.4. The initial strength occurs rapidly within the first 7 days and continued slowly over time through the pozzolanic reaction.

It was concluded that silty sands, which met one of the preliminary requirements for lime stabilization, was just as suitable as those soils that met both requirements. Silty sands required a minimum of 3% of lime to reach a pH of 12.4, while the other soil types (MH, SC, and ML) required a minimum of 4-7% lime. Performing the Eades and Grim pH test provides the least amount of lime necessary to produce stabilization effects. However for unconfined compression samples higher lime contents than obtained with pH test were used. The sampling locations of lime stabilized samples were verified by unconfined compression testing. All sensor locations qualified as lime stabilized samples for both the 6% lime content and the field lime content. In compression strength, silty sands surpassed the strength of the inorganic silt by at least 197% for the field lime content and 141% for the 6% lime content. In contrast to compression strength, the inorganic silt performed better in its untreated state by 157% for resilient modulus as opposed to the silty sands. When lime was added to the soil, the inorganic silt still performed the best, and was at least 121% higher than that of silty sands with the highest fines. The other silty sands produced stresses ranging from 137,900 to 186,165 kPa (20,000 to 27,000 psi) at confining pressures of 41.37 kPa (6 psi).

Most of the soil samples collected from the cement test section can be classified sand (SM) or A-4. The values of the 7-day UCS for the cement treated soils were slightly less than the NCDOT specified minimum value of 1378.95 kPa (200 psi). Attempts to conduct cyclic IDT on the cement treated specimens were unsuccessful as no standard or calibrated method for such a test exist.

CHAPTER 5 FIELD IMPLEMENTATION AND TESTING OF TEST SECTIONS

5.1 Introduction

This chapter describes the field testing component of this project, which was carried out at a test site constructed with various types of deep stabilization of the subgrade. Together with Chapter 4 (Laboratory program) these chapters constitute a summary of the experimental component of this project

5.2 General Description of the Test Sections

In coordination with NCDOT a test section was selected for this project. The section was located along the northbound lane of new Highway NC 16 bypass (between Station 247+00 and 266+42). A general location map of the test site is shown in Figure 5.1 (a more detailed map was presented in Figure 4.1 of the preceding chapter).

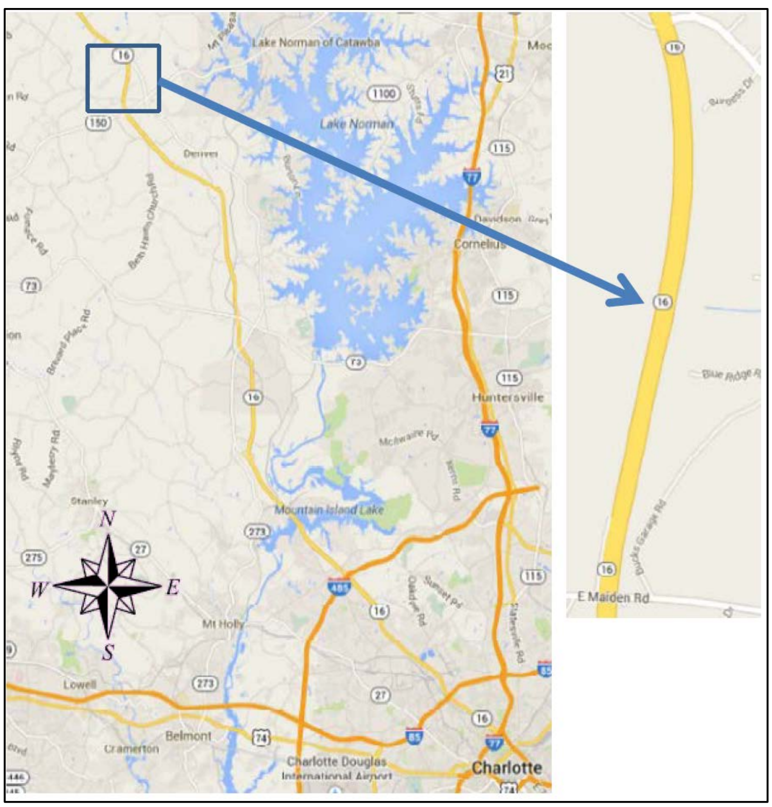

Figure 5.1 Location map of test section of this project

General description of the geology and geotechnical conditions of the site is presented at the beginning of Chapter 4. The design pavement structure for this project consisted of an HMA layer of 180 mm (7.09 in.), which in turn consisted of 80 mm S9.5C underlain by 100 mm I19.0C HMA mix types. The HMA layer was underlain by an aggregate base course (ABC) base of 200 mm (8 in.) and below the ABC layer, a chemically stabilized subgrade layer. Two chemically stabilized test sections were constructed in this study, one involving lime stabilized subgrade and the other section used cement as the stabilizing chemical additive. The HMA and base layers of all the test sections were constructed to the same specifications while the thicknesses of the stabilized subgrade were varied. For the control sections at the test sites, the stabilized subgrade layers were 200 mm (8 in.) at the lime section and 180 mm (7 in.) at the cement section, in accordance with the current NCDOT practices. The deep layers of subgrade stabilization at the test sections are described in the following subsections.

5.2.1 Lime stabilized test sections

Construction of the lime stabilized test sections took place from July 14-15, 2010 between Stations 247+00 and 255+52 of the northbound lanes as shown schematically in Figure 5.2 (only the stabilized subgrade layers are shown). As shown in this figure, the control sections (Lime 1 and Lime 4) involved an 200 mm (8 in.) depth of stabilization located from Station 247+00 to 250+48 (Lime 1) and from Station 254+57 to 255+52 (Lime 4). Section Lime 2 involved a 305 mm (12 in.) stabilization depth and was located from Station 250+48 to 252+42. Test section Lime 3 was located from Station 252+42 to 254+57 and involved lime stabilization with a thickness of 406 mm (16 in.).

The lime was applied to the subgrade soil at a rate of 15 kg/m^2 (3.07 psf) per every 200 mm (8 in.) depth of subgrade stabilization, i.e., for the control test sections of Lime 1 and Lime 4. For the 300 mm (12 in.) deep stabilized subgrade test section (Lime 2) the lime dosage used was 22.5 kg/m^2 (4.61 psf), and for the 400 mm (16 in.) deep stabilized subgrade test section (Lime 3) the application rate was 30 kg/m^2 (6.14 psf). The lime was delivered in slurry form using a spreader truck regulated to apply the specified rates as shown in Figure 5.3

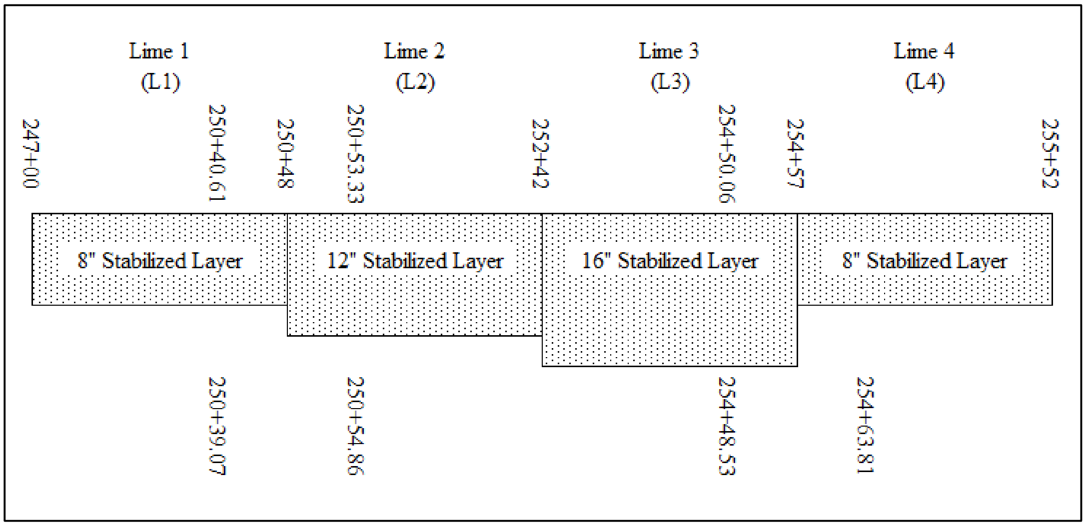

Figure 5.2 Schematic showing the location of the lime stabilized test sections

Figure 5.3 Truck spreading lime slurry for stabilization

After the appropriate amount of lime was placed for each test section, a soil reclaimer machine, as the one shown in Figure 5.4, was used to mix and homogenize the soil and lime together to the specified depth (depths as per Figure 5.2).

When mixing was complete, the test section was left to mellow for a period of 48 hours. The soil reclaimer remixed the soil after the mellowing period of 48 hours. Compaction was achieved with a sheep's-foot roller making one pass per roller width per inch of stabilization depth. In other words for the standard 200 mm (8in.) stabilized layer eight passes per roller width were used. For Test Section Lime 3, a total of sixteen passes per roller width were used given the 400 mm (16in.) lime stabilized thickness for this test section. After sheep foot roller compaction four passes per roller width were carried out using a smooth drum roller compactor. The compacted layer was then graded to the desired final grade line. Tack coat was applied over the entire roadway surface to seal the molding moisture in the stabilized layer and allowed to cure for seven days.

Figure 5.4 Machine mixing lime into subgrade soil

5.2.2 Cement stabilized test sections

The cement stabilized test sections were constructed from August 2-3, 2010 between Stations 258+26 and 266+42 in the northbound lanes of Highway NC16. The location of the different cement test sections are shown in Figure 5.5 (only the subgrade layers are shown).

As shown in Figure 5.5, the control sections (Cement 1 and Cement 4) involved a 175 mm (7 in.) depth of stabilization located from Stations 258+26 to 260+29 (Cement 1) and from Stations 264+39.5 to 266+42 (Cement 4). Section Cement 2 used a 250 mm (10 in.) cement subgrade stabilization thickness and was located from Stations 260+29 to 262+34. Test section Cement 3 was located from Stations 262+34 to 2264+39.5 and involved subgrade cement stabilization with a thickness of 356 mm (14 in.).

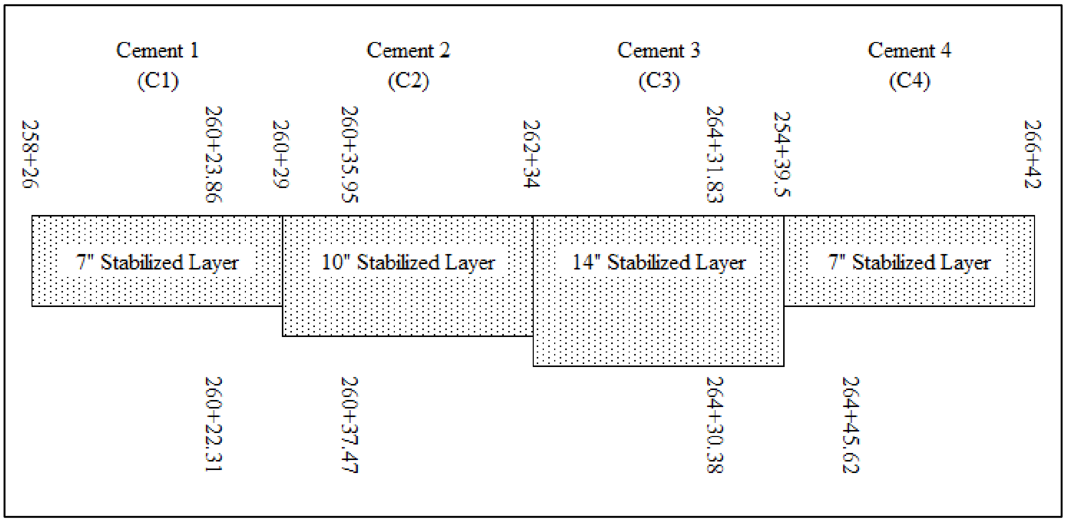

Figure 5.5 Schematic showing the location of the cement stabilized test sections

Dry form of cement was applied at a dosage rate of 25 kg/m2 (5.12 psf) per every 175 mm (7 in.) depth of subgrade stabilization (i.e., the control 175 mm test section of cement stabilized layer used a rate of 25 kg/m2, the 254 mm deep stabilized subgrade test section layer used a rate of 35.7 kg/m2 (7.31 psf), and for the 356 mm deep stabilized subgrade test section a rate of 50 kg/m2 (10.24 psf) was used. The cement used was a Portland Cement, Type I. A photo showing the spreading of the cement is shown in Figure 5.6.

Mixing of the cement, water, and subgrade soil to the specified depth of the test section was achieved using a soil reclaimer which was pulled by a water truck as shown in Figure 5.7. Immediately after mixing, a sheep's-foot roller was used to compact the soil-cement subgrade mixture. Similarly to the lime subgrade stabilization, one pass per roller width per inch of stabilization was used for all the cement stabilized test sections. In other words, seven passes per roller width for the 175 mm (7 in.) standard cement stabilized test sections was used for Sections Cement 1 and 4. For Section Cement 3, a total of fourteen passes per roller width was specified for the 356 mm (14 in.) deep cement stabilized section. After compaction with the sheep foot roller 4 passes of a smooth drum roller were applied to smooth the surface and finalize the compaction process. Grading operations were undertaken after the compaction to finish the stabilized layer to final grade line. Tack coat was applied to seal and cure the stabilized layer for a period of seven days before the ABC stone base was placed.

5.3 Sampling and Quality Control of Test Sections during Stabilization

The objectives of field sampling of the chemically stabilized subgrade test sections are to provide quality control and assurance of the field stabilization process, and to determine the differences between field and lab stabilization of the soils. In order to achieve these objectives, three forms of field sampling and testing were conducted at several stations of the stabilized test sections. First, a set of samples were collected and prepared on site immediately after final mixing of stabilized soils and cured for 7 days to determine unconfined compressive strength (UCS) gain as a result of the stabilizing agent. The data provide quality control data of field stabilization process. Another set of samples were also collected by a member of the NCDOT Geopavement Unit to determine UCS values for quality control. Finally, in addition to the UCS sampling, an NCDOT certified division inspector completed depth verification and density checks for quality control.

Figure 5.6 Cement truck with spreading machine

Figure 5.7 Mixing machine with water truck attached

5.3.1 Quality Control and Unconfined Compressive Strength (UCS) Testing

Field Compaction Quality Control

In accordance with NCDOT practice, a certified inspector performed the moisture content and density tests of the stabilized layers after final compaction. By completing a density test in accordance with ASTM D2167, “Standard Test Method for density and unit weight of soil in place by the Rubber Balloon Method”, the inspector was able to determine the percent of maximum dry density attained during the compaction. NCDOT specifications state that chemically treated soil must be compacted to 97% of maximum dry density as determined in accordance with AASHTO T-99. The air pressure specified by the NCDOT Conventional Density Testing Manual was 27.58 kPa (4 psi). The hole used for testing measured 100 mm (4 in.) in diameter by 150 mm (6 in.) deep.

The last quality control test to be completed was checking the moisture content of the stabilized layer. After completing the density test using the balloon method, the soil removed from the test hole was pulverized and compacted into a mold in accordance with AASHTO T-99. 300 grams (0.66 lb) from the compacted sample were taken and placed in a pan on a burner to dry the soil and obtain the dry soil mass. NCDOT specifications state that the moisture content during compaction shall be at optimum ± 2%. These tests were completed by an NCDOT inspector on site but being that the values passed the recommended NCDOT limits they were only recorded as meeting specification.

However, samples were collected by the UNCC research team for moisture content determination at UNC Charlotte laboratory. The samples were placed in zip-lock bags, stored in a cooler, and transported to the lab for moisture content determination. These values were compared to the optimum moisture content values for each section based on NCDOT's preliminary geotechnical evaluation of the project site (Table 5.1).

Stabilized Depth Verification Quality Control

In order to determine the effective depth of stabilization, an NCDOT certified inspector augured a hole approximately 25.4 mm (1 in.) deeper than the thickness of the stabilized layer (i.e., 230 mm in the 200 mm lime stabilized test section). After auguring was complete, an indicator compound, phenolphthalein, was slowly poured into the hole. Phenolphthalein is typically clear but turns pink when it comes in contact with some chemical additives including lime and cement. The depth of the color change line was recorded as the depth of the stabilized layer. The depth of stabilization shall be no greater than 25.4 mm (1.0 in.) or less than 12.7 mm (0.5 in.) of the specified value according to the NCDOT Standard Specifications for Roads and Structures Section 501-11 (NCDOT, 2006). If the section was found to be more than 12.7 mm (0.5 in.) less than the specification, the section would have to be replaced with lime treated soil having the required thickness at no cost to NCDOT. In accordance with the NCDOT Specifications for Roads and Structures Section 501-11 depth verification tests were performed at random intervals of no more than 152.4 m (500 ft.).

Being that the values met the recommended NCDOT limits they were only recorded as such. Although the stabilized thickness may be verified through this method, it is only an indication of mixing depth but not a verification of adequate compaction at that depth.

Table 5.1: Moisture Contents at Time of Compaction versus OMC

Location		Field compaction moisture content (w%)	OMC (w%)
Test section	Station		
Lime 1 (8” Stabilized)	248+33.31	11.65	20.2
	248+86.65	12.67	
	249+50.00	16.86	
	250+39.37	16.82	
Lime 2 (12” Stabilized)	250+55.16	12.14	20.2
	251+00.00	14.12	
	251+45.98	13.56	
	252+00.00	14.37	
Lime 3 (16” Stabilized)	252+60.03	28.03	20.2
	253+13.37	27.38	
	253+50.00	28.93	19.2
	254+46.26	27.59	
Lime 4 (8” Stabilized)	254+65.46	24.77	19.2
	255+00.00	21.43	
	255+65.23	18.58	
	255+85.43	20.29	
Cement 1 (7” Stabilized)	258+75.48	14.58	18.0
	259+21.20	16.24	
	259+66.92	14.78	
	260+33.38	12.32	
Cement 2 (10” Stabilized)	260+36.10	14.21	18.0
	260+55.26	15.87	
	261+00.00	15.15	
	261 +67.50	16.87	
Cement 3 (14” Stabilized)	262+8.28	7.00	18.0
	263+17.50	9.72	
	263+57.37	10.01	
	264+30.38	9.75	
Cement 4 (7” Stabilized)	264+45.62	8.52	18.0
	264+83.83	10.37	
	265+13.76	10.49	
	265+61.69	9.76	

5.3.2 Unconfined Compressive Strength (UCS) Testing

Samples were collected at four different locations within each subsection of the lime and cement test sections totaling thirty-two different collection locations for the chemically stabilized test sections after final mixing of the stabilizing agent into the subgrade soils. The samples were sieved through a No. 4 sieve prior to compacting in three standard Proctor mold samples per sampling location in accordance with AASHTO T-99. Extruded samples were placed in a zip-lock bag with a moist sponge, placed in cool chambers and transported back to the laboratory for curing in environmental chambers a temperature of 21° C (70° F) and 100% humidity at UNC Charlotte. Figures 5.8 and 5.9 show the field sieving process performed to prepare the stabilized soil mixture and the sample compaction of UCS specimens in the field. NCDOT also collected bulk samples and prepared them on site at the same time as the UNC Charlotte research team. The samples prepared by NCDOT's Geopavement Unit personnel were cured in the molds and tested at the Materials and Testing Unit in Raleigh, North Carolina.

When lime or cement is used for soil stabilization in the state of North Carolina, NCDOT has specified requirements for minimum unconfined compressive strength. For lime stabilized soils the minimum unconfined compressive strength after seven days of curing is 413.69 kPa (60 psi). For cement treated soils the minimum unconfined compressive strength after seven days of curing is 1378.95 kPa (200 psi). These values have been determined by NCDOT to be equivalent to a structural number (SN) of one for eight inches of lime stabilization and seven inches of cement stabilization. All samples were produced in accordance with AASHTO T-99.

The UCS values of the samples collected during field stabilization process are compared with the natural soil strength samples to determine the strength gain attributed to chemical stabilization (Table 5.2). Some locations do not have natural soil strength data as the soil sampling for laboratory testing was completed over one year prior to the commencement of construction activities on site resulting in some of the constructed test sections not overlapping the sampling locations. There is also limited data for laboratory stabilized soil samples as these were completed specifically for only selected locations.

Figure 5.8 Sieving the material for compaction samples

Figure 5.9 Compacting a UCS sample in the field

Table 5.2: UCS of Field Stabilized Samples Compared to the Subgrade Soil Strength

Location: Test section	Location: Station	Laboratory Natural Soil Strength, kPa (psi)	UNCC Strength of Field Stabilized Soil, kPa (psi) N=3	NCDOT Field Stabilized Soil Strength, kPa (psi) N = 1
Lime 1 (8” Stabilized)	248+33.31	206.2 (29.9)	390.2 ±.56.1 (56.6 ± 8.1)	-
	248+86.65	200.4 (29.07)	479.9 ± 71.5 (69.6 ± 10.4)	-
	249+50	199.5 (28.93)	353.0 ± 186.0 (51.2 ± 27.0)	256.5 (37.2)
	250+39.37	110.8 (16.07)	692.2 ± 6.1 (100.4 ± 0.9)	668.8 (97.0)
Lime 2 (12” Stabilized)	250+55.16	185.7 (26.93)	672.9 ± 23.7 (97.6 ± 3.4)	-
	251+00	-	663.3 ± 106.7 (96.2 ± 15.5)	599.8 (87.0)
	251+45.98	257.4 (37.33)	475.0 ± 49.3 (68.9 ± 7.2)	580.5 (84.2)
	252+00	133.4 (19.35)	550.2 ± 31.8 (79.8 ± 4.6)	496.4 (72.0)
Lime 3 (16” Stabilized)	252+60.03	226.1 (32.8)	460.6 ± 51.0 (66.8 ± 7.4)	866.0 (125.6)
	253+13.37	289.4 (41.97)	522.6 ± 30.6 (66.8 ± 7.4)	-
	253+50	185.1 (26.85)	511.6 ± 99.9 (74.2 ± 14.5)	1147.3 (166.4)
	254+46.26	-	337.2 ± 45.3 (48.9 ± 6.6)	-
Lime 4 (8” Stabilized)	254+65.46	136.2 (18.3)	370.9 ± 49.6 (58.3 ± 7.2)	-
	255+00	-	433.0 ± 31.2 (62.8 ± 4.5)	491.6 (71.3)
	255+65.23	-	402.0 ± 73.1 (58.3 ± 10.6)	-
	255+85.43	-	271.7 ± 15.1 (39.4 ± 2.2)	-
Cement 1 (7” Stabilized)	258+75.48	129.6 (18.8)	3374.6 ± 585.6 (489.5 ± 84.9)	2513.1 (364.5)
	259+21.20	160.6 (23.3)	3396.8 ± 447.5 (492.7 ± 64.9)	2840.6 (412.0)
	259+66.92	156.5 (22.7)	900.5 ± 88.5 (130.6 ± 12.8)	2845.5 (412.7)
	260+33.38	-	-	2614.5 (379.2)
Cement 2 (10” Stabilized)	260+36.10	229.6 (33.3)	2416.6 ± 36.7 (350.5 ± 5.3)	2078.8 (301.5)
	260+55.26	86.9 (12.6)	1915.5 ± 62.4 (277.8 ± 9.0)	1572.7 (228.1)
	261+00	201.3 (29.2)	1507.9 ± 115.6 (218.7 ± 16.8)	1277.6 (185.3)
	261+67.50	160.0 (23.2)	3257.6 ± 148.9 (472.5 ± 21.6)	3139.9 (455.4)
Cement 3 (14” Stabilized)	262+8.28	-	1244.6 ± 51.6 (180.5 ± 7.5)	1370.7 (198.8)
	263 +17.50	192.4 (27.9)	1632.0 ± 68.9 (236.7 ± 10.0)	1978.8 (287.0)
	263+57.37	95.1 (13.8)	1666.7 ± 33.2 (241.7 ± 4.8)	1879.5 (272.6)
	264+30.38	-	2221.0 ± 360.0 (322.1 ± 52.2)	1885.7 (273.5)
Cement 4 (7” Stabilized)	264+45.62	134.4 (19.5)	2124.7 ± 21.1 (308.2 ± 3.1)	-
	264+83.83	-	898.8 ± 20.8 (130.4 ± 3.0)	1965.0 (285.0)
	265+13.76	212.4 (30.8)	1087.6 ± 212.6 (157.7 ± 30.8)	2176.0 (315.6)
	265+61.69	200.6 (29.1)	925.0 ± 115.5 (134.2 ± 16.8)	2416.6 (350.5)

5.4 Field Testing of Stabilized Test Sections

This section presents the key piece of the field testing component of this project. In order to assess the improvement of the stabilized layers two types of field measurements were performed. Dynamic Cone Penetration (DCP) testing was performed to measure the stiffness/structural strength of the base, stabilized subgrade, and subgrade layers and to assess the effectiveness of the compaction of the deep subgrade stabilization layers. Falling weight deflectometer (FWD) testing was conducted to determine the average layer moduli of the stabilized layers and monitor any potential changes in strength due to deep subgrade stabilization. The details of the field testing and data analysis are presented in the following subsections.

5.4.1 Dynamic Cone Penetrometer (DCP) Testing

Dynamic cone penetrometer (DCP) field tests were carried at various locations within the different test sections. The tests were carried out in general accordance with ASTM D6951. The DCP equipment used is shown schematically in Figure 5.10.

DCP testing was performed at the project site over a period of 4 days: August 31, September 3, 8 and 9, 2010. Four different locations were tested within each subsection of the lime and cement test sections. The DCP locations were selected to be adjacent to the location of sampling for UCS testing. At the time of the test, the base layer had been placed, but neither the intermediate nor the surface HMA layers had been placed. All testing was completed in the right lane of the northbound direction of travel. At each location, three DCP tests were conducted approximately 300 mm (12 in.) apart. A total of 96 DCP tests were completed across both lime and cement test sections. Figure 5.11 shows a photo of the DCP test being performed.

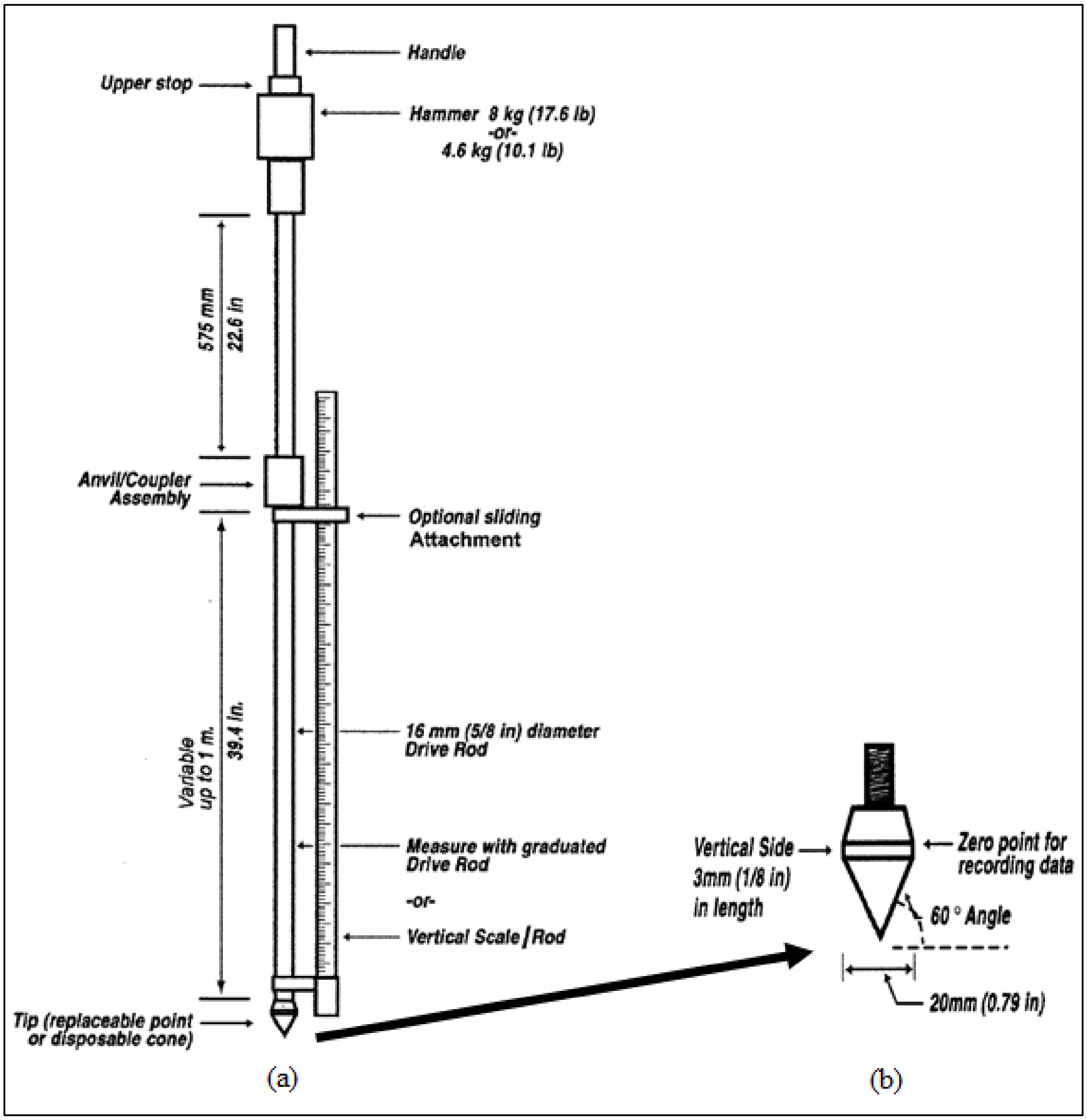

Figure 5.10 (a) Schematic of DCP testing equipment, (b) DCP cone diagram (ASTM D6951)

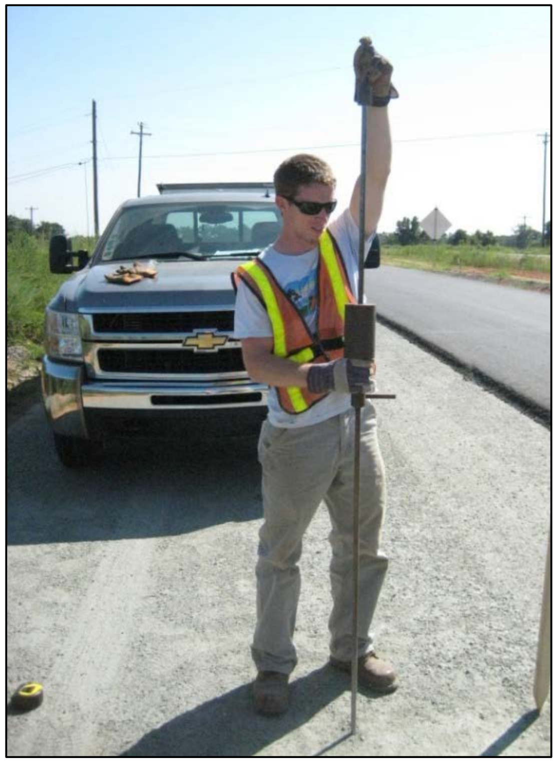

Figure 5.11 Performing DCP testing

5.4. 2 Falling Weight Deflection (FWD) Testing

FWD is a widely used non-destructive pavement test to determine the structural properties of each layer in a pavement structure. The testing equipment is usually trailer mounted and can be towed by any vehicle with a tow hitch. A circular plate measuring 300 mm (12 in.) in diameter is used to apply a load to the pavement surface determined by the user. A load frame mounted above the plate allows for a range of load applications capable of simulating different types of vehicles. A series of geophones are located on a beam set longitudinally to the trailer. The sensors contact the ground and measure the deflection of the pavement surface during the pulse loading. The geophones are adjustable but NCDOT uses standard distances of 0 mm (0 in), 203 mm (8 in), 305 mm (12 in), 406 mm (24 in), 609 mm (36 in), 812 mm (48 in) and 1524 mm (60 in) from the center of the load plate. The testing equipment and personnel were provided by the NCDOT Pavement Management Unit based in Statesville, NC. The test equipment used was a Dynatest Model 8000 Falling Weight Deflectometer and is presented in Figure 5.12. FWD testing was performed on three occasions to obtain data during different seasons and before the HMA layers were laid. Testing was performed on August 31, 2010, May 25, 2011, and October 20, 2011.

Testing in August 2010 was completed at the same time as the DCP testing. At this time, the HMA layers (surface and intermediate) had not been laid; therefore, testing was performed on top of the ABC stone base. (Figure 5.13)When testing was performed in May 2011, the HMA surface had been laid. (Figure 5.14 and 5.15) Note: Only stabilized subgrades are shown

The testing in October 2011 was conducted after the road had been opened to traffic. Special care was taken at the time of testing to ensure that the tests were conducted at the same locations

Figure 5.12 FWD testing equipment used by NCDOT

5.5 Analysis of Field Testing Data

Data collected from testing was analyzed using different methods to determine the modulus values of each layer within the pavement structure. Both DCP and FWD test data were analyzed for layer strengths. Existing correlations were used in conjunction with DCP data. Two analysis methods were used to estimate layer modulus values from FWD data, including Boussinesq equation for determination of composite modulus in accordance with NCDOT current practice and back calculation method.

5.5.1 DCP Data Analysis

5.5.1.1 Depth Verification for Quality Control

In order to determine the effective depth of stabilization, an NCDOT certified inspector augured a hole approximately 1 inch deeper than the thickness of the stabilized layer (i.e., 9 inches in the 8 inch lime stabilized test section). After auguring was complete, an indicator compound, phenolphthalein, was slowly poured into the hole. Phenolphthalein is typically clear but turns pink when it comes in contact with basic substances including lime and cement. When the solution changed colors, the depth to the color change line was recorded as the depth of the stabilized layer. The depth of stabilization shall be no greater than 1.0 inch or less than 0.5 inch of the specified value according to the NCDOT Standard Specifications for Roads and Structures Section 501-11. If the section was found to be more than 0.5 inch shallower than specification, the section would have to be replaced with lime treated soil having the required thickness at no cost to NCDOT. In accordance with the NCDOT Specifications for Roads and Structures Section 501-11 depth verification tests were performed at random intervals of no more than 500 feet. These tests were completed on site by an NCDOT inspector but due to the value being within the given limits the values were not recorded. Although the stabilized thickness may be verified through this method, it is only an indication of mixing depth but not a verification of adequate compaction at that depth.

As mentioned in Chapter 4, DCP testing was completed across both lime and cement stabilized test sections in August-September 2010. Field DCP testing occurred at the lime- and cement-test sections approximately 46 and 36 days, respectively, after the stabilization process was completed. Using the data collected from this testing, the depth of the stabilized layer was verified by creating plots of depth below the surface (in millimeters) versus cumulative number of blows. By extending the trend lines from the graphical plots, the intersections of the lines correspond to the depth of the layer interfaces. Based on these interfaces, the thickness of the ABC stone base and the stabilized subgrade layers were estimated. Figure 5.13 illustrates a typical graphical plot to estimate and verify the constructed thicknesses of the base and stabilized subgrade layers using DCP data. These values were then compared to the design thicknesses for the pavement structure in each test section. All depth verification plots for all DCP tests can be found in Appendix B.

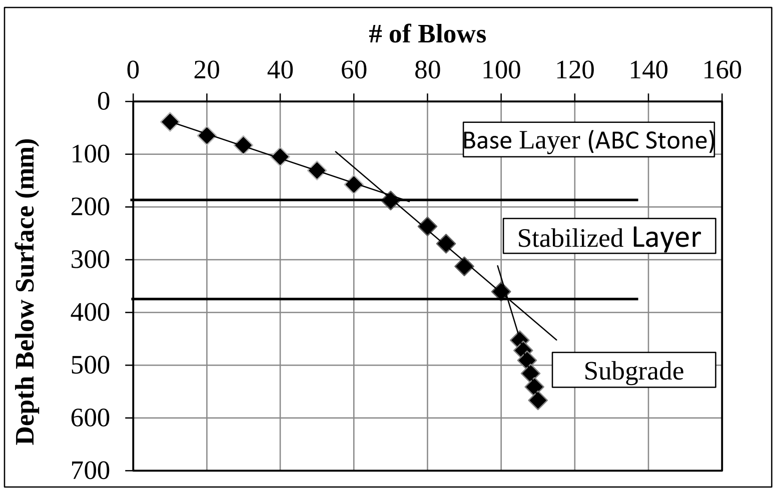

Figure 5.13 Typical depth verification plot for 200mm lime stabilized test section

5.5.1.2 DCP Correlations

DCP testing is widely used by state DOTs due to its ease of use and low cost. Since it has been used frequently in the last few decades, many correlations to geotechnical engineering properties for specific sites have been developed through research. For the purpose of this research, the DCP Index (DCPI, mm/blow) was plotted versus depth for all DCP tests. Figure 5.14 presents a typical DCPI versus depth plot taken from DCP data.

The data was analyzed using the correlation found in ASTM D6951-09 in which the DCPI is converted into CBR using Equation 5.1. After converting the data into CBR, the modulus value of each layer was estimated using Equation 5.2 (AASHTO, 1993) and

Equation 5.3 (Powell et al., 1984). The latter correlation has been heavily used in the industry, as well as in other research such as that conducted by Chen et al. (2005). Table 5.3 presents CBR values for each pavement structure layer tested with the DCP. The values were averaged from 12 DCP tests, completed at 4 different test locations within each subsection. At each test location, 3 DCP tests were performed. Note that the CBR value decreases as the stabilization depth increases in both lime and cement test sections.

Table 5.4 presents the results from analysis using current correlations between DCP and elastic modulus (E) in conjunction with test data from August through.

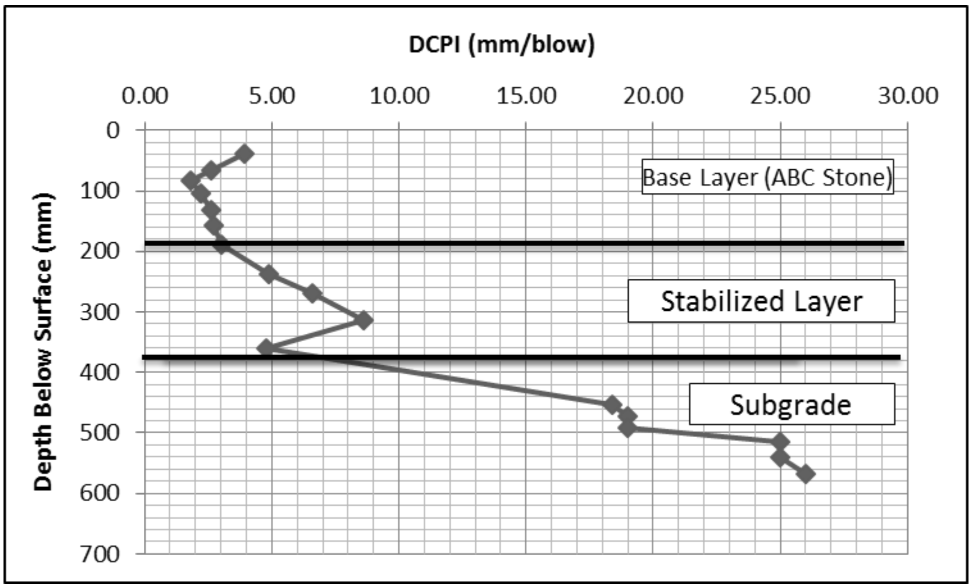

Figure 5.14 Typical plot of DCPI (mm/blow) versus depth below surface

$$CBR = \frac{292}{DCP^{1.12}} \tag{5.1}$$

$$E(psi) = 1500 * CBR \tag{5.2}$$

$$E(psi) = 2550 * CBR^{0.64} \tag{5.3}$$

Table 5.4 presents the results from analysis using current correlations between DCP and elastic modulus (E) in conjunction with test data from August through September 2010.

Table 5.3: DCP-CBR Values by Test Section

Test Section	Layer	Average CBR (%) for each test section N=12
Lime 1 (8" Stabilized)	ABC Base	88 ± 7
	Stabilized Soil	37 ± 3
	Subgrade	15 ± 3
Lime 2 (12" stabilized)	ABC Base	92 ± 6
	Stabilized Soil	35 ± 10
	Subgrade	16 ± 11
Lime 3 (16" Stabilized)	ABC Base	88 ± 7
	Stabilized Soil	22 ± 9
	Subgrade	9 ± 4
Lime 4 (8" Stabilized)	ABC Base	95 ± 5
	Stabilized Soil	51 ± 12
	Subgrade	18 ± 10
Cement 1 (7" Stabilized)	ABC Base	61 ± 17
	Stabilized Soil	48 ± 7
	Subgrade	12 ± 6
Cement 2 (10" Stabilized)	ABC Base	80 ± 12
	Stabilized Soil	68 ± 16
	Subgrade	10 ± 3
Cement 3 (14" Stabilized)	ABC Base	97 ± 5
	Stabilized Soil	63 ± 18
	Subgrade	10 ± 3
Cement 4 (7" Stabilized)	ABC Base	90 ± 9
	Stabilized Soil	67 ± 21
	Subgrade	17 ± 6

September 2010. The table presents the average value taken from 12 DCP tests performed within each subsection. The correlation by Powell et al. (1984) presented a smaller range of values across each test section as evident in the standard deviation values. Analyzing the DCP data using the formulas for CBR and modulus conversion in NCDOT Chemical Stabilization Subgrade/Base QA Field Manual (2004) result in values greater than those obtained with these two correlations (Powell et al. 1984 and AASHTO 1993). The results produced similar scatters as those of AASHTO (1993). Therefore, the results obtained using correlations from NCDOT (2004) are not presented in this report. Based on the lower standard deviation, it can be assumed that the correlation by Powell et al. (1984) more correctly represents actual layer strengths determined using DCP versus using the AASHTO 1993 correlation.

Table 5.4: DCP Correlation Results Based on Tests Performed from Aug-Sept 2010

Test Section	Layer	Based AASHTO, 1993 MPa (ksi)		Based Powell et al. (1984) MPa (ksi)	
		Modulus	Standard Deviation	Modulus	Standard Deviation
Lime 1 (8" stabilized)	ABC Base	913.6 (132.5)	40.3 (5.8)	308.9 (44.9)	8.7 (1.3)
	Stabilized soil	377.5 (54.8)	25.3 (3.7)	175.8 (25.5)	7.5 (1.1)
	Subgrade	157.7 (22.9)	28.3 (4.1)	100.5 (14.6)	11.7 (1.7)
Lime 2 (12" stabilized)	ABC Base	949.8 (137.8)	47.5 (6.9)	317.2 (46.0)	10.1 (1.5)
	Stabilized soil	363.7 (52.8)	81.3 (11.8)	171.6 (24.9)	24.5 (3.6)
	Subgrade	162.0 (23.5)	97.6 (14.2)	102.3 (14.8)	37.4 (5.4)
Lime 3 (16" stabilized)	ABC Base	908.4 (131.8)	41.8 (6.1)	308.3 (44.7)	9.0 (1.3)
	Stabilized soil	231.0 (33.5)	88.2 (12.8)	128.3 (18.6)	33.0 (4.8)
	Subgrade	95.7 (13.9)	32.9 (4.8)	73.0 (10.6)	16.2 (2.3)
Lime 4 (8" stabilized)	ABC Base	980.8 (142.3)	25.6 (3.7)	323.8 (47.0)	5.4 (0.8)
	Stabilized soil	526.6 (76.4)	128.8 (18.7)	217.5 (31.5)	34.8 (5.0)
	Subgrade	187.9 (27.3)	101.9 (14.8)	112.5 (16.3)	38.0 (5.5)
Cement 1 (7" stabilized)	ABC Base	626.6 (90.9)	172.9 (25.1)	243.1 (35.3)	42.1 (6.1)
	Stabilized soil	493.0 (71.5)	46.4 (6.7)	208.5 (30.2)	12.6 (1.8)
	Subgrade	119.8 (17.4)	53.7 (7.8)	84.8 (12.2)	22.8 (3.3)
Cement 2 (10" stabilized)	ABC Base	815.7 (118.3)	130.8 (19.0)	287.8 (41.7)	30.3 (4.4)
	Stabilized soil	672.7 (97.6)	155.2 (22.5)	254.4 (36.9)	36.6 (5.3)
	Subgrade	101.7 (14.8)	33.7 (4.9)	75.9 (11.0)	16.0 (2.3)
Cement 3 (14" stabilized)	ABC Base	999.7 (145.0)	26.8 (3.9)	327.8 (47.5)	5.7 (0.8)
	Stabilized soil	652.4 (94.6)	179.5 (26.0)	249.5 (36.2)	45.7 (6.6)
	Subgrade	100.8 (14.6)	27.3 (4.0)	75.5 (11.0)	13.5 (2.0)
Cement 4 (7" stabilized)	ABC Base	933.4 (135.4)	87.7 (12.7)	313.7 (45.5)	19.0 (2.8)
	Stabilized soil	692.1 (100.4)	190.0 (27.6)	259.1 (37.6)	47.5 (6.9)
	Subgrade	172.4 (25.0)	40.1 (5.8)	106.4 (15.4)	16.1 (2.3)

The modulus values of the ABC stone base layers for all the tests are practically equal across the test sections and the chemical additives used. The lime stabilized subgrade layers have lower modulus values and strength gained than the cement stabilized soil layers. This observation confirmed ACI (2009) findings that cement stabilized subgrade layers gain strength faster than lime stabilized soil. For the lime stabilized subgrade, it appears that the higher the stabilized subgrade thickness, lower the modulus value. This may be due to slow pozzolanic reaction and possibly less effective compaction due to deep stabilization. When compared with the typical range of values recommended in the Mechanistic-Empirical Pavement Design Guide for different soil types (Table 5.5), the values calculated using correlation by Powell et al. (1984) tend to group towards the lower range while those by AASHTO (1993) seem to cluster within the upper band of the range.

Table 5.5: Comparison of DCP Correlation Results with Subgrade M_r Values Provided in M-EPDG for Different Soil Types

Test Section	Subgrade Soil Classification	M-EPDG M_r range by soil type, MPa (ksi)	AASHTO Correlation, MPa (ksi)	Powell et al. (1984) Correlation, MPa (ksi)
Lime 1 (8" Stabilized)	SM/MH	55.2 - 227.5 (8.0 - 33.0)	129.4 -186.0 (18.8 - 27.0)	88.8 - 112.2 (9.2 - 20.0)
Lime 2 (12" Stabilized)	SM/ML	117.2 - 227.5 (17.0 - 33.0)	64.4 - 226.4 (9.3 - 37.7)	64.9 - 139.7 (9.4 - 20.2)
Lime 3 (16" Stabilized)	SM/MH	55.2 - 227.5 (8.0 - 33.0)	62.8 - 128.6 (9.1 - 18.7)	56.8 - 89.2 (8.3 - 12.9)
Lime 4 (8" Stabilized)	SC	148.2 - 213.7 (21.5 - 33.0)	86.0 - 289.8 (12.5 - 42.1)	74.5 - 150.5 (10.8 - 21.8)
Cement 1 (7" Stabilized)	SM	165.5 - 227.5 (24.0 - 33.0)	66.1 - 173.5 (9.6 - 25.2)	62.0 - 107.6 (8.9 - 15.5)
Cement 2 (10" Stabilized)	SM/ML	117.2 - 227.5 (17.0 - 33.0)	68.0 - 135.4 (9.9 - 19.7)	59.9 - 91.9 (8.7 - 13.3)
Cement 3 (14" Stabilized)	SM	165.5 - 227.5 (24.0 - 33.0)	73.5 - 128.1 (10.6 - 18.6)	62.0 - 89.0 (9.0 - 13.0)
Cement 4 (7" Stabilized)	SM/ML	117.2 - 227.5 (17.0 - 33.0)	132.3 - 212.5 (19.2 - 30.8)	90.3 - 122.5 (13.1 - 17.7)

5.5.2 FWD Data Analysis

5.5.2.1 Suitability of FWD Data for Analysis

The data from all three test periods were plotted to determine if the data sets were suitable for analysis by available backcalculation methods. A data set was deemed reasonable if the deflection basin produced a curve with smooth transition curvature. Figure 5.15 presents a comparison among deflection basins as recorded during different testing periods. Based on these plots, the data from August 2010 was deemed unsuitable for backcalculation due to the irregular shape of the deflection basins. When testing was conducted in August 2010, the HMA layer had not yet been placed and larger loading plate was not used which contributed to significant deflection the pavement structure at loading point. Based on the smooth bowl shaped deflection basins of the data from May and October of 2011, they were deemed suitable for analysis using the backcalculation method.

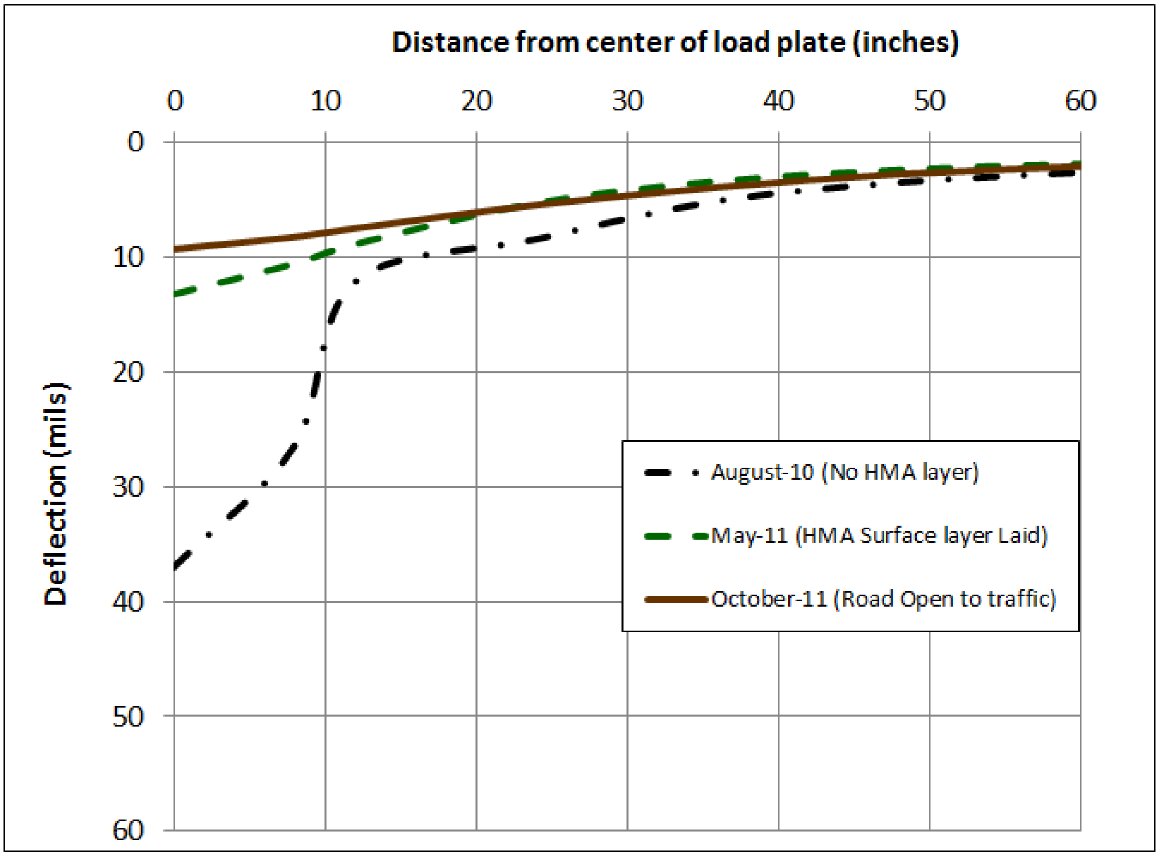

Figure 5.15 Typical deflection basin plot based on season

5.5.2.2 FWD Deflection Basin Comparison

Plots were created showing the comparison between the deflection basins across the lime and cement test sections for both May and October 2011 test dates. The plots are presented in Figure 5.16 through Figure 5.19. By comparing deflection basins across the entire test section, the strength difference between sections was easily visible. Table 5.6 presents the range of ambient and pavement surface temperatures for each test section from both May 2011 and October 2011 test dates. The deflection basins presented for comparison were averages of the third FWD drop from all test locations within each subsection. As the stabilized depth increased, the FWD maximum deflection decreased which indicated that the pavement structure with a thicker stabilized subgrade soil layer exhibited a higher strength.

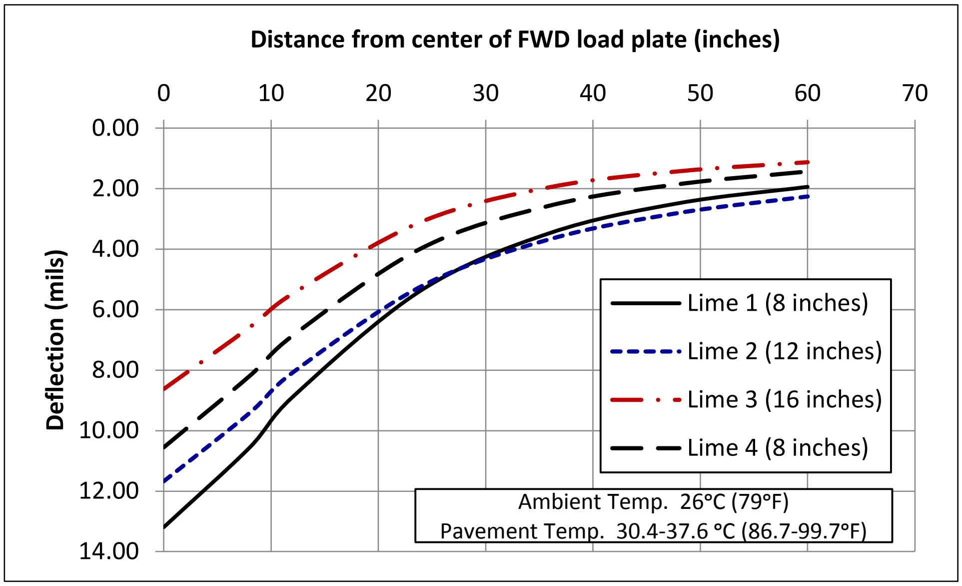

Figure 5.16 Deflection basin comparison – May 2011, lime test section

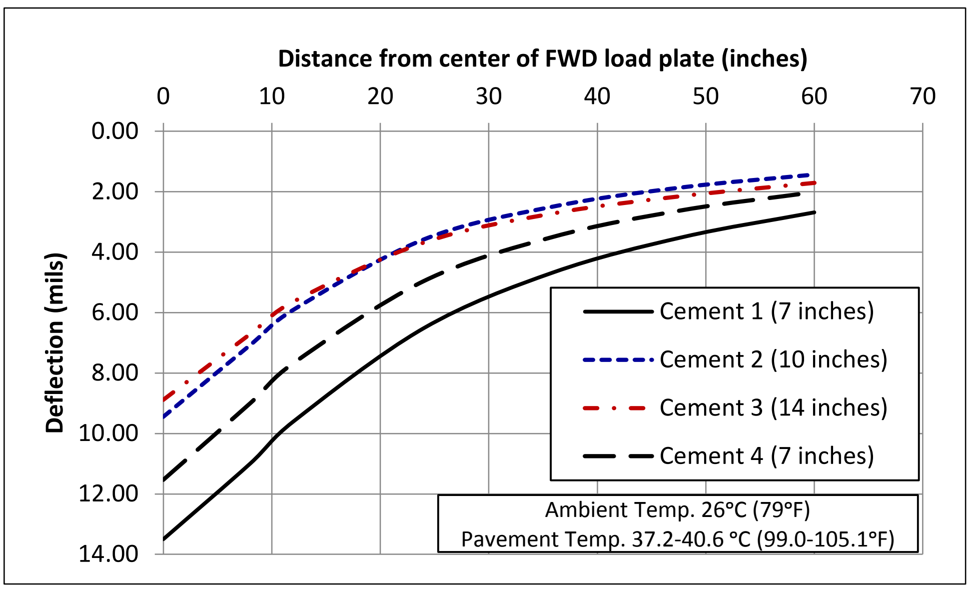

Figure 5.17 Deflection basin comparison – May 2011, cement test section

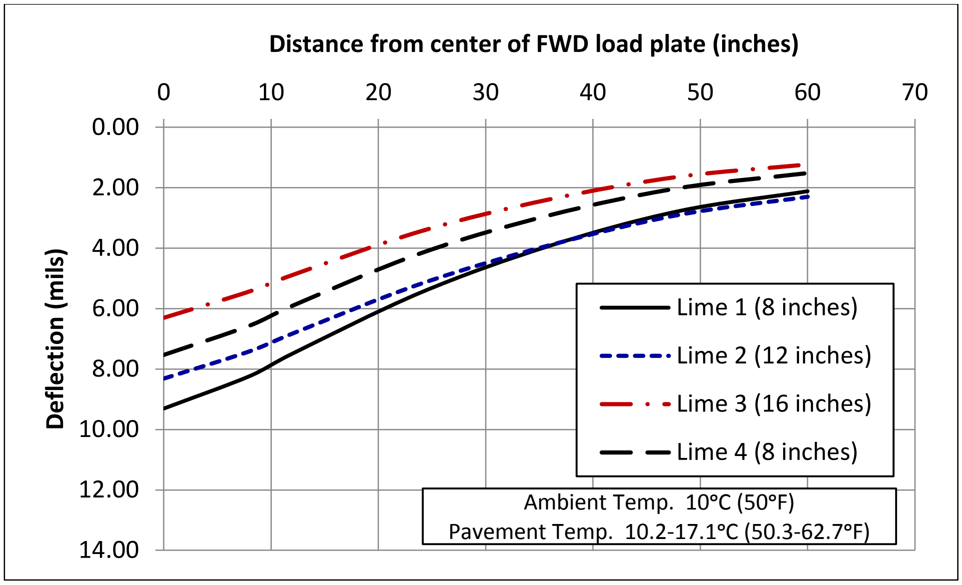

Figure 5.18 Deflection basin comparison – October 2011, lime test section

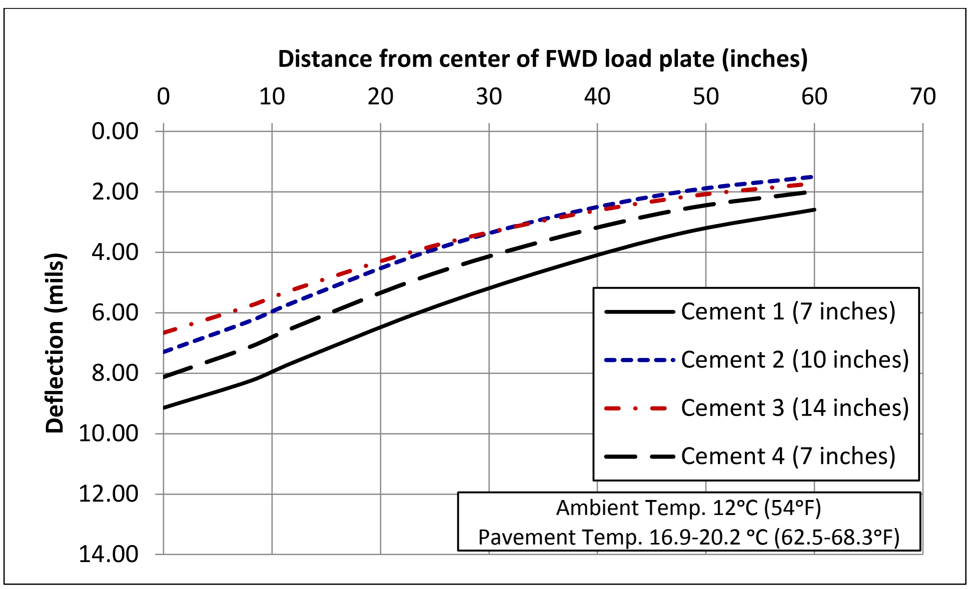

Figure 5.19 Deflection basin comparison – October 2011, cement test section

Table 5.6: Ambient and pavement surface temperature during FWD testing performed in May and October 2011

Test Date	Test Section	Ambient Temperature °C (°F)	Pavement Surface Temperature °C (°F)
5/24/2011	Lime	26 (79)	30.4-37.6 (86.7-99.7)
5/24/2011	Cement	26 (79)	37.2-40.6 (99.0-105.1)
10/20/2011	Lime	10 (50)	10.2-17.1 (50.3-62.7)
10/20/2011	Cement	12 (54)	16.9-20.2 (62.5-68.3)

5.5.2.3 NCDOT FWD Analysis Method

The NCDOT uses FWD testing to estimate the in-situ structural stiffness/strength of pavement structures throughout the state. By using this testing method, NCDOT can optimize the rehabilitation schedule. This method uses the deflection at the center of the FWD load plate to determine a composite modulus value for the entire pavement structure, and the deflection at 915 mm (36 in.) from the center of the load plate to calculate a resilient modulus value for the subgrade soil. The theory behind this method stems from the works of Boussinesq in which a set of close formed equations for a semi-infinite linear elastic, median half-space was developed based on a point load (Stubstad, 2005). The subgrade modulus was calculated using Equation 5.4.

$$E_{subgrade} = 238.7\left(\frac{P}{36D_{36}}\right) \tag{5.4}$$

D36 (mils) is the deflection at 36 inches from the center of the load plate, P is the applied load (Ib) from the FWD load frame and $E_{subgrade}$ is the computed modulus of subgrade soil (psi).

Equation 5.5 was used to calculate the composite modulus of the entire pavement structure where P is the applied load (pounds), μ is the Poisson's ratio, r is the radius of the load plate (inches), Do (mils) is the deflection measured at the center of the load plate and Ecomp is the computed composite modulus (psi). The results for May and October 2011 testing are presented in Figures 5.20 - 5.21 and summarized in Table 5.7.

$$E_{comp} = 2\left[1000P\left(\frac{1-\mu^2}{\pi r D_0}\right)\right] \tag{5.5}$$

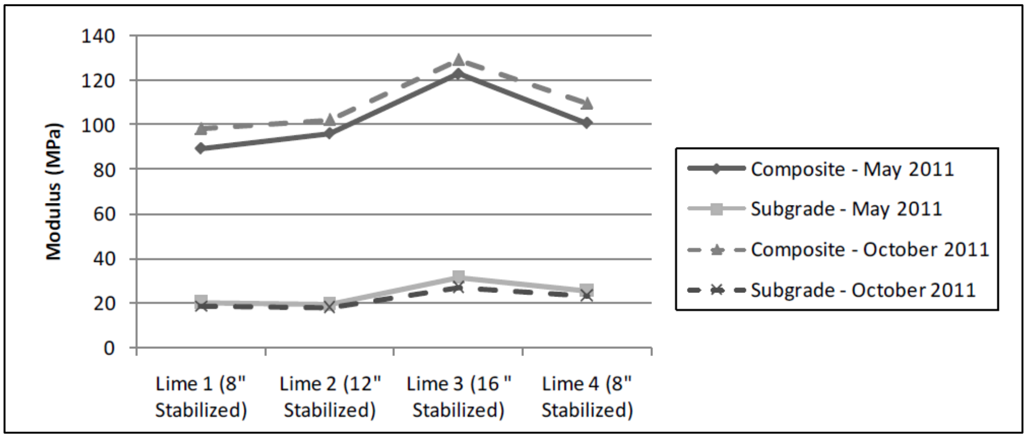

Figure 5.20 NCDOT method results for lime test section

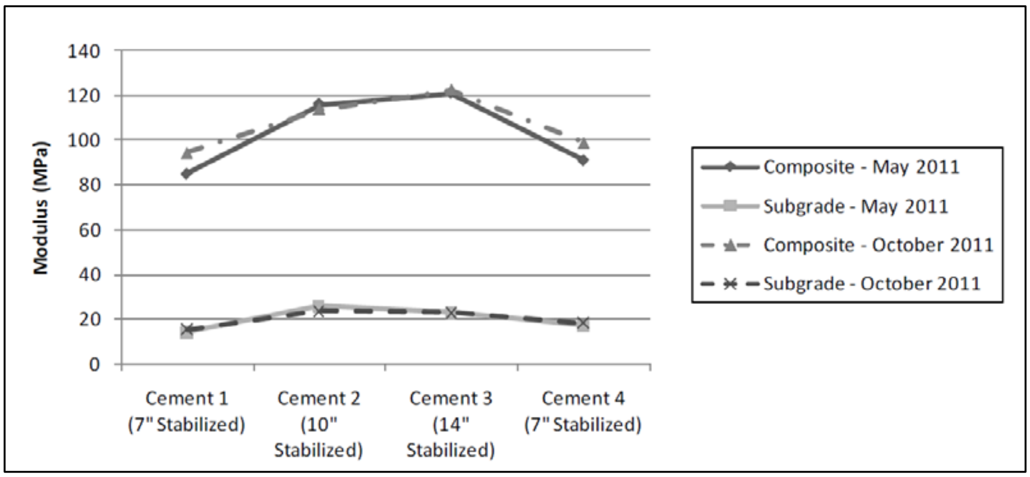

Figure 5.21 NCDOT method results for cement test section

5.5.2.4 Backcalculation Analysis Method

EVERCALC© is a back calculation software program designed by Washington State Department of Transportation (WSDOT) to estimate the elastic moduli of the different layers of a pavement structure. It is based on Waterways Engineering Station Elastic Layer Analysis (WESLEA - developed by the Waterways Experiment Station, US Army Corps of Engineers) as the layered elastic solution to backcalculate the strength modulus of each layer and a modified Augmented Gauss-Newton algorithm for optimization. The software also calculates the stresses and strains at various depths and critical points within the pavement structure.

Table 5.7: NCDOT FWD Analysis Method Results

May 2011				October 2011			
Test Section		Modulus, MPa (ksi)	Standard Deviation, kPa (ksi)	Test Section		Modulus, MPa (ksi)	Standard Deviation, kPa (ksi)
Lime 1 (8" Stabilized) N=10	Composite	616.0 (89.3)	105.8 (15.3)	Lime 1 (8" Stabilized) N=10	Composite	675.7 (98.4)	120.2 (17.4)
	Subgrade	140.1 (20.3)	40.6 (5.9)		Subgrade	128.7 (18.7)	34.1 (4.9)
Lime 2 (12" Stabilized) N=7	Composite	662.8 (96.1)	151.3 (21.9)	Lime 2 (12" Stabilized) N=7	Composite	706.8 (102.5)	138.1 (20.0)
	Subgrade	134.1 (19.5)	55.8 (8.1)		Subgrade	124.9 (18.1)	44.2 (6.4)
Lime 3 (16" Stabilized) N=7	Composite	848.2 (123.0)	52.5 (7.6)	Lime 3 (16" Stabilized) N=7	Composite	891.1 (129.2)	66.1 (9.6)
	Subgrade	218.5 (31.7)	24.7 (3.6)		Subgrade	187.9 (27.3)	28.2 (4.1)
Lime 4 (8" Stabilized) N=5	Composite	695.5 (100.9)	91.3 (13.2)	Lime 4 (8" Stabilized) N=5	Composite	756.5 (109.7)	103.0 (14.9)
	Subgrade	176.7 (25.6)	54.5 (7.9)		Subgrade	159.7 (23.2)	44.4 (6.4)
Cement 1 (7" Stabilized) N=8	Composite	633.0 (92.2)	49.3 (7.2)	Cement 1 (7" Stabilized) N=8	Composite	664.0 (96.3)	54.1 (7.8)
	Subgrade	96.1 (13.9)	12.1 (1.8)		Subgrade	101.8 (14.8)	9.8 (1.4)
Cement 2 (10" Stabilized) N=7	Composite	895.1 (129.8)	77.1 (11.2)	Cement 2 (10" Stabilized) N=7	Composite	817.7 (118.6)	73.3 (10.4)
	Subgrade	175.6 (25.5)	29.2 (4.2)		Subgrade	159.5 (23.1)	22.0 (3.2)
Cement 3 (14" Stabilized) N=8	Composite	937.9 (136.0)	116.0 (16.8)	Cement 3 (14" Stabilized) N=8	Composite	883.2 (128.1)	91.7 (13.3)
	Subgrade	155.1 (22.5)	16.8 (2.4)		Subgrade	152.5 (22.1)	16.7 (2.4)
Cement 4 (7" Stabilized) N=5	Composite	723.2 (104.9)	39.5 (5.7)	Cement 4 (7" Stabilized) N=5	Composite	698.6 (101.3)	38.1 (5.5)
	Subgrade	117.1 (17.0)	4.5(0.7)		Subgrade	120.2 (17.4)	5.0 (0.7)

EVERCALC© can only backcalculate up to five layers, ten sensors, and 12 drops per station. There must be more deflection sensors than the number of layer moduli that are to be estimated. If needed, the software can estimate the stiff layer depth and correct the asphalt moduli for temperature. These are all part of the WESLEA layered elastic theory method. There are many basic assumptions of the layered elastic theory used in EVERCALC©:

Layers are indefinitely long horizontally

Layers have uniform thickness

Bottom layer is semi-infinite in the vertical direction

Layers are composed of homogeneous, isotropic, linearly elastic materials characterized by elastic modulus and Poisson’s ratio.

The backcalculation is an inverse technique which uses the deflection basin data collected from the FWD test to determine the modulus. The field information required for the computation is the load plate radius, the number of sensors and locations, number of layers, loads for all three drops, deflections below every sensor, and for each drop, asphalt temperature, and layer thicknesses. Other information needed for each layer are the Poisson's ratio and the initial and range values for the moduli. EVERCALC© uses assumed modulus values and computes deflection values which are then compared with the actual deflections. Each unknown layer modulus is individually varied to get a new set of estimated deflections. The program performs a maximum of ten iterations to closely match the estimated and measured FWD surface deflections

ELMOD: is a product of Dynatest, the original commercial developer and largest supplier of FWD equipment. Accompanying the equipment, the company has developed a backcalculation program known as ELMOD (Evaluation of Layer Moduli and Overlay Design) to analyze the deflection basins recorded during testing.

ELMOD uses data input by the user including depths of each layer in the pavement structure, pavement and air temperature, FWD deflections as measured by the geophones, and seed (or fixed) moduli values to calculate a "theoretical" deflection basin for the given pavement structure. The "actual" deflection basin is input by the user from FWD data and is plotted against the theoretical deflection basin. The program assesses the error among the two deflection basins and adjusts the layer moduli values by approximately 10% and re-analyzes the basins. This iterative process is conducted until the error between the theoretical and actual deflection basin is reduced to a minimum.

The disadvantage of using these methods of analysis are that several pavement structures may produce the same solution. When multi-layer pavement structures (>3 layers) are analyzed, the user can reduce the error in results by providing a fixed modulus for any of the pavement layers. The depth to bedrock or stiff layer can also be adjusted to reduce the root-mean-square-error produced by running an analysis.

5.5.2.5 3-Layer Backcalculation Analysis

Backcalculation was performed using a 3-layer pavement structure for both lime and cement test sections for the two testing periods, May and October 2011. Both ELMOD and EVERCALC 5.0 backcalculation software programs were utilized for this analysis to compare the results from the two different software packages. To perform the analysis as a 3-layer pavement structure, the ABC stone base and the stabilized base for each test section were combined to create a composite base layer, much the same way as the process performed for the forward calculation analysis. Both ELMOD and EVERCALC 5.0 returned almost identical results for all test locations for both the lime and cement test sections as presented in Figure 5.22. The figure presents the comparison of results for the composite base layer (ABC stone plus stabilized subbase) in lime test section 3 (16 inches stabilized subbase). Note that the values at all test sections are very close when comparing between ELMOD and EVERCALC. The comparison graphs for all other test section layers are located in Appendix F. Table 5.8 presents the average modulus value for each of the 3 layers in the pavement structure analyzed with ELMOD and EVERCALC. The values in Table 5.8 are presented only for the May testing period as the analysis was not performed on the October 2011 data.

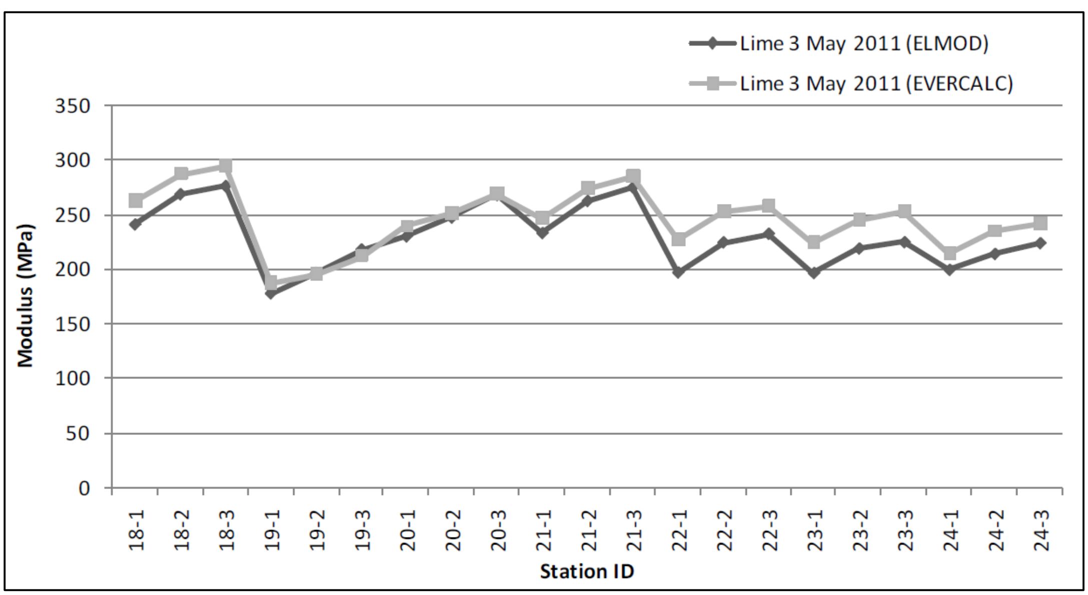

Figure 5.22 Graph of 3-layer backcalculation results (ELMOD vs. EVERCALC) for lime test section 3 for ABC/stabilized subgrade composite base layer

Table 5.8: 3-layer backcalculation result comparison (ELMOD vs. EVERCALC)

ELMOD			
	HMA Modulus (MPa)	Composite Base Layer Modulus (MPa)	Subgrade Modulus (MPa)
Lime 1	2613 ± 299	172 ± 67	172 ± 44
Lime 2	2911 ± 757	212 ± 27	159 ± 65
Lime 3	2981 ± 262	230 ± 29	260 ± 27
Lime 4	2590 ± 154	172 ± 16	213 ± 58
Cement 1	2635 ± 327	226 ± 51	115 ± 15
Cement 2	2402 ± 467	295 ± 55	207 ± 33
Cement 3	2245 ± 358	408 ± 110	173 ± 14
Cement 4	2153 ± 348	251 ± 32	140 ± 7
EVERCALC			
	HMA Modulus (MPa)	Composite Base Layer Modulus (MPa)	Subgrade Modulus (MPa)
Lime 1	2733 ± 406	189 ± 80	171 ± 43
Lime 2	3007 ± 841	227 ± 37	156 ± 64
Lime 3	3051 ± 407	245 ± 29	258 ± 25
Lime 4	2707 ± 312	187 ± 29	211 ± 57
Cement 1	3214 ± 489	207 ± 62	116 ± 15
Cement 2	2697 ± 604	295 ± 63	207 ± 33
Cement 3	2512 ± 516	403 ± 108	172 ± 13
Cement 4	2470 ± 480	251 ± 36	140 ± 8

5.5.2.6 4-Layer Backcalculation Analysis

Figures 5.23 and 5.24 present the pavement structures used for analysis in the ELMOD backcalculation software. For this backcalculation analysis method, the modulus values of the pavement layers were not fixed. The results obtained from the 4 –layer backcalculation analysis are presented in Table 5.9.

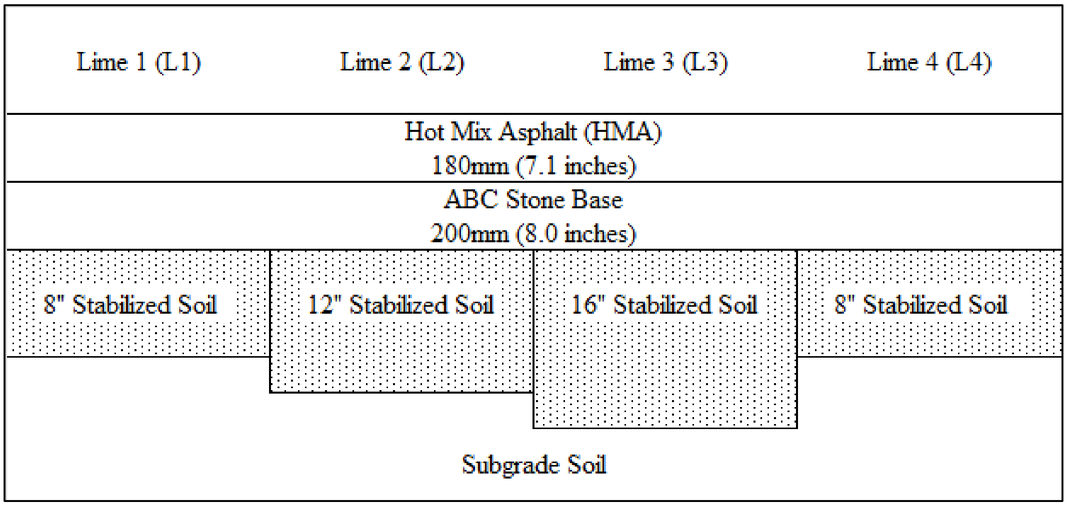

Figure 5.23 Lime test section pavement profile used in ELMOD

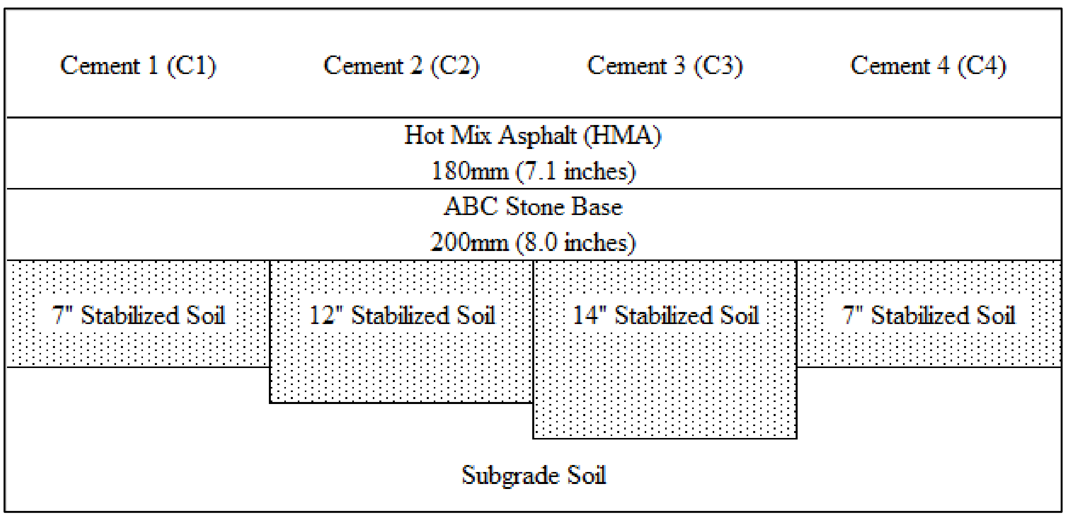

Figure 5.24 Cement test section pavement profile used in ELMOD

Table 5.9: ELMOD results for 4-layer pavement structure

May 2011								
	HMA		ABC Base		Stabilized Subgrade		Subgrade	
Test Section	Modulus, MPa (ksi)	Standard Deviation, MPa (ksi)	Modulus, MPa (ksi)	Standard Deviation, MPa (ksi)	Modulus, MPa (ksi)	Standard Deviation, MPa (ksi)	Modulus, MPa (ksi)	Standard Deviation, MPa (ksi)
Lime 1 (8" Stabilized) N=10	2280.1 (330.7)	227.9 (33.1)	276.6 (40.1)	41.2 (6.0)	207.1 (30.0)	60.8 (8.8)	156.7 (22.7)	85.4 (12.4)
Lime 2 (12" Stabilized) N=7	2594.4 (376.3)	524.2 (76.0)	274.8 (39.9)	70.3 (10.2)	300.4 (43.6)	52.8 (7.7)	142.4 (20.7)	60.4 (8.8)
Lime 3 (16" Stabilized) N=7	2667.6 (386.9)	166.7 (24.2)	324.4 (47.1)	41.3 (6.0)	272.4 (39.5)	38.5 (5.6)	301.1 (43.7)	67.9 (9.8)
Lime 4 (8" Stabilized) N=5	2254.5 (327.0)	60.1 (8.7)	288 (41.8)	50.1 (7.3)	208.3 (30.2)	45.8 (6.6)	210.6 (30.5)	85.5 (12.4)
Cement 1 (7" Stabilized) N=8	2237.8 (324.6)	227.9 (33.0)	356.4 (51.7)	41.8 (6.1)	256.4 (37.2)	69.4 (10.1)	104.2 (15.1)	17.6 (2.5)
Cement 2 (10" Stabilized) N=7	2210.4 (320.6)	282.4 (41.0)	410 (59.5)	71.1 (10.3)	386.5 (56.1)	80.7 (11.8)	194.5 (28.2)	39.5 (5.7)
Cement 3 (14" Stabilized) N=8	2325.8 (337.3)	191.8 (27.8)	391.6 (56.8)	66.2 (9.6)	608.4 (88.2)	195.3 (28.3)	185.9 (27.0)	21.7 (3.2)
Cement 4 (7" Stabilized) N=5	1969 (285.6)	159.5 (23.1)	364.7 (52.9)	45.8 (6.6)	290.9 (42.2)	118.2 (17.1)	139 (20.2)	16.6 (2.4)

October 2011								
	HMA		ABC Base		Stabilized Subgrade		Subgrade	
Test Section	Modulus,MPa (ksi)	Standard Deviation, MPa (ksi)	Modulus, MPa (ksi)	Standard Deviation, MPa (ksi)	Modulus, MPa (ksi)	Standard Deviation, MPa (ksi)	Modulus, MPa (ksi)	Standard Deviation, MPa (ksi)
Lime 1 (8" Stabilized) N=10	6,601.6 (957.5)	434.4 (63.0)	533.9 (77.4)	170.8 (24.8)	198.4 (28.8)	64.2 (9.3)	127.1 (18.4)	42.9 (6.2)
Lime 2 (12" Stabilized) N=7	7,101.1 (1,029.9)	815.0 (118.2)	626.9 (90.9)	72.7 (10.5)	174.4 (25.3)	37.8 (5.5)	133.4 (19.3)	46.2 (6.7)
Lime 3 (16" Stabilized) N=7	7,690.5 (1,115.4)	1,159.7 (168.2)	593.1 (86.0)	172.0 (24.9)	268.9 (39.0)	42.7 (6.2)	168.0 (24.4)	28.2 (4.1)
Lime 4 (8" Stabilized) N=5	6,195.0 (898.6)	265.0 (38.4)	639.1 (92.7)	117.0 (17.0)	206 (29.9)	65.0 (9.4)	134.0 (19.4)	27.1 (3.9)
Cement 1 (7" Stabilized) N=8	7,367.0 (1,068.5)	691.3 (100.3)	675.4 (98.0)	125.3 (18.2)	126.3 (18.3)	42.4 (6.2)	113.2 (16.4)	17.1 (2.5)
Cement 2 (10" Stabilized) N=7	6,241.9 (905.3)	729.4 (105.8)	846.3 (122.7)	181.5 (26.3)	207.8 (30.1)	22.4 (3.3)	126.2 (18.3)	36.9 (5.3)
Cement 3 (14" Stabilized) N=8	6,537.9 (948.2)	803.4 (116.6)	759.6 (110.2)	194.7 (28.2)	256.4 (37.2)	74.3 (10.8)	173.2 (25.1)	42.3 (6.1)
Cement 4 (7" Stabilized) N=5	6,028.2 (874.3)	568.8 (82.5)	681.1 (98.8)	117.8 (17.1)	254.9 (37.0)	83.6 (12.1)	129.0 (18.7)	22.3 (3.2)

5.5 Discussion and Summary

This chapter presented a summary of the field quality control sampling, testing, and data analysis of the lime and cement stabilized subgrade test sections. Several means including UCS sampling, DCP, and FWD were used to assess the improvement due to chemical stabilization over the natural subgrade soils of the test sections. Except for one sample, the 7-day UCS values of samples collected after mixing the lime additive at the site are equal or greater than 413.69 kPa (60 psi) in accordance with NCDOT minimum target value for quality control specimens. For the cement test sections (except for control test section (Cement 4) where the values obtained by the research team were generally lower but when combined with values obtained by NCDOT geopavement engineer on site), the UCS values were general at or greater than 1378.95 kPa (200 psi) of NCDOT minimum target value for quality control for specimens and less than the maximum 4136.85 kPa (600 psi) value.

Though NCDOT inspector on site tested and confirmed chemical stabilization to the required depths, an attempt was made by the research team to verify the thicknesses of the stabilized subgrade layers using the DCP data. The result is inconclusive considering that no undisturbed samples are taken for laboratory UCS testing. From the analysis of DCP data, the modulus values of the ABC stone base layers are practically the same for all the test sections. The chemical additive and thickness of the stabilized subgrade has no significant influence on the stiffness/strength of the compacted unbound aggregate base layer. This implies that the current standard NCDOT subgrade stabilization layer is sufficient to provide confinement of the unbound aggregate base layer. Strength values of the stabilized subgrade in the cement test sections are practically equivalent irrespective of the stabilized depth. In the lime stabilized test sections however, the thicker the stabilized subgrade layer is, lower the estimated modulus value.

Results of the composite modulus from analysis of FWD test data are consistent across the test sections (Table 5.7). The deep subgrade stabilization sections return consistently higher composite modulus values than the control test sections for all the tests. Similarly, the 3-layer analysis of the FWD data reveals that, when base and stabilized subgrade layers were combined, the composite base/subbase modulus values of the deep layers of subgrade stabilization were higher than those of the control sections. Equally, with the 4-layer pavement analysis of the FWD data of May 2011, the back calculated modulus values of deep layers of subgrade stabilization were higher than the values of the control sections. However, from the analysis of FWD data of October 2011, the modulus values of the lime stabilized subgrades were statistically the same, while for the cement test sections, the modulus values of the deep layers of subgrade stabilization were slightly higher than those of the control sections. From the back calculations of the FWD data, the HMA and the base layers exhibited slight increase in modulus values compared to the control sections.

The results obtained from Phase II of this project will be used as input in modeling the responses of the test sections under traffic load. In Chapter 6, these results will serve as input data to calculate pavement responses and predict the performance indicators from deep layers of subgrade stabilization. In Chapter 7, a simplified cost/-effectiveness analysis of the deep layers of subgrade stabilization test site studied in the project will be presented.

CHAPTER 6 PERFORMANCE PREDICTION OF DEEP SUBGRADE STABILIZATION LAYER

6.1 Background

The performance of the deep subgrade stabilization test sections studied in this project and presented in chapter 5 was predicted using the following two analysis methods:

(1) the Effective Modulus Method (NCDOT, 2000), and

(2) the MEPDG Performance Indicators (AASHTO, 2008).

Pavement improvements from deep layers of subgrade stabilization were evaluated by comparing the performance indicators of standard NCDOT subgrade stabilization pavement (control test sections) with those of deep subgrade stabilization pavement structures studied in this project. It will be recalled that four test sections per chemical additives were constructed and studied. The test site is laid out starting with the first control section, followed by deep subgrade stabilization section 1 and then deep subgrade stabilization section 2 and ending with control test section 2 (Figures 5.14 and 5.15). The control test sections 1 and 2 are designed and constructed to the current specification of NCDOT, while deep subgrade stabilization test sections 1 and 2 are composed of chemical stabilized layers approximately 1.5 and 2 times the stabilized depth of the control test section. The following sections describe, discuss, and present in detail, the analysis methods and results of the performance of the test sections studied in this project.

6.2 Performance Prediction based on Effective Modulus (E_p) Method

In this analysis method, performance improvement was based on the estimated HMA overlay thickness required for the standard NCDOT subgrade stabilization pavement structures (control sections) to attain the same structural number (SN) as the 2 deep subgrade stabilization pavement test sections studied in this project. The method, described in NCDOT (2000), involves determining the effective modulus (Ep) of the entire pavement structure, i.e. the composite modulus (Ecomp) (computed using equation 5.5), using FWD data collected from the field test sections. The effective structural number (SNeff) of each test section is estimated as follows:

$$SN_{eff} = 0.0045 * h_{comp} * E_p^{\frac{1}{3}} \qquad (6.1)$$

Where,

h_{comp} = total depth of pavement structure (inches); and,

E_p = effective modulus of pavement layer (psi).

The next step in this analysis was to determine the required overlay SN value (SN(req-ovl)) for current NCDOT subgrade stabilization pavement structure to attain the SN of a deep subgrade stabilization pavement structure. The SN(req-ovl) value was obtained as difference of the values of the SNeff for the deep subgrade stabilization pavement structure (SNeff-dp) and that of the current NCDOT subgrade stabilization pavement structure (SNeff-st):

$$SN_{(req-ovl)} = SN_{(eff-dp)} - SN_{(eff-st)} \qquad (6.2)$$

Table 6.1 presents the estimated values of (SNeff-st), and (SNeff-dp) for the Ecomp determined from FWD data obtained at the field test sections. The SN values in Table 6.1 were estimated using in Equation 6.1 the average   for May and October 2011.

$$h_{(HMA-ovl)} = \frac{SN_{(HMA-ovl)}}{a} \qquad (6.3)$$

Where:

a = 0.017/mm (0.44/in).

Since the structural number (SN) values of the deep subgrade stabilization test sections are higher than that of the control section (Table 6.1), the deep subgrade stabilization sections are expected to support more standard-axle load repetition to failure. This is a direct indication of performance improvement from deep layers of subgrade stabilization test section. In extension, deep layers of subgrade stabilization are expected to extend the pavement lives. To address the equivalency between the control test section and the deep test sections, addition of HMA overlay over the control test section is proposed. The HMA overlay thickness ($h_{(HMA\text{-}ovl)}$) required for the standard NCDOT subgrade stabilization pavement (control test sections) in order to attain same SN as the deep layer of subgrade stabilization pavement is estimated using Equation 6.3 below. The $SN_{(req\text{-}ovl)}$ values are computed from Equation 6.2 and the values are summarized in Table 6.1. NCDOT (2000) recommends a value of 0.017/mm (0.44/in) for layer coefficient (a). This value corresponds to surface and intermediate SuperPave HMA mix types.

Table 6.1: $SN_{eff\text{-}st}$ and $SN_{eff\text{-}dp}$ from Composite Modulus Values Determined for Subgrade Stabilization Test Section

Subgrade Stabilization Test Section		Total Pavement Structure Thickness, mm (in.)	May 2011	October 2011	$SN_{eff\text{-}st}$ & $SN_{eff\text{-}dp}$
Additive	Type		Composite Modulus, MPa (ksi)	Composite Modulus, MPa (ksi)	
Lime	Current NCDOT	582 (22.9)	616.0 (89.3)	675.7 (98.4)	4.77*
	Deep	683 (26.9)	662.8 (96.1)	706.8 (102.5)	5.60#
	Deep	785 (30.9)	848.2 (123.0)	891.1 (129.2)	6.97#
Cement	Current NCDOT	556 (21.9)	633.0 (92.2)	664.0 (96.3)	4.55*
	Deep	632 (24.9)	895.1 (129.8)	817.7 (118.6)	5.59#
	Deep	734 (28.9)	937.9 (136.0)	883.2 (128.1)	6.62#

* current NCDOT subgrade stabilization pavement structure ($SN_{eff\text{-}st}$)
\# deep subgrade stabilization pavement structure ($SN_{eff\text{-}dp}$)

The HMA overlays ($h_{(HMA\text{-}ovl)}$) thicknesses determined using Equation 6.3 are summarized for the lime and cement test sections in Table 6.2.

Table 6.2: Estimated HMA Overlay Thicknesses (h(HMA-ovl)) Required for Current NCDOT Subgrade Stabilization Structure to attain the same SN of the Deep Subgrade Stabilization Structures

Deep Subgrade Stabilization		HMA Overlay Thickness Required for Current NCDOT pavement structures, mm (in)
Test section	Depth of stabilization mm (in)	
Lime	305 (12)	48 (1.9)
	406 (16)	127 (5.0)
Cement	254 (10)	60 (2.4)
	356 (14)	119 (4.7)

The results in Table 6.2 should be interpreted as the additional HMA thickness required for test sections constructed at the current NCDOT subgrade stabilization to attain the same structural number (SN) as the test sections constructed with deep subgrade stabilization thicknesses above. This analysis was based on the required overlay thickness for an existing pavement structure to attain a specified SN and does not consider any long term pavement degradation

6.3 Performance Prediction Based on the MEPDG Performance Indicators

The second analysis used was based on the MEPDG performance indicators (AASHTO, 2008). This was done by predicting the pavement responses at critical locations of the deep subgrade stabilization test sections using EVERSTRESS and Abaqus models coupled with the MEPDG equations to predict the performance of the constructed test sections. Though several damage modes are responsible for the eventual failure of pavements, in many pavement analyses, the damage mode that predicts the lowest number of load repetitions (Nf) is usually assumed to cause a pavement to fail. The performance indicators typically predicted in pavements include: fatigue damage, and permanent deformation. Considering the proximity of the test sections and the lack of long term performance data on the test sections, thermal cracking damage was ignored in this study.

Detail of the analysis method and framework used to establish equivalency between the control sections and deep subgrade stabilization sections were thoroughly detailed in Chapter 3 section 3.2. Illustrative sketches of the test section and schematic demonstrating the equivalency framework used in this study were also presented in section 3.2. Methods of calculating pavement responses at critical pavement locations using EVERSTRESS multi-layer elastic analysis were detailed in section 3.4 of chapter 3. The pavement responses calculation using a viscoelastic, non-linear 3D FE model under dynamic moving load was developed and was successfully validated with field measured data. Full details of the Abaqus FE numerical analysis model, the loading method, mesh sensitivity analysis, and radiation are presented in Appendix A.

Performance indicators for permanent deformation of the pavement structures were predicted for HMA and subgrade rutting. The failure criterion of a 12.5 mm (0.5 in.) rutting was used to predict the numbers of load repetition resulting from HMA. The predicted numbers of load repetition to failure of HMA based on MEPDG mathematical relationships (AASHTO, 2008) were very large and although HMA rutting is the major component of rutting in NC, rutting is not considered the critical distress for this study. Furthermore, the predicted numbers of load repetition due to subgrade rutting based on damage model in Wang and Al-Qadi (2008) were unrealistically large, therefore subgrade rutting was also eliminated as a critical distress mode for the deep subgrade stabilization performance.

The number of load repetitions (Nf) to cause fatigue cracking were determined by inputting the calculated tensile strains values, the material parameters, HMA thickness, and volumetric properties in the MEPDG load related fatigue cracking equations presented in Section 3.4.4.1 of this report. The longitudinal tensile strains on top of the HMA was calculated using the Abaqus model (Appendix A) and EVESTRESS method (Chapter 3). The material parameters (modulus values) used were field data from FWD testing and viscoelastic properties of HMA (Kim et al., 2005).

6.3.1 Relationship Between N_f and HMA Thickness (h_{HMA})

The number of axle-load applications (N_f) was computed for the four test sections after calculating the pavement responses. By reducing the HMA thicknesses of the deep subgrade stabilization test sections, new pavement responses and number of axle-load applications were computed. All damage data for the deep subgrade stabilization sections produced a simplified exponential model of the form presented in Equation 6.4 to predict the number of load repetitions to failure (N_f) as a function of HMA thickness (h_{HMA}) for fatigue cracking (alligator or bottom-up, longitudinal or top-down). Figures 6.1 and 6.2 for lime subgrade stabilization sections are presented here to show the trend of N_f versus HMA thicknesses for the deep subgrade stabilization. The longitudinal strain using the MEPDG fatigue cracking

$$N_f = k_1 e^{k_2 h_{HMA}} \tag{6.4}$$

Where,

k_1 and k_2 = best fit constants.

The analysis for bottom-up (alligator) and top-down (longitudinal) distresses are similar. Although the longitudinal distress model is not yet calibrated, it produced the lowest number of load repetitions (Nf) to failure. Therefore, longitudinal cracking was selected as the critical distress used to predict the performance improvement of deep subgrade stabilization. The parameters of the exponential model for the different deep subgrade stabilization test sections are presented in Tables 6.3 and 6.4.

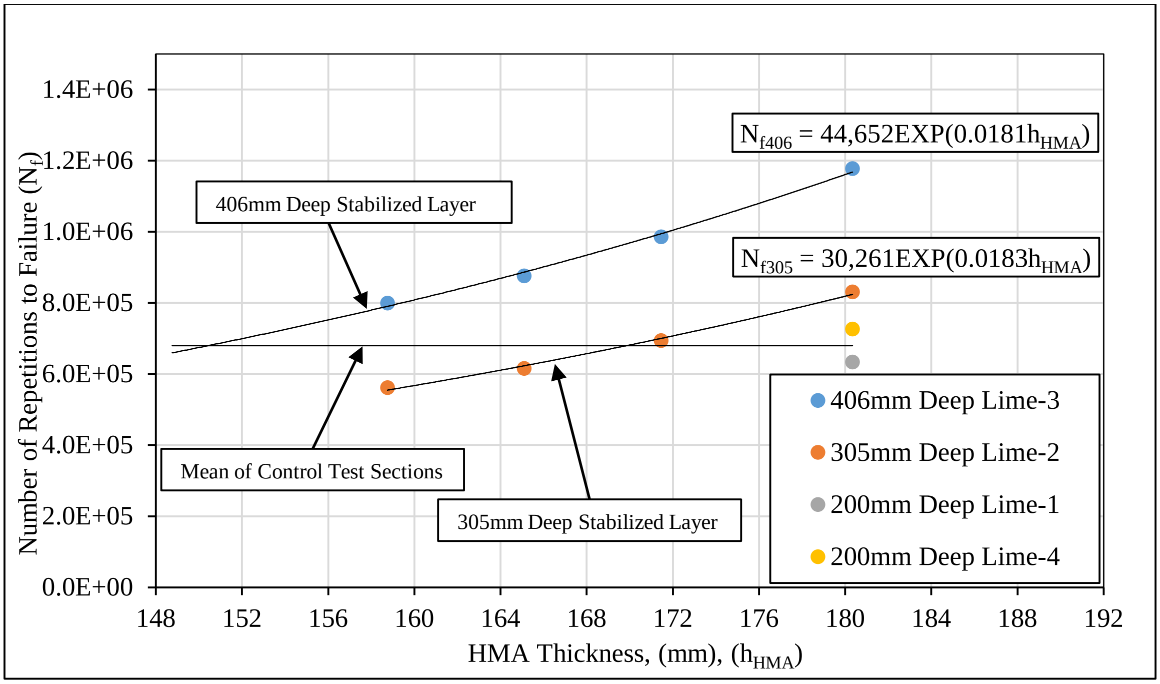

Figure 6.1 Load related top-down cracking model: lime test section, May 2011 (Based on EVERSTRESS)

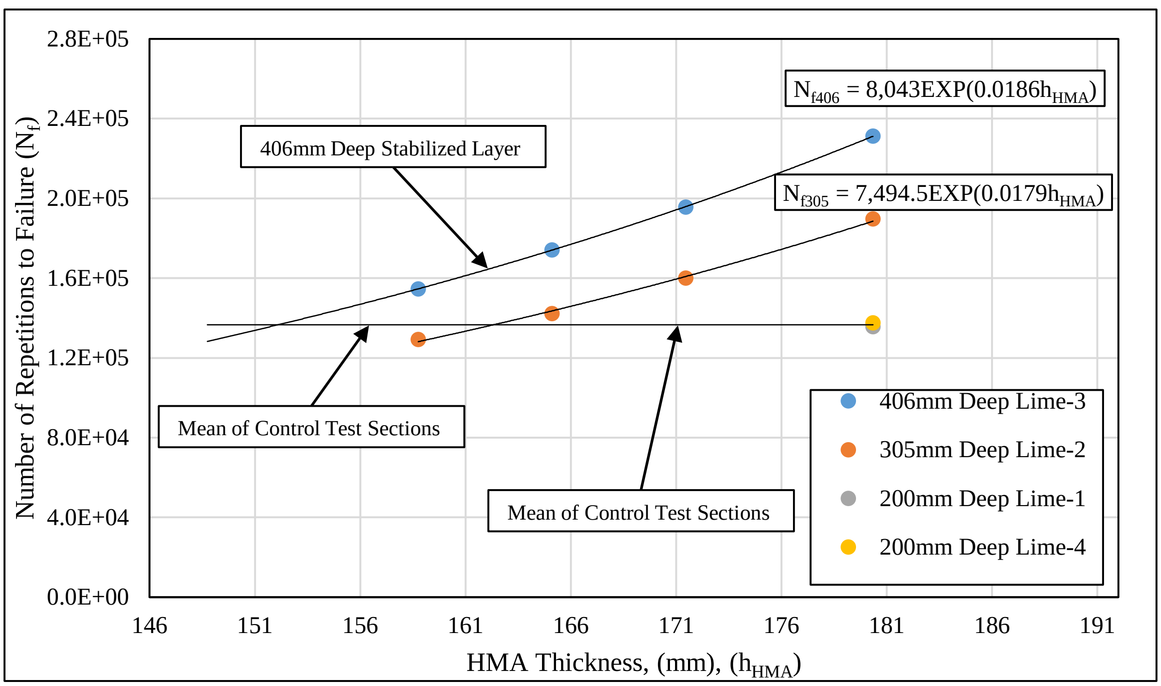

Figure 6.2 Load related top-down cracking model: lime test section, May 2011 (Based on Abaqus)

Table 6.3: Comstant Parameters (k_1 & k_2) of the simplified Exponential Damage Model of the Deep Subgrade Stabilization Test Sections (EVERSTRESS)

Deep Subgrade Stabilization		Load Related Fatigue Cracking Top-Down (longitudinal)			
		FWD in May, 2011		FWD in October, 2011	
Test Section Type	Thickness, mm (in.)	k_1	k_2	k_1	k_2
Lime Test Section	305 (12)	30,261	0.0183	112,949	0.0199
	406 (16)	44,652	0.0181	144,257	0.0203
Cement Test Section	254 (10)	88,889	0.0148	205,179	0.0174
	356 (14)	103,524	0.0152	67,171	0.0247

Table 6.4: Constant Parameters (k_1 & k_2) of the simplified Exponential Damage Model of the Deep Subgrade Stabilization Test Sections (Abaqus Viscoelastic FE)

Deep Subgrade Stabilization		Load Related Fatigue Cracking Top-Down (longitudinal)			
		Top-Down (longitudinal)		FWD in October, 2011	
Test Section Type	Thickness, mm (in.)	k_1	k_2	k_1	k_2
Lime Test Section	305 (12)	7,496	0.0179	-	-
	406 (16)	8,051	0.0186	-	-
Cement Test Section	254 (10)	3,295	0.0204	-	-
	356 (14)	4,091	0.0201	-	-

6.3.2 Determination of Equivalent HMA Thickness of Deep Subgrade Stabilization Test Section

In order to determine the reduced HMA thickness of a deep subgrade stabilization test section that was equivalent to the full pavement structure of the standard NCDOT subgrade stabilization test section, Equation 6.4 was reorganized as follows.

$$h_{HMA} = \frac{1}{k_2} Ln\left(\frac{N_f}{k_1}\right) \tag{6.5}$$

For Equation 6.5 the controlling number of load repetition to failure (Nf) was predicted with the current NCDOT standard pavement section for this project. This includes HMA layer of 180 mm (7.1 inches), ABC stone base layer of 200 mm (8 inches), and either a lime subgrade stabilization layer of 200 mm (8 inches) or a cement subgrade stabilization layer of 178 mm (7 inches). The HMA thickness of the deep subgrade stabilization test sections resulting in the same controlling number of load repetition to failure (Nf) were estimated by substituting the corresponding k1 and k2 for the deep subgrade stabilization type, thickness, and fatigue cracking failure mechanism from Tables 6.3 and 6.4. The reduced HMA thicknesses of the deep subgrade stabilization test sections resulting in equivalent pavement structure as the current NCDOT standard subgrade stabilization test sections based on load related longitudinal fatigue cracking are summarized in Tables 6.5 and 6.6. The reduction in HMA thicknesses due to the performance improvement of the deep subgrade stabilization test sections are summarized in Table 6.7.

In confirmation of the conclusion of chapter, the pavement response values calculated using EVERSTRESS and Abaqus Viscoelastic FE (under moving load condition) are significantly different with EVERSTRESS resulting in much higher values of Nf, as can be deduced from parameters in tables 6.3 and 6.4. The lower Nf values predicted with response calculated is Abaqus can be attributed to the using of the Principal maximum stain in the damage model. For this comparative analysis the impact of using this pavement response to predict performance is minimal in the reduced HMA values. Better comparable values were obtained for the time that section of 406mm deep subgrade stabilization section. Notwithstanding, the comparable range of HMA thickness reductions were predicted by both EVERSTRESS and Abaqus Viscoelastic FE for the lime deep subgrade stabilization test sections based on FWD field of May, 2011. Though the HMA thickness reductions predicted for the cement test sections by EVERSTRESS was more than order of magnitude greater than those predicted with Abaqus Viscoelastic FE, the same expected trend of the deeper subgrade stabilized layer (406 mm thick) predicting higher HMA thickness reduction than the deep subgrade stabilized layer of (305 mm) is obtained from the methods.

Table 6.5: Reduced HMA thickness of the deep subgrade stabilization test sections from load-related longitudinal fatigue cracking damage models (EVERSTRESS).

Test Section Type	Current NCDOT Standard Subgrade Stabilization Thickness, mm (in)	Deep Subgrade Stabilization		
		Thickness, mm (in)	Reduced HMA thickness for deep subgrade stabilization, mm (in)	
			FWD in May, 2011	FWD in October, 2011
Lime	200 (8)	305 (12)	170 (6.70)	172 (6.78)
		406 (16)	150 (5.92)	157 (6.17)
Cement	178 (7)	254 (10)	145 (5.70)	161 (6.35)
		356 (14)	131 (5.15)	159 (6.25)

Table 6.6: Reduced HMA thickness of the deep subgrade stabilization test sections from load-related longitudinal fatigue cracking damage models (Abaqus FE)

Test Section Type	Current NCDOT Standard Subgrade Stabilization Thickness, mm (in)	Deep Subgrade Stabilization		
		Thickness, mm (in)	Reduced HMA thickness for deep subgrade stabilization, mm (in)	
			FWD in May, 2011	FWD in October, 2011
Lime	200 (8)	305 (12)	162 (6.38)	-
		406 (16)	152 (5.99)	-
Cement	178 (7)	254 (10)	165 (6.49)	-
		356 (14)	157 (6.16)	-

Table 6.7: HMA Thickness Reduction due to Performance Improvement of Deep Subgrade Stabilization

Model for calculating response	Lime HMA Thickness, mm (in.)			Cement HMA Thickness, mm (in.)		
	Deep Stabilization Thickness	Test Date		Deep Stabilization Thickness	Test Date	
		May	October		May	October
EVERSTRESS	305 (12)	10 (0.40)	8 (0.35)	254 (10)	35 (1.40)	19 (0.75)
	406 (16)	30 (1.15)	23 (0.95)	356 (14)	49 (1.95)	21 (0.85)
Abaqus FE	305 (12)	18 (0.70)	-	254 (10)	15 (0.60)	-
	406 (16)	28 (1.10)	-	356 (14)	23 (0.95)	-

6.4 Summary

In this chapter, the performance of deep subgrade stabilization test sections was predicted using two different approaches. The first approach was based on the effective modulus method utilizing the composite modulus values presented in Table 5.7. The predicted SN values are presented in Table 6.1. The SN values of the deep stabilized subgrade sections were greater than those of the control sections. Further, the HMA overlay thickness required to increase the SN of the control test section to the SN values of the deep subgrade stabilizations sections were computed and presented in Table 6.2. Since SN is an index of the condition or an indication of the strength of a pavement, higher SN indicates a pavement with better structural strength if under the same climatic/environmental, soil, and operating conditions. With higher SN, deep subgrade stabilization layer pavement demonstrates better strength or condition than the current NCDOT pavement structure.

The second method used to predict the performance of the test sections is based on MEPDG performance indicators. For this analysis, the equivalency framework developed in Chapter 3 section 3.2 was implemented. The pavement responses at critical locations were calculated using EVERSTRESS and Abaqus FE. The response data were used with the appropriate MEPDG damage models to predict pavement performance. Load-related longitudinal fatigue cracking was found to be the critical damage mode to cause failure. The predicted N_f values of the deep subgrade stabilization test sections are greater than those of the control sections (Figures 6.1 & 6.2). The performance improvement demonstrates that deep subgrade stabilization will extend the life of pavements.

Analysis of the load repetition values (N_f) in accordance with the equivalency framework method produced values of reduced HMA thicknesses of the deep subgrade stabilization sections The estimated HMA overlay thicknesses in Table 6.2 and the reduced HMA thicknesses in Tables 6.6 and 6.7 will be used in Chapter 7 to assess the cost effectiveness of deep subgrade stabilization.

CHAPTER 7 QUANTIFICATION OF COST-EFFECTIVENESS OF DEEP SUBGRADE STABILIZATION PERFORMANCE

7.1 Introduction

Performance analysis conducted in Chapter 6 has already demonstrated that deep subgrade stabilization extends life of pavements. This Chapter presents a simplified assessment of the cost-effectiveness of the deep subgrade stabilization methods and depth considered in this research project. The cost effectiveness depends on the long term maintenance cost savings of the as-built test sections and the constructions cost savings from the deep subgrade stabilization test sections for the reduced HMA thickness. To quantify the cost effectiveness of deep subgrade stabilization, the following simplified approaches were used:

Cost analysis of the estimated HMA overlays based on the effective modulus method and result are presented in Chapter 6 (Table 6.2).

Construction cost savings analysis from the predicted HMA thickness reduction due to deep subgrade stabilization as shown in Chapter 6 (Tables 6.5, 6.6, and 6.7)

The cost of each test section comprises of the cost of earthwork, subgrade stabilization, the ABC layer, and the HMA layer. For convenience and simplicity, the cost analyses of the test sections are carried out solely on the basis of unit construction costs of: (1) the subgrade stabilization and (2) HMA layer. Though each layer of pavement has multiple, components, material costs, and construction operation costs; to simplify, the total construction cost of an in-spec NCDOT test section was considered as follows:

$$C_T = C_{SG} + C_{SB} + C_B + C_{HMA} \qquad (7.1)$$

Where:

C_T = total cost of in-spec NCDOT pavement section;

C_{SG} = earthwork operation cost;

C_{SB} = cost of subgrade stabilization for the in-spec NCDOT pavement section;

C_B = cost of construction of the base layer; and,

C_{HMA} = cost of the in-spec construction of the HMA layer for the site.

Similarly, the total construction cost of a deep subgrade stabilization test section can also be expressed as:

$$C_{T(D)} = C_{SG(D)} + C_{SB(D)} + C_{B(D)} + C_{HMA(D)} \quad (7.2)$$

Where:

$C_{T(D)}$ = total cost of deep subgrade stabilization pavement section;

$C_{SG(D)}$ = earthwork operation cost;

$C_{SB(D)}$ = cost of deep subgrade stabilization of pavement sections;

$C_{B(D)}$ = cost of construction of the base layer; and,

$C_{HMA(D)}$ = cost of the HMA layer for the deep subgrade stabilization pavement of the site.

Since the same earthwork operation and base layer construction materials/operation are implemented for in-spec NCDOT subgrade and deep subgrade stabilizations, Equation (7.2) can be written as:

$$C_{T(D)} = C_{SG} + C_{SB(D)} + C_B + C_{HMA(D)} \quad (7.3)$$

All construction costs used were actual costs for the test sections obtained from Blythe Construction, the project’s general contractor. Cost of HMA layers were broken down into two components on NCDOT highway projects: (1) aggregate and asphalt concrete, and (2) binder. Similarly, the costs of subgrade stabilization were split into cost of chemical additive and cost of subgrade stabilization operation. For this analysis, the site preparation and base layer costs were ignored, since these costs are the same for all the test sections. The HMA pavement layer for the test site (NC-16 bypass project) consisted of an intermediate HMA layer (I19.0C) of 100mm (3.95 inches) thickness, and a surface HMA layer (S9.5C) of 80mm (3.15 inches) thickness. The cost for the intermediate HMA layer was $35.00 per metric ton while the cost for the surface layer HMA was $38.00 per metric ton. The aggregate cost includes all aggregate material from the Job Mix Formula (JMF) provided to NCDOT from the contractor. The cost of binder varied throughout the life of the project ranging from \$475.23 per metric ton to \$765.88 per metric ton. The key parameters used for cost analysis are summarized in the Table 7.1. The construction costs of the deep subgrade stabilization were estimated on proportional depth of stabilization from the lump sum provided by the contractor and may be different from the unit cost paid out by NCOT.

Table 7.1: Summary of the keys parameters for cost analysis

HMA					Binder	
Mix Type	Thickness mm (in)	G_{mm}	Field Compaction (%)	Cost \$/Metric ton	% in JMF	Cost \$/Metric ton
S9.5C	80 (3.15)	2.541	93.2	38.50	5.6	650.00
I19.0C	100 (3.95)	2.589	95.0	35.00	4.8	

Type of Subgrade Stabilization and Additive					
Lime Additive			Cement Additive		
Depth, mm (in)	Additive Cost (\$/m^2)	Construction Cost (\$/m^2)	Depth, mm (in)	Additive Cost (\$/m^2)	Construction Cost (\$/m^2)
200 (8)	3.29	2.64	178 (7)	2.79	2.1
305 (12)	4.93	3.13	254 (10)	4.19	2.95
406 (16)	6.57	3.62	356 (14)	5.59	3.80

7.2 Cost Analysis of the Estimated HMA Overlay Thickness Based on the Effective Modulus Method

In order to quantify the cost effectiveness of the performance improvement of deep subgrade stabilization, cost analysis of in-spec NCDOT pavement section plus the estimated HMA overlay thickness (as presented in Table 6.2) is compared with the cost of construction of deep subgrade stabilization pavement structure. For this analysis, the cost of the required HMA overlay thickness is added to the total cost compared with Equation 7.1. However, the as-build deep subgrade stabilization pavement structure, was expressed based on Equation 7.3. In Equation 7.3, the cost of the HMA layer is CHMA (the cost of the in-spec construction of the HMA layer for the site). The cost effectiveness of the performance improvement of deep subgrade stabilization is expressed as follows:

$$\Delta C_M = (C_T + C_{HMA(OV)}) - C_{T(D)} \tag{7.4}$$

Where,

ΔC_M = cost effectiveness from deep subgrade stabilization pavement section;

C_T = total cost of in-spec NCDOT pavement section (Equation 7.1);

$C_{HMA(OV)}$ = cost of the required HMA overlay thickness (Table 6.2); and,

$C_{T(D)}$ = total cost of the as-built deep subgrade stabilization pavement section (Equation 7.3).

In this case, $C_{HMA(D)}$ is the same as C_{HMA}. Simplification of Equation 7.4 after substituting for C_T and $C_{T(D)}$ becomes:

$$\Delta C_M = (C_{HMA(OV)} + C_{SB}) - C_{SB(D)} \tag{7.5}$$

This cost effectiveness analysis reduces to comparing the costs of the required HMA overlay thickness and of subgrade stabilization for the in-spec (standard) NCDOT pavement section with cost of the deep subgrade stabilization layer, Equation 7.5 is illustrated in the block diagram presented in Figure 7-1.

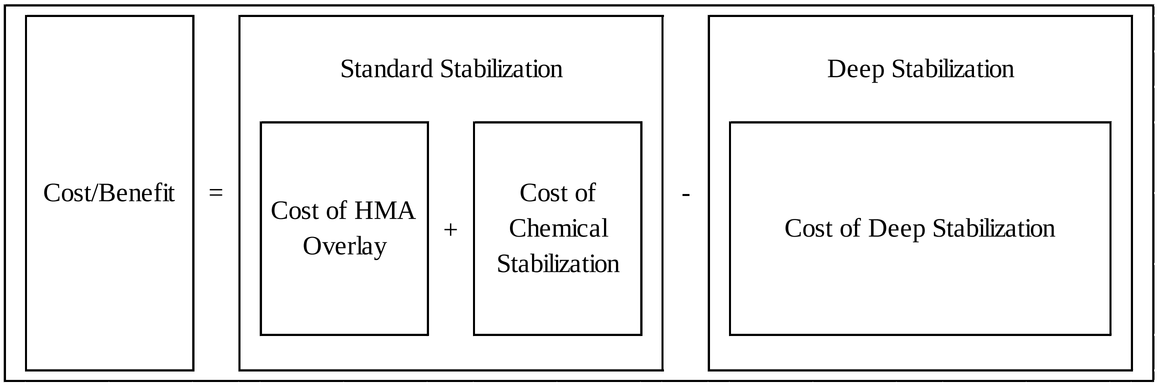

Figure 7.1 Block diagram for computing cost benefit of deep subgrade stabilization based on the effective modulus

Table 7-2 presents the cost effectiveness of the deep subgrade stabilization layers for both the lime and cement test sections using field data collected from May, 2011 and October, 2011. These cost effectiveness values were computed in terms of cost per unit area in \$/m2. . The benefit cost analysis was computed for HMA overlays of either surface mix type (S9.5C) or intermediate mix type (I19.0C).

Table 7.2: Estimated Cost Benefit of Deep Subgrade Stabilization Pavement computed based on Effective Modulus Values.

Deep Subgrade Stabilization		HMA Overlay Thickness Required for Current NCDOT pavement structures, mm (in)	Estimated Benefit, \$/m^2	
Test section	Depth of stabilization mm (in)		Surface Mix (S9.5C)	Intermediate Mix (I19.0C)
Lime	305 (12)	48 (1.9)	6.37	5.67
	406 (16)	127 (5.0)	18.22	16.33
Cement	254 (10)	60 (2.4)	8.37	7.50
	356 (14)	119 (4.7)	16.57	14.84

7.3 Construction Cost Savings based on HMA Reduction from M-EPDG Load Related Longitudinal Cracking

To estimate the construction cost savings due to performance improvement of deep subgrade stabilization, the cost of the in-spec NCDOT pavement section is compared with the cost of a new predicted pavement structure of the deep subgrade stabilization section. The new predicted pavement structure of the deep subgrade stabilization section consists of the as-built deep subgrade stabilization layer, the base layer, and the reduced HMA layer thickness. The methodology for predicting reduced HMA layer thickness was discussed in detailed in Chapter 3. The reduced HMA layer thicknesses for the test sections studied in this project are presented in Tables 6.5 and 6.6. For this construction cost savings analysis, Equations 7.1 (for as-built in-spec NCDOT pavement structure) is compared with reduced HMA thickness in equation 7.3. In Equation 7.3, the cost of the reduced HMA layer thickness CHMA(D) is used. The cost effectiveness due to performance improvement of deep subgrade stabilization in this case is expressed as follows:

$$\Delta C_S = C_T - C_{T(D)} \tag{7.6}$$

Where,

ΔC_T = construction cost savings from deep subgrade stabilization pavement sections;

C_T = total cost of in-spec NCDOT pavement section (Equation 7.1); and,

$C_{T(D)}$ = total cost of the as-built deep subgrade stabilization pavement section with reduced HMA layer thickness (Equation 7.3).

After substituting for C_T and $C_{T(D)}$, in equation 7.6 above can be simplified to become equation 7.7 below.

$$\Delta C_S = \left(C_{HMA} + C_{SB}\right) - \left(C_{HMA(D)} + C_{SB(D)}\right) \tag{7.7}$$

Where,

$C_{HMA(D)}$ = cost of reduced HMA layer thickness (thicknesses are in Table 6.5 and 6.6);

From Equation 7.7, the cost savings can be simplified to difference in cost of constructing the HMA and stabilized layers of the in-spec standard NCDOT pavement section and those of the deep subgrade stabilization sections. The construction cost savings in Equation 7.7 is illustrated in the block diagram presented in Figure 7.2. It is the difference in cost of constructing the HMA and stabilized layers of standard NCDOT pavement section, and those of the deep subgrade stabilization section. This analysis is limited to the assessment of the potential cost benefit of deep subgrade stabilization and assumed that the reduced thickness is feasible, constructible, and that the controlling distress is top-down longitudinal cracking.

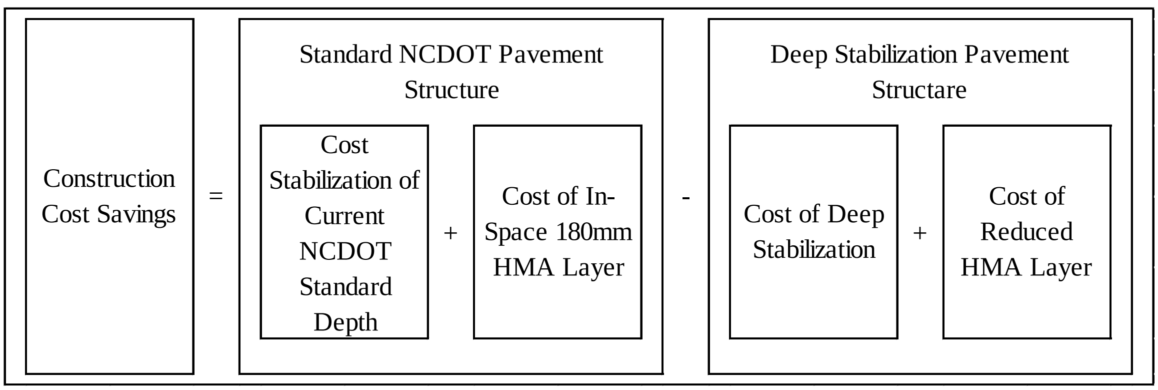

Figure 7.2 Block diagram illustrating the framework cost savings from deep subgrade stabilization based on longitudinal fatigue cracking performance

In this analysis, the field applications of the chemical additive contents are assumed the same for the standard NCDOT subgrade stabilization as the deep subgrade stabilization. Therefore, it is expected that material cost of the chemical additives can easily be estimated in the contract price. Although, the unit cost of constructed HMA does not fluctuate widely, the overall pavement cost is significantly impacted by the fluctuation in the price of binder. In the following section, the effects of the unit cost ($/MT) of binder and the construction cost of deep subgrade stabilization on pavement construction cost savings were studied. The binder unit cost was varied from $500/MT to $1000/MT while the deep subgrade stabilization construction costs were varied (from 10% to 30%) as a percent of the construction cost of the in-spec NCDOT subgrade stabilization. Plots of the estimated construction cost savings in $\$/m^2$ of roadway for the range of 10 – 30% of stabilization construction cost and binder unit cost ranging from $500/MT – $1000/MT are presented in

Figure 7.3 to 7.10. Only the values corresponding to the pavement performance predicted from responses calculated with Abaqus FE VLE model are presented in the Figures. The figures below are generated using FWD data collected in May, 2011 to calculate pavement responses. The performance indicator based on longitudinal fatigue damage model of MEPDG was predicted for the deep subgrade stabilization test sections. Similar analysis and plot were generated using the same data and damage model for the pavement responses calculated using EVERSTRESS. The corresponding Figures are provided in Appendix C. From these figures, the construction cost savings in $/m^2 of a roadway can be estimated if the unit cost of the binder and the increase in stabilization construction cost due to deep stabilization is known.

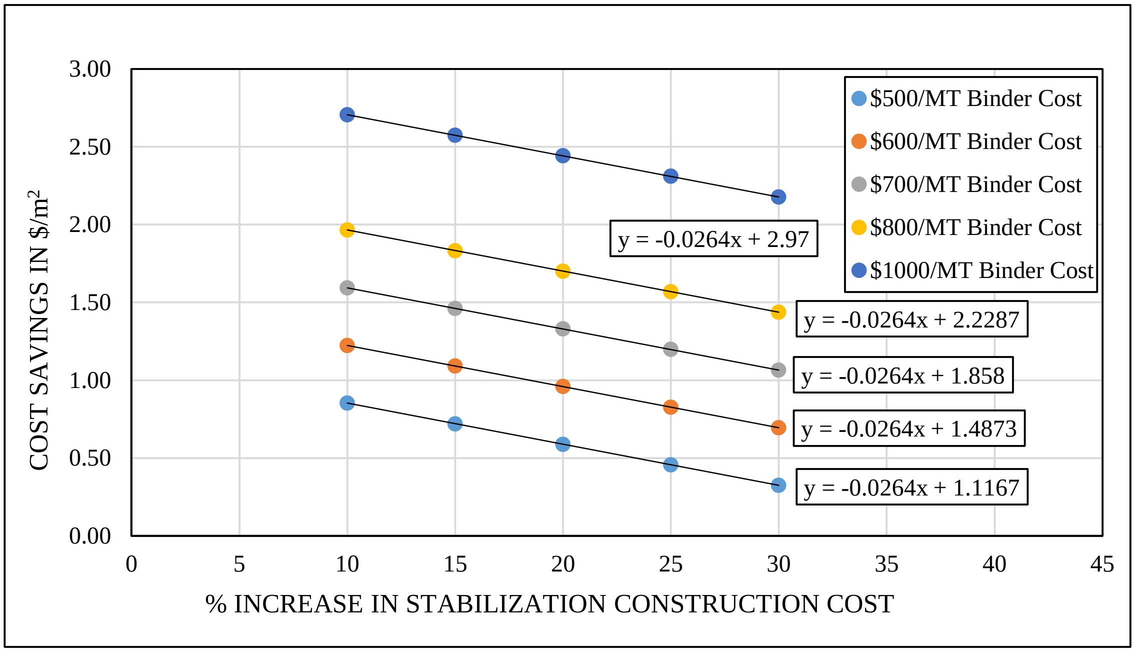

Figure 7.3 Cost Savings versus % increase in Stabilization Construction Cost for various Binder costs (Lime of 406 mm, S9.5C mix, Abaqus FE analysis of May 2011 data)

Another key objective of this cost analysis is to determine the limiting stabilization construction cost beyond which deep subgrade stabilization does not result in cost savings for a unit cost of asphalt binder assuming the reduced HMA thickness is feasible. The cost which is expressed as percent of the construction cost of standard NCDOT stabilization depth is the cost of stabilizing beyond the standard NCDOT depth. This analysis was performed for all of the cost savings plots in Figures 7.3 - 7.10 and for those based on EVESTRESS analysis shown in Appendix C. The values of limiting stabilization construction cost (as % of the contract price of construction cost of standard NCDOT stabilization depth) are summarized in Tables 7.3 and 7.4. The values were computed for various unit cost of binders, chemical additives and model of calculating pavement response (EVERSTRESS and Abaqus FE VLE models)

In Table 7.3, the cells shaded in “orange” color imply that no construction savings are possible for the range of unit cost of binder less than $1000/MT. The cells shaded in “gray” color indicate that construction cost savings are unlikely for those ranges of unit cost of binder. Since the values are less than 10% which is the cost increase formulated by the research team as lowest value any contractor will bid for deep stabilization construction. It should be noted that the “unlikely/no savings” ranges occur only in the 305-mm deep lime subgrade stabilization pavement section based on pavement responses calculated using EVESTRESSS. However, when the more rigorous Abaqus FE analysis was used to calculate pavement responses and the values used to predict the performance, significant construction cost savings were estimated. Savings were estimated for binder unit cost of $500/MT with subgrade stabilization cost construction of up 36.55% for 305-mm deep lime subgrade stabilization pavement section. It is convenient to conclude that 305-mm deep lime subgrade stabilization has high potential of construction cost savings. In table 7.4, all the deep cement subgrade stabilization indicates likelihood and strong potential of construction cost savings.

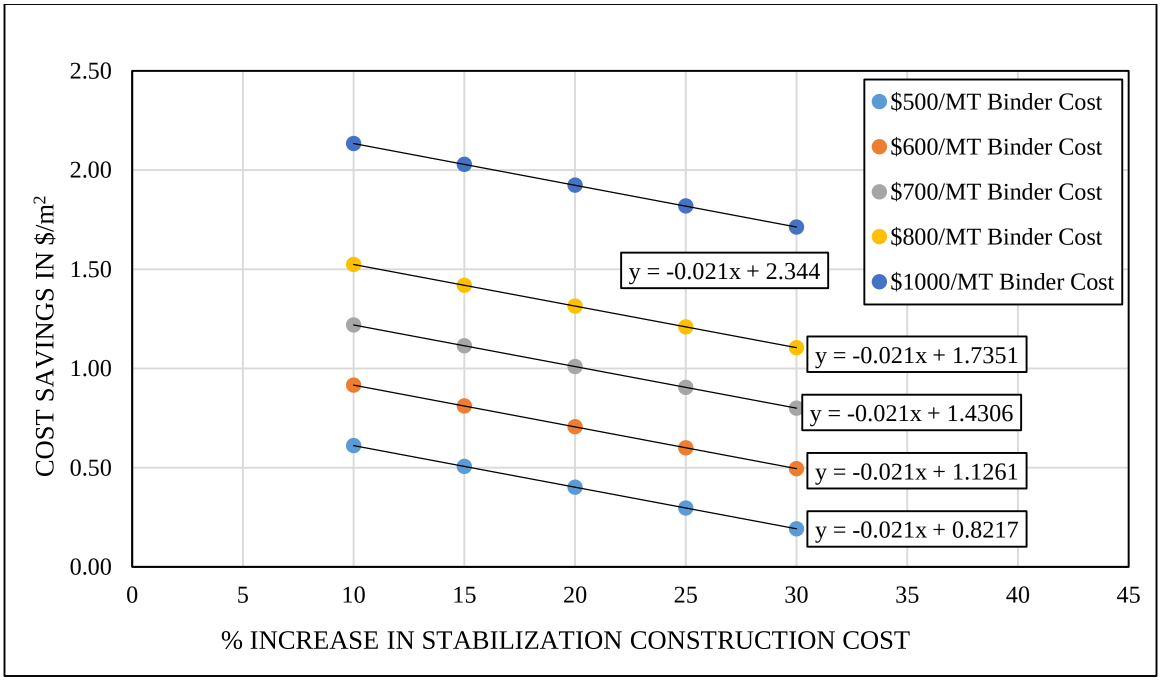

Figure 7.4 Cost Savings versus % increase in Stabilization Construction Cost for various Binder costs (Cement of 356 mm, S9.5C mix, based on Abaqus FE analysis of May 2011 data)

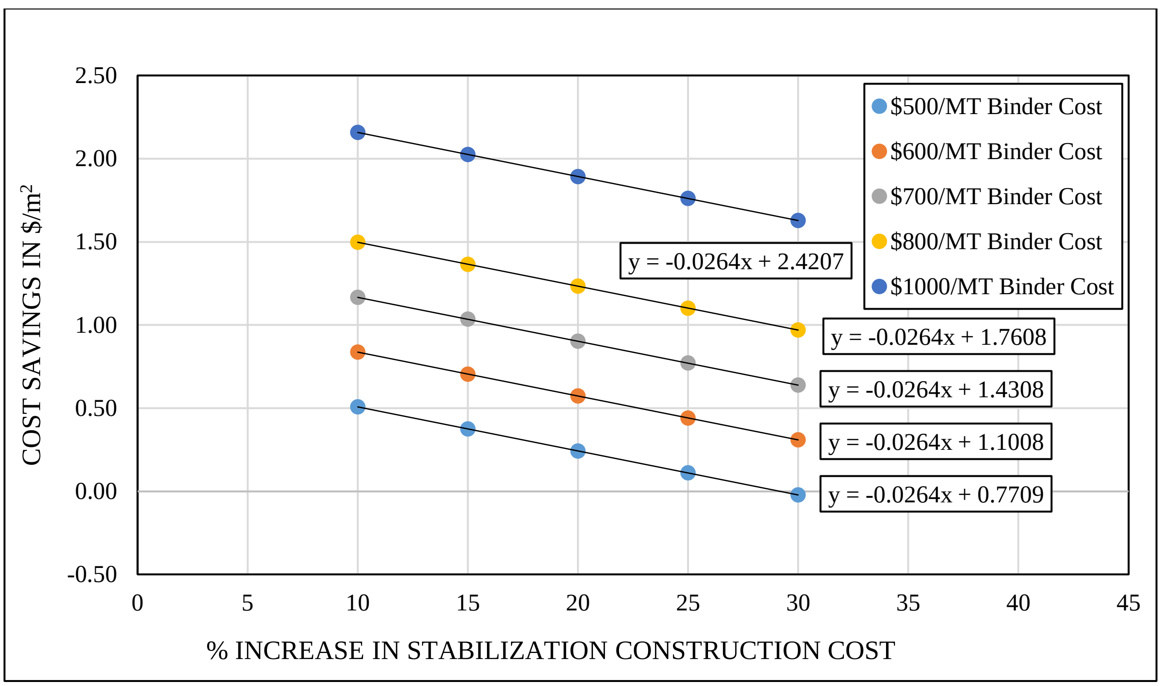

Figure 7.5 Cost Savings versus % increase in Stabilization Construction Cost for various Binder costs (Lime of 406 mm, I19.0C mix, Abaqus FE analysis of May 2011 data)

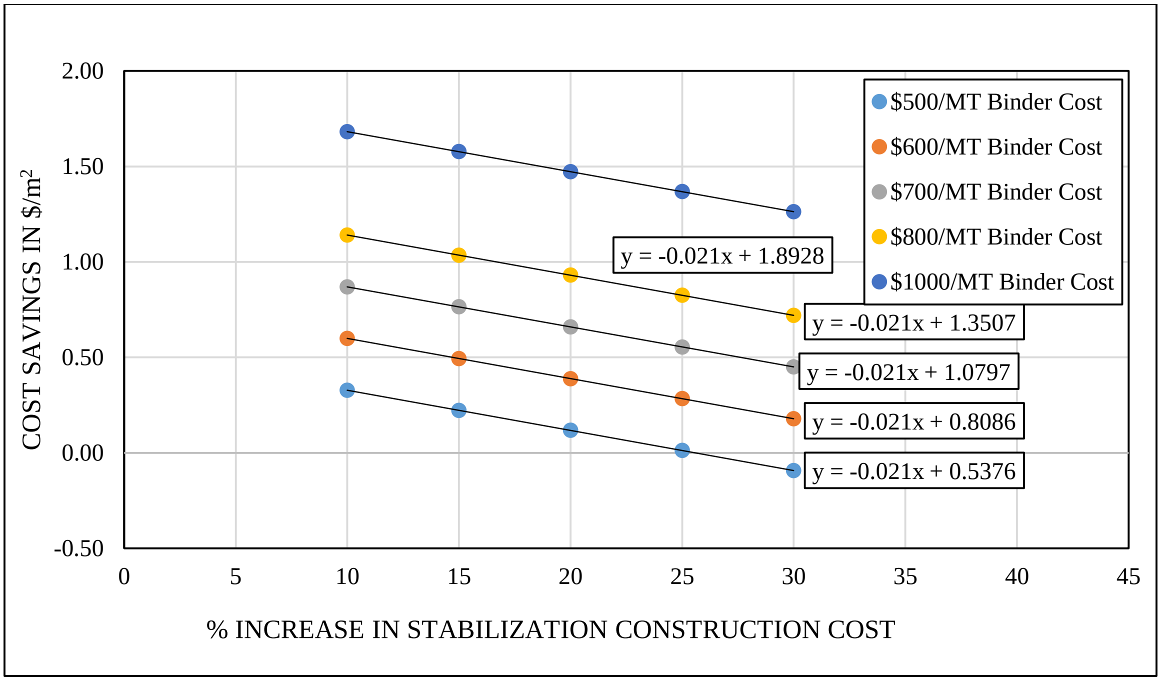

Figure 7.6 Cost Savings versus % increase in Stabilization Construction Cost for various Binder costs (Cement of 356 mm, I19.0C mix, based on Abaqus FE analysis of May 2011 data)

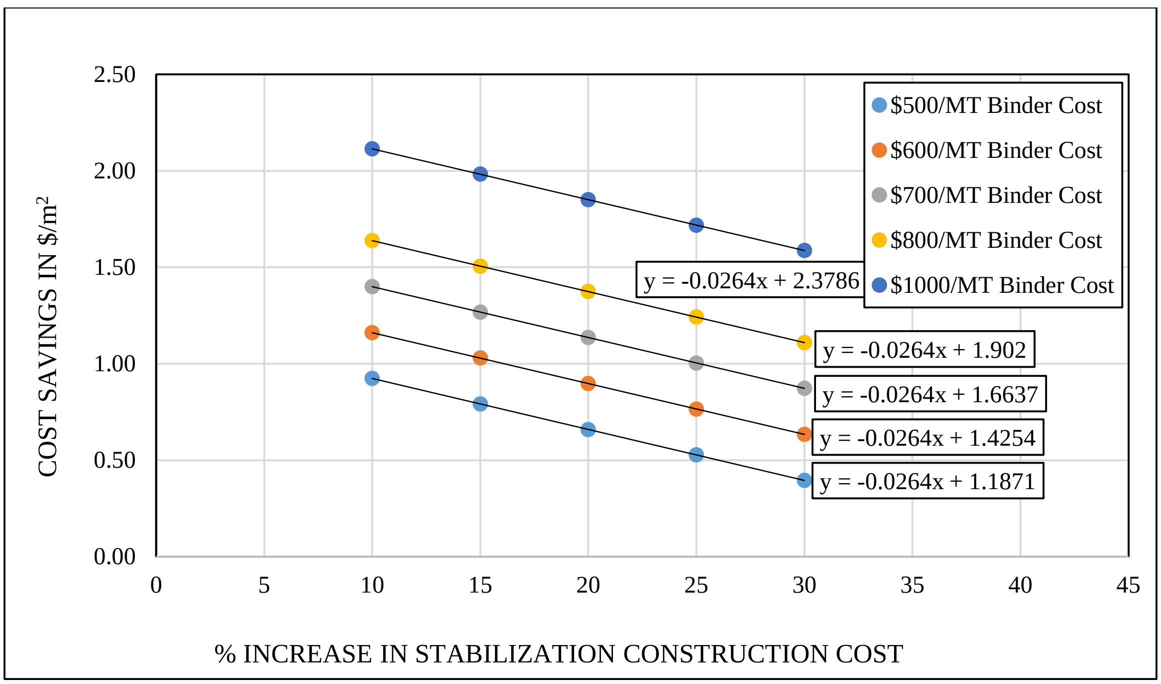

Figure 7.7 Cost Savings versus % increase in Stabilization Construction Cost for various Binder costs (Lime of 305 mm, S9.5C mix, Abaqus FE analysis of May 2011 data)

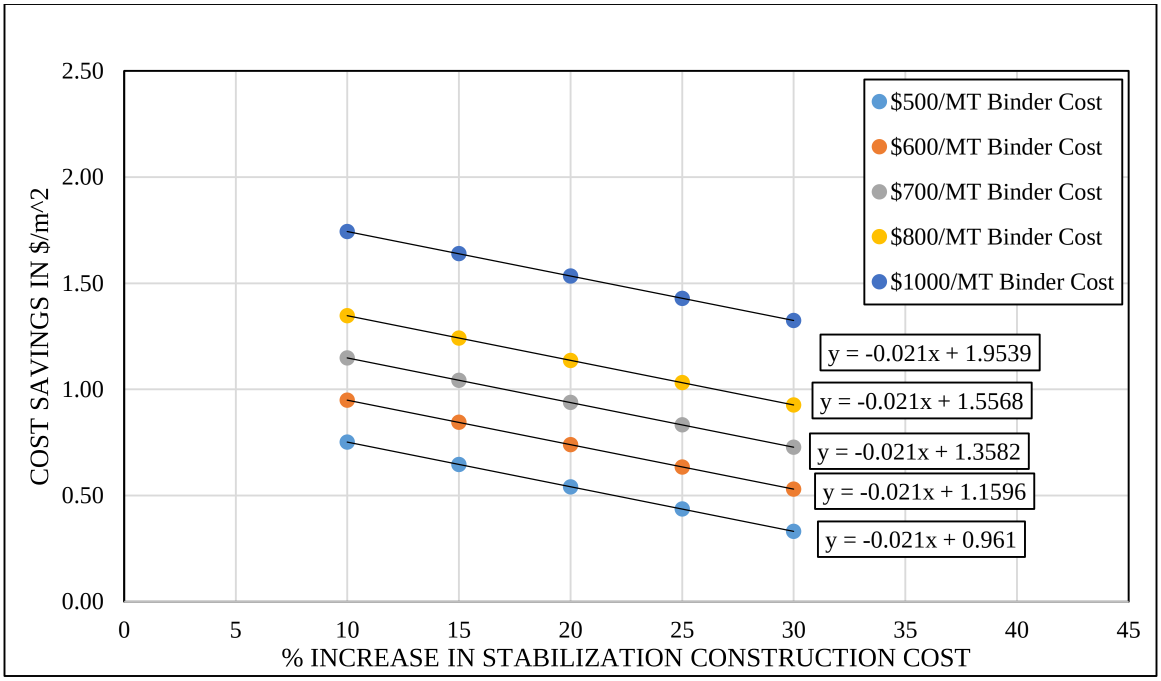

Figure 7.8 Cost Savings versus % increase in Stabilization Construction Cost for various Binder costs (Cement of 254 mm, S9.5C mix, based on Abaqus FE analysis of May 2011 data)

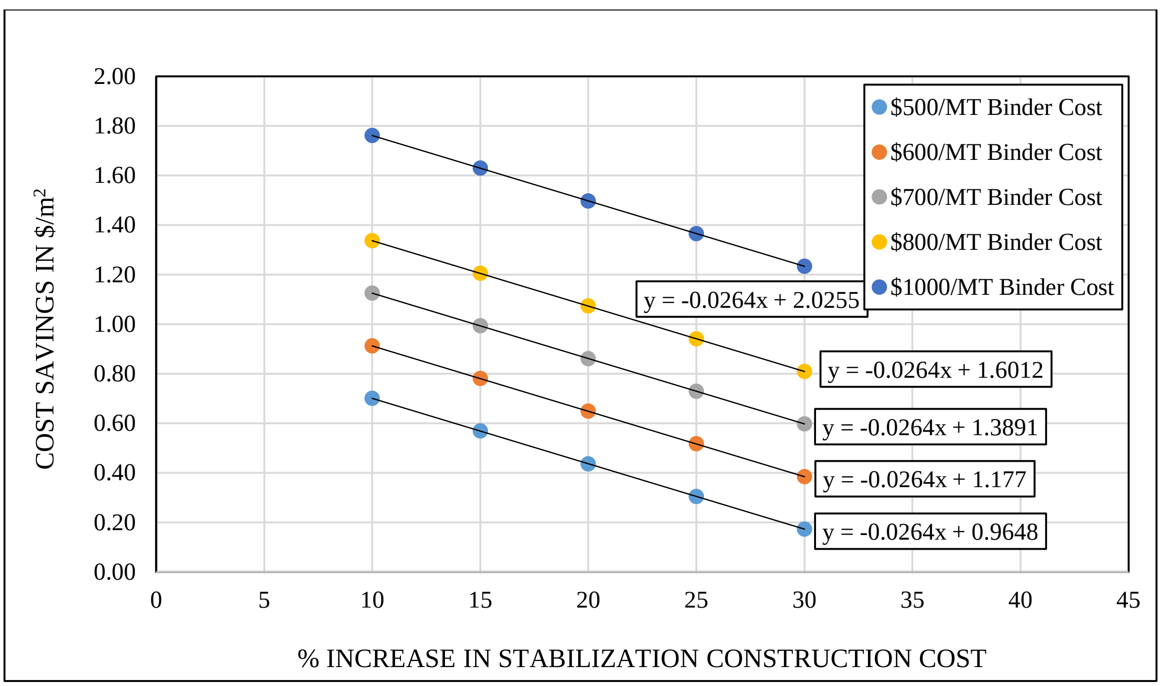

Figure 7.9 Cost Savings versus % increase in Stabilization Construction Cost for various Binder costs (Lime of 305 mm, I19.0C mix, Abaqus FE analysis of May 2011 data)

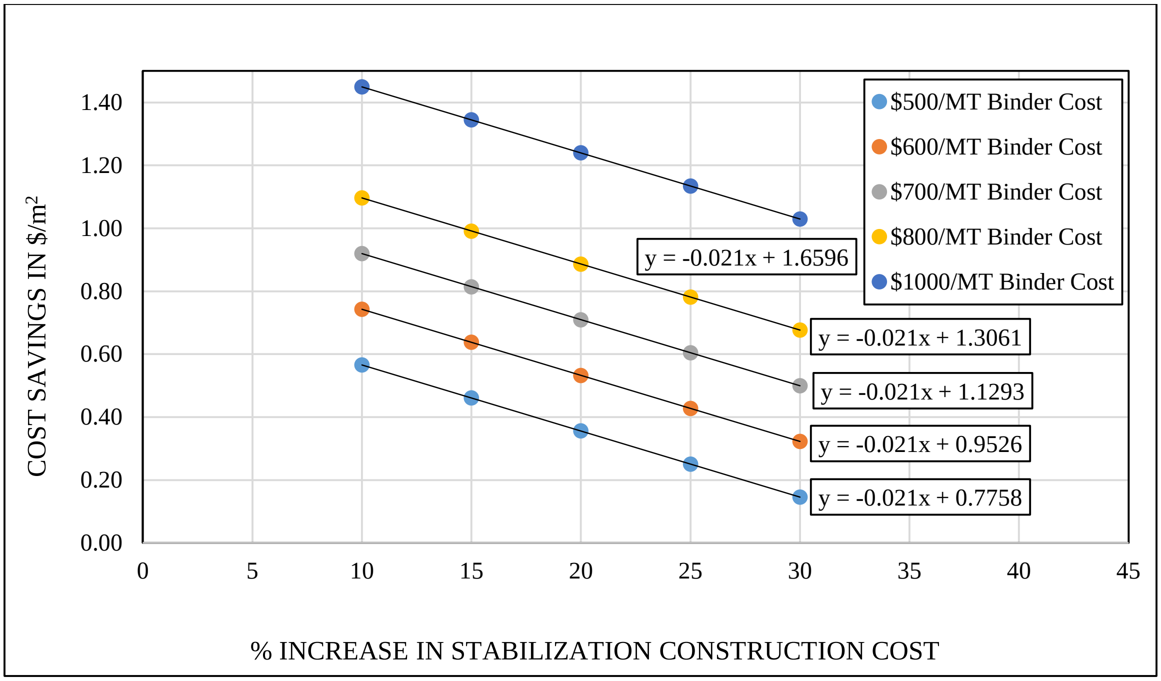

Figure 7.10 Cost Savings versus % increase in Stabilization Construction Cost for various Binder costs (Cement of 254 mm, I19.0C mix, based on Abaqus FE analysis of May 2011 data)

Table 7.3: Stabilization Construction Cost % Increase corresponding to "No Cost Savings for Deep Lime Subgrade Stabilization ("S" = S9.5C; "I" = I19.0C)

Binder ($/MT)	The limiting % increase of stabilization construction cost at which "no cost savings" accrues from deep "lime" subgrade stabilization											
	Response Analysis by EVERSTRESS								Response Analysis by Abaqus FE VLE model			
	406 mm Stabilized Layer				305 mm Stabilized Layer				406 mm Stab. Layer		305 mm Stab. Layer	
	May, 2011		Oct., 2011		May, 2011		Oct., 2011		May, 2011		May, 2011	
	"S"	"I"	"S"	"I"	"S"	"I"	"S"	"I"	"S"	"I"	"S"	"I"
500	54.21	40.17	12.53	1.77	-2.67	-7.35	-14.58	-18.32	42.30	29.20	44.97	36.55
600	69.25	53.56	24.06	12.03	2.34	-2.88	-10.57	-14.75	56.34	41.70	53.99	44.58
700	84.30	66.95	35.59	22.30	7.36	1.58	-6.56	-11.18	70.38	54.20	63.02	52.62
800	99.34	80.35	47.13	32.56	12.38	6.05	-2.55	-7.61	84.42	66.70	72.05	60.65
1000	129.42	107.13	70.19	53.10	22.40	14.97	5.48	-0.47	112.50	91.69	90.10	76.72

	No Construction Savings
	Construction Savings unlikely (% increase < 10)

Table 7.4: Stabilization Construction Cost % Increase corresponding to “No Cost Savings for Deep Cement Subgrade Stabilization (“S” = S9.5C; “I” = I19.0C)

Binder ($/MT)	The limiting % increase of stabilization construction cost at which “no cost savings” accrues from deep “cement” subgrade stabilization											
	Response Analysis by EVERSTRESS								Response Analysis by Abaqus FE VLE model			
	356 mm Stabilized Layer				254 mm Stabilized Layer				356 mm Stab. Layer		254 mm Stab. Layer	
	May, 2011		Oct., 2011		May, 2011		Oct., 2011		May, 2011		May, 2011	
	“S”	“I”	“S”	“I”	“S”	“I”	“S”	“I”	"S"	"I"	"S"	"I"
500	233.76	204.94	24.16	11.80	195.48	174.90	75.70	64.53	39.13	25.60	45.76	36.94
600	264.65	232.44	37.40	23.59	217.54	194.54	87.69	75.20	53.62	38.50	55.22	45.36
700	295.54	259.93	50.63	35.37	239.61	214.18	99.66	85.86	68.12	51.41	64.68	53.78
800	326.42	287.43	63.87	47.16	261.67	233.82	111.64	96.52	82.62	64.32	74.13	62.20
1000	388.20	342.43	90.35	70.73	305.80	273.10	135.60	117.84	111.62	90.13	93.04	79.03

7.4 Summary of Cost Effectiveness Analysis

Both cost analysis methods presented in this chapter demonstrate that the pavement performance improvement due to deep subgrade stabilization results in:

(1) Significant benefit in terms of estimated overlay or “maintenance/rehabilitation” required for the in-spec NCDOT standard pavement to attain the extended life of the deep subgrade stabilization pavement structure.

(2) Construction cost savings with deep subgrade stabilization for binder unit cost as low at $500/MT, if the reasonably priced stabilization construction cost increases.

CHAPTER 8 CONCLUSIONS

8.1 Conclusions

This study investigates the performance improvement of deep layers of subgrade stabilization sections of a constructed project site in North Carolina. The pavement responses were calculated using multilayer elastic linear analysis program (EVERSTRESS©) and a finite element numerical model (ABAQUS). Furthermore, a viscoelastic, non-linear 3D finite element with stress-dependent soil model was implemented to adequately simulate responses of pavement under moving axle load. The performance of the test sections was predicted using the damage models in MEPDG. An equivalency framework was developed to establish HMA thicknesses for which a deep subgrade stabilization pavement section has the same predicted performance value as the control pavement section.

Based mainly on field data collected at the test site, the actual performance values of the deep subgrade stabilization and control pavement test sections were predicted for specific type of distresses. To establish cost effectiveness of deep subgrade stabilization, cost analysis of the predicted HMA overlay thickness and reduced HMA thickness for the control and deep subgrade stabilization test sections, respectively was conducted. From this study, the following conclusions may be reached:

1. EVERSTRESS© 5.0 (similar to JULEA implemented in MEPDG) can be used to calculate pavement responses.
2. More consistent and accurate pavement responses were obtained from viscoelastic non-linear 3D FE model developed in this study.
3. The equivalency framework developed in study is capable of estimating the reduced HMA thickness of deep subgrade stabilization section.
4. The laboratory unconfined compression and resilient modulus results indicated that the recommended field application rates of lime were adequate. This finding was generally confirmed by the test results of QC samples collected during field operation.

5. Unconfined compression results of samples prepared during field stabilization operation at the test sites reported by NCDOT were generally comparable. However, NCDOT values were consistently higher.
6. An attempt was made to verify the actual effective thickness of the stabilized layer using DCP. The result was inconclusive as no undisturbed samples of the layer were tested.
7. From the analysis of DCP data, the chemical additive and thickness of the stabilized subgrade studied did not significantly influence the stiffness/strength of the compacted unbound aggregate base layer, implying that the current standard NCDOT subgrade stabilization layer may be sufficient to provide confinement.
8. Analysis of the FWD tests revealed that:
   a. Composite modulus values of the deep subgrade stabilization were consistently higher.
   b. The same trend was observed with 3-layer or 4-layer analysis of the FWD date. For the 3-layer analysis the base and the stabilized subgrade layers were combined in each test section.
   c. From the back calculations of the FWD data, the HMA and the base layers appeared to exhibit slightly higher modulus values than those of the control sections.
9. Load-related longitudinal distress (top-down fatigue cracking) was the critical failure mode of the pavement structures in this study. For both EVERSTRESS© and Abaqus FE, the longitudinal fatigue damage model predicted the lowest number of load repetitions to failure.
10. Two (2) methods were used in this study to predict the performance of the test sections. Both methods indicated that deep subgrade stabilization increases the strength and improve the service life of pavement. Using the equivalency framework developed in this study HMA thickness reduction can be predicted for deep subgrade stabilization pavement.
11. Cost-effectiveness of deep subgrade stabilization layer depends on the model used to evaluate pavement response. The viscoelastic, non-linear 3D FE implemented

in Abaqus produces a more consistent result. Cost analysis study of the test sections demonstrated cost effectiveness of deep subgrade stabilization layers.

8.2 Recommendations

This study was performed at a test site with limited field data (2 FWD tests). More long-term data and monitoring at the test site are needed. Field data from other sites with subgrade stabilization to depths greater than the current NCDOT standard depth are needed. The data are required to further validate this study. A life cycle analysis is needed to truly assess the long-term cost-effectiveness of deep subgrade stabilization layer. A well-conceived and comprehensive data collection program including traffic monitoring data, climatic/environmental data, and maintenance/rehabilitation data should be implemented. Efforts are needed to determine spatio-temporal variation in material properties of stabilized layers. Also, best compaction practices of deep subgrade stabilization should be investigated.

.

CHAPTER 9 REFERENCES

AASHTO (1993), AASHTO Guide for Design of Pavement Structures, 1993

AASHTO (2008), Mechanistic-Empirical Pavement Design Guide, Interim Edition: A Manual of Practice

Achampong, F., Usmen, M., Kagawa, T., and Session. (1997). "Evaluation of Resilient Modulus for Lime- and Cement-Stabilized Synthetic Cohesive Soils." Transportation Research Record. 1589, 70-75.

ACI. (2009). *Report on Soil Cement*, American Concrete Institute, Farmington Hills.

Al-Qadi, I. L., Wang, H., Yoo, P. J., and Dessouky, S. H. (2008). "Dynamic analysis and in situ validation of perpetual pavement response to vehicular loading." Transportation Research Record No. 2087: Journal of the Transportation Research Board, 29-39.

Appea, Alexander K., Imad L. Al-Qadi. (2000). "Assessment of Falling Weight Deflectometer Data for Stabilized Flexible Pavements."*Transportation Research Record*, 1(1709), 19-25.

ARA, Inc., ERES Consultants Division. (2004). "Guide for Mechanistic-Empirical Design of New and Rehabilitated Pavement Structures, NCHRP 1-37A Final Report," ERES Consultants Division, *Transportation research Board, National Research Council, Washington, D.C.*

Arabani, M., and Karami, M. (2007). "Geomechanical properties of lime stabilized clayey sands." Arabian Journal for Science and Engineering, 32(1), 11-26.

ASTM D2166. (2006). "Standard Test Method for Unconfined Compressive Strength of Cohesive Soil." ASTM International West Conshohocken, Pennsylvania.

ASTM D422. (1998). "Standard Test Method for Particle Size Analysis of Soils." ASTM International, West Conshohocken, Pennsylvania.

ASTM D4318. (2006). "Standard Test Method for Liquid Limit, Plastic Limit and Plasticity Index of Soils." ASTM International, West Conshohocken, Pennsylvania.

ASTM D5102. (2009). "Standard Test Method for Unconfined Compressive Strength of Compacted Soil Lime Mixtures." ASTM International, West Conshohocken, Pennsylvania.

ASTM D698. (2000). "Standard Test Method for Laboratory Compaction Characteristics of Soil Using Standard Effort." ASTM International, West Conshohocken, PA.

ASTM D854. (2000). "Standard Test Method for Specific Gravity of Soils,” ", ASTM International, West Conshohocken, Pennsylvania.

ASTM International.(2007). “D698-07 Standard Test Methods for Laboratory Compaction Characteristics of Soil Using Standard Effort,” West Conshohocken, Pennsylvania.

ASTM International.(2008). “D2167-08. “Standard Test Method for Density and Unit Weight of Soil in Place by the Rubber Balloon Method.” West Conshohocken, Pennsylvania.

Bell, F. G. (1996). "Lime stabilization of clay minerals and soils." ENGINEERING GEOLOGY -AMSTERDAM-, 42(4), 223-238.

Bell, F., and Coulthard, J. (1990). "Stabilization of clay soils with lime." Municipal Engineer, 7, 125-140.

Castel, A., and Arulanandan, K. (1979). "New Approach to Predict Lime Reactivity of Soils." Journal of the Geotechnical Engineering Division, 105(4), 563-568.

Cebon, D. (1986). "Road Damaging Effects of Dynamic Axle Loads." Proc., International Symposium on Heavy Vehicle Weights and Dimensions, 37-53.

Chen, Dar-Hao, Deng-Fong Lin, Pen-Hwang Liau, and John Bilyeu. (2005). "A Correlation Between Dynamic Cone Penetrometer Values and Pavement Layer Moduli." *Geotechnical Testing Journal* 28(1), pp. 42-49.

Consoli, N. C., da Silva Lopes, L., and Heineck, K. S. (2009). "Key Parameters for the Strength Control of Lime Stabilized Soils." Journal of materials in civil engineering, 21(5), 210.

Cook, R. D., Malkus, D. S., and Plesha, M. E. (1989). Concepts and Applications of Finite Element Analysis, Wiley, New York.

Crisman, B., and Facchin, G. (2005). "Advanced numerical methods to evaluate pavements response: comparison and parametric analysis."

Daita, R. K., Drnevich, V. P., Kim, D., Joint Transportation Research, P., Purdue University. School of Civil, E., Indiana. Dept. of, T., and United States. Federal Highway, A. (2005). "Family of compaction curves for chemically modified soils." Joint Transportation Research Program, School of Civil Engineering, Purdue University, West Lafayette, Ind.

Desai, C. S. (1979). "Elementary finite element method." Civil Engineering and Engineering Mechanics Series, Englewood Cliffs: Prentice-Hall, 1979, 1.

Eades, J., and Grim, R. (1966). "A quick test to determine lime requirements for lime stabilization." Highway Research Record, 139, 61-72.

El-Rawi, N., and Samadi, M. M. Y. A.-. (1995). "Optimization of Cement-Lime-Chemical Additives to Stabilize Jordanian Soils." Journal of Islamic Academy of Sciences, 8(4), 167-174.

Elseifi, M. A., Al-Qadi, I. L., and Yoo, P. J. (2006). "Viscoelastic Modeling and Field Validation of Flexible Pavements." Journal of engineering mechanics /, 132(2), 172-176.

George, K. P., (2004). "Prediction of resilient modulus from soil index properties." University of Mississippi, University, Miss.

George, S., Ponniah, D., and Little, J. (1992). "Effect of temperature on lime-soil stabilization." Construction and Building Materials, 6(4), 247-252.

Gillespie, T. D., S. M. Karimihas, D. Cebon, M. W. Sayers, M. A. Nasim, W. Hansen and N. Ehsan (1993). "NCHRP Report 353: Effects of Heavy-Vehicle Characteristics on Pavement Response and Performance. TRB, National Research Council."Washington, D.C.

Graves, R.E., and Eades, J.L. (1987) “Strength Development from Carbonate Cementation in Silicia/Carbonate Systems”, Final Report, Department of Geology, University of Florida.

Haddad, Y. M. (1995). Viscoelasticity of engineering materials, Chapman & Hall, London.

Hadi, M. N., and Bodhinayake, B. C. (2003). "Non-linear finite element analysis of flexible pavements." ADVANCES IN ENGINEERING SOFTWARE, 34(11-12), 657-662.

Heckel, G., Illinois. Dept. of Transportation. Bureau of, M., and Physical, R. (1997). Alternative materials for the modification and stabilization of unstable subgrade soils, Illinois Dept. of Transportation, Bureau of Materials and Physical Research Springfield; Springfield, VA.

Herrin, M. and Mitchell, H. (1961) “Lime-soil mixtures”, Highway Research Board, Bulletin 304, pp. 99-121.

Hibbit, Karlsson & Sorenson, Inc (2005), ABAQUS/Standard User's Manual, Version 6.5, Pawtucket, RI.

Hicks, R. G., and Monismith, C. L. (1971). "Factors influencing the resilient response of granular materials." Highway Research Record 345, 15-31.

Holt, C.C., Freer-Hewish, R.J., and Ghataora, G.S. (2000), “The use of Lime-treated British Clays in Pavement Construction. Part 2: The Effect of Mellowing on the Stability Process”, Journal: Proceedings of The Institution of Civil Engineers-transport - PROC INST CIVIL ENG-TRANSPORT , vol. 141, no. 4, pp. 207-216,

Hopkins, T. C., University of Kentucky Transportation, KTC., and United States. Federal Highway, A. (2004). "Resilient modulus of Kentucky soils."

Hopkins, T.C., Beckham, T. L., and Hunsucker, D. Q. (1995), Modification of Highway Soil Subgrades,” Research Report KTC-94-11, University of Kentucky Transportation Center, College of Engineering.

Hopkins, Tommy C.; Beckham, Tony L.; Sun, Liecheng; Ni, Bixian; and Butcher, Barry, (2002). "Long-Term Benefits of Stabilizing Soil Subgrades", Kentucky Transportation Center Research Reports. Paper 253.

Hua, J. (2000). "Finite element modeling and analysis of accelerated pavement testing devices and rutting phenomenon." ETD Collection for Purdue University.

Hua, J., and White, T. (2002). "A study of nonlinear tire contact pressure effects on HMA rutting." International Journal of Geomechanics, 2, 353.

Huang, H. (1995). "Analysis of accelerated pavement tests and finite element modeling of rutting phenomenon." ETD Collection for Purdue University, AAI9601511.

INDOT, (2008). “Design Procedures for Soil Modification or Stabilization” 13 p.

Ingles, O. G., and Metcalf, J. B. (1973). Soil stabilization: principles and practice, Wiley, NY.

Kavak, A., and Akyarh, A. (2007). "A field application for lime stabilization." Environmental Geology, 51(6), 987-997.

Kim, Y. R., Momen, M., and King, M. (2005). Typical dynamic moduli for North Carolina asphalt concrete mixtures, North Carolina Department of Transportation, Research and Analysis Group, and North Carolina State University Dept. of Civil, Construction and Environmental Engineering, Raleigh, N.C.

Kitazume, M., Nakamura, T., and Ohishi, K. (2003). "Laboratory Tests on Long-Term Strength of Cement Treated Soil." Geotechnical Special Publication, 120, 586-597.

Kruntcheva, M. R., Collop, A. C., and Thom, N. H. (2006). "Properties of asphalt concrete layer interfaces." Journal of Materials in Civil Engineering, 18, 467.

Lav A.H., Lav M.A. and Goktpe A.B., (2006). "Analysis and design of a stabilized fly ash as pavement base material." Journal of Fuel, 85, pp. 2359-2370.

Lee, K., Prezzi, M., and Kim, N. (2007). "Subgrade Design Parameters from Samples Prepared with Different Compaction Methods." Journal of transportation engineering, 133(2), 82.

Liao, Y. (2007). "Viscoelastic FE Modeling of Asphalt Pavements and Its Application to U.S. 30 Perpetual Pavement." Ohio University.

Little, D. (1990). "Comparison of In-Situ Resilient Moduli of Aggregate Base Courses with and without Low Percentages of Lime Stabilization." Innovations and uses for lime, 65-77.

Little, D. N. (1995). "Stabilization of pavement subgrades and base courses with lime", Kendall/Hunt Publishing Company, Dubuque, Iowa.

Little, D. N. (1999). "Evaluation of Structural Properties of Lime Stabilized Soils and Aggregates". Volume 1: Summary of Findings, Prepared for the National Lime Association. 97 p.

Little, D. N., and Nair, S. (2009). "Recommended practice for stabilization of subgrade soils and base materials." http://onlinepubs.trb.org/onlinepubs/nchrp/nchrp_w144.pdf.

Little, D., (2012). Lime Stabilization of Subgrade Soils for Structural Purposes: Past Evidence and Future Needs. Lime: Building on the 100-Year Legacy of the ASTM Committee C071-25

Little, Dallas N. (1996). "Assessment of In-situ Structural Properties of Lime-Stabilized Clay Subgrades". Transportation Research Record, 1(1546), pp. 13-23.

Logan, D. L. (1992). A first course in the finite element method, PWS-KENT, Boston.

Loulizi, A., Al-Qadi, I. L., and Elseifi, M. (2006). "Difference between in situ flexible pavement measured and calculated stresses and strains." Journal of transportation engineering, 132, 574-579.

Lund, O. L., Ramsey, W. J., and Nebraska. Dept. of, R. (1958). Experimental lime stabilization in Nebraska, Nebraska Dept. of Roads, Lincoln, Neb.

Mallela, J., Harold Von Quintus, P., Smith, K., and Consultants, E. (2004). "Consideration of Lime-Stabilized Layers in Mechanistic-Empirical Pavement Design."

Mallick, R. B., and El-Korchi, T. (2009). Pavement engineering: principles and practice, CRC Press : Taylor & Francis Group, Boca Raton; London; New York.

Mateos, M., and Davidson, D. (1963). "Compaction Characteristics of Soil-Lime-Fly Ash Mixtures." Highway Research board of the national Academy of Sciences, National Research Council, washington, DC Highway Research record, 29, 27-41.

McElvaney, J. and Ir. Bunadi Djatnika.(1991). “Strength Evaluation of Lime-Stabilised Pavement Foundations.”*Australian Road Research*, 21(1), pp. 40-52.

Mikhail, M. Y., and Mamlouk, M. S. (1998). "Effect of Traffic Load on Pavement Serviceability." ASTM special technical publication., 1348, 7.

Miller, Gerald A. (2000). “A Comparative Evaluation of Stabilized Subbase Courses. *Geotechnical Special Publication*, 1(94), pp. 388-400

MnDOT.(2008). *User Guide for the Dynamic Cone Penetrometer*, Mn/ROAD, Maplewood.

Montapara, A., Al-Qadi, Imad L., et al. (2007). "Loading Responses Comparison between Laboratory Testing and Numerical Modeling for Hot-Mix Asphalt Spcimens." 4th Iinternational SIIV Congress - Palemro (Italy).

Mooney, M. A., Toohey, N. M., Colorado, D. T. D. A. R., Innovation, B., and United States. Federal Highway, A. (2010). Accelerated curing and strength-modulus correlation for lime-stabilized soils, Colorado Department of Transportation, DTD Applied Research and Innovation Branch, Denver, CO.

Muench, S., Mahoney, J., and Pierce, L. (2003). "WSDOT Pavement Guide Interactive." Washington State Department of Transportation Materials Laboratory, Olympia, Wash.100

Mulungye, R. M., Owende, P. M. O., and Mellon, K. (2007). "Finite element modelling of flexible pavements on soft soil subgrades." Materials and Design, 28(3), 739-756.

Nalbantoglu, Z. (2006). "Lime stabilization of expansive clay", Expansive soils: recent advances in characterizations and treatment, Taylor & Francis, London, 341-348.

National Lime Association (NLA). 1988. Chemical Lime Facts, (Bulletin 214), 5th Edition, Arlington, VA.

National Lime Association, (2004). "Lime Treated Soil Construction Manual Lime Stabilization and Lime Modification."

National Research Council (1987). Lime stabilization: Reactions, Properties, Design, and Construction, Transportation Research Board, National Research Council. Committee on, Lime

Nazzal, Munir D. and Louay N. Mohammad. (2010). “Estimation of Resilient Modulus of Subgrade Soils Using Falling Weight Deflectometer.” *Transportation Research Record*, (1)2186, pp. 1-10

NCHRP 04-36 “Characterization of Cementitiously Stabilized Layers for Use in Pavement Design and Analysis” Completed not yet published (NCHRP report 789)

NCHRP 1-37A (2004). Guide for Mechanistic-Empirical Design of New and Rehabilitated Pavement Structures. National Cooperative Highway Research Program. Transportation Research Board.

New York Transportation Department (2008). “Standard Specifications for Bases and Subbases”. Section 300.

North Carolina Department of Transportation. (2006). “Standard Specifications for Roads and Structures”, North Carolina Department of Transportation, Raleigh.

North Carolina Department of Transportation.(2009). *Conventional Density Testing*, North Carolina Department of Transportation – Materials and Tests Unit, Raleigh.

O’Flaherty, C., and Andrews, D. (1968). "Frost Effects in Lime and Cement-Treated Soils." Highway Research Record, 235, 49-60.

O'Connor, M., Parsons, R. L., Kansas. Dept. of Transportation.. (2006). Lime application methods, Kansas Department of Transportation ;, Topeka, Kan.; Springfield, Va.

Ozier, J., and Moore, R. (1976). "Factors Affecting the Unconfined Compressive Strength of Salt-lime Treated Clay." 641, 17-24.

Perl, M., Uzan, J., and Sides, A. (1983). "Visco-elasto-plastic constitutive law for a bituminous mixture under repeated loading." Transportation Research Record (911).

Powell, W. D., Potter, J. F., Mayhew, H. C., and Nunn, M. E., (1984). “The Structural Design of Bituminous Roads,” TRRL Report LR 1132, 62 pp.

Prusinski, J. R., and Bhattacharja, S. (1999). "Effectiveness of Portland Cement and Lime in Stabilizing Clay Soils." Transportation research record.(1652), 215.

Puffer, W. (1981).“Engineering Trade-offs in Subgrade Stabilization.”*Railway Track and Structures*, 77(6), pp. 25-26, 28, 30114

Puppala, A. J., Mohammad, L. N., and Allen, A. (1996). "Engineering Behavior of Lime-Treated Louisiana Subgrade Soil." Transportation research record.(1546), 24-31.

Qubain, B., Seksinsky, E., and Li, J. (2000). "Incorporating subgrade lime stabilization into pavement design." Transportation Research Record: Journal of the Transportation Research Board, 1721(-1), 3-8.

Rao, S., and Shivananda, P. (2005). "Role of curing temperature in progress of lime-soil reactions." Geotechnical and Geological Engineering, 23(1), 79-85.

Rogers, C., and Glendinning, S. (2000). "Lime requirement for stabilization." Transportation Research Record: Journal of the Transportation Research Board, 1721(-1), 9-18.

Romanoschi, S. A., and Metcalf, J. B. (2001). "Characterization of asphalt concrete layer interfaces." Transportation Research Record: Journal of the Transportation Research Board, 1778(-1), 132-139.

Russell, Harrison S. and Mustaque Hossain. (2000). “Design Resilient Modulus of Subgrade Soils from FWD Tests.” *Geotechnical Special Publication*, 1(98), pp. 87-103

Schapery, R. (1984). "Correspondence principles and a generalized integral for large deformation and fracture analysis of viscoelastic media." International Journal of Fracture, 25(3), 195-223.

Schoute, E. J. (1999). “Chemical Stabilization of Soft Clay,” MS Thesis, Memoirs of the Centre of Engineering Geology in the Netherlands, No. 188, pp.15-39.

Siddharthan, R. V., Krishnamenon, N., El-Mously, M., and Sebaaly, P. E. (2002). "Investigation of tire contact stress distributions on pavement response." Journal of transportation engineering, 128, 136.

Sivaneswaran, N., Pierce, L., and Mahoney, J. (1999). "Everseries software." Washington State Department of Transportation, Olympia.

Smith, Charles R., Dwayne E. Lewis, James Turner, and David M. Jared.(2008). "Georgia's Use of Lime in Full-Depth Reclamation."*Transportation Research Record*, (1)2059, pp. 89-94.

Solanki, P., and Zaman, M., (2014). "Effect of Wet-Dry Cycling on the Mechanical Properties of Stabilized Subgrade Soils" Geo-Congress 2014 Technical Papers, GSP 234, pp 3625-3634.

Solanki, P., Khoury, N., and Zaman, M. M. (2009). "Engineering Properties and Moisture Susceptibility of Silty Clay Stabilized with Lime, Class C Fly Ash, and Cement Kiln Dust." Journal of materials in civil engineering, 21(12), 749.

Stubstad, Richard, Y. Jane Jiang and Erland Lukanen.(2005). "Forwardcalculation of Pavement Moduli with Load-Deflection Data."*Transportation Research Record* - Pavement Rehabilitation, Strength and Deformation Characteristics, and Surface Properties-Vehicle Interaction 2007, (1)2005, p 104-111.

Sweeney, D. A., Wong, D. K. H., Fredlund, D. G.,(1988). "The effect of lime on a highly plastic clay with special emphasis on aging." National Research Council, Transportation Research Board, Washington, D.C.

Sweere, G. T. H. (1990). Unbound granular bases for roads. PhD thesis, Faculty of Civil Engineering, Delft University of Technology, Delft, The Netherlands.

Thompson, M. (1972). "Deep-plow lime stabilization for pavement construction." Journal of the Transportation Engineering Division, 98(2), 311-323.

Thompson, M. R. (1964). "Lime-reactivity of Illinois soils as it relates to compressive strength."

Tutumluer, E., and Kim, M. (2006). "Considerations for Nonlinear Analyses of Pavement Foundation Geomaterials in the Finite Element Modeling of Flexible Pavements." ASCE, 133-144.

USACE. (1994). "Soil stabilization for pavements." Dept. of the Army, Navy, and Air Force, [Washington, DC].

Uzan, J. (1985). "Characterization of granular material." Transportation Research Record (1022), 52-59.

Uzan, J. _2005_. "Viscoelastic-viscoplastic model with damage for asphalt concrete" J. Material in Civil Engineering, 17(5), 528–534.

Uzan, J. and Levenberg, E. (2007). "Advanced Testing and Characterization of Asphalt Concrete Materials in Tension”. International Journal of Geomechanics, 7(2), 158-165.

Vorobieff, G., and Murphy, G. (2003). “A New Approach to Pavement Design Using Lime Stabilized Subgrades”. Proceedings of the 21st ARRB and 11th REAAA Conference. Transport. Our Highway to a Sustainable Future. ARRB Transport Research, Limited, Cairns, Australia, 12 p.

Wang, H. and Al-Qadi, I. (2008) Comparison between Mechanistic Analysis and In-Situ Response of Full-Depth Flexible Pavements. Airfield and Highway Pavements: pp. 1-15.

Webster, S.L., Grau, R.H., Williams, R.P., 1992. Description and application of Dual Mass Dynamic Cone Penetrometer. U.S. Army Engineers, Waterways Experiment Station, Instruction Report, No. GL-92-3.

Wiseman, G. and J. Greenstein. (1983). “Comparison of Methods of Determining Pavement Parameters from Deflection Bowl Measurements,” Proceedings from the 7th Asian Regional Conference on Soil Mechanics and Foundation Engineering

Yin, H., Solaimanian, M., Kumar, T., and Stoffels, S. (2007). "The effect of loading time on flexible pavement dynamic response: a finite element analysis." Mechanics of Time-Dependent Materials, 11(3), 265-288.

Yoo, P. J. (2008). "Flexible pavement dynamic response analysis and validation for various tire configurations." University of Illinois at Urbana-Champaign.

Yoo, P. J., and Al-Qadi, I. L. (2006). "Flexible pavement response to different loading amplitudes." Airfield and highway pavements : meeting today's challenges with emerging technologies : proceedings of the 2006 Airfield and Highway Pavement Specialty Conference, April 30-May 3, 2006, Atlanta, Georgia., 39-49.

Yoo, P., Al-Qadi, I., Elseifi, M., and Janajreh, I. (2006). "Flexible pavement responses to different loading amplitudes considering layer interface condition and lateral shear forces." International Journal of Pavement Engineering, 7(1), 73-86.

Yun, T. (2008). "Development of a Viscoplastic Constitutive Model using Rate-Dependent Yield Criterion for HMA in Compression." Ph.D. Dissertation, North Carolina State University.

APPENDICES

APPENDIX A

A.1. Survey of Deep Layers of Subgrade Stabilization Practices in the United States

The summary of an online survey questions sent to state transportation agencies in the USA is presented in Table A.1 below.

Table A.1 Survey Questions

Number	Question
1	Name and Title
2	Responsibility
3	Unit
4	State and division
5	Email
6	Phone Number
7	Does your agency/company use or perform soil stabilization of pavement subgrade?
8	Have you ever experimented with subgrade stabilization?
9	Was the stabilization done with chemical additives? (lime cement fly ash)
10	What is the type of stabilization?
11	Short description of the criteria for selecting stabilization method/type.
12	Typical percent content of chemical additives used for subgrade stabilization (example 6% cement or cement of 25 kg/m^2 to a depth of 20 cm)
13	What is the typical depth of cement stabilized subgrade used in pavement by your organization/agency
14	What is the typical depth of lime stabilized subgrade used in pavement by your organization/agency
15	If you stabilize deeper than 7' for cement specify the depths
16	If you stabilize deeper than 8' for lime specify the depths
17	Design and mix ratio criteria for cement (what method do your division use to test the samples and what criteria must they meet?)
18	Design and mix ratio criteria for lime (what method do your division use to test the samples and what criteria must they meet?)

A.2. Validation of Viscoelastic Finite Element Modeling of Asphalt Pavement under Moving Wheel Loads

A.2.1 Non-Linear Behavior of Hot-Mix Asphalt

The behavior of hot-mix asphalt layer depends on factors such as temperature, loading time, and rate of loading. The best way to simulate non-linear behavior and solve such problems computationally is using finite element method. In FEM, the behavior of viscoelastic material is successfully represented by Prony series. The Prony series representation of viscoelastic material provides efficient numerical solution to linear viscoelastic boundary value problems.

A.2.1.1 Prony Series Representation in Abaqus

In ABAQUS, viscoelastic material is defined by a Prony series expansion of the dimensionless shear relaxation modulus $g_R(t)$ given by,

$$g_R(t) = 1 - \sum_{i=1}^{N} g_i (1 - e^{-t/\tau_i}) \tag{A.1}$$

Where,

g_i = Prony series parameters;

τ_i = relaxation times; and,

N = number of Prony series terms.

The time dependent bulk $K(t)$ and shear $G(t)$ moduli can be determined from relaxation modulus $E(t)$ using the following relationship:

$$G(t) = \frac{E(t)}{2(1+\nu)} \tag{A.2}$$

$$K(t) = \frac{E(t)}{3(1-2\nu)} \tag{A.3}$$

Where,

$G(t)$ = shear relaxation modulus;

$E(t)$ = relaxation modulus;

$K(t)$ = bulk relaxation modulus; and,

ν = Poisson's ratio.

In ABAQUS, time dependent shear and bulk moduli is defined in one of the four ways: by direct specification of Prony series parameters, by providing creep test data, by providing relaxation test data, or by providing frequency-dependent test data (ABAQUS User's Manual, 2003). In this study, frequency dependent modulus data obtained from dynamic modulus test is used to define viscoelastic material properties. The laboratory determined modulus data is defined in tabular form by providing real and imaginary part of ωg^* and ωk^*, where ω is angular frequency. ABAQUS will determine the Prony series parameters from frequency data by performing non-linear square fit (ABAQUS User's manual, 2003). The real and imaginary parts of shear moduli are defined as:

$$\omega R(g^*) = G_l / G_\infty \tag{A.4}$$

$$\omega I(g^*) = 1 - (G_s / G_\infty) \tag{A.5}$$

Where,

$R(g^*)$, $I(g^*)$ = real and imaginary parts of shear modulus respectively;

G_∞ = long-term shear modulus;

G_s, G_l = storage and loss modulus respectively;

ω = angular frequency = $2\pi f$ rad/sec; and,

f = frequency in Hz.

At any particular frequency, the storage and loss modulus are obtained from shear modulus using following relationship.

$$G_s(\omega) = G\cos\varphi \tag{A.6}$$

$$G_I(\omega) = G \sin \varphi \tag{A.7}$$

Where,

φ = phase angle in radians.

Similarly, real and imaginary parts of bulk moduli are calculated.

A.2.2 Quasi-Static Analysis

In Abaqus/Standard, a quasi-static analysis is used to analyze time dependent material response such as creep, swelling, and viscoelasticity. The main different between dynamic analysis and quasi-static analysis is first consider the effect of inertia while later neglects it. A research done by Monismith et al. (1988) showed that for flexible pavements, a quasi-static analysis is a reasonable approximation (Monismith, et al., 1988). The quasi-static analysis can be linear or non-linear (ABAQUS User's Manual, 2003). In this study, *VISCO procedure, an option in ABAQUS step module, is considered most appropriate to capture the visco-elastic behavior of HMA and thus used to perform the analysis for this project.

A.2.3 Pavement Layer Interaction

Most of the mechanistic design methods for flexible pavement assume full-bond between pavement layers. Even in layered elastic theory, stress-strain compatibility is assumed between layer interfaces. But, full-bond is not achieved all the time and in practice, pavement interface properties are functions of traffic loading, time, and temperature (Kruntcheva, et al., 2006). Many researchers used friction models to define layer interaction and found results in good agreement with field measured data (Romanoschi and Metcalf, 2001,Elseifi, et al., 2006, Yoo, et al., 2006). In this study, for comparison, layer interaction properties defining with isotropic Coulomb friction model is compared with full-bond condition.

A. 2.3.1 Tied or Coulomb Friction Model

A Coulomb friction model relates maximum shear stress at the interface to normal stress between the contacting bodies (ABAQUS Analysis User's manual, 2003). The two surfaces in contact resist movement up to a certain magnitude of shear stress and then start sliding relative to each other. The maximum shear stress at which sliding begins is defined as a fraction of contact pressure at the interface. Mathematically, a Coulomb friction model is defined by:

$$\mu = \frac{\tau_{\max}}{\sigma} \tag{A.8}$$

Where,

μ = coefficient of friction;

$\tau_{\max}$ = maximum shear stress; and,

σ = normal stress at the interface.

In ABAQUS, a simple friction model is defined by coefficient of friction (μ). The coefficient of friction is a positive number representing slope of the relationship between shear stress and normal stress at the contact (Yoo, 2008). The contacting surfaces carry maximum shear stress $\tau_{\max}$ before they start sliding relative to each other; this state is known as sticking. The friction coefficient can be varied from 0 to 1 corresponding to friction angle between 0 and 45^0.

In pavements, layer interfaces can be modeled as two small sliding rigid bodies. According to Romanoschi and Metcalf (2001) the pavement surfaces in contact are of very large area and remain in contact with no gap-opening. This condition is included in ABAQUS by using "No Separation" algorithm (Romanoschi and Metcalf, 2001, Yoo, 2008). The parameter prevents separation of two surfaces once the contact has been established.

ABAQUS also provides option to tie and constraint sliding of surfaces of rigid bodies in contact. This option assumes perfect contact and irrespective of the induced transverse stresses the surfaces remain in full contact. This option is also evaluate and the data compared with those of the Coulomb friction model.

A.2.4 Trapezoidal Loading Amplitude Method

In FE model, moving wheel load is simulated by gradually shifting tire imprint area over the loading area. The approximation of tire imprint by circular contact area is a simplified assumption and gives erroneous results. The actual contact area is non-circular and can be represented more accurately by two semi-circles and a rectangle given below.

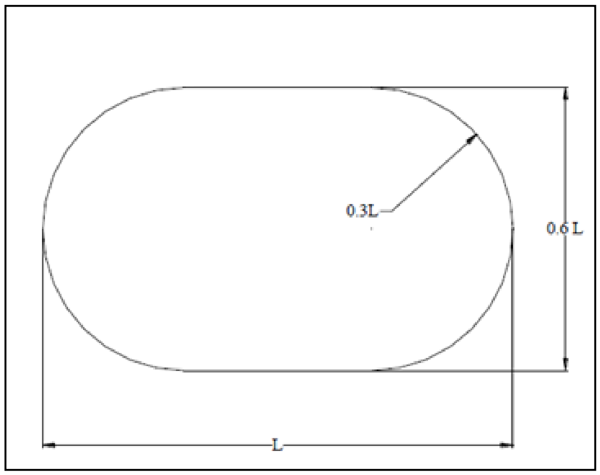

Figure A.1 Assumed Tire-Pavement Contact Area

By assuming length of tire imprint as L and width 0.6L, the area of contact can be determined by,

$$A_c = \pi(0.3L)^2 + (0.4L)(0.6L) = 0.5227L^2 \quad \text{(A.9)}$$

Where,

A_c = the contact area = $\dfrac{tireload}{tirepressure}$; and,

L = total length of tire patch given by,

$$L = \sqrt{\frac{A_c}{0.5227}} \quad \text{(A.10)}$$

To simulate a moving load, a step load function is applied to a first set of elements and then moves to the next set of elements in direction of traffic. When load is applied on the last set of elements in wheel path, a single wheel pass is completed. A loading sequence for a particular element in wheel path is given below (Figure A.2).

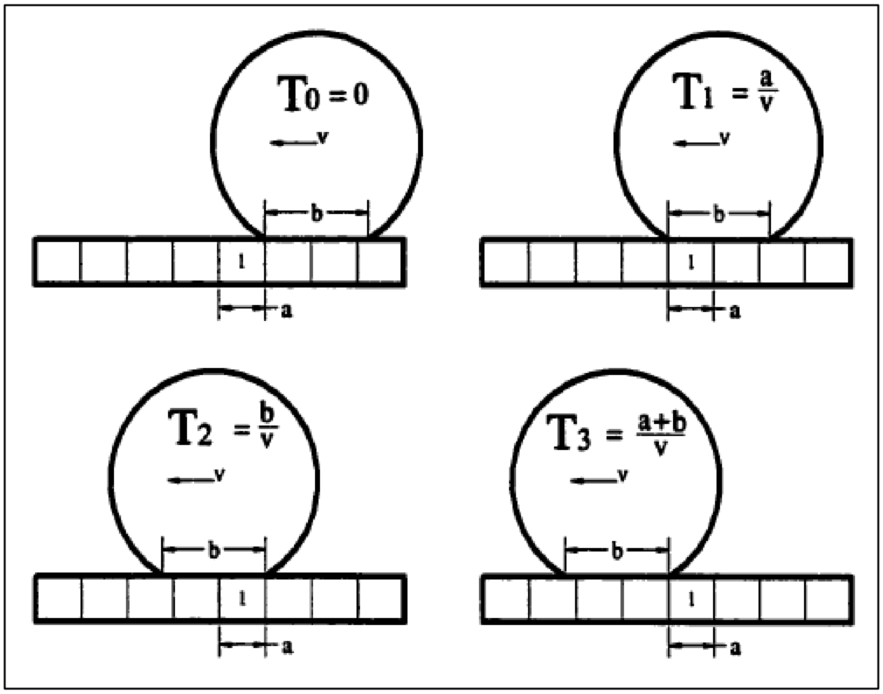

Figure A.2 Time Calculation of Step Loading (Hua, 2000)

At time T_0, a wheel load is approaching element 1 so the load on element 1 is zero. At time T_1, element 1 is covered by tire and pressure on element 1 is at its maximum. The time needed to travel can be found out by dividing length of element 1 by vehicle speed. At time T_2, element 1 is still covered by tire imprint and load is still at its maximum. At time T_3, as vehicle leaves the surface of element 1, the load drops from maximum to zero (Hua, 2000).The variation of amplitude with respect to time is given in Figure A.3.

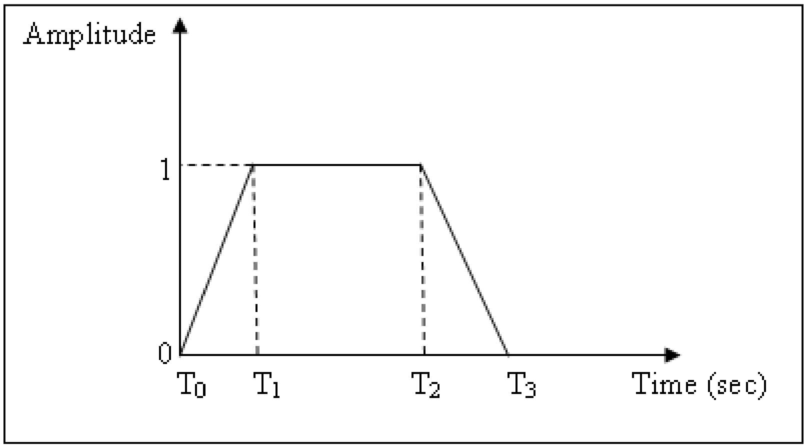

Figure A.3 Variation of Amplitude with respect to Time

The different time intervals are calculated as follows:

From T_0 to T_1:

$$t_1 = T_1 - T_0 = \frac{a}{s} \tag{A.11}$$

From T_1 to T_2:

$$t_2 = T_2 - T_1 = \frac{b-a}{s} \tag{A.12}$$

From T_2 to T_3:

$$t_3 = T_3 - T_2 = \frac{a+b}{s} - \frac{b}{s} = \frac{a}{s} \tag{A.13}$$

Total time duration,

$$T(\text{sec}) = t_1 + t_2 + t_3 = \frac{a+b}{s} \tag{A.14}$$

Where,

a = element length, mm;

b = tire imprint length, mm; and,

s = vehicle speed, mm/sec.

In ABAQUS, the trapezoidal loading amplitude data is given in tabular format. The time-amplitude data is shown below.

Table A.2 Time-Amplitude Data

Time (sec)	Amplitude
T_0	0
T_1	1
T_2	1
T_3	0

In reality, the contact pressure between tire and pavement surface is non-uniform. The actual pressure distribution depends on tire inflation pressure, tire load, type of tire as well as pavement's material properties such as stiffness. However, in order to simplify the analysis, contact pressure was assumed to be uniform over the contact area.

A. 2. 1 Viscoelastic FE Modeling of Asphalt Pavement under Moving Wheel Load

The research team of University of North Carolina at Charlotte (UNCC) has studied the effect of heavy vehicles on asphalt pavements in Charlotte, NC. As a part of that research, stresses and strains were measured at different sections of a pavement under different vehicle configurations with the help of sensors. In this study, a FE model with linear viscoelastic theory and trapezoidal impulsive loading amplitude method is used to predict response of asphalt pavements computationally. The results were compared with field measured data to validate the numerical model developed for this project.

In present research, pavement response of minor arterial street section under Charlotte Area Transit System (CATS) bus is simulated using ABAQUS. From Figure A.4, it is seen that HMA layer of the minor street section consists of 63.5 mm (2.5 inches) surface layer, 57.2 mm (2.25 inches) intermediate layer and 203.2 mm (8 inches) base layer. The front single tire, single axle of CATS bus has axle load of 42.3 kN and exerts tire pressure of 844.6 kPa (0.8446 N/mm^2). The tire-pavement contact area is assumed to be non-circular and its dimensions are determined using Equations A.9 and A.10.

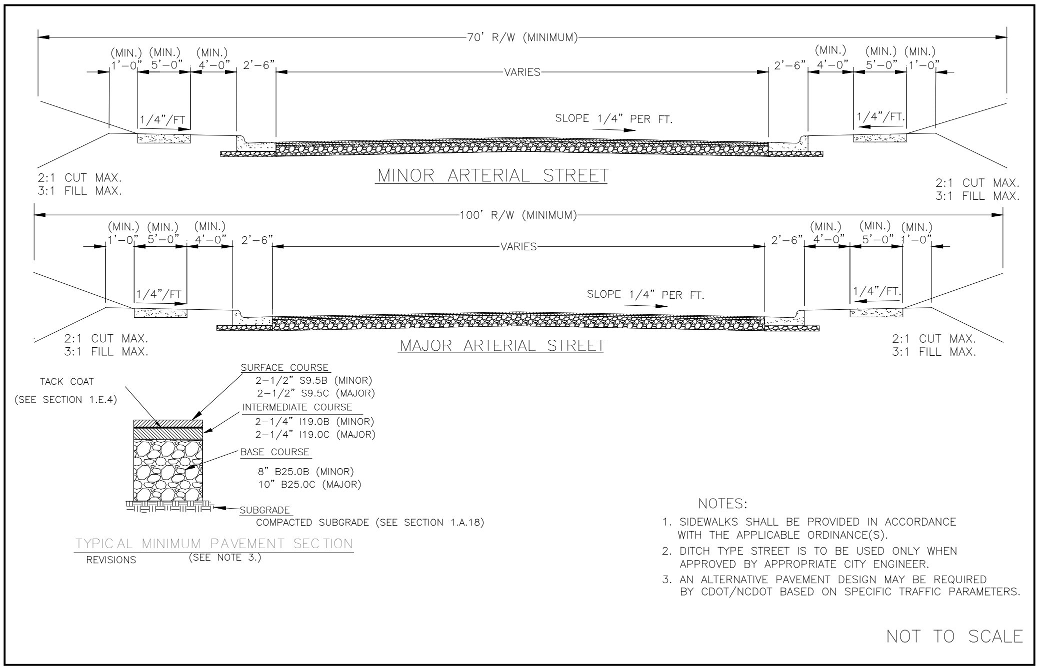

Figure A.4 Typical Arterial Street Sections of Charlotte Land Development Standards

The research team of UNCC performed falling weight deflectometer (FWD) test to determine dynamic modulus of pavement layers. FWD test data in conjunction with the forward calculation method is used to calculate instantaneous moduli of HMA and subgrade layer. The field test was conducted at 10Hz and 64° F. Detailed information about the procedure is presented elsewhere (Cranford, 2011). For comparison, FE responses using equivalent laboratory determined HMA moduli for similar HMA types are determined. The equivalent laboratory data were obtained from the study conducted by Kim, et al. (2005) on typical dynamic moduli for North Carolina Asphalt Concrete Mixtures.

FWD test gives the dynamic modulus of composite HMA layer and not the dynamic modulus of surface, intermediate and base layers separately. Therefore, laboratory determined dynamic modulus at different loading frequencies is calculated for the composite layer using Equation A.15.

$$E^*_{composite} = \frac{\sum E^*_{layer} \times h_{layer}}{h_{total}} \qquad \text{(A.15)}$$

From FWD test, the instantaneous moduli of HMA and subgrade layers were 13597.7 N/mm^2 (1,972,179 psi) and 153.66 N/mm^2 (22,287 psi), respectively. While equivalent laboratory determined dynamic modulus of HMA layer was 10111.78 N/mm^2. (1,466,589.7) psi.

In ABAQUS, to define viscoelastic material properties of HMA, dynamic modulus ($E^*_{composite}$) is calculated at different frequencies using time-temperature superposition (t-TS) principle. The unknowns, sigmoidal coefficients and shift factor coefficients in t-TS principle are determined by referring to the work done by Kim et al. (2005). The phase angle for a particular frequency and temperature is evaluated by curve fitting of the experimental data. The viscoelastic material properties for FWD and laboratory test are assumed the same for this analysis.

The characteristics of HMA layer is given in the table below.

Table A.3 Characteristics of HMA Layer

	Course	Mix type	Shift Function Coefficients			Sigmoidal Coefficients			
			α1	α2	α3	a	b	d	e
HMA	Surface	S[1]9.5[2]B[3]	0.00067	-0.14940	1.49840	1.3257	3.21009	1.54126	0.49085
	Intermediate	I19.5B	0.00075	-0.15933	1.51615	1.36605	3.19382	1.56800	0.44184
	Base	B25.0B	0.00087	-0.15998	1.51815	1.25921	3.26262	1.71818	0.48357

Note: [1]S for surface mix, I for intermediate mix, and B for base mix

[2]Nominal maximum aggregate size (in mm)

[3]Traffic volume indicator

The viscoelastic material properties of composite HMA layer at 10 Hz and 64° F are given below:

Table A.4 Viscoelastic Material Properties of Composite HMA Layer

Frequency (Hz)	E* (N/mm^2)	φ (Deg)	G*(N/mm^2)	k*(N/mm^2)
0.01	1203.6814	27.41	445.8079	1337.4238
0.05	2189.8566	26.01	811.0580	2433.1740
0.1	2794.4640	25.05	1034.9867	3104.9600
0.5	4701.9841	23.59	1741.4756	5224.4268
1	5751.6890	21.34	2130.2552	6390.7655
5	8678.6011	18.31	3214.2967	9642.8901
10	10111.7786	16.83	3745.1032	11235.3095
25	12111.7618	15.74	4485.8377	13457.5131

Where:

E* = dynamic modulus N/mm^2;

G* = shear dynamic modulus N/mm^2;

k* = bulk dynamic modulus N/mm^2; and,

φ = phase angle in degrees.

In ABAQUS, the material properties required to define HMA and subgrade layer are given below:

Table A.5 Material Properties of HMA and Subgrade using FWD Test

	Elastic Properties		Viscoelastic Properties				
Layer	E (N/mm^2)	ν	ωg*_real	ωg*_imag	ωk*_real	ωk*_imag	Freq. (Hz)
HMA	13597.7	0.35	1.11365	-1.14754	1.11365	-1.14754	0.01
			1.93001	-2.95535	1.93001	-2.95534	0.05
			2.37796	-4.08795	2.37796	-4.08795	0.1
			3.78174	-7.66019	3.78174	-7.66018	0.5
			4.20654	-9.76700	4.20654	-9.76700	1
			5.47954	-15.55889	5.47953	-15.55888	5
			5.88398	-18.45188	5.88398	-18.45186	10
			6.60327	-22.42907	6.60326	-22.42905	25
Subgrade	153.66	0.35	------				

The stress-strain data from the field was measured for a vehicle speed of 16 km/h (10 mph) and a surface temperature recorded during the test of 64^0F. A finite element model is developed by incorporating the above mentioned material properties. The model has dimensions 1,800 mm × 15,000 mm (70.0 in. x 590.6 in.). The composite HMA layer is 325 mm (12.75 inches) thick and subgrade thickness is 1300 mm (51.2 inches), approximately 4 times the thickness of composite HMA layer. The bottom of subgrade layer is fixed in all directions and horizontal motion perpendicular to the boundaries of a pavement model is constrained.

The loading area has dimensions of 130 mm × 9, 000 mm (5.1 in. x 354.3 in.). The width of loading area is equal to width of a tire. The longitudinal dimension of loading area is very large in order to capture pavement response for one complete loading cycle. If the longitudinal dimension is small, then pavement model fails to capture evolution of strain smoothly. For example, in case of longitudinal strain at the bottom of HMA layer, when vehicle approaches a data observing point, strain at the bottom of HMA layer is compressive. As vehicle approaches closer and closer, the data observing point starts experiencing tensile strain and it has maximum strain when load is exactly above it. Therefore, in order to capture this strain transition from compression to tension, the length of loading area is kept large otherwise there will be a sharp variation in strain magnitude. Moreover from field loading test on the instrumented test section, it is observed that the strain response data for front axle of CATS is captured in approximately 2sec. Therefore, length of loading area can be estimated by:

Length of loading area = vehicle speed (mm/sec) × time traveled (sec)

In this case, for vehicle speed of 16 kmph (10 mph), results in

Length of loading area = 4444.48 × 2 = 8888.96mm

Hence, length of loading area is estimated as 9000mm.

In FE model, the loading area has divided into small elements to simulate a moving load (Figure A.5). The moving load is simulated by using trapezoidal loading amplitude method as discussed before. The trapezoidal impulsive loading is applied to a first set of elements and moves longitudinally to the next set of elements. In total, 90 different increments were required to achieve one full passage of vehicle. When load is applied on the last set of elements, a single wheel pass is completed. The loading and unloading time for a particular set of elements is determined using Equations A.11 - A.14.

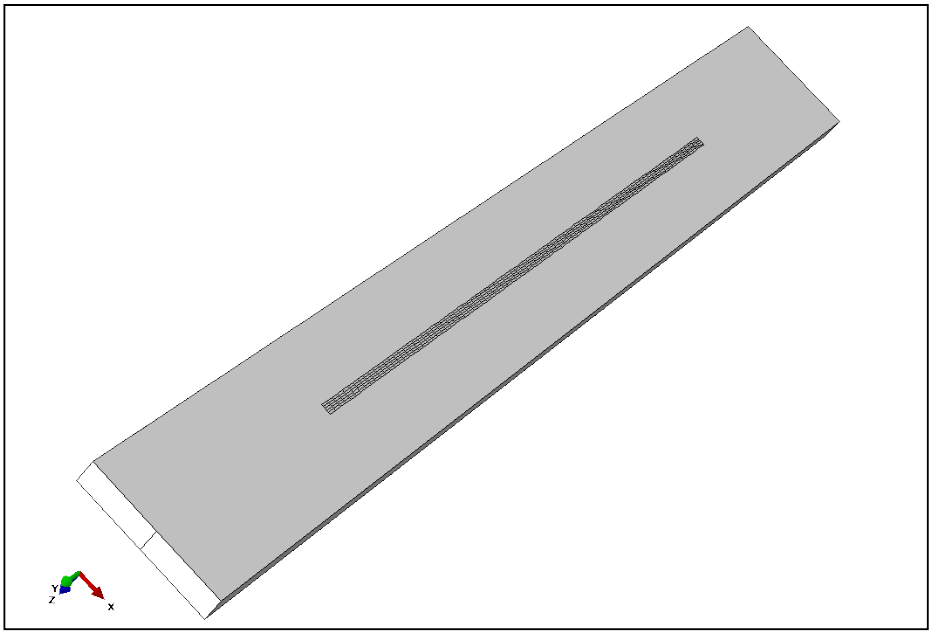

Figure A.5 Loading Area on HMA surface

After several iterations, an element length (a) of 100 mm less than half of the tire imprint length (b) of 219 mm was found to be optimal for this analysis. For a vehicle speed of (s) of 4444.48 mm/sec, using Equations 3.29 – 3.32, the time-amplitude data for the CATS bus for the first set of elements is presented in Table A.6 below.

Table A.6 Time-Amplitde data for vehicle speed of 16 kmph (10 mph)

Time (sec)	Amplitude
0	0
0.0225	1
0.0495	1
0.072	0

For comparison, Coulomb friction model and tie constraint are used to define layer interaction. In Coulomb friction model, the friction parameter μ was set to 1. The model is discretized with 8-node linear brick reduced integration elements (C3D8R) to improve the rate of convergence. A fine mesh is used near the loading area and coarse mesh away from it. The bias mesh is used along the depth of subgrade with higher number of elements near top of subgrade. The total number of elements in FE model was 121,563. The discretized FE model is shown in Figure A.6.

The FE results are compared with experimental data. In FE model, strain is calculated at the center of loading area. A pictorial representation of strain variation in FE model is given below. From Figure A.7 it is seen that inelastic strain at any time is maximum at the bottom of HMA layer while vertical displacement is maximum at the pavement surface and its magnitude decreases along the depth of a pavement shown in Figure A.8.

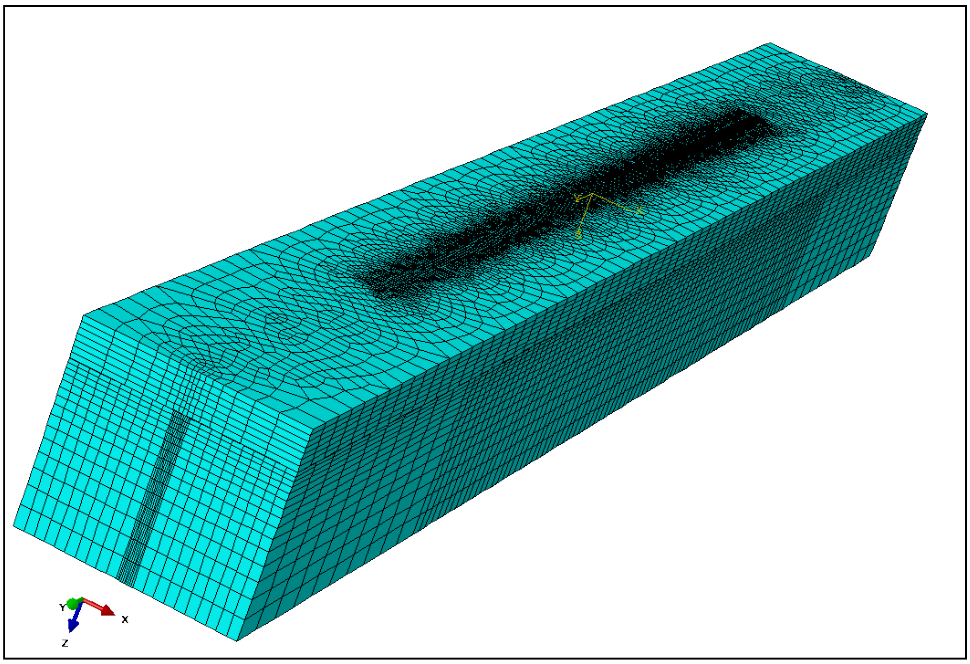

Figure A.6 FE Model of Asphalt Pavement

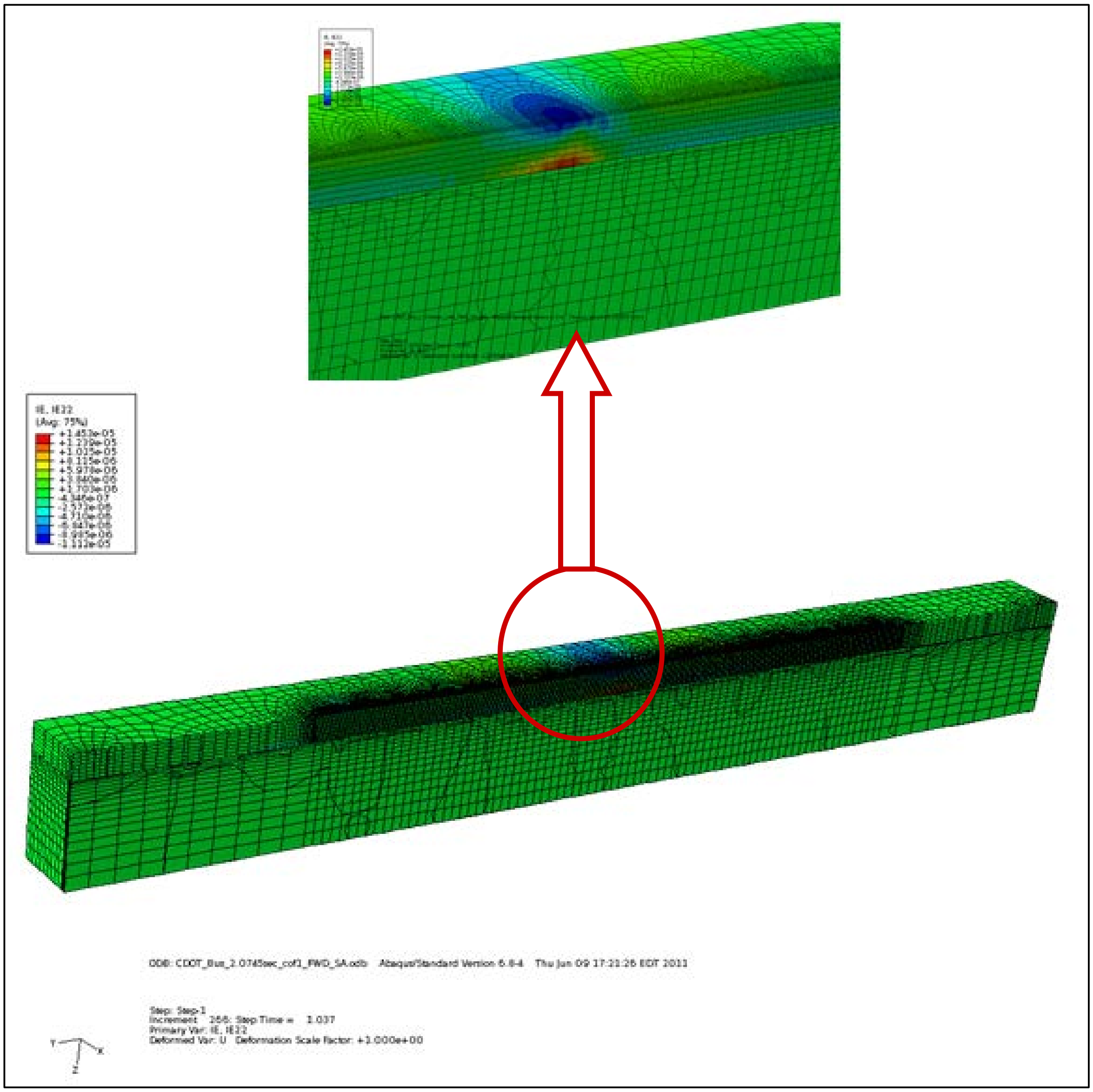

Figure A.7 Inelastic Strain (IE22) Distribution in a Pavement Structure

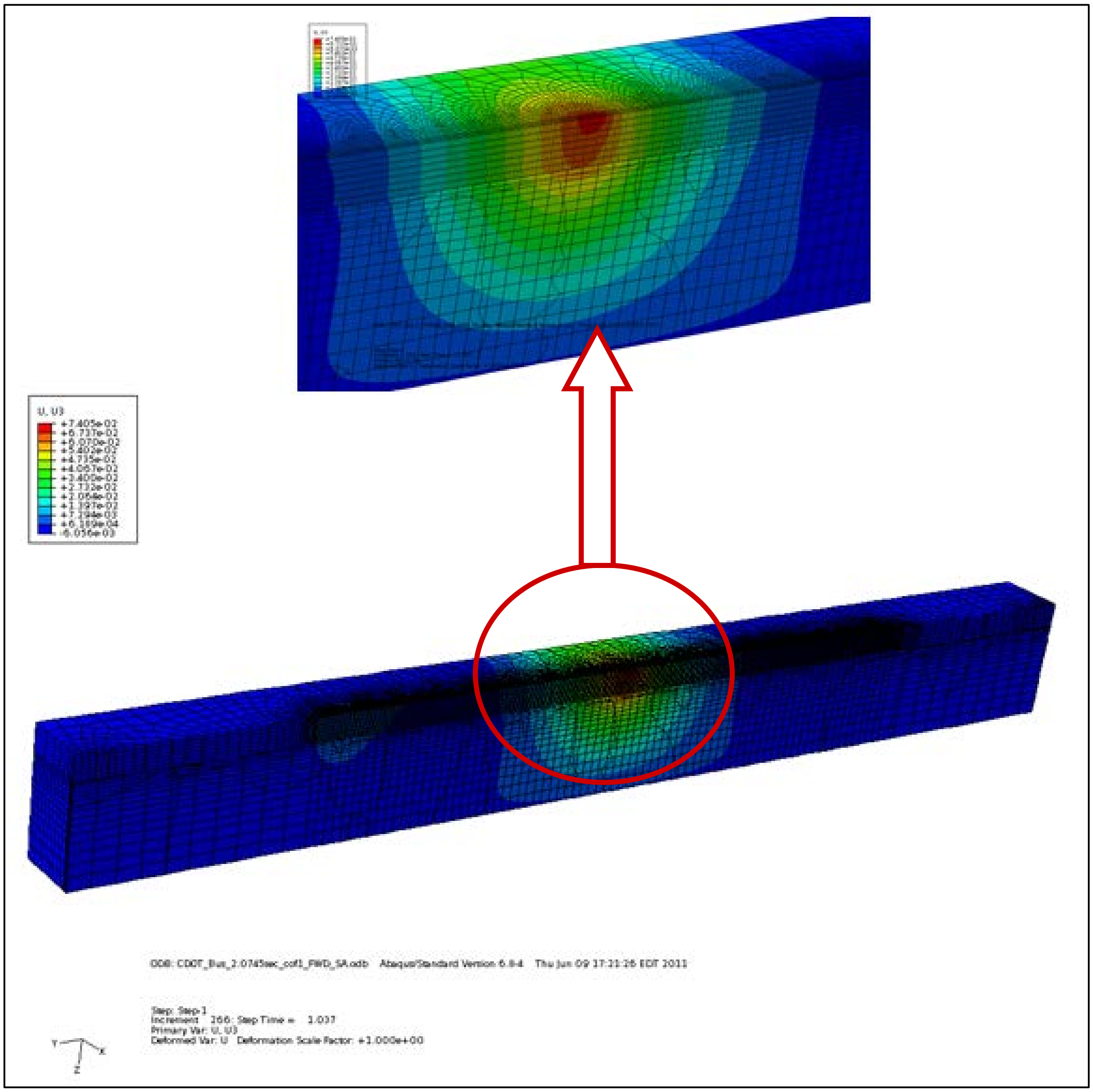

Figure A.8 Variation of Vertical Displacement (U3) in a Pavement System

Figures A.9 and A.10 compare measured and calculated longitudinal and transverse strain respectively at the bottom of HMA layer at 16 kmph. It is observed that FWD modulus with layer friction coefficient 1 predicts longitudinal strain with an error of approximately 5%, while 10% error is observed in case of transverse strain.

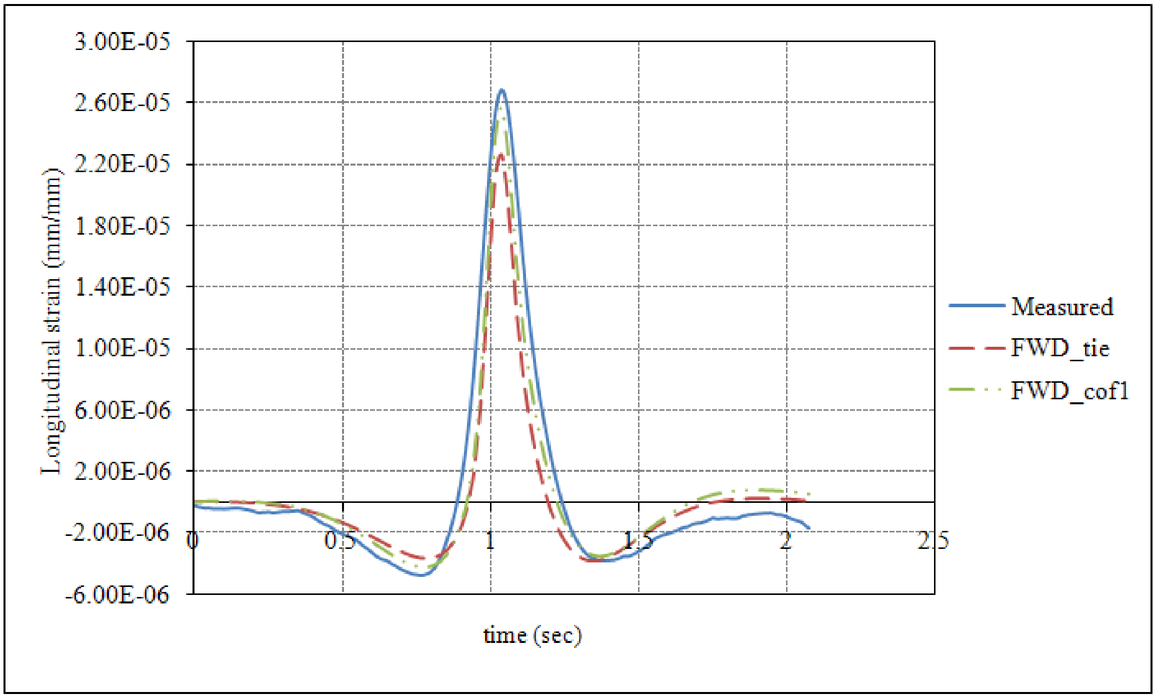

Figure A.9 Longitudinal Strain (TE22) at the Bottom of HMA Layer using FWD Data

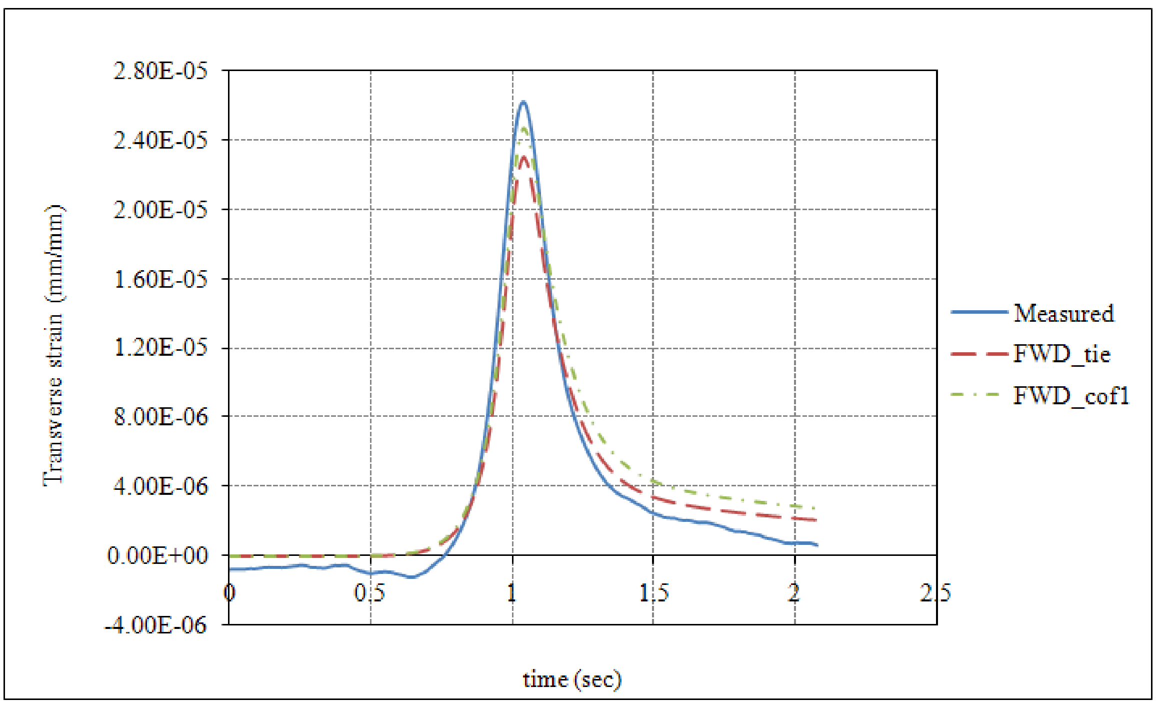

Figure A.10 Transverse strain (TE11) at the bottom of HMA layer using FWD data

In pavement response using FWD data, FE model with tie constraint gives a higher percentage error than friction model. This is because the tie constraint assumes displacement continuity at layer interface. As layers are fully bonded to each other, it increases the strength of a pavement structure and resists shear stresses as one body. Whereas in case of friction model, pavement interfaces start sliding relative to each other once shear stress reaches maximum shear strength at the interface. This increases shear stresses at the interface. Therefore, strain at the interface is greater for Coulomb friction model than tie constraint. In this case, layer interaction using tie constraint underpredicts pavement response and gives approximately 16% error in longitudinal and transverse strain.

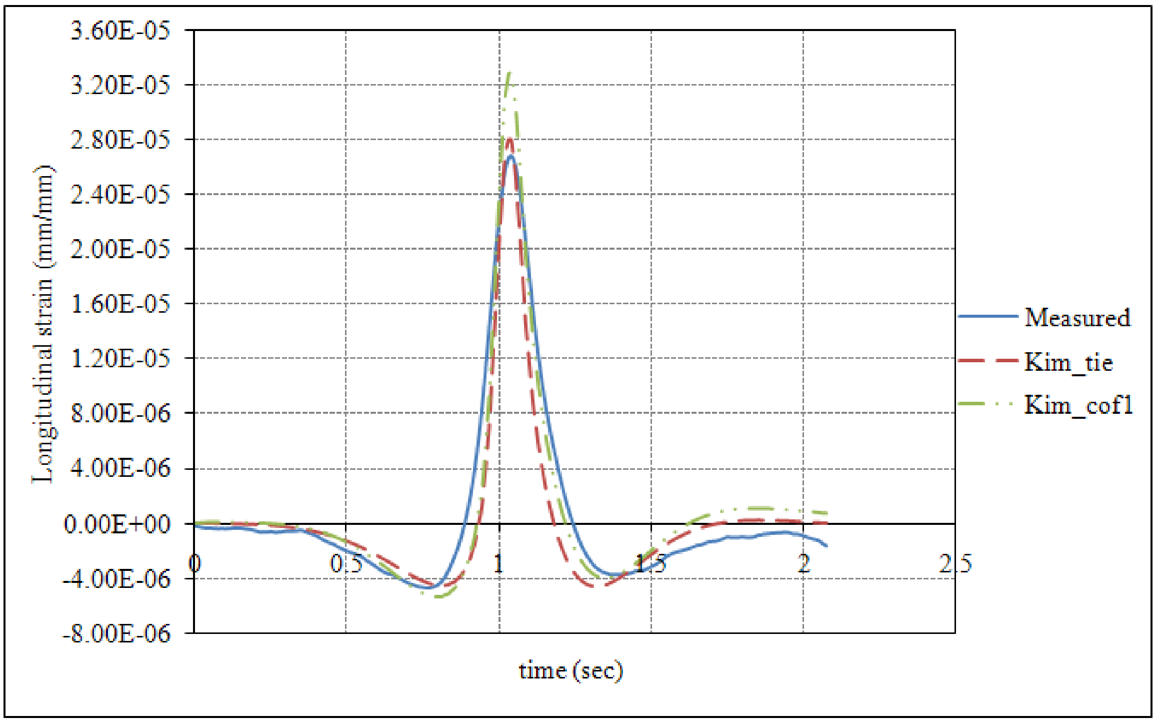

Figure A.11 Longitudinal Strain (TE22) at the Bottom of HMA Layer using Laboratory Data

The FE model response using equivalent laboratory determined modulus and tie constraint is in good agreement with field data. The difference between measured and calculated longitudinal strain is 3% (Figure A.11) while approximately 8% error is observed in case of transverse strain (Figure A.12). Using Coulomb friction model, percentage error is approximately 14% and 18% for longitudinal and transverse strains respectively.

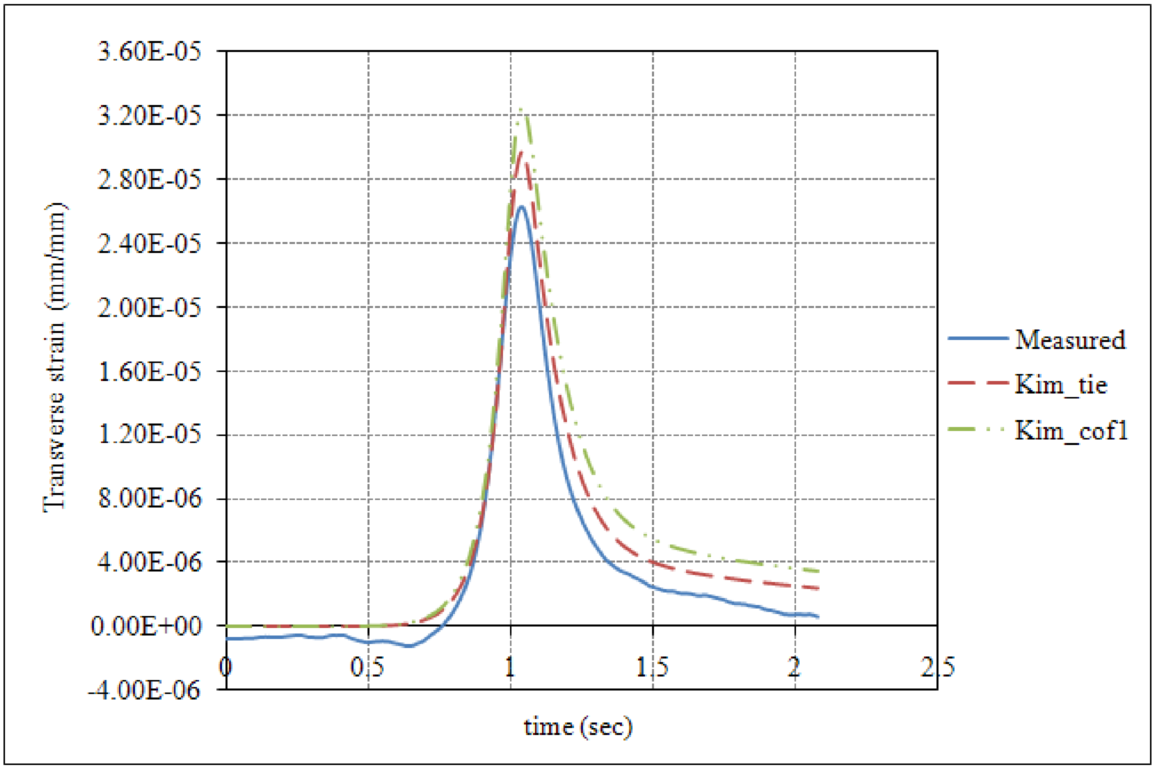

Figure A.12 Transverse Strain (TE11) at the Bottom of HMA Layer using Laboratory Data

Figure A.13 represents variation of shear modulus over time. It is seen that, at any time, shear modulus determined by Kim is less than FWD data. As relaxation modulus $E(t)$ is directly proportional to shear modulus $G(t)$, strain determined by Kim is more than FWD data. Therefore, strain calculated using Kim data is more than FWD data (Tables A.7 and A.8).

In this study, even though strain prediction using Kim laboratory data with tie constraint gives better results than FWD test data, according to Yoo (2008) FE model with tie constraint underpredicts pavement response and gives incorrect results at some of the layer interfaces when compared with field measured values. The author further concluded that appropriate friction model to simulate contact conditions increases the reliability of FE model. The same behavior is observed with results obtained from FWD data. Also, laboratory determined instantaneous modulus of HMA layer is calculated at controlled temperature and loading, whereas modulus obtained using FWD is determined from field test. Therefore, it is always recommended to use actual field measured data in FE model with proper frictional interface properties to simulate pavement response.

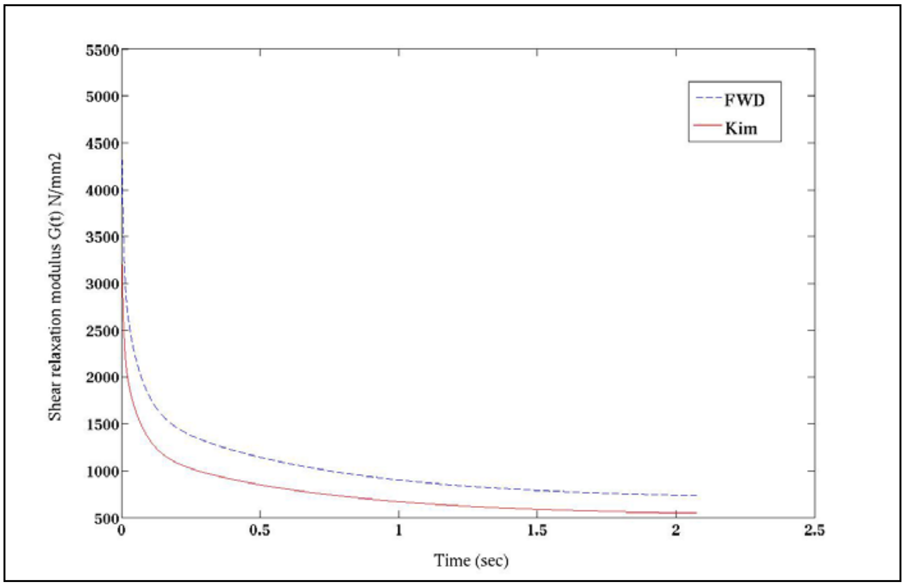

Figure A.13 Variation of Time Dependent Shear Modulus

Table A.7 Comparison of transverse strain (TE11) at the bottom of HMA layer

Transverse strain (TE11)			
	ABAQUS	Measured	Absolute % error
FWD_tie	2.3026E-05	2.7485E-05	16.2238
FWD_cof=1	2.4636E-05		10.3652
Kim_tie	2.9766E-05		8.2987
Kim_cof=1	3.2507E-05		18.2706

Table A.8 Comparison of longitudinal strain (TE22) at the bottom of HMA layer

Longitudinal strain (TE22)			
	ABAQUS	Measured	Absolute % error
FWD_tie	2.6255E-05	3.1611E-05	16.9429
FWD_cof=1	2.9989E-05		5.1306
Kim_tie	3.2554E-05		2.9818
Kim_cof1	3.6052E-05		14.0494

Even though the strain prediction using Kim et al. (2005) laboratory data with the tie constraint gives better results than the FWD test data, it is noted that according to Yoo (2008) the FE model with the tie constraint under predicts pavement response and gives incorrect results at some of the layer interfaces when compared with field measured. The author further concludes that an appropriate friction model to simulate contact conditions increases the reliability of a FE model. The behavior is observed with results obtained from the FWD data. Also, the laboratory determined instantaneous modulus of HMA layer is calculated at a controlled temperature and loading, whereas the modulus obtained using FWD is determined from a field test. Therefore, it is always recommended to use actual field measured data in a FE model with proper frictional interface properties to simulate the pavement response. The validated model in this chapter is used to predict the responses of the actual test sections and the values used to estimate the HMA equivalent thicknesses of the deep subgrade stabilization layers.

APPENDIX B

B.1 Resilient Modulus Data from the Lime Test Section

Table B.1: Resilient Modulus for Location 1 (G) Subgrade Layer

Chamber Confining Pressure σ_c kPa (psi)	**Nominal Maximum Axial Stress σ_d kPa (psi)**	**Resilient Modulus M_R kPa**	**Resilient Modulus M_R psi**	**Resilient Modulus M_R kPa**	**Resilient Modulus M_R psi**
-	-	Trial 1		Trial 2	
41.4 (6)	13.8 (2)	36,628.4	5,312	54,144	7,853
41.4 (6)	27.6 (4)	34,365.7	4,984	49,260	7,144
41.4 (6)	41.4 (6)	32,304.1	4,685	45,403	6,585
41.4 (6)	55.2 (8)	32,128.9	4,660	43,458	6,303
41.4 (6)	69.0 (10)	32,696.4	4,742	42,931	6,226
27.6 (4)	13.8 (2)	32,168.4	4,665	49,290	7,149
27.6 (4)	27.6 (4)	28,454.7	4,127	40,404	5,860
27.6 (4)	41.4 (6)	25,887.4	3,755	36,120	5,239
27.6 (4)	55.2 (8)	26,194.4	3,799	34,940	5,067
27.6 (4)	69.0 (10)	27,363.1	3,969	35,326	5,123
13.8 (2)	13.8 (2)	23,561.7	3,417	35,234	5,110
13.8 (2)	27.6 (4)	19,790.9	2,870	28,685	4,160
13.8 (2)	41.4 (6)	18,891.4	2,740	26,069	3,781
13.8 (2)	55.2 (8)	19,994.5	2,900	26,045	3,777
13.8 (2)	69.0 (10)	21,041.5	3,052	26,533	3,848
	Compaction Level (%)	81.0		82.7	
	Moisture Content (%)	18.2		20.0	
	Trial 1	$M_R = 2{,}535(\sigma_d)^{-.09238}(\sigma_c)^{.44454}$, $R^2=.96$			
	Trial 2	$M_R = 4{,}008(\sigma_d)^{-.18725}(\sigma_c)^{.46014}$, $R^2=.98$			

Table B.2: Resilient Modulus for Location 2 (H) Subgrade Layer

Chamber Confining Pressure σ_c kPa (psi)	**Nominal Maximum Axial Stress σ_d kPa (psi)**	**Resilient Modulus M_R kPa**	**Resilient Modulus M_R psi**	**Resilient Modulus M_R kPa**	**Resilient Modulus M_R psi**
-	-	Trial 1		Trial 2	
41.4 (6)	13.8 (2)	36,238.8	5,256	40,914	5,934
41.4 (6)	27.6 (4)	33,531.0	4,863	34,430	4,993
41.4 (6)	41.4 (6)	31,446.9	4,561	31,532	4,573
41.4 (6)	55.2 (8)	31,064.0	4,505	29,897	4,336
41.4 (6)	69.0 (10)	31,813.4	4,614	31,990	4,640
27.6 (4)	13.8 (2)	31,408.8	4,555	37,806	5,483
27.6 (4)	27.6 (4)	26,163.3	3,795	28,446	4,126
27.6 (4)	41.4 (6)	24,439.1	3,544	24,570	3,563
27.6 (4)	55.2 (8)	24,758.7	3,591	23,574	3,419
27.6 (4)	69.0 (10)	25,856.3	3,750	25,477	3,695
13.8 (2)	13.8 (2)	20,910.9	3,033	26,969	3,911
13.8 (2)	27.6 (4)	17,682.7	2,565	20,099	2,915
13.8 (2)	41.4 (6)	16,914.4	2,453	17,647	2,559
13.8 (2)	55.2 (8)	17,842.1	2,588	17,546	2,545
13.8 (2)	69.0 (10)	18,721.7	2,715	19,138	2,776
	Compaction Level (%)	84.8		81.6	
	Moisture Content (%)	17.0		23.1	
	Trial 1	$M_R = 2,157(\sigma_d)^{-.09958}(\sigma_c)^{.52727}$, $R^2 = 96$			
	Trial 2	$M_R = 2,988(\sigma_d)^{-.22895}(\sigma_c)^{.47060}$, $R^2 = .93$			

Table B.3: Resilient Modulus for Location 3 (N) Subgrade Layer

Chamber Confining Pressure σ_c kPa (psi)	**Nominal Maximum Axial Stress σ_d kPa (psi)**	**Resilient Modulus M_R kPa**	**Resilient Modulus M_R psi**	**Resilient Modulus M_R kPa**	**Resilient Modulus M_R psi**
-	-	Trial 1		Trial 2	
41.4 (6)	13.8 (2)	128,747.0	18,673	158,832	23,036
41.4 (6)	27.6 (4)	116,942.9	16,961	150,431	21,817
41.4 (6)	41.4 (6)	103,591.3	15,024	134,789	19,549
41.4 (6)	55.2 (8)	97,464.4	14,136	127,802	18,535
41.4 (6)	69.0 (10)	94,413.7	13,693	125,108	18,145
27.6 (4)	13.8 (2)	124,361.3	18,036	153,876	22,317
27.6 (4)	27.6 (4)	108,963.1	15,803	142,220	20,626
27.6 (4)	41.4 (6)	96,346.0	13,973	130,777	18,967
27.6 (4)	55.2 (8)	88,487.3	12,834	121,595	17,635
27.6 (4)	69.0 (10)	84,935.1	12,318	115,537	16,757
13.8 (2)	13.8 (2)	100,032.9	14,508	129,483	18,779
13.8 (2)	27.6 (4)	85,484.4	12,398	117,437	17,032
13.8 (2)	41.4 (6)	76,172.8	11,048	107,860	15,643
13.8 (2)	55.2 (8)	71,329.5	10,345	101,422	14,710
13.8 (2)	69.0 (10)	70,575.6	10,236	98,581	14,298
	Compaction Level (%)	105.7		105.8	
	Moisture Content (%)	21.5		22.0	
	Trial 1	$M_R= 13{,}867(\sigma_d)^{-.23220}(\sigma_c)^{.27531}$, R^2=.98			
	Trial 2	$M_R=18{,}413(\sigma_d)^{-.18103}(\sigma_c)^{.21596}$, R^2=.97			

Table B.4: Resilient Modulus for Location 4 (O) Subgrade Layer

Chamber Confining Pressure σ_c kPa (psi)	**Nominal Maximum Axial Stress σ_d kPa (psi)**	**Resilient Modulus M_R kPa**	**Resilient Modulus M_R psi**	**Resilient Modulus M_R kPa**	**Resilient Modulus M_R psi**
-	-	Trial 1		Trial 2	
41.4 (6)	13.8 (2)	88,567.7	12,845	84,470	12,251
41.4 (6)	27.6 (4)	76,649.6	11,117	79,961	11,597
41.4 (6)	41.4 (6)	69,171.8	10,032	73,151	10,609
41.4 (6)	55.2 (8)	66,193.9	9,600	73,578	10,671
41.4 (6)	69.0 (10)	64,792.9	9,397	75,162	10,901
27.6 (4)	13.8 (2)	82,253.4	11,929	78,552	11,393
27.6 (4)	27.6 (4)	67,029.7	9,721	69,290	10,049
27.6 (4)	41.4 (6)	59,120.8	8,574	64,742	9,390
27.6 (4)	55.2 (8)	56,407.5	8,181	64,099	9,297
27.6 (4)	69.0 (10)	55,972.4	8,118	65,536	9,505
13.8 (2)	13.8 (2)	68,248.0	9,898	60,195	8,730
13.8 (2)	27.6 (4)	53,606.9	7,775	52,234	7,576
13.8 (2)	41.4 (6)	47,204.7	6,846	49,443	7,171
13.8 (2)	55.2 (8)	45,611.9	6,615	50,733	7,358
13.8 (2)	69.0 (10)	46,235.1	6,706	53,491	7,758
	Compaction Level (%)	100.8		103.4	
	Moisture Content (%)	23.3		22.5	
	Trial 1	$M_R = 8{,}800(\sigma_d)^{-.24039}(\sigma_c)^{.31202}$, R^2=.97			
	Trial 2	$M_R = 7{,}128(\sigma_d)^{-.09927}(\sigma_c)^{.34285}$, R^2=.95			

Table B.5: Resilient Modulus for Location 1 (G) Stabilized Layer

Chamber Confining Pressure σ_c kPa (psi)	**Nominal Maximum Axial Stress σ_d kPa (psi)**	**Resilient Modulus M_R kPa**	**Resilient Modulus M_R psi**	**Resilient Modulus M_R kPa**	**Resilient Modulus M_R psi**	***Percent Increase %***
-	**-**	**Soil**		**Lime**		**-**
41.4 (6)	13.8 (2)	64,645	9,376	140,636	20,397	*118*
41.4 (6)	27.6 (4)	54,558	7,913	128,310	18,609	*135*
41.4 (6)	41.4 (6)	46,409	6,731	114,603	16,621	*147*
41.4 (6)	55.2 (8)	42,291	6,134	105,173	15,254	*149*
41.4 (6)	69.0 (10)	40,618	5,891	97,464	14,135	*140*
27.6 (4)	13.8 (2)	60,601	8,789	117,918	17,102	*95*
27.6 (4)	27.6 (4)	46,863	6,797	102,580	14,878	*119*
27.6 (4)	41.4 (6)	38,949	5,649	91,694	13,299	*135*
27.6 (4)	55.2 (8)	35,355	5,128	86,433	12,536	*144*
27.6 (4)	69.0 (10)	34,301	4,975	84,270	12,222	*146*
13.8 (2)	13.8 (2)	48,681	7,060	90,705	13,155	*86*
13.8 (2)	27.6 (4)	36,876	5,348	78,769	11,424	*114*
13.8 (2)	41.4 (6)	31,008	4,497	72,011	10,444	*132*
13.8 (2)	55.2 (8)	28,611	4,150	69,293	10,050	*142*
13.8 (2)	69.0 (10)	28,108	4,077	68,706	9,965	*144*
	Compaction Level (%)	95.7		95.9		
	Moisture Content (%)	19.8		20.7		
	G Soil	$M_R = 14,549(\sigma_d)^{-.30351}(\sigma_c)^{.18391}$, $R^2 = .96$				
	G Lime	$M_R = 11,581(\sigma_d)^{-.21567}(\sigma_c)^{.38925}$, $R^2 = .98$				

Table B.6: Resilient Modulus for Location 2 (H) Stabilized Layer

Chamber Confining Pressure σ_c kPa (psi)	**Nominal Maximum Axial Stress σ_d kPa (psi)**	**Resilient Modulus M_R kPa**	**Resilient Modulus M_R psi**	**Resilient Modulus M_R kPa**	**Resilient Modulus M_R psi**	**Resilient Modulus M_R kPa**	**Resilient Modulus M_R psi**	***Percent Increase %***
-	**-**	**Soil**		**Lime 1**		**Lime 2**		-
41.4 (6)	13.8 (2)	44,275	6,421	240,187	34,835	205,237	29,766	*364-442*
41.4 (6)	27.6 (4)	37,801	5,482	240,029	34,812	209,001	30,312	*453-611*
41.4 (6)	41.4 (6)	32,757	4,751	232,803	33,764	206,036	29,882	*529-611*
41.4 (6)	55.2 (8)	29,843	4,328	223,750	32,451	199,976	29,003	*570-650*
41.4 (6)	69.0 (10)	28,838	4,182	213,814	31,010	194,205	28,166	*573-641*
27.6 (4)	13.8 (2)	40,291	5,844	222,922	32,331	187,075	27,132	*364-453*
27.6 (4)	27.6 (4)	30,983	4,494	213,083	30,904	180,359	26,158	*482-588*
27.6 (4)	41.4 (6)	26,286	3,812	207,595	30,108	178,525	25,892	*579-690*
27.6 (4)	55.2 (8)	24,176	3,506	204,126	29,605	177,905	25,802	*636-744*
27.6 (4)	69.0 (10)	23,740	3,443	201,989	29,295	178,539	25,894	*652-751*
13.8 (2)	13.8 (2)	30,519	4,426	188,509	27,340	158,233	22,949	*418-518*
13.8 (2)	27.6 (4)	23,275	3,376	184,524	26,762	158,095	22,929	*579-693*
13.8 (2)	41.4 (6)	19,920	2,889	183,097	26,555	151,656	21,995	*661-819*
13.8 (2)	55.2 (8)	18,887	2,739	181,849	26,374	153,297	22,233	*712-863*
13.8 (2)	69.0 (10)	18,836	2,732	182,373	26,450	155,641	22,573	*726-868*
	Compaction Level (%)	95.5		94.7		94.9		
	Moisture Content (%)	24.0		24.8		24.8		

H Soil	$M_R = 14{,}549(\sigma_d)^{-.30351}(\sigma_c)^{.18391}$, $R^2 = .96$
H Lime 1	$M_R = 25{,}110(\sigma_d)^{-.05130}(\sigma_c)^{.20166}$, $R^2 = .96$
H Lime 2	$M_R = 19{,}622(\sigma_d)^{-.02593}(\sigma_c)^{.24509}$, $R^2 = .98$

Table B.7: Resilient Modulus for Location 3 (N) Stabilized Layer

Chamber Confining Pressure σ_c kPa (psi)	**Nominal Maximum Axial Stress σ_d kPa (psi)**	**Resilient Modulus M_R kPa**	**Resilient Modulus M_R psi**	**Resilient Modulus M_R kPa**	**Resilient Modulus M_R psi**	**Resilient Modulus M_R kPa**	**Resilient Modulus M_R psi**	***Percent Increase %***
-	-	**Soil 1**		**Soil 2**		**Lime**		-
41.4 (6)	13.8 (2)	69,335	10,056	67,936	9,853	182,852	26,520	*164-169*
41.4 (6)	27.6 (4)	60,767	8,813	57,484	8,337	173,450	25,156	*185-202*
41.4 (6)	41.4 (6)	51,848	7,520	50,885	7,380	157,434	22,833	*204-209*
41.4 (6)	55.2 (8)	46,792	6,786	44,487	6,452	143,569	20,822	*207-223*
41.4 (6)	69.0 (10)	44,522	6,457	41,715	6,050	132,516	19,219	*198-218*
27.6 (4)	13.8 (2)	62,558	9,073	59,993	8,701	166,895	24,205	*167-178*
27.6 (4)	27.6 (4)	50,270	7,291	47,148	6,838	153,336	22,239	*205-225*
27.6 (4)	41.4 (6)	42,896	6,221	39,991	5,800	140,412	20,364	*227-251*
27.6 (4)	55.2 (8)	39,204	5,686	36,585	5,306	131,385	19,055	*235-259*
27.6 (4)	69.0 (10)	37,733	5,473	35,330	5,124	125,633	18,221	*233-256*
13.8 (2)	13.8 (2)	50,403	7,310	47,203	6,846	152,109	22,061	*202-222*
13.8 (2)	27.6 (4)	39,878	5,784	36,647	5,315	137,762	19,980	*245-276*
13.8 (2)	41.4 (6)	34,189	4,959	31,283	4,537	125,853	18,253	*268-302*
13.8 (2)	55.2 (8)	31,718	4,600	29,180	4,232	118,263	17,152	*273-305*
13.8 (2)	69.0 (10)	30,978	4,493	28,669	4,158	113,607	16,477	*267-296*
	Compaction Level (%)	96.6		95.8		95.2		
	Moisture Content (%)	18.6		19.3		20.5		

N Soil 1	$M_R = 14{,}549(\sigma_d)^{-.30351}(\sigma_c)^{.18391}$, $R^2 = .96$
N Soil 2	$M_R = 6{,}312(\sigma_d)^{-.32986}(\sigma_c)^{.38086}$, $R^2 = .99$
N Lime	$M_R = 22{,}329(\sigma_d)^{-.19631}(\sigma_c)^{.17607}$, $R^2 = .97$

Table B.8: Resilient Modulus for Location 4 (O) Stabilized Layer

Chamber Confining Pressure σ_c kPa (psi)	**Nominal Maximum Axial Stress σ_d kPa (psi)**	**Resilient Modulus M_R kPa**	**Resilient Modulus M_R psi**	**Resilient Modulus M_R kPa**	**Resilient Modulus M_R psi**	***Percent Increase %***
-	**-**	**Soil**		**Lime**		**-**
41.4 (6)	13.8 (2)	106,714	15,477	214,669	31,134	*101*
41.4 (6)	27.6 (4)	103,088	14,951	218,270	31,656	*112*
41.4 (6)	41.4 (6)	94,244	13,668	216,602	31,414	*130*
41.4 (6)	55.2 (8)	85,521	12,403	214,980	31,179	*151*
41.4 (6)	69.0 (10)	77,271	11,207	211,081	30,614	*173*
27.6 (4)	13.8 (2)	97,678	14,166	197,535	28,649	*102*
27.6 (4)	27.6 (4)	93,353	13,539	197,901	28,702	*112*
27.6 (4)	41.4 (6)	88,116	12,780	198,528	28,793	*125*
27.6 (4)	55.2 (8)	81,758	11,858	198,313	28,762	*143*
27.6 (4)	69.0 (10)	76,223	11,055	198,938	28,853	*161*
13.8 (2)	13.8 (2)	86,860	12,597	173,701	25,192	*100*
13.8 (2)	27.6 (4)	83,818	12,156	172,331	24,994	*106*
13.8 (2)	41.4 (6)	79,884	11,586	172,306	24,990	*116*
13.8 (2)	55.2 (8)	75,616	10,967	175,220	25,413	*132*
13.8 (2)	69.0 (10)	71,499	10,370	177,861	25,796	*149*
	Compaction Level (%)	96.3		94.5		
	Moisture Content (%)	34.5		34.6		
	O Soil	$M_R = 13{,}338(\sigma_d)^{-.15960}(\sigma_c)^{.14351}$, $R^2 = .89$				
	O Lime	$M_R = 22{,}024(\sigma_d)^{.00280}(\sigma_c)^{.19100}$, $R^2 = .99$				

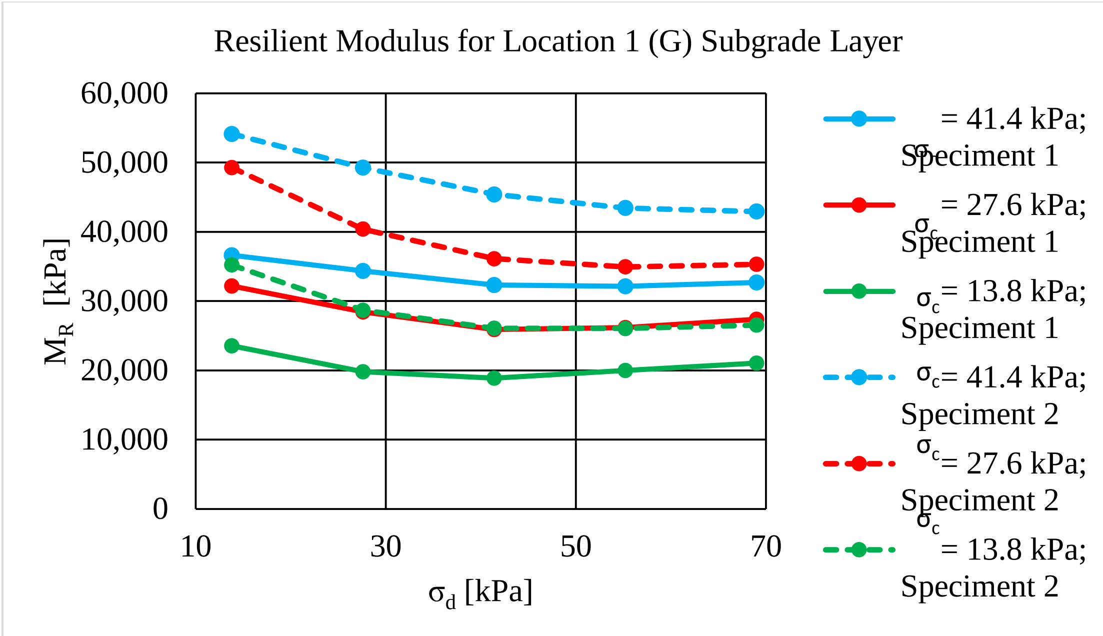

Figure B.1 Resilient Modulus of Subgrade Layer for Location 1 (G)

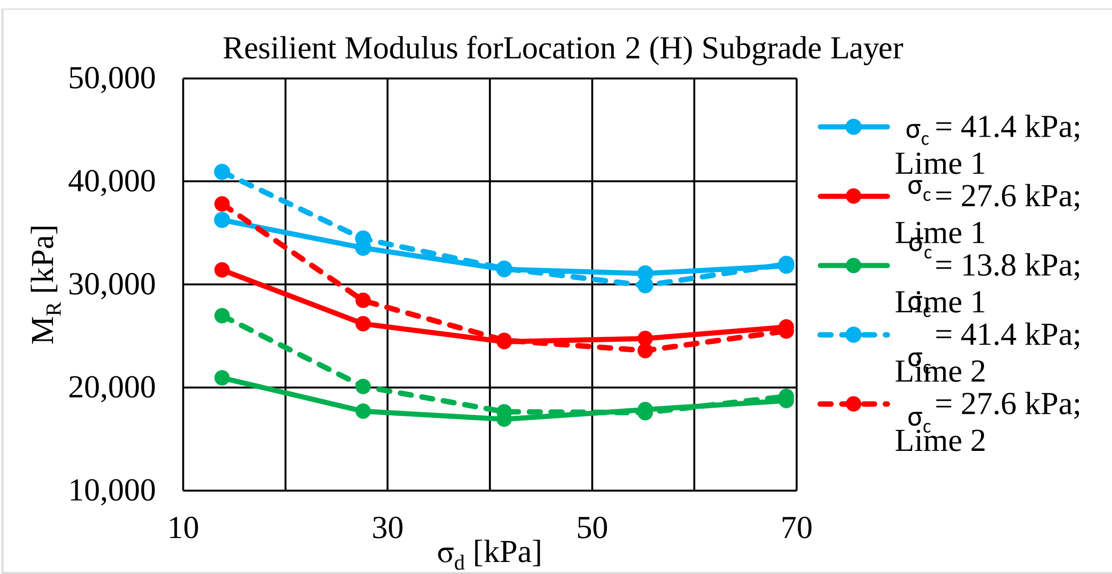

Figure B.2 Resilient Modulus of Subgrade Layer for Location 2 (H)

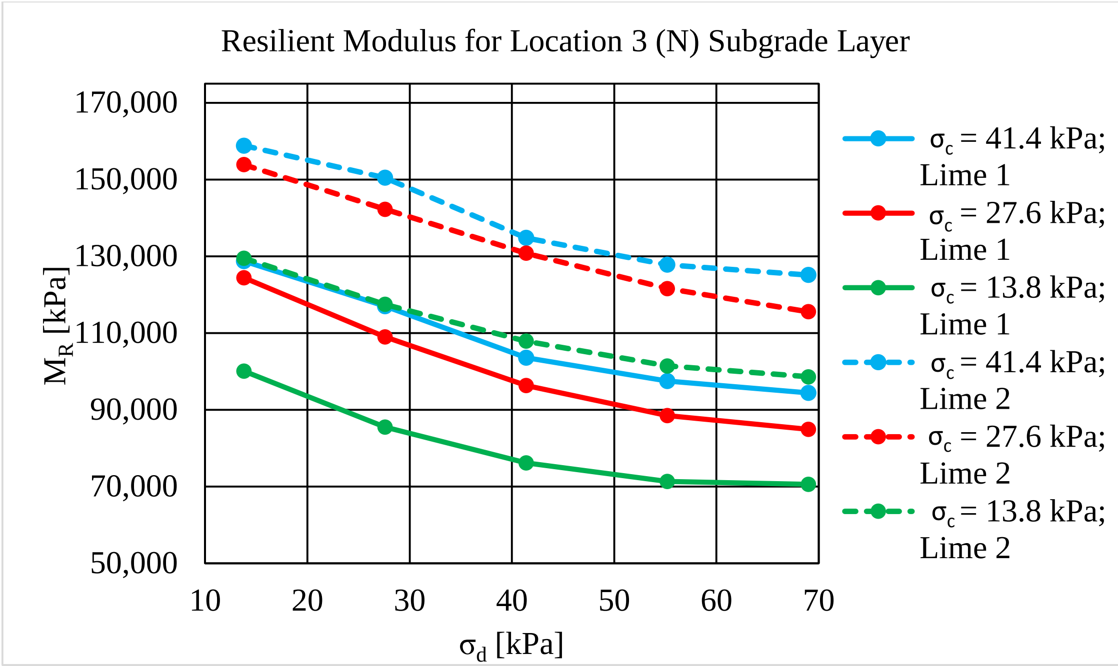

Figure B.3 Resilient Modulus of Subgrade Layer for Location 3 (N)

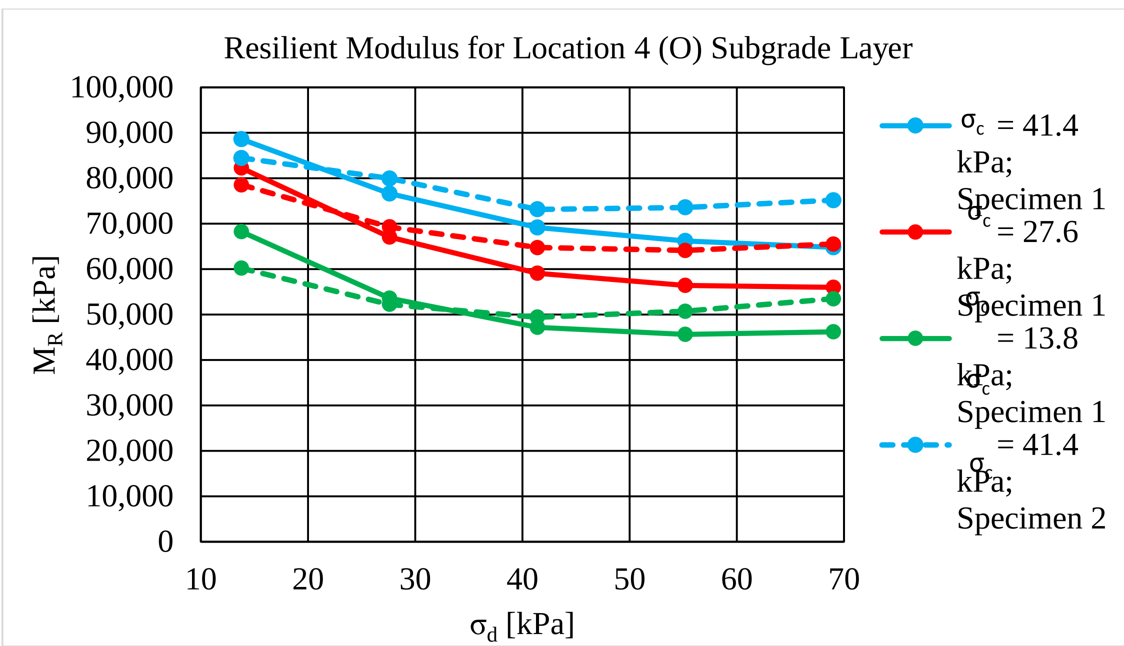

Figure B.4 Resilient Modulus of Subgrade Layer for Location 4 (O)

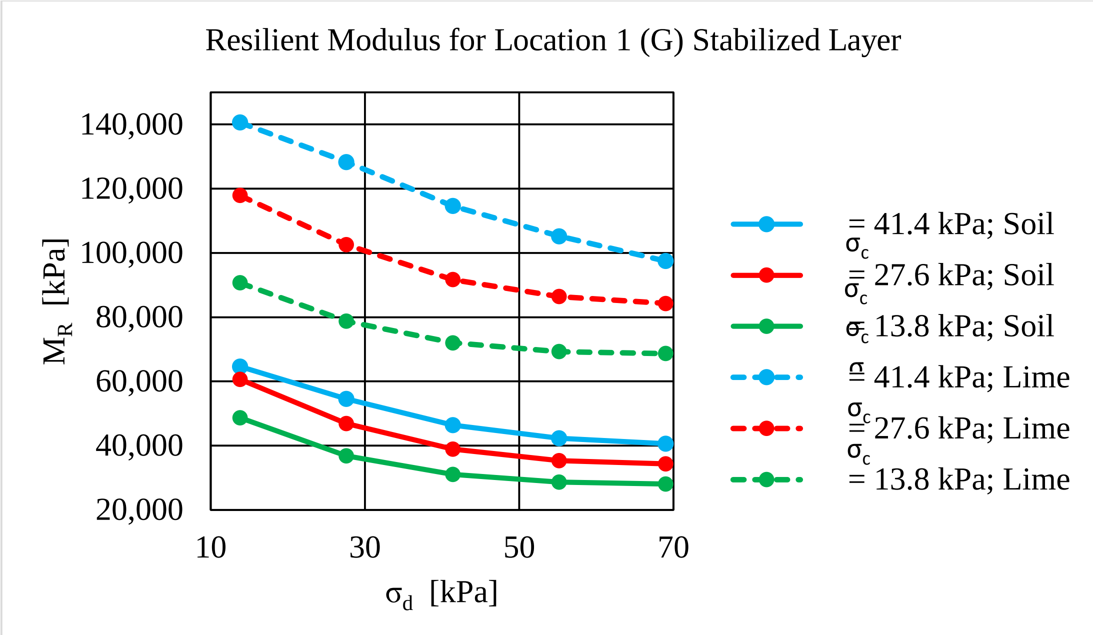

Figure B.5 Resilient Modulus of Stabilized Layer for Location 1 (G)

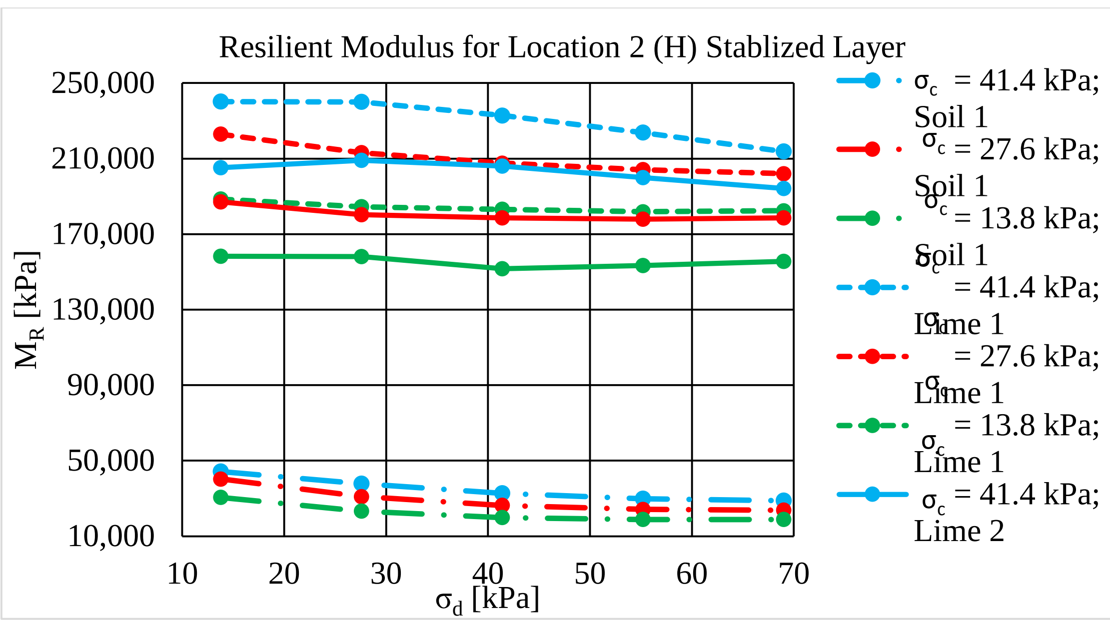

Figure B.6 Resilient Modulus of Stabilized Layer for Location 2 (H)

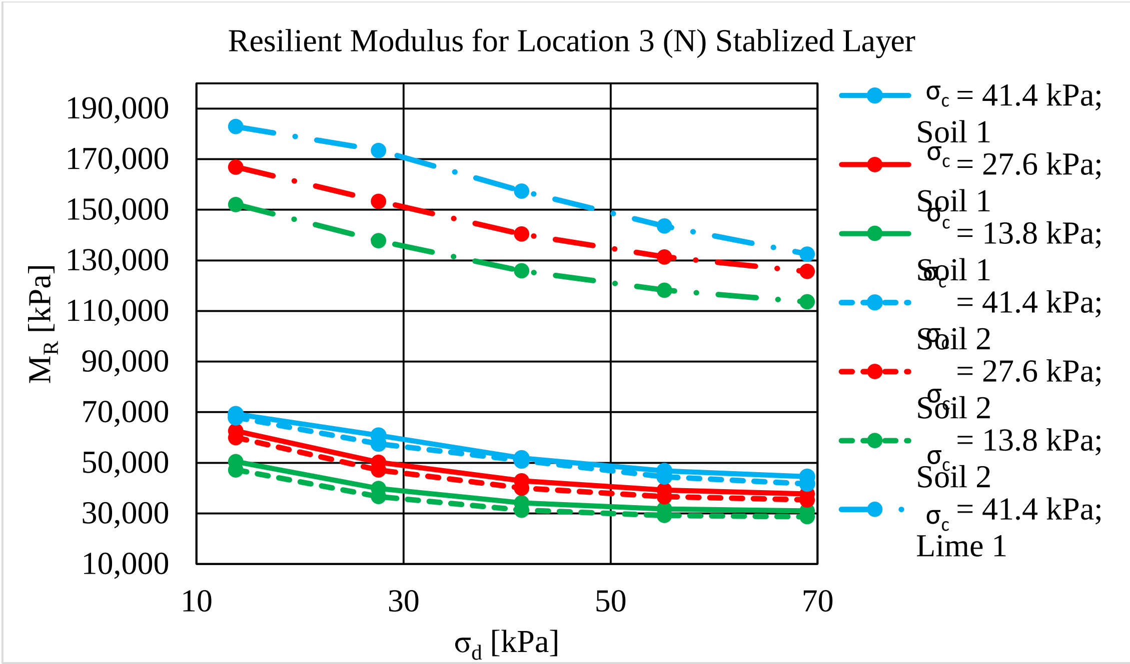

Figure B.7 Resilient Modulus of Stabilized Layer for Location 3 (N)

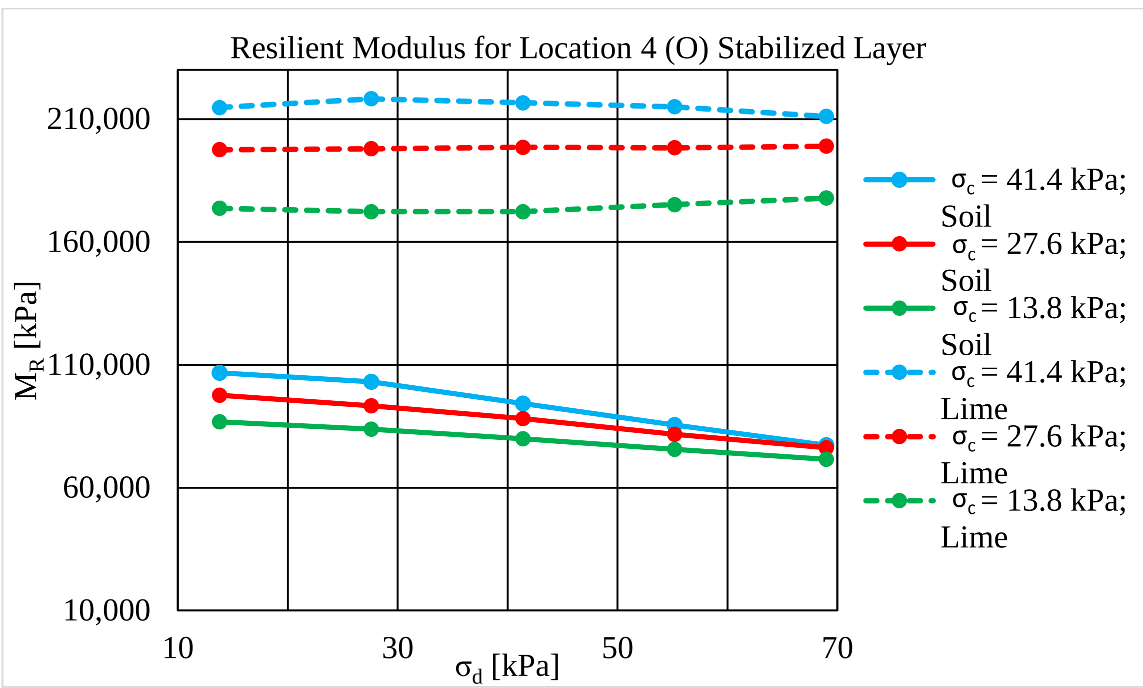

Figure B.8 Resilient Modulus of Stabilized Layer for Location 4 (O)

B. 2 Depth Verification using DCP Data Analysis

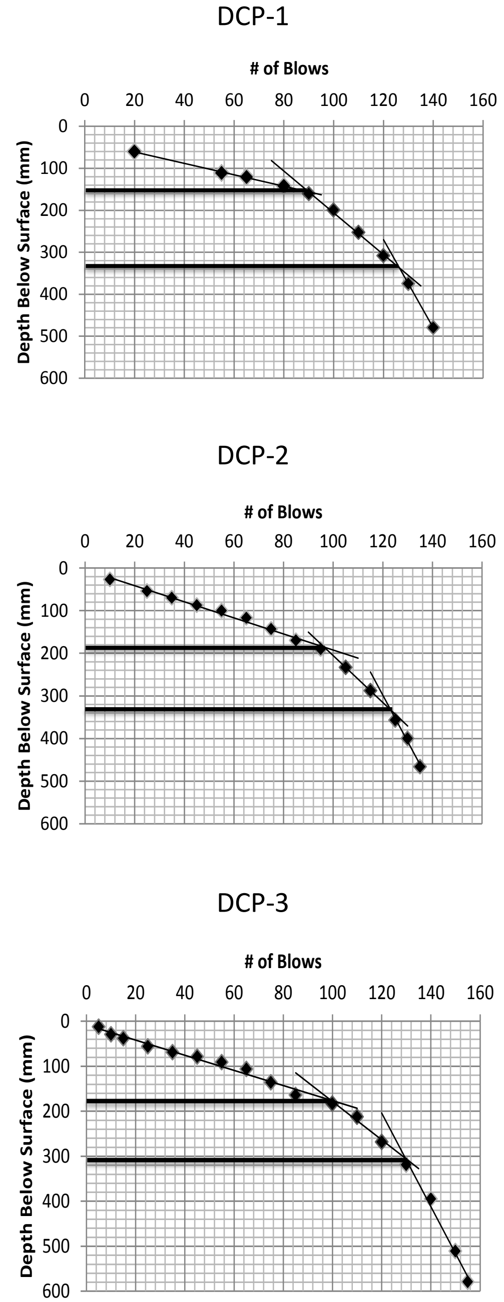

Figure B. 9 LIME 1 DCP LOCATION: L-1 (STA 248+33.31)

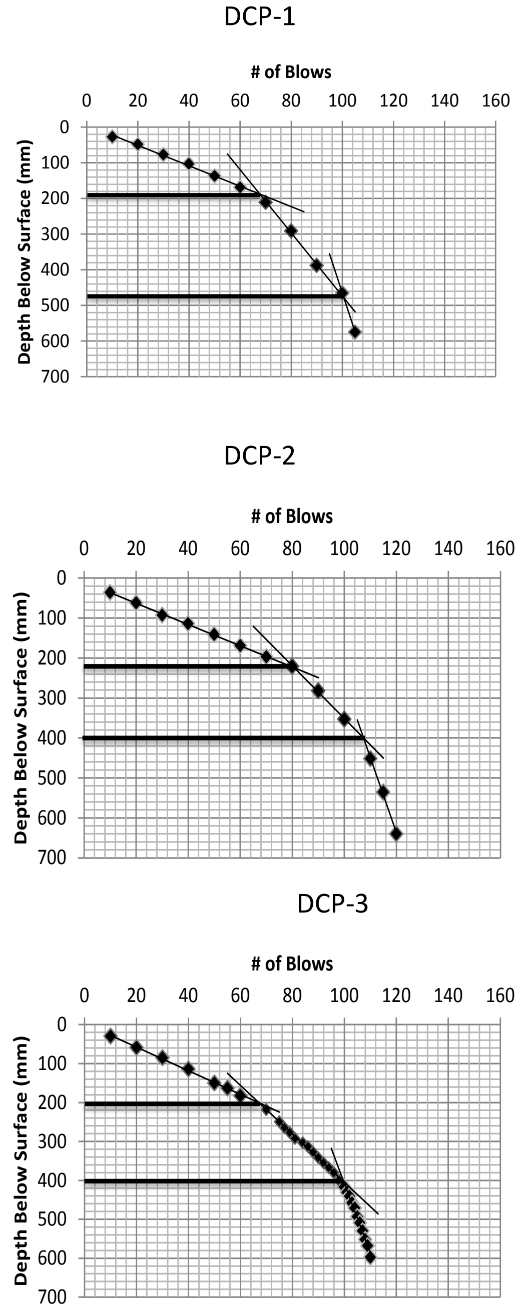

Figure B. 10 LIME 1 DCP LOCATION: L-2 (STA 248+86.65)

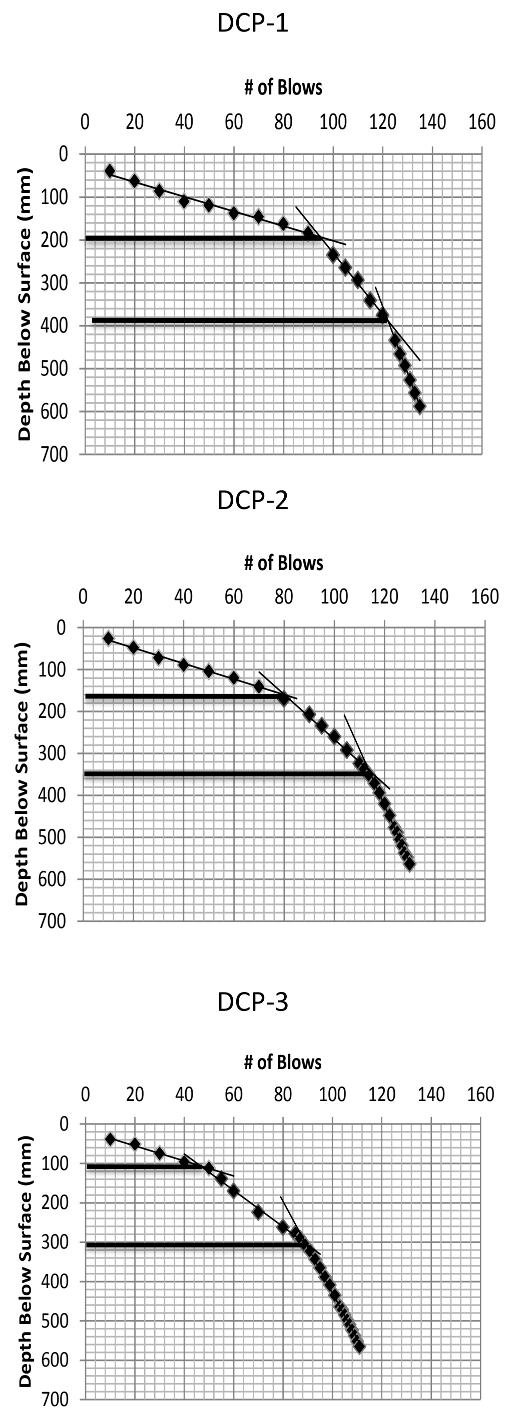

Figure B. 11 LIME1 DCP LOCATION: L-3 (STA 249+50)

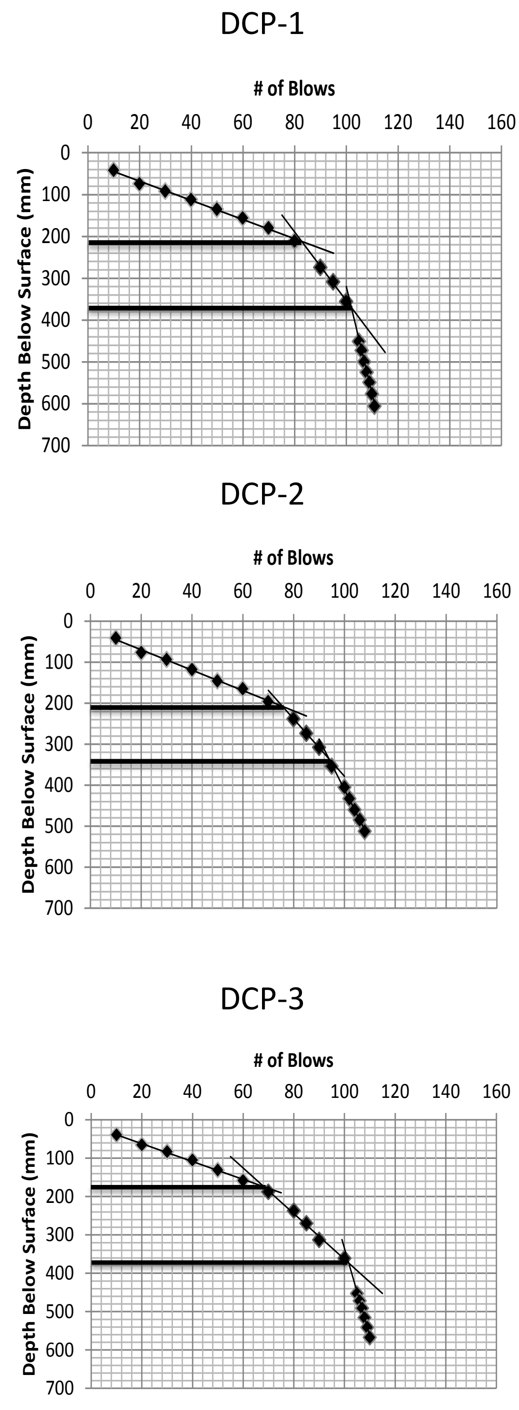

Figure B. 12 LIME 1 DCP LOCATION: L-4 (STA 250+39.37)

DCP-1

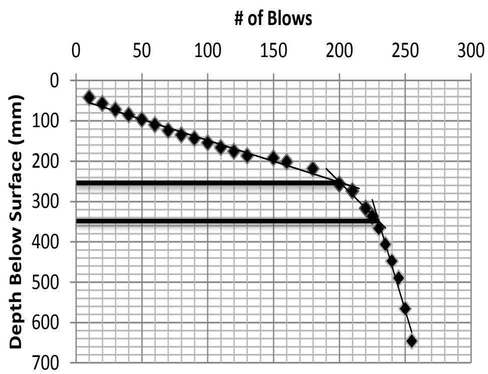

DCP-2

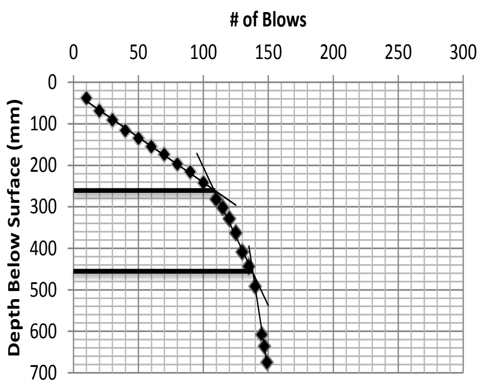

DCP-3

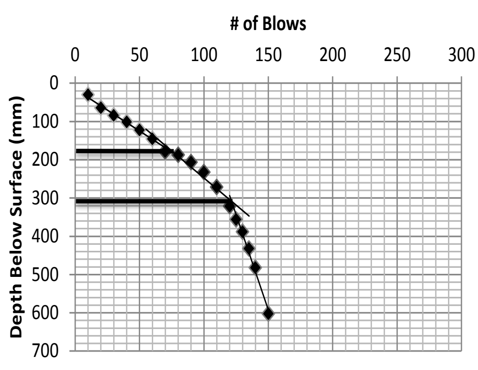

Figure B. 13 LIME 2 DCP LOCATION: L-5 (STA 250+55.16)

DCP-1

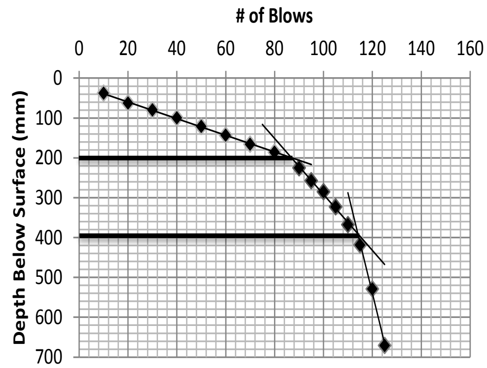

DCP-2

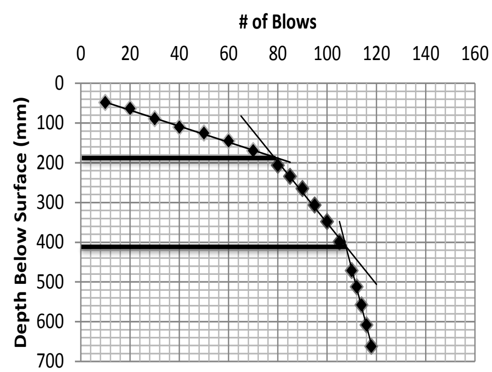

DCP-3

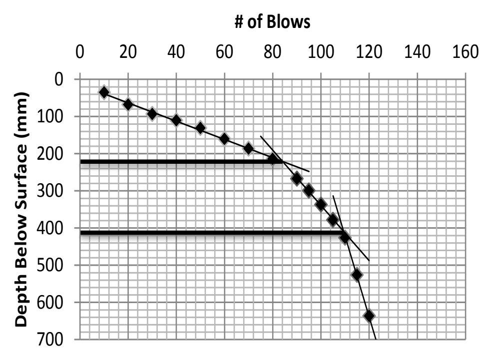

Figure B. 14 LIME 2 DCP LOCATION: L-6 (STA 251+00)

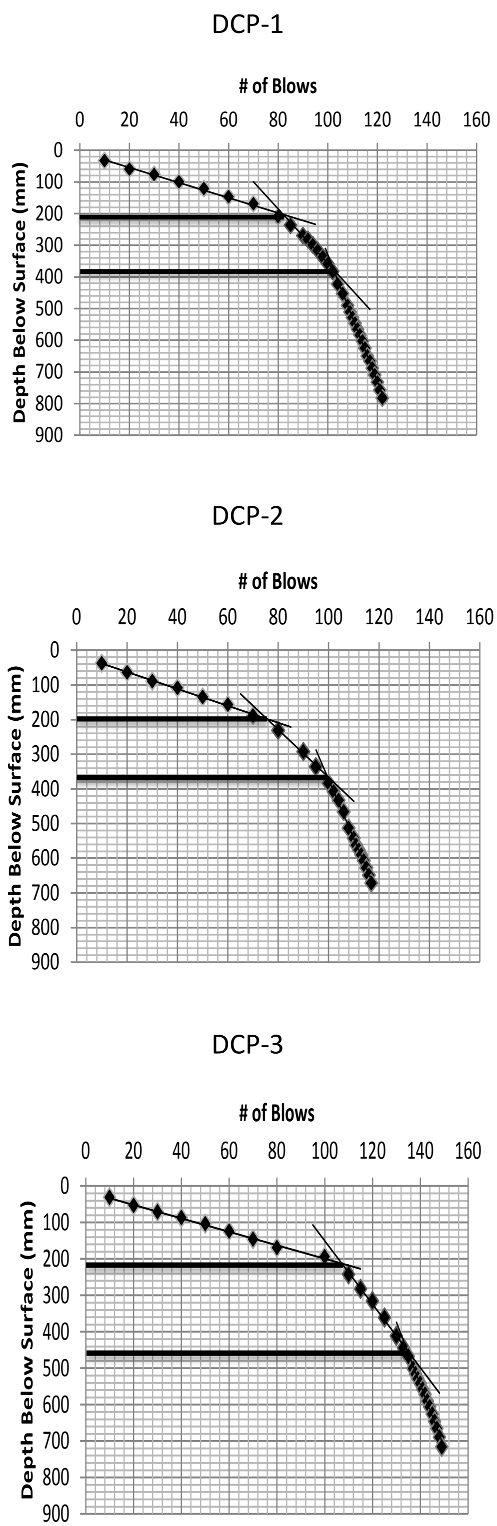

Figure B. 15 LIME 2 DCP LOCATION: L-251 (STA 251+45.98)

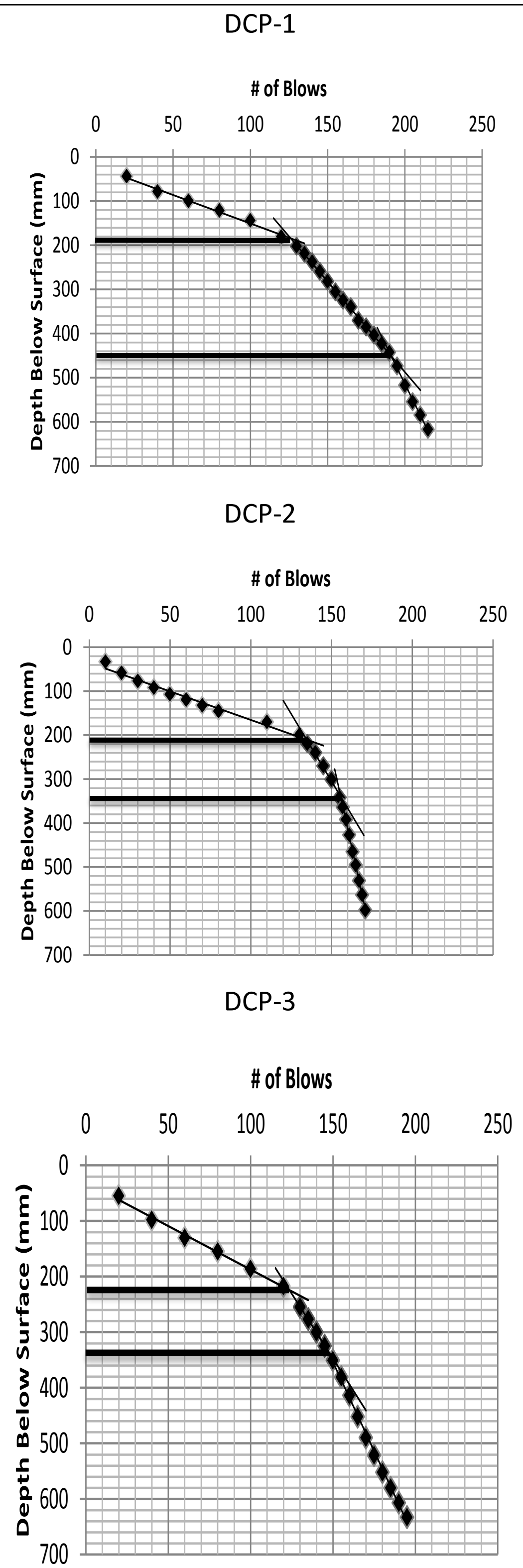

Figure B. 16 LIME 2 DCP LOCATION: L-7 (STA 252+00)

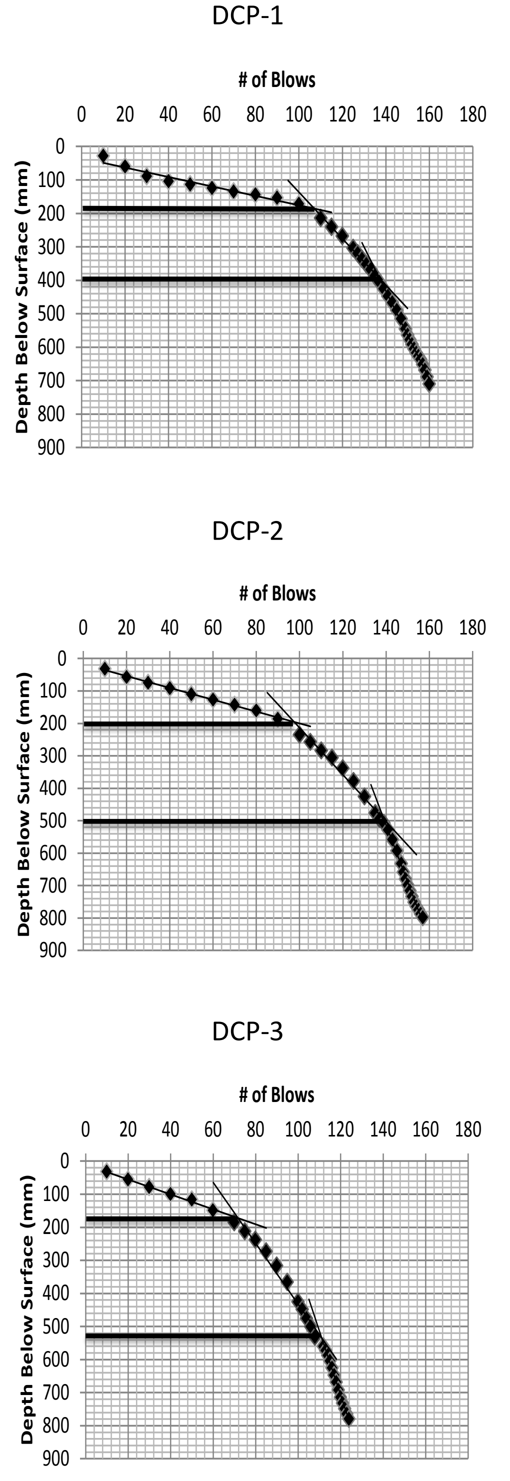

Figure B. 17 LIME 3 DCP LOCATION: L-8 (STA 252+60.03)

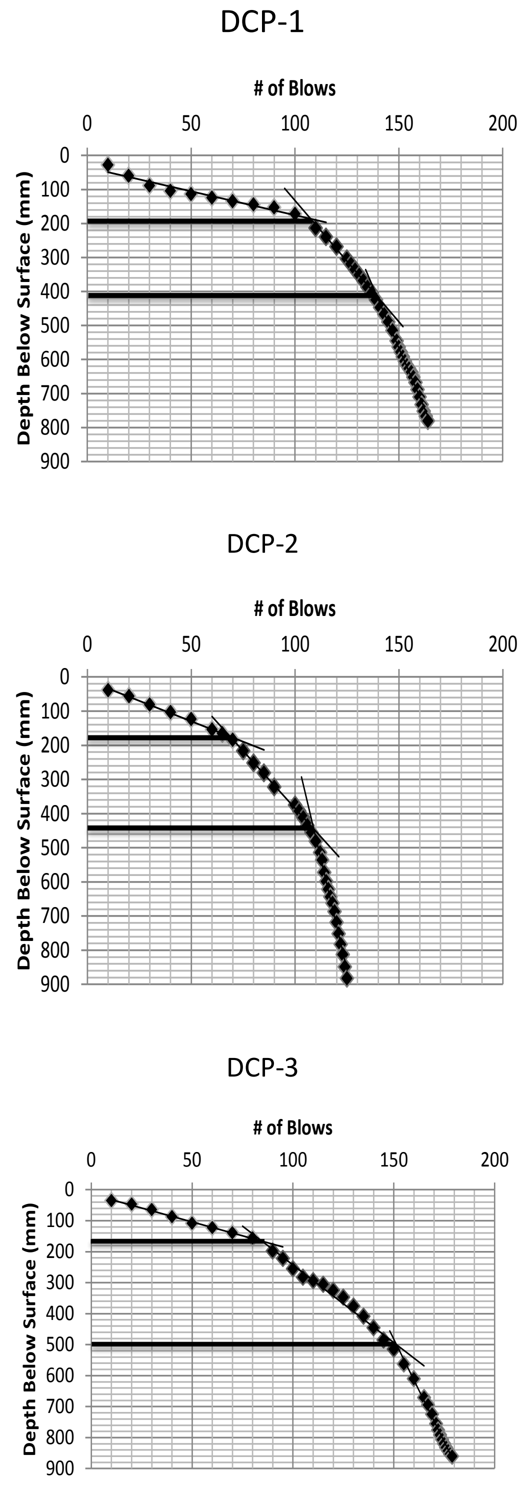

Figure B. 18 LIME 3 DCP LOCATION: L-9 (STA 253+13.37)

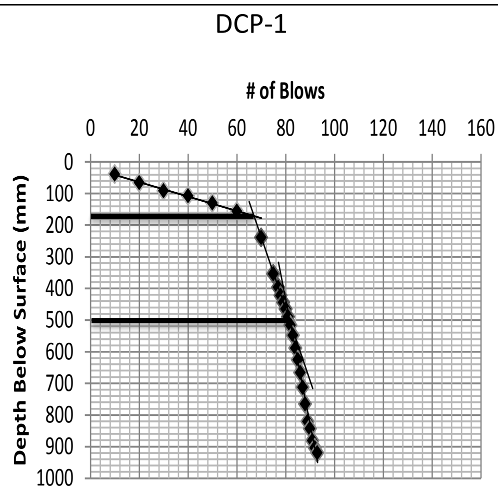

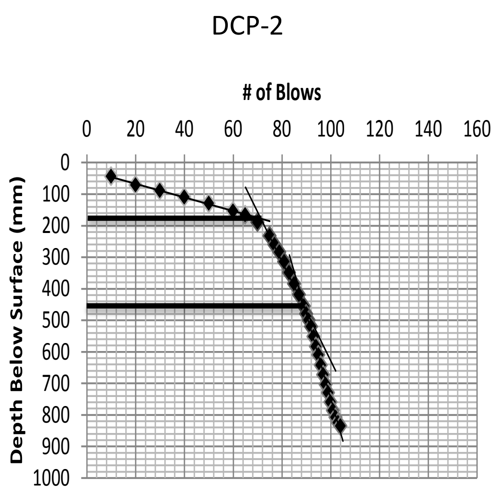

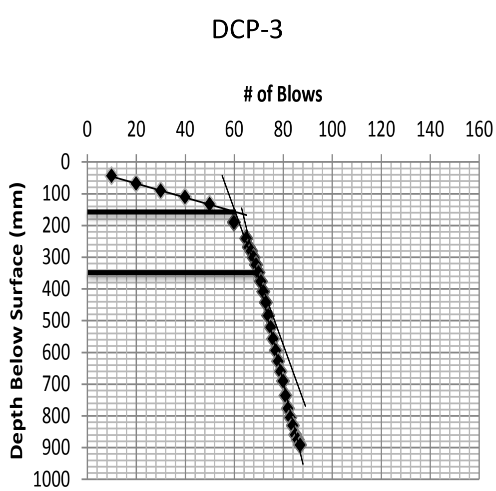

Figure B. 19 LIME 3 DCP LOCATION: L-10 (STA 253+50)

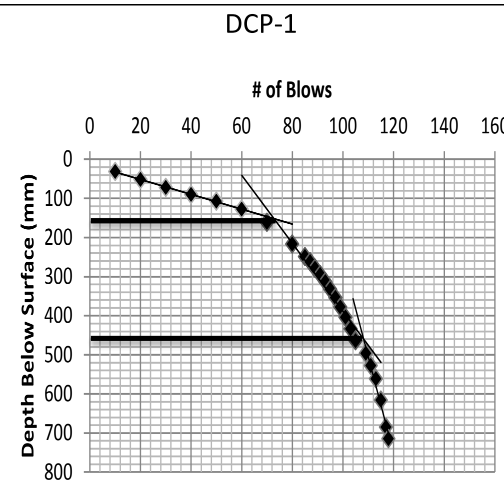

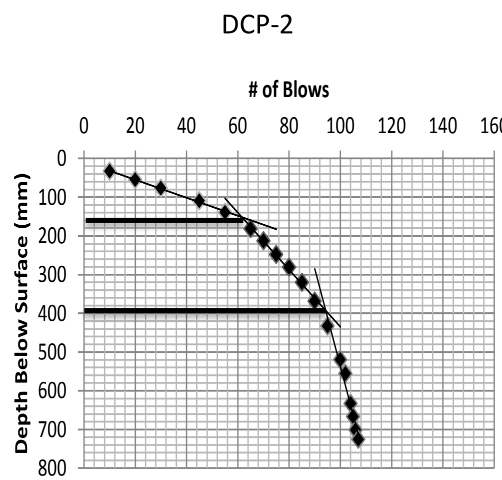

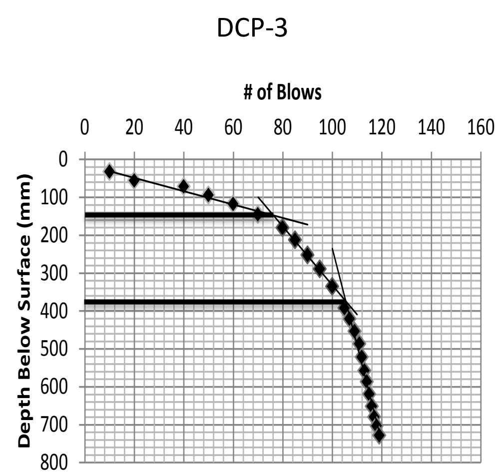

Figure B. 20 LIME 3 DCP LOCATION: L3-S (STA 254+46.26).

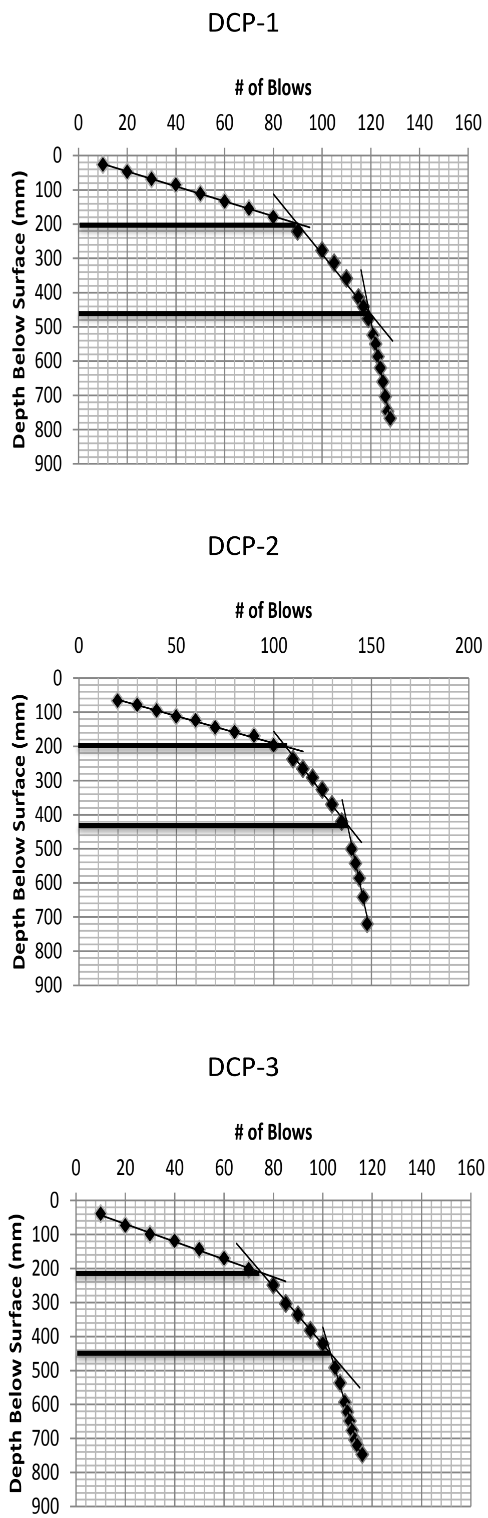

Figure B. 21 LIME 4 DCP LOCATION: L4-S (STA 254+65.46)

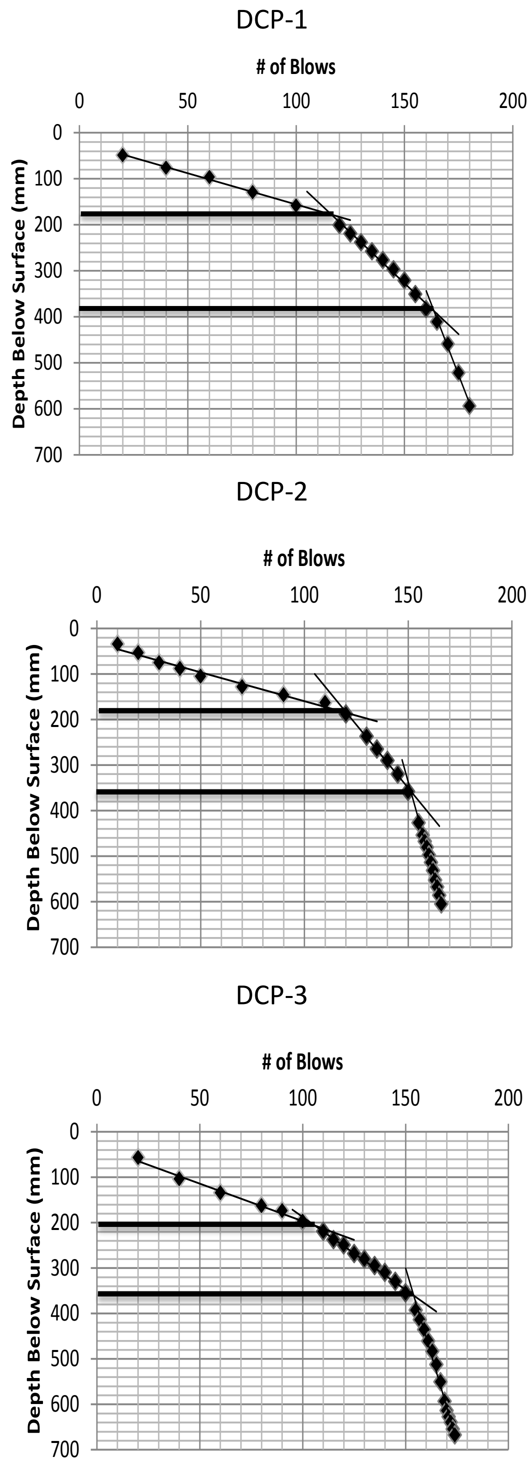

Figure B. 22 LIME 4 DCP LOCATION: L-11 (STA 255+00)

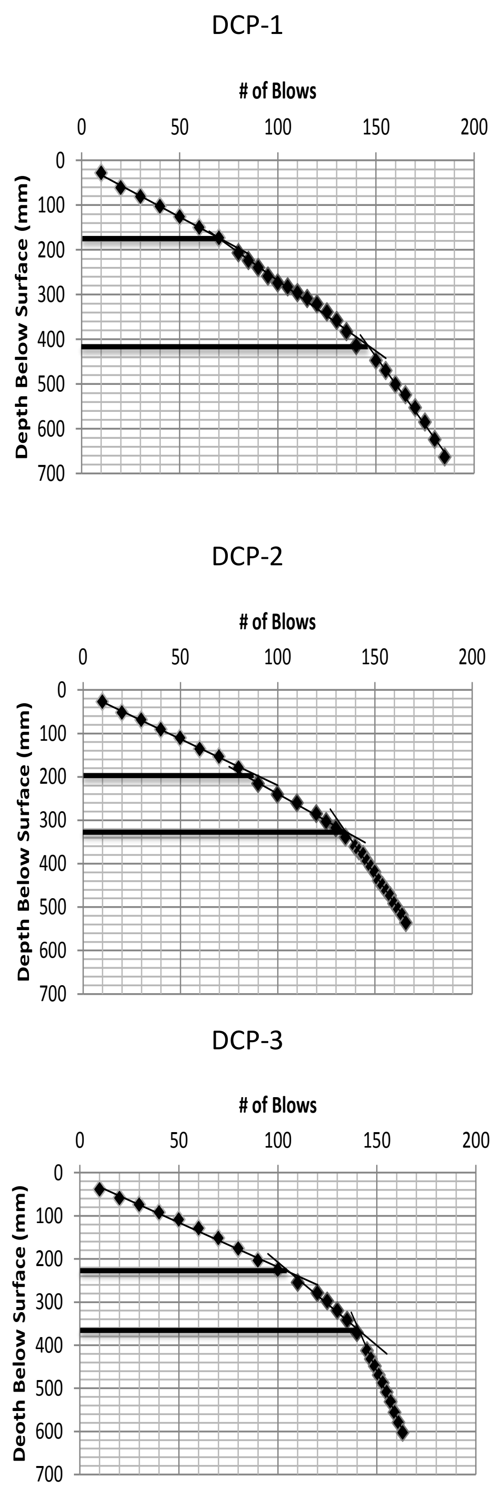

Figure B. 23 LIME 4 DCP LOCATION: L-12 (STA 255+65.23)

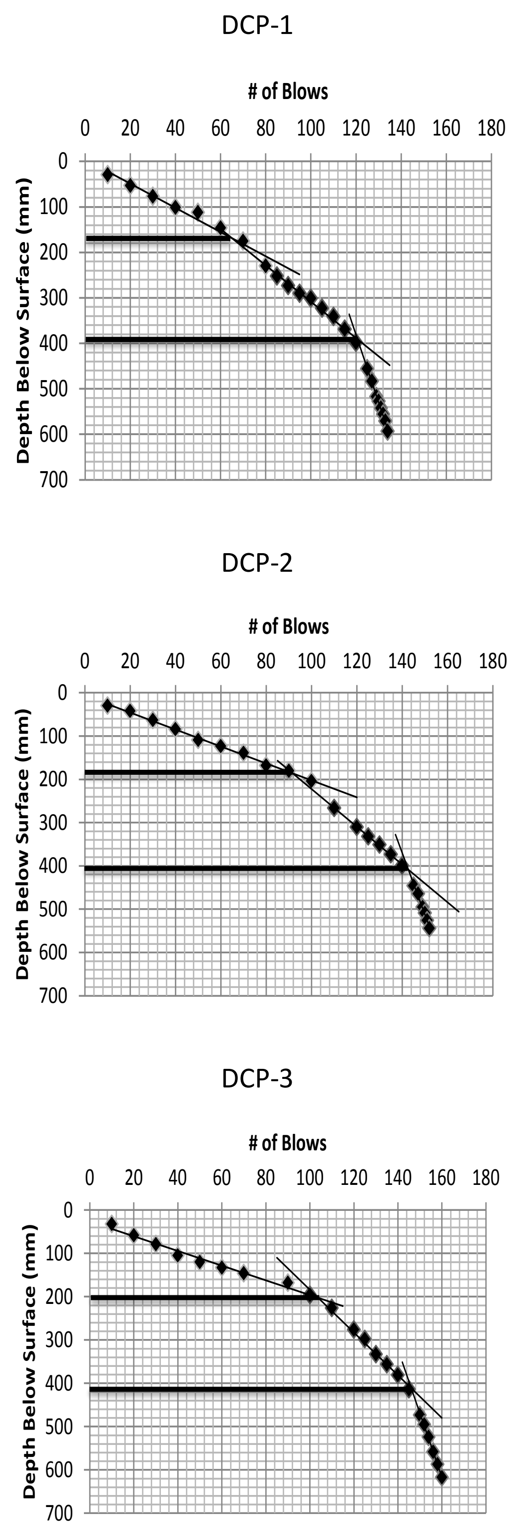

Figure B. 24 LIME 4 DCP LOCATION: L-13 (STA 255+85.43)

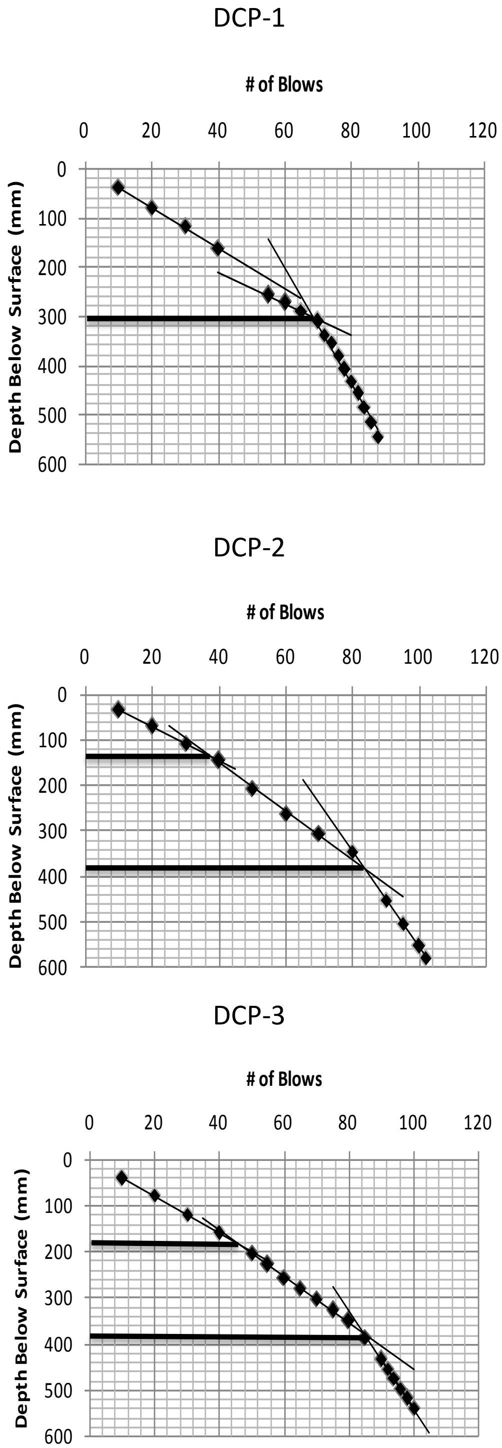

Figure B. 25 CEMENT 1 DCP LOCATION: C-1 (STA 258+75.48)

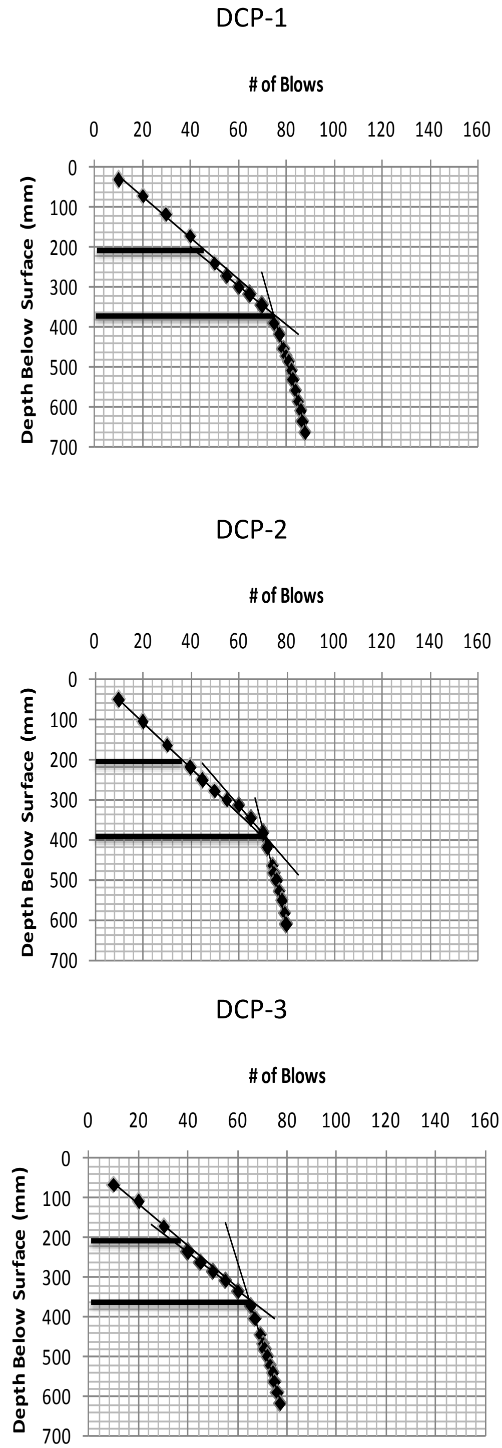

Figure B. 26 CEMENT 1 DCP LOCATION: C-2 (STA 259+21.20)

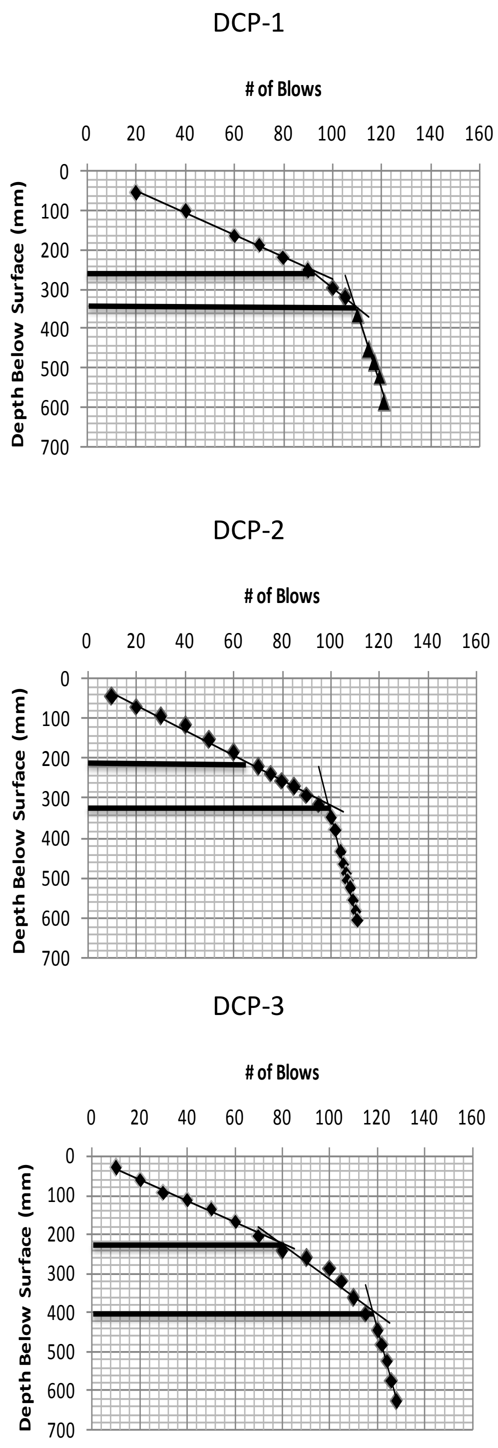

Figure B. 27 CEMENT1 DCP
LOCATION: C-3 (STA 259+66.92)

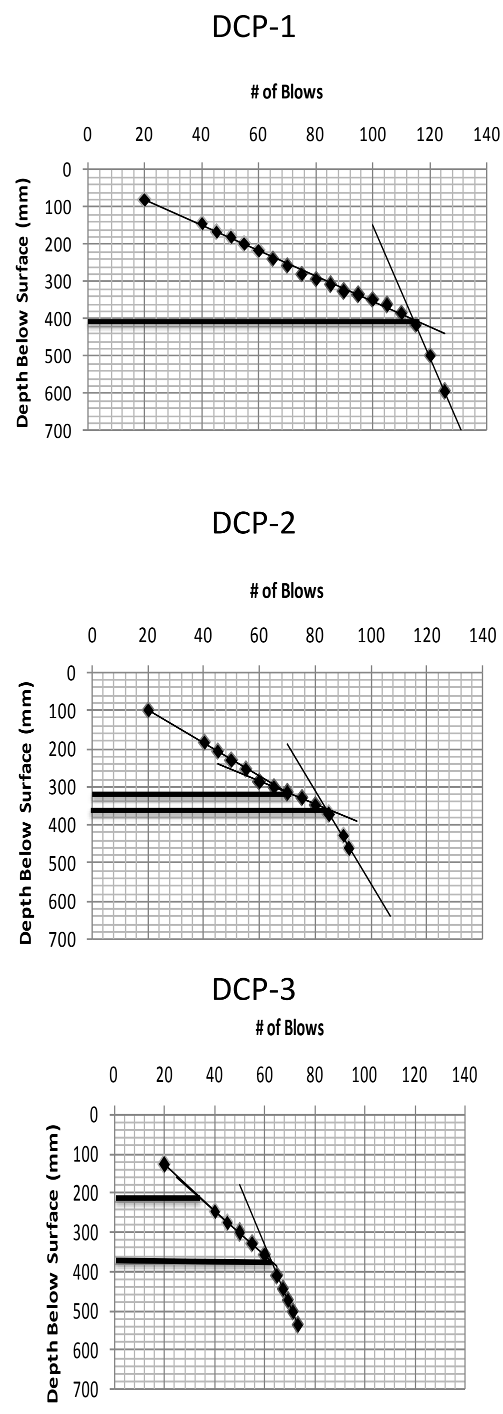

Figure B. 28 CEMENT 1 DCP
LOCATION: C1-S (STA 260+23.00)

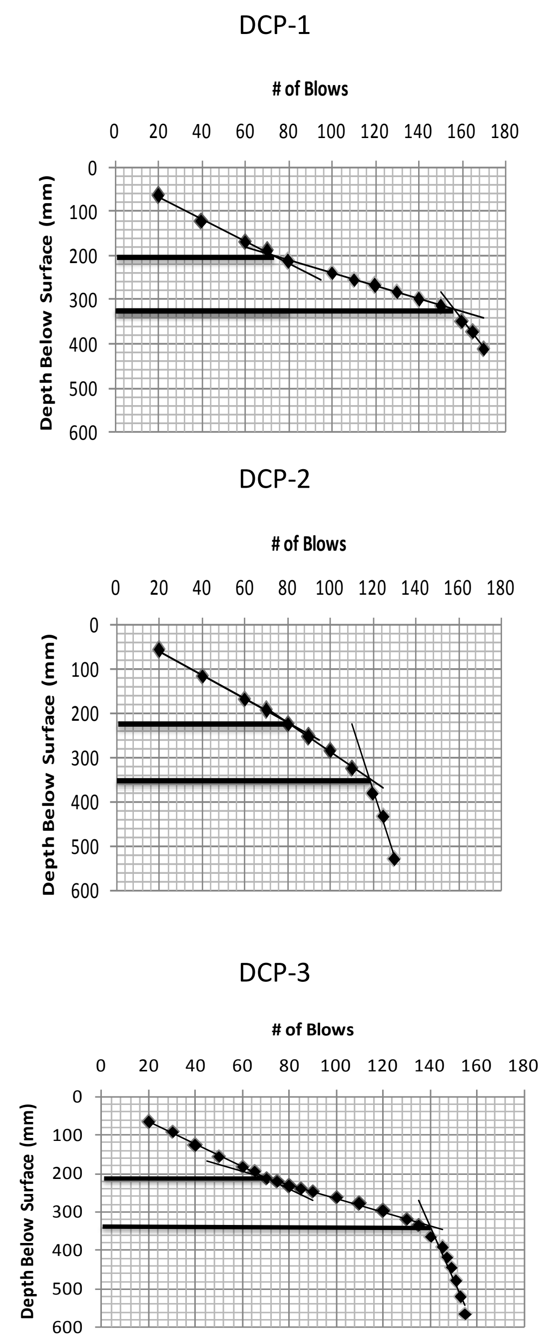

Figure B. 29 CEMENT 2 DCP LOCATION: C2-S (STA 260+36.096)

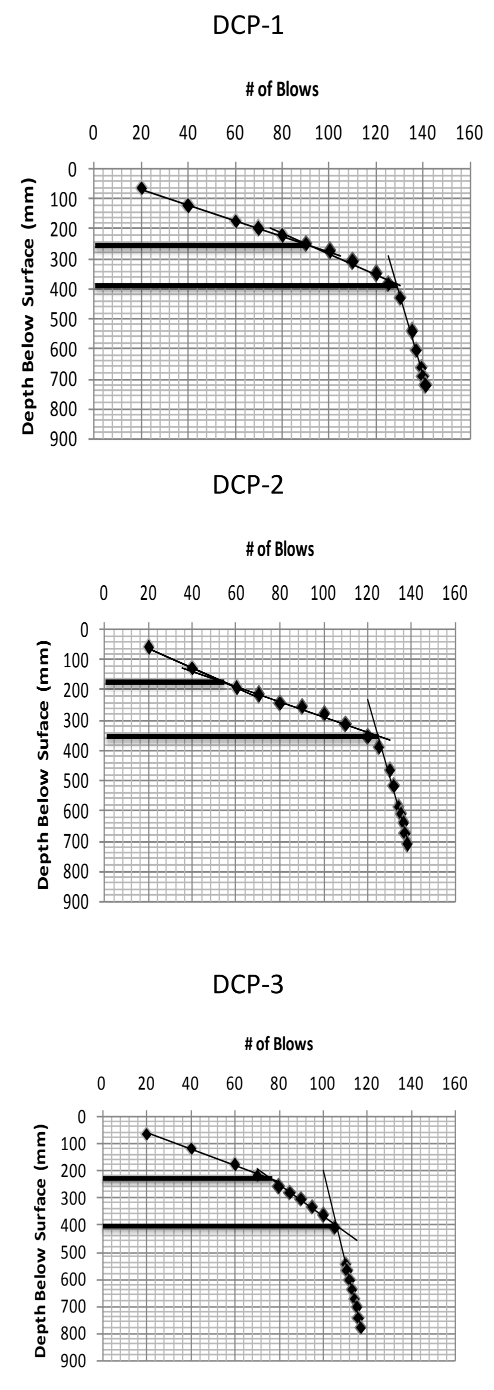

Figure B. 30 CEMENT 2 DCP LOCATION: C-4 (STA 260+55.26)

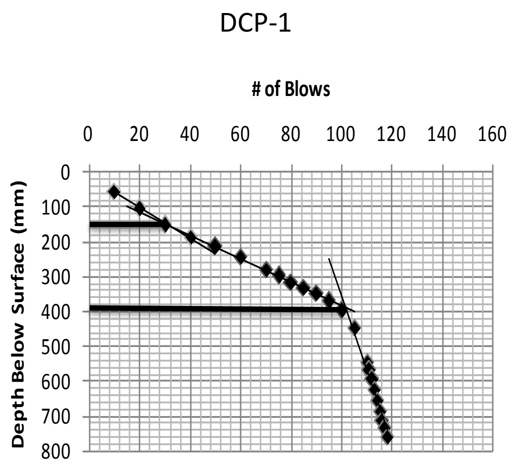

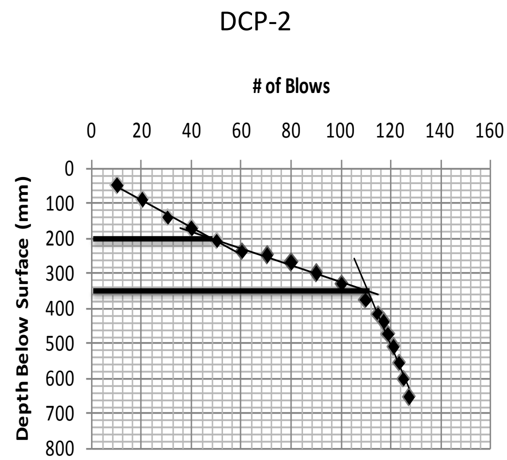

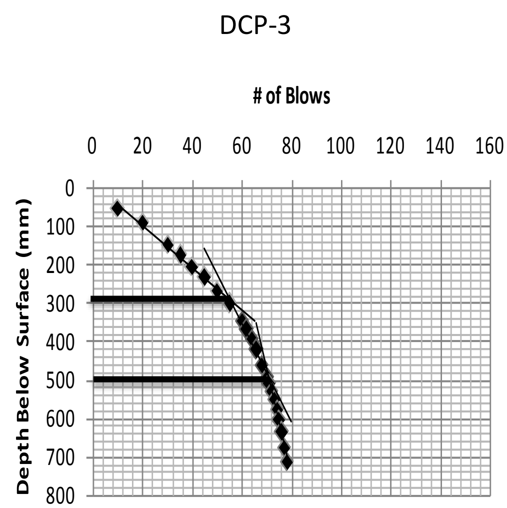

Figure B. 31 CEMENT 2 DCP LOCATION: C-5 (STA 261+00)

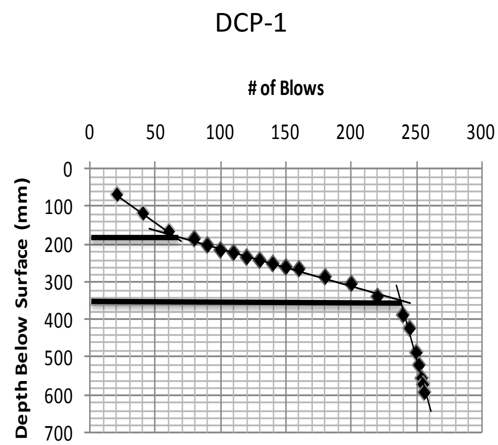

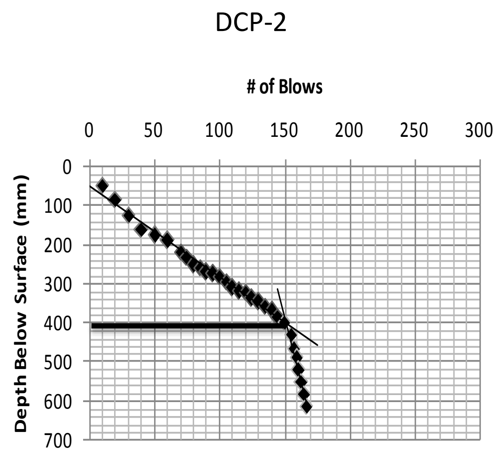

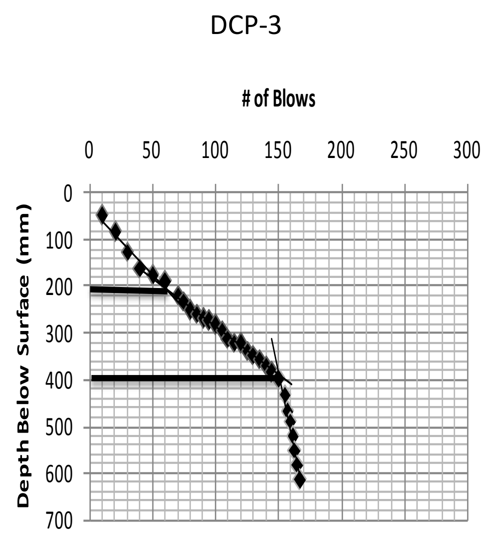

Figure B. 32 CEMENT 2 DCP LOCATION: C-6 (STA 261+67.50)

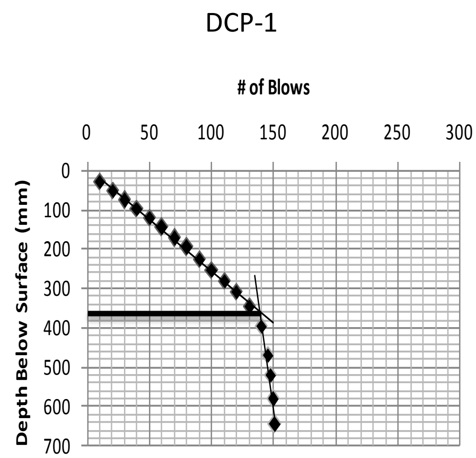

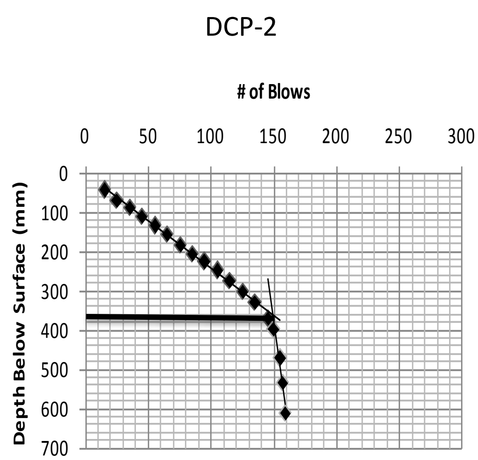

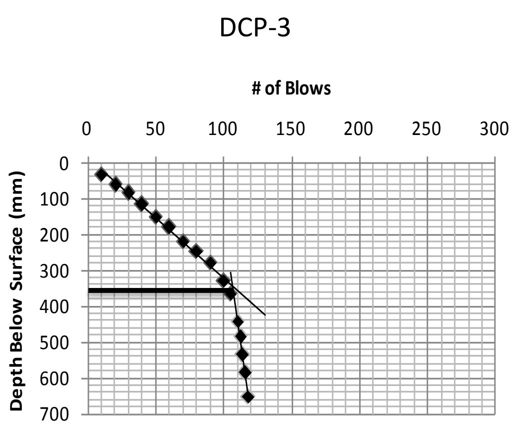

Figure B. 33 CEMENT 3 DCP
LOCATION: C-7 (STA 262+8.28)

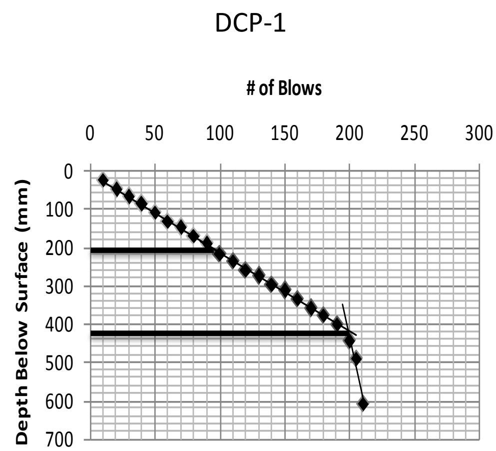

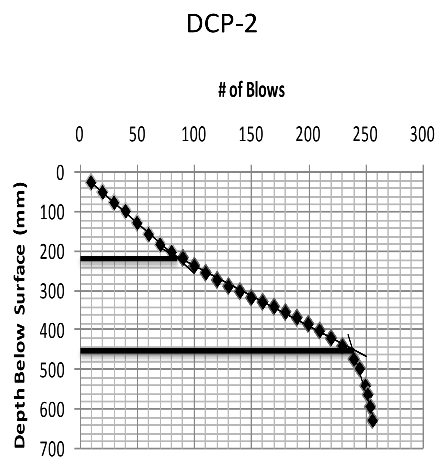

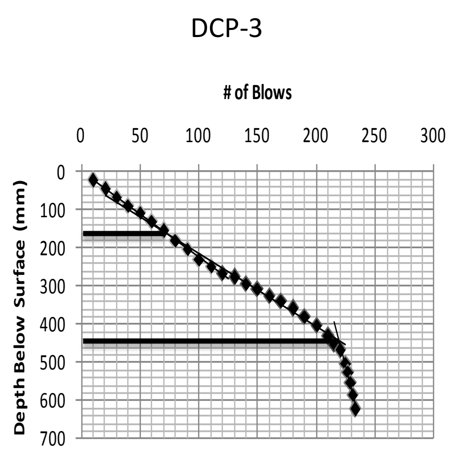

Figure B. 34 CEMENT 3 DCP
LOCATION: C-8 (STA 263+17.50)

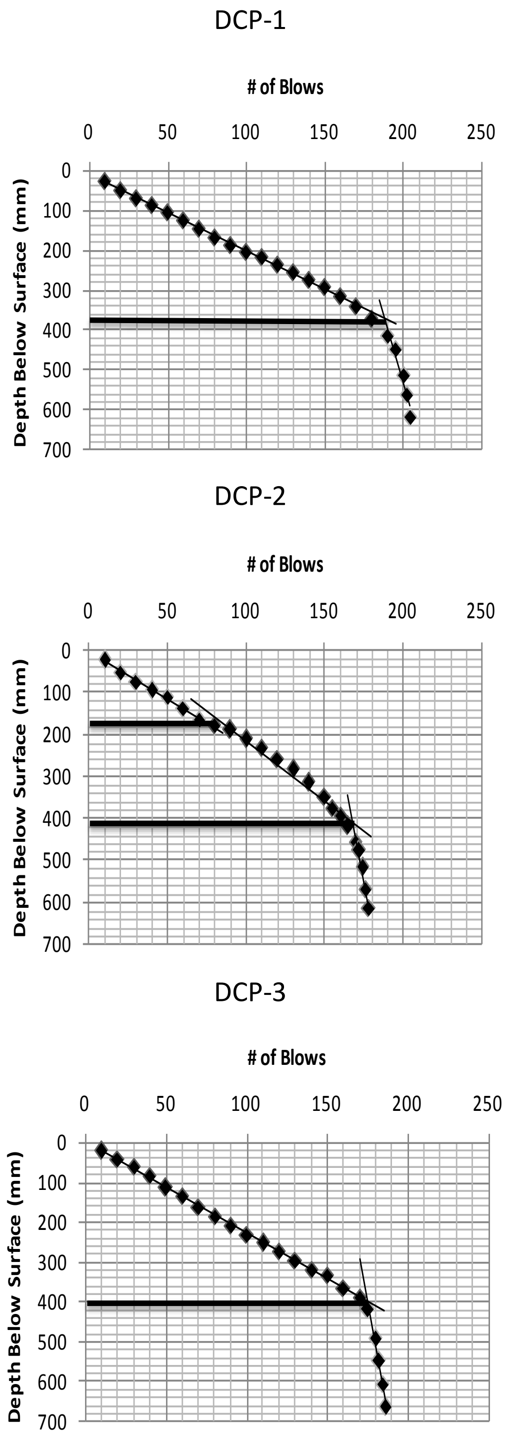

Figure B. 35 CEMENT 3 DCP LOCATION: C-9 (STA 263+57.37)

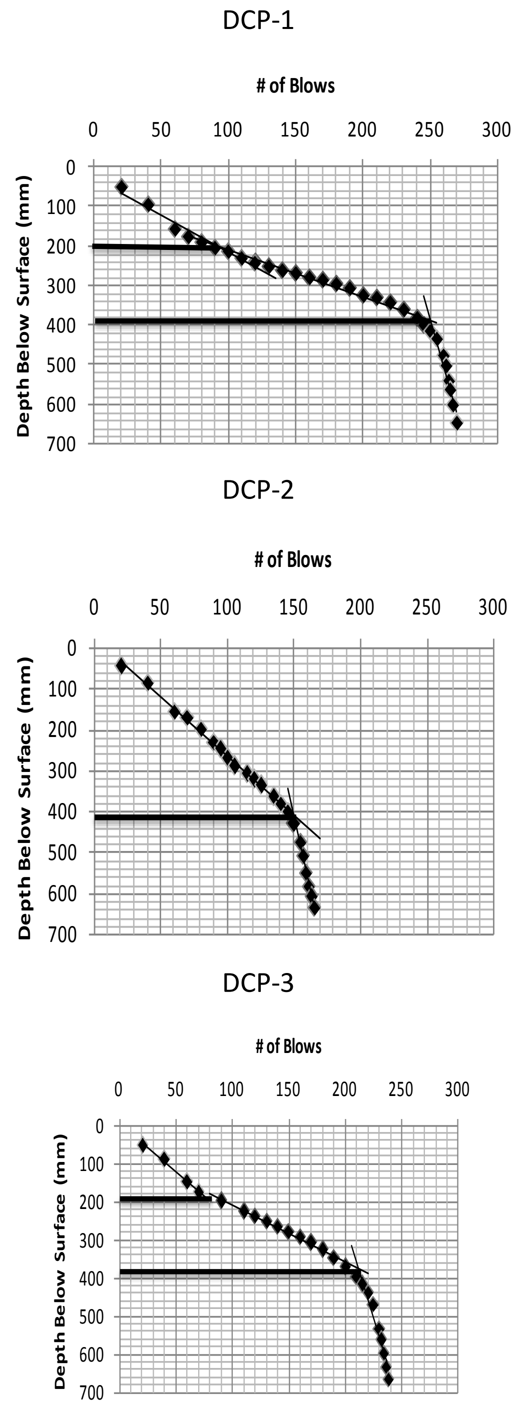

Figure B. 36 CEMENT 3 DCP LOCATION: C3-S (STA 264+30.38)

DCP-1

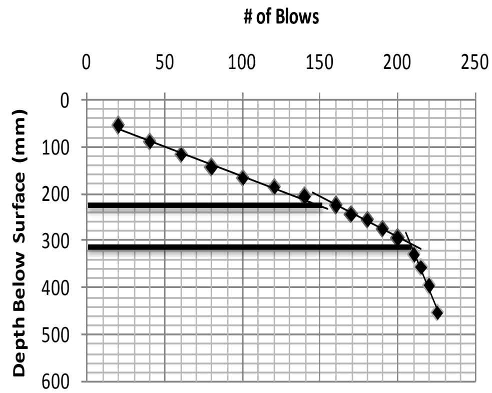

DCP-2

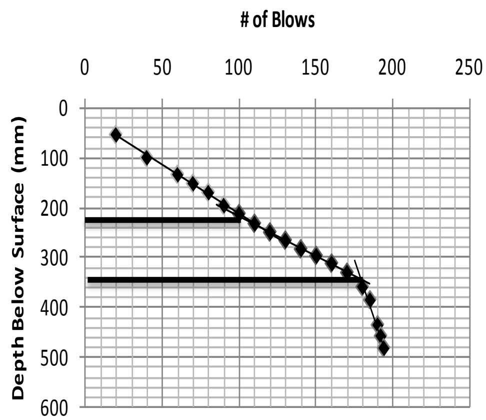

DCP-3

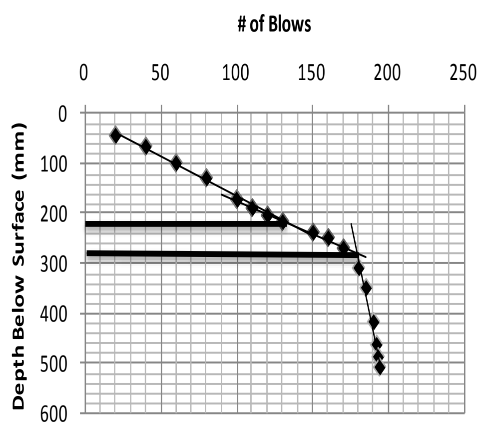

Figure B. 37 CEMENT 4 DCP
LOCATION: C4-S (STA 264+45.62)

DCP-1

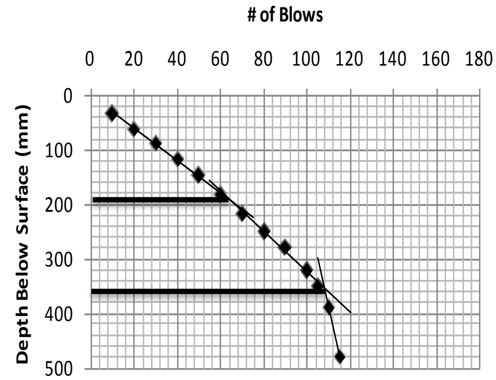

DCP-2

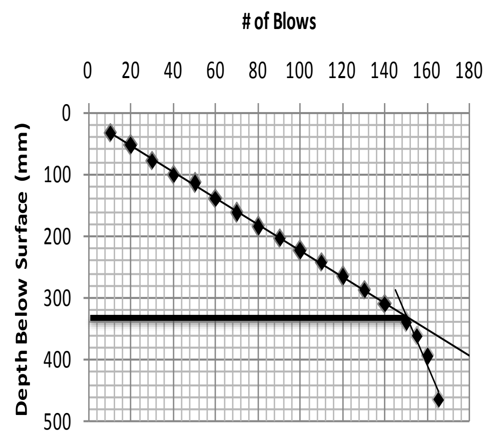

DCP-3

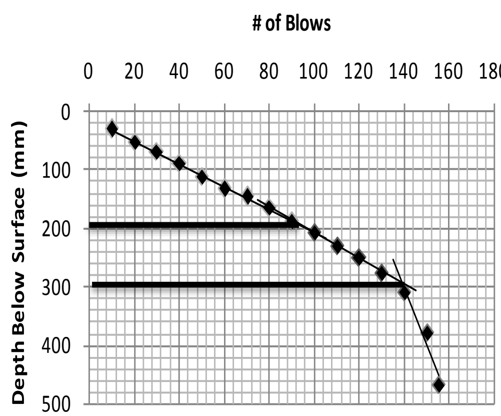

Figure B. 38 CEMENT 4 DCP
LOCATION: C-10 (STA 264+83.83)

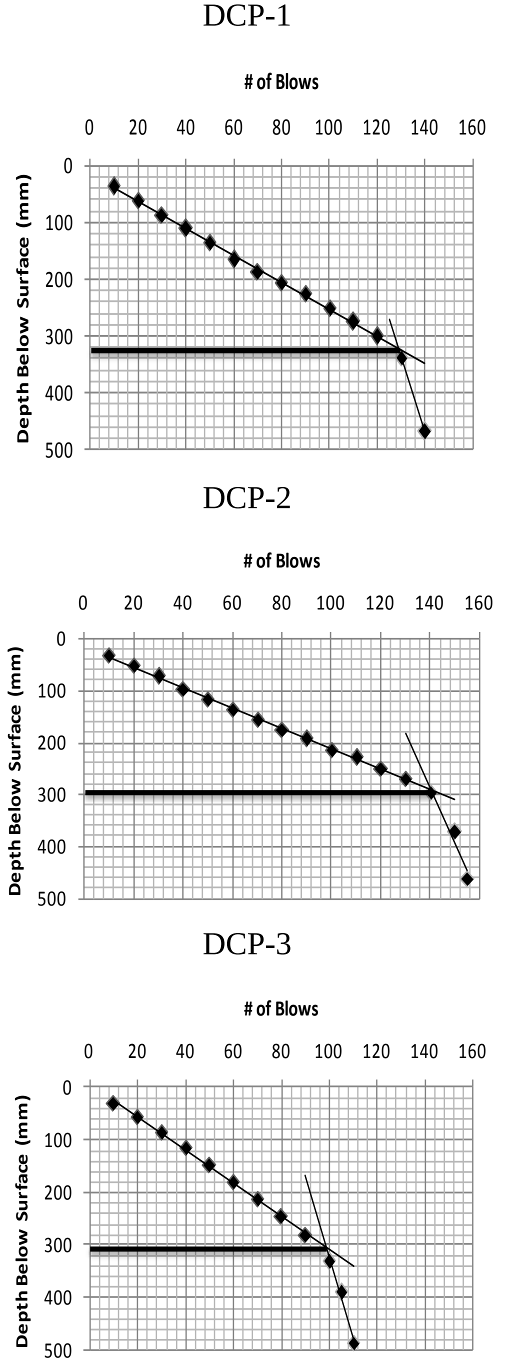

Figure B. 39 CEMENT 4 DCP
LOCATION: C-11 (STA 265+13.76)

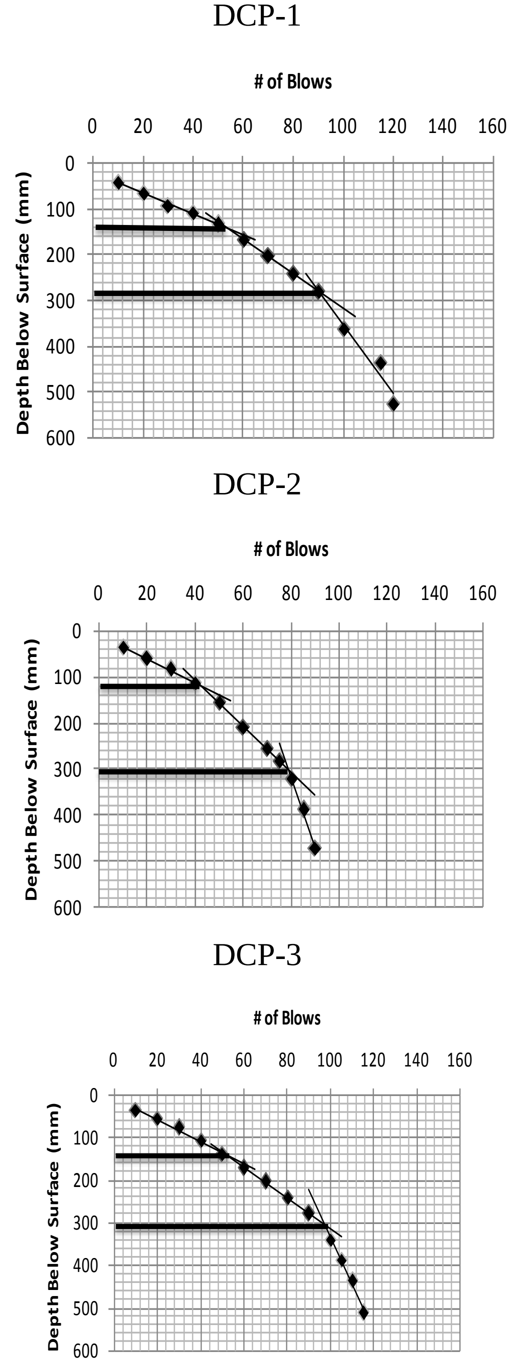

Figure B. 40 CEMENT 4 DCP
LOCATION: C-12 (STA 265+61.69)

APPENDIX C

C.1. Predicted Longitudinal Strains

C.1.1 Lime Test Section

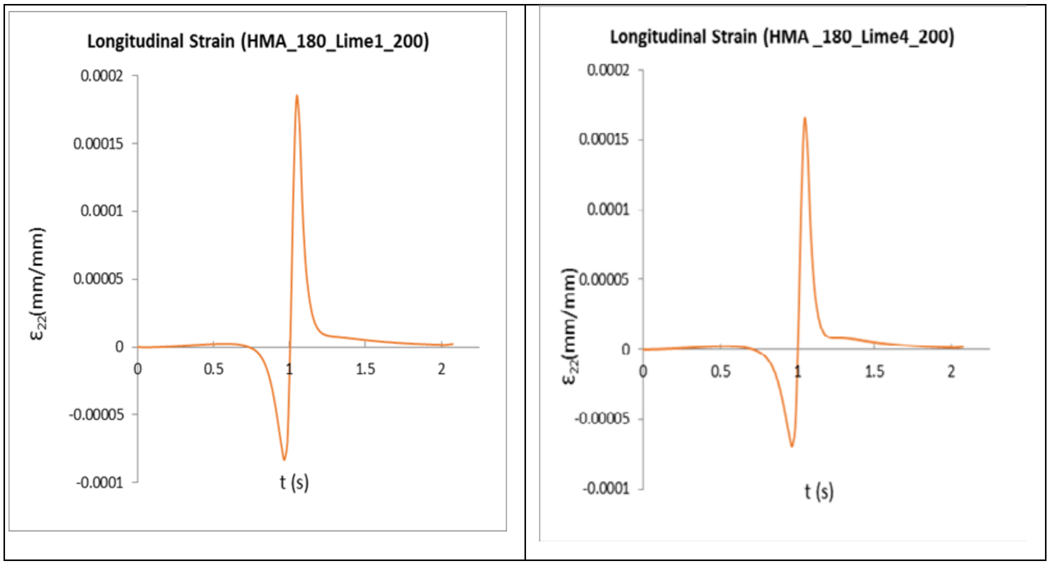

Figure C.1.1.1 Calculated longitudinal strains at the bottom of HMA of control lime subgrade stabilization layer test sections consisting: for (a) 180-mm HMA, 200-mm ABC, 200-mm stabilized layer; (b) 180-mm HMA, 200-mm ABC, 200-mm stabilized layer.

Figure C.1.1.2 Calculated longitudinal strains at the bottom of HMA of deep lime

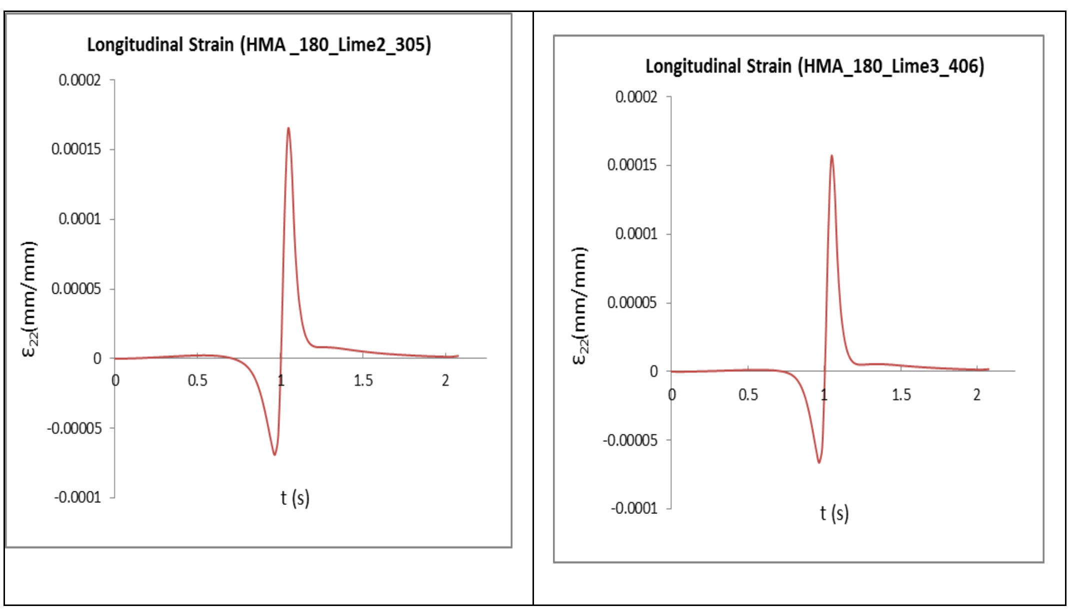

subgrade stabilization layer test sections consisting: for (a) 180-mm HMA, 200-mm ABC, 305-mm stabilized layer; (b) 180-mm HMA, 200-mm ABC, 406-mm stabilized layer.

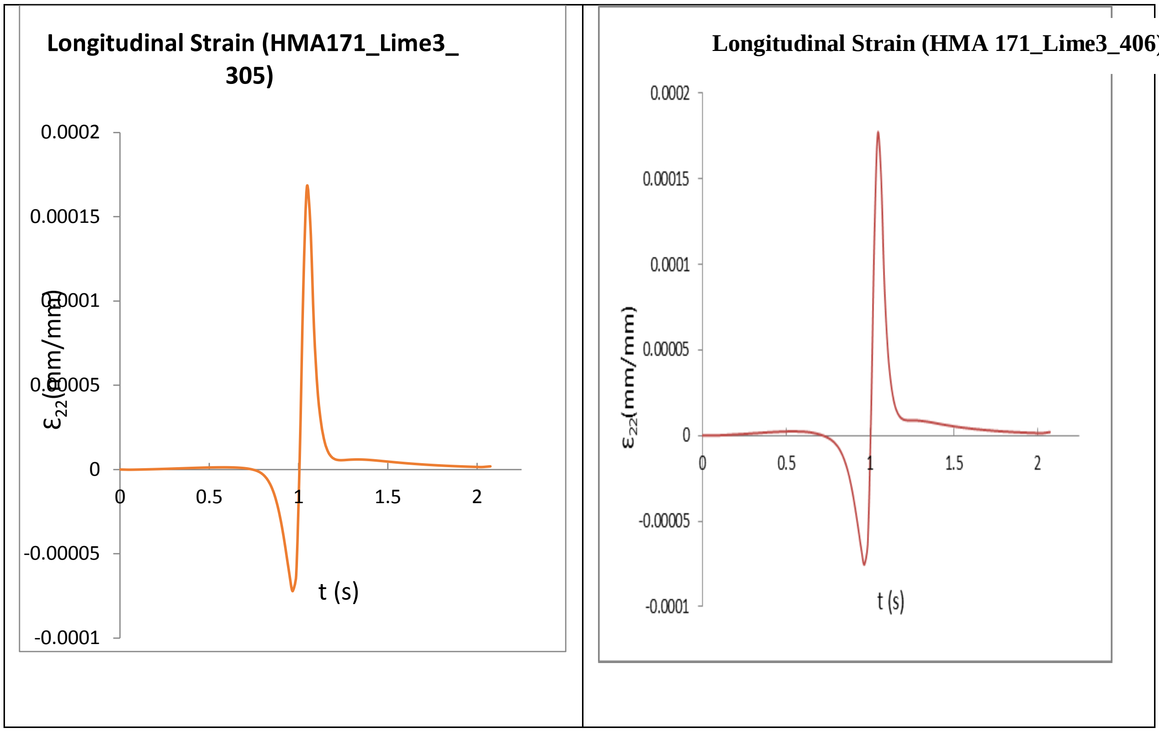

Figure C.1.1.3 Calculated longitudinal strains at the bottom of HMA of deep lime subgrade stabilization layer test sections consisting: for (a) 171-mm HMA, 200-mm ABC, 305-mm stabilized layer; (b) 171-mm HMA, 200-mm ABC, 406-mm stabilized layer.

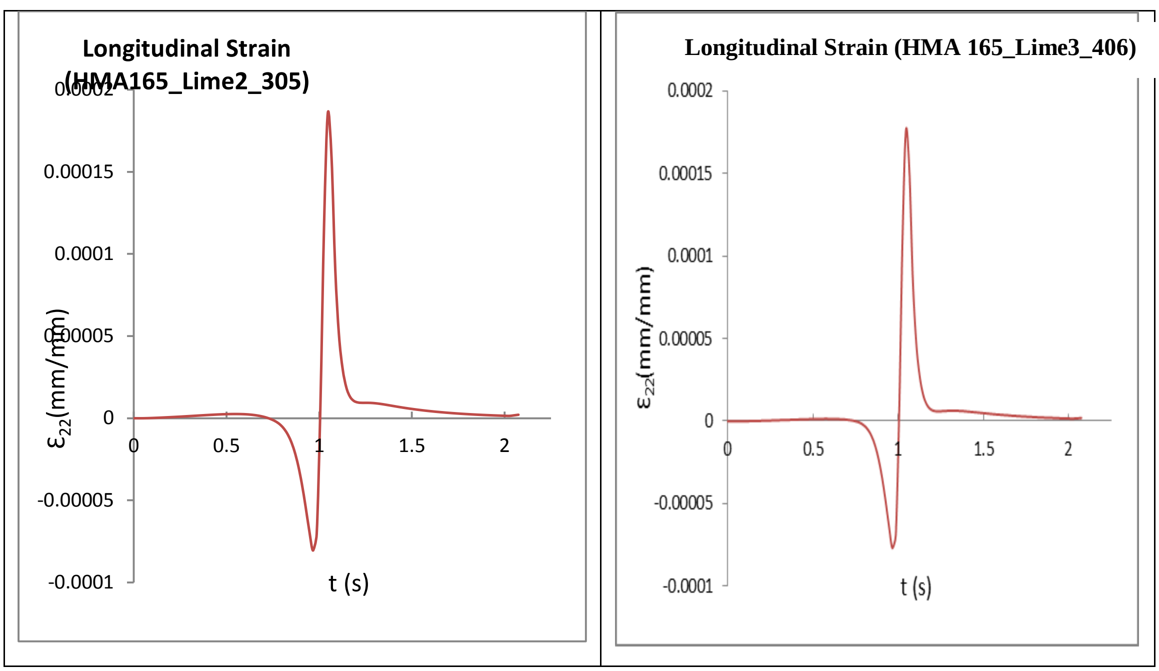

Figure C.1.1.4: Calculated longitudinal strains at the bottom of HMA of deep lime subgrade stabilization layer test sections consisting: for (a) 165-mm HMA, 200-mm ABC, 305-mm stabilized layer; (b) 165-mm HMA, 200-mm ABC, 406-mm stabilized layer.

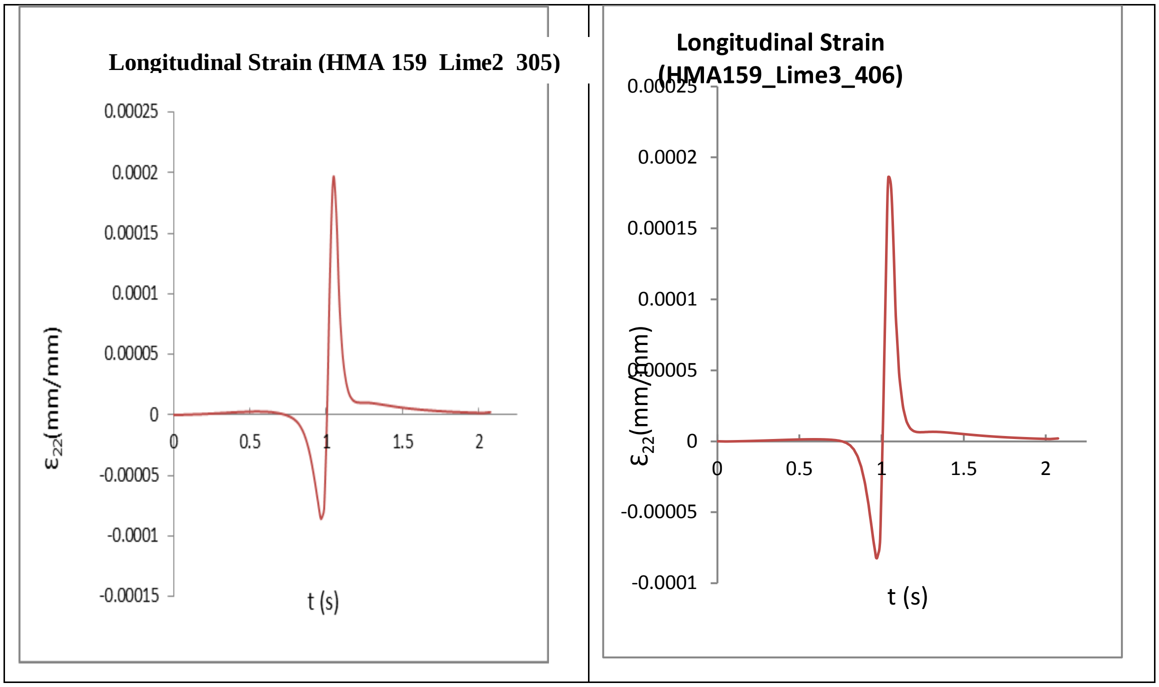

Figure C.1.1.5: Calculated longitudinal strains at the bottom of HMA of deep lime subgrade stabilization layer test sections consisting: for (a) 159-mm HMA, 200-mm ABC, 305-mm stabilized layer; (b) 159-mm HMA, 200-mm ABC, 406-mm stabilized layer.

C.1.2 Cement Test Sections

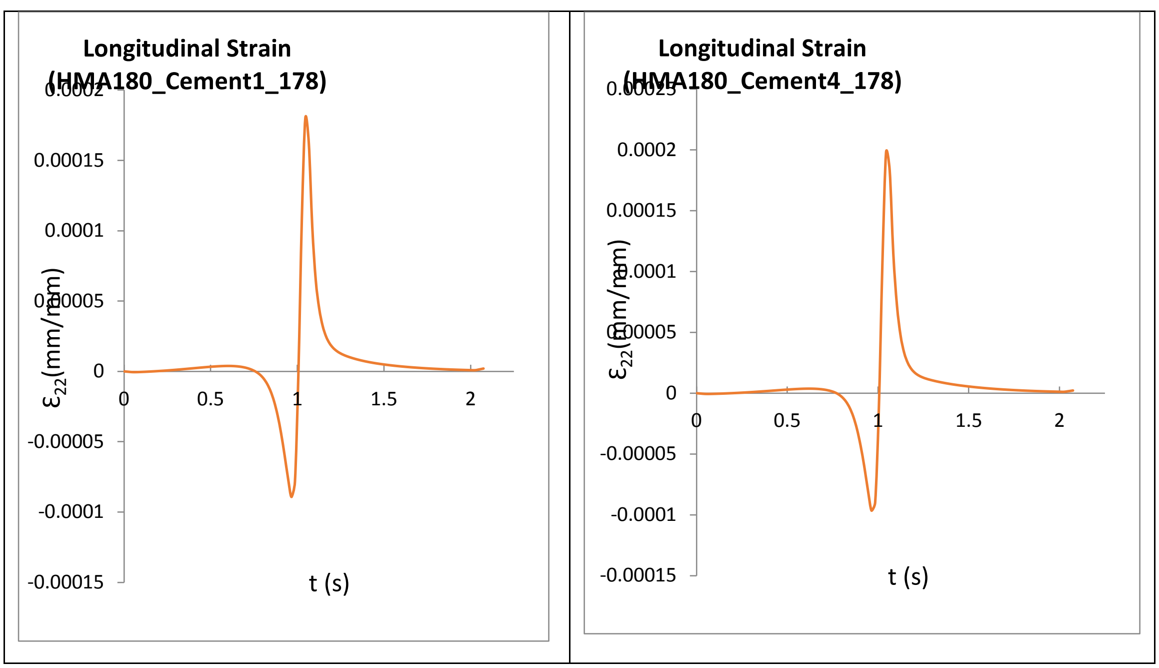

Figure C.1.2.1: Calculated longitudinal strains at the bottom of HMA of control cement subgrade stabilization layer test sections consisting: for (a) 180-mm HMA, 200-mm ABC, 178-mm stabilized layer; (b) 180-mm HMA, 200-mm ABC, 178-mm stabilized layer.

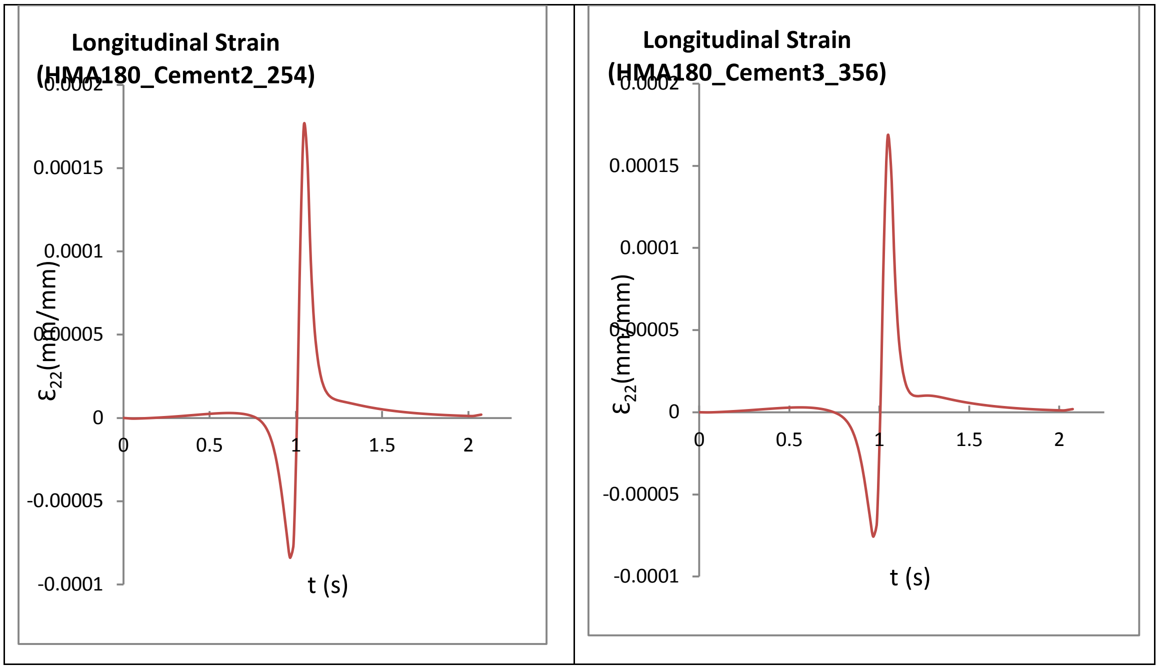

Figure C.1.2.2: Calculated longitudinal strains at the bottom of HMA of deep cement subgrade stabilization layer test sections consisting: for (a) 180-mm HMA, 200-mm ABC, 254-mm stabilized layer; (b) 180-mm HMA, 200-mm ABC, 356-mm stabilized layer.

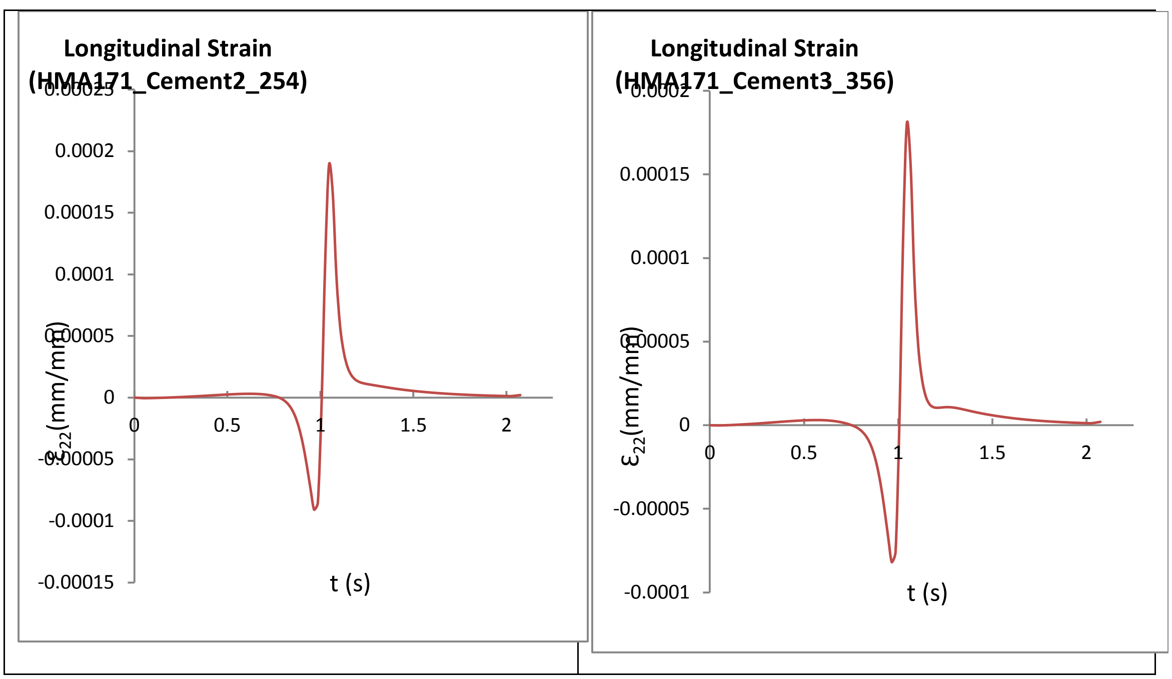

Figure C.1.2.3: Calculated longitudinal strains at the bottom of HMA of deep cement subgrade stabilization layer test sections consisting: for (a) 171-mm HMA, 200-mm ABC, 254-mm stabilized layer; (b) 171-mm HMA, 200-mm ABC, 356-mm stabilized layer.

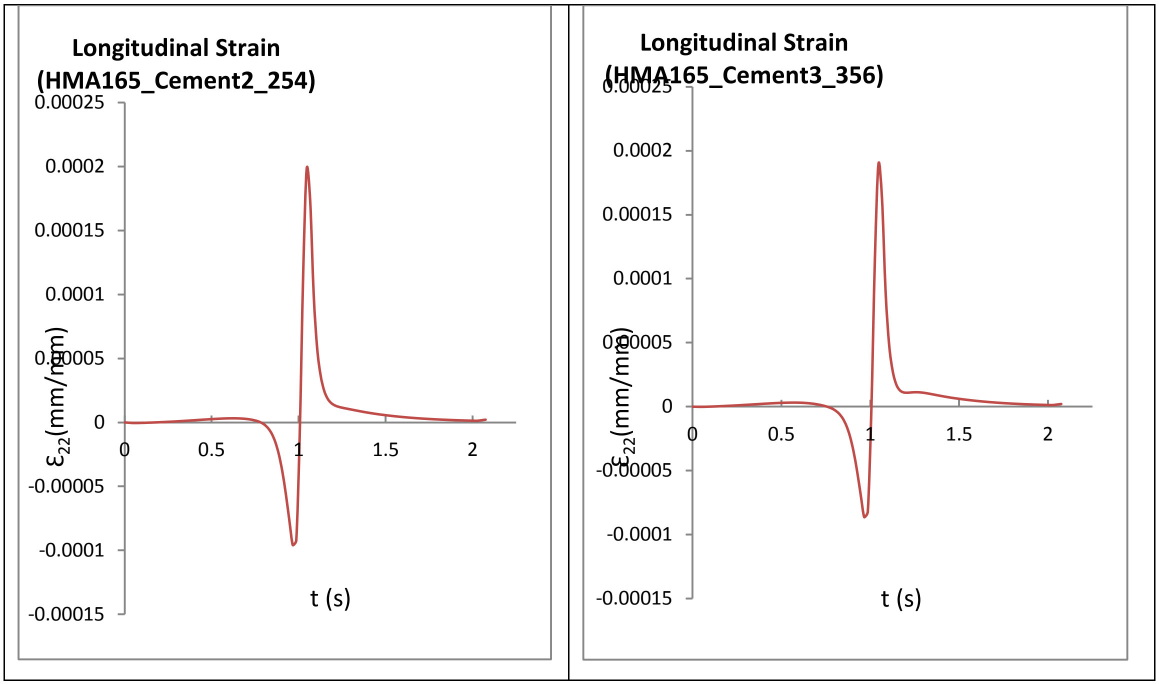

Figure C.1.2.4: Calculated longitudinal strains at the bottom of HMA of deep cement subgrade stabilization layer test sections consisting: for (a) 165-mm HMA, 200-mm ABC, 254-mm stabilized layer; (b) 165-mm HMA, 200-mm ABC, 356-mm stabilized layer.

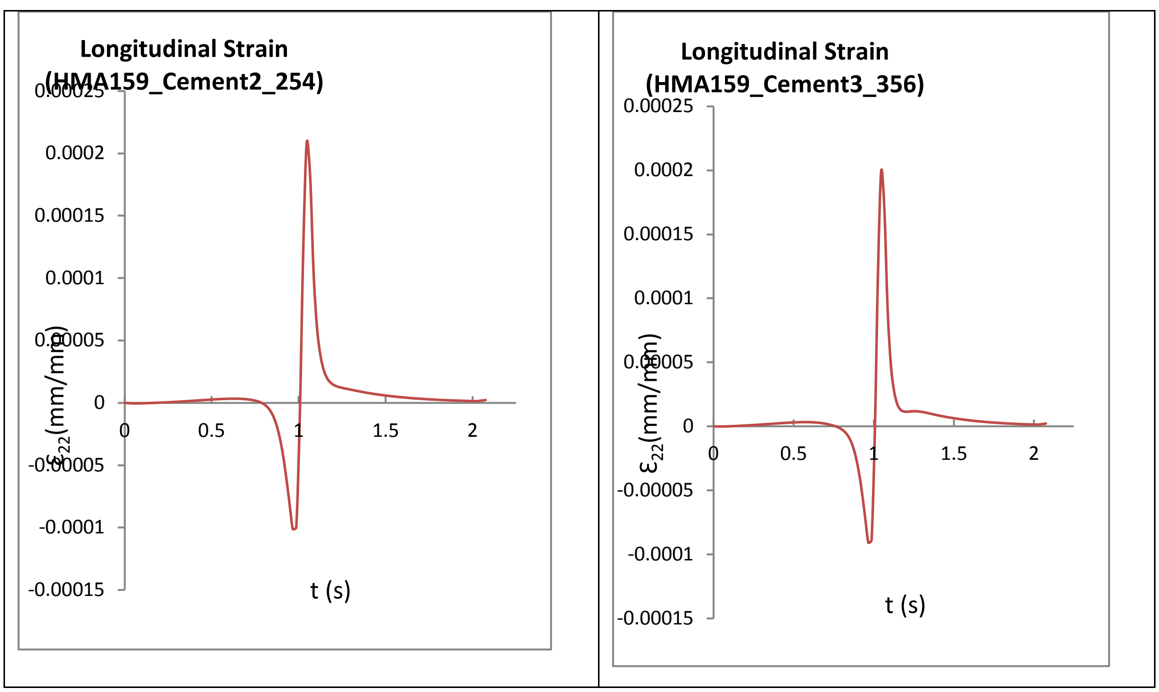

Figure C.1.2.5: Calculated longitudinal strains at the bottom of HMA of deep cement subgrade stabilization layer test sections consisting: for (a) 159-mm HMA, 200-mm ABC, 254-mm stabilized layer; (b) 159-mm HMA, 200-mm ABC, 356 -mm stabilized layer.

C.2. Variations of Load Repetitions to Failure with HMA Thickness

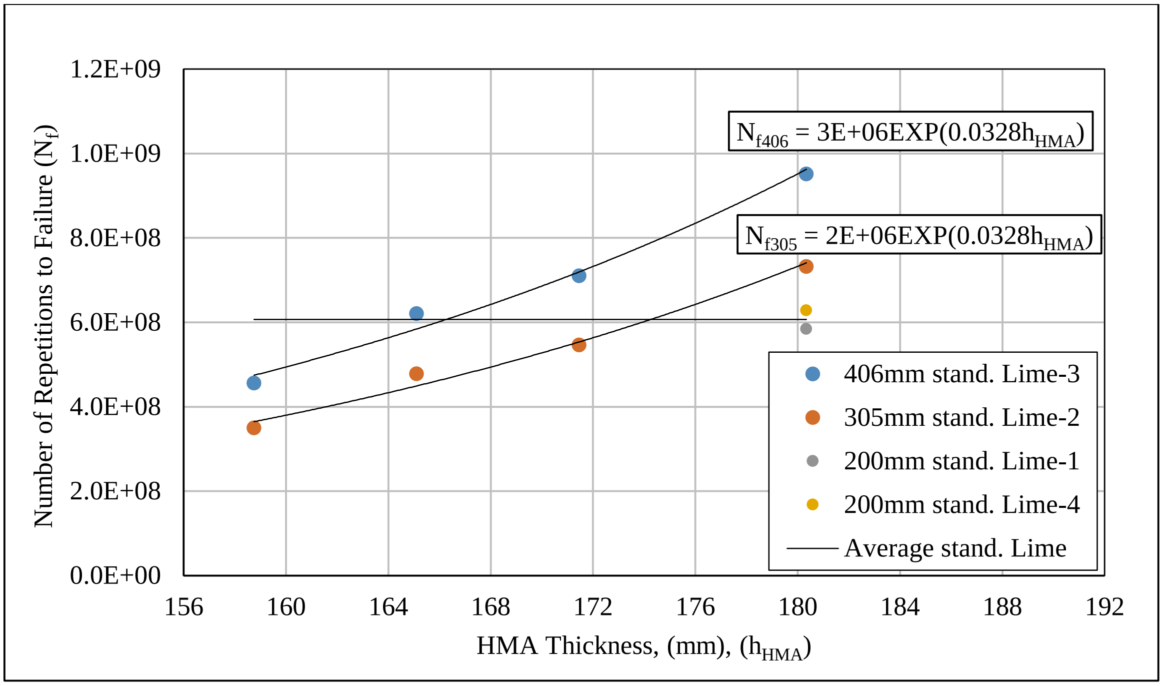

Figure C.2.2 Load related bottom-up cracking model: lime test section, May 2011 (Based on EVERSTRESS)

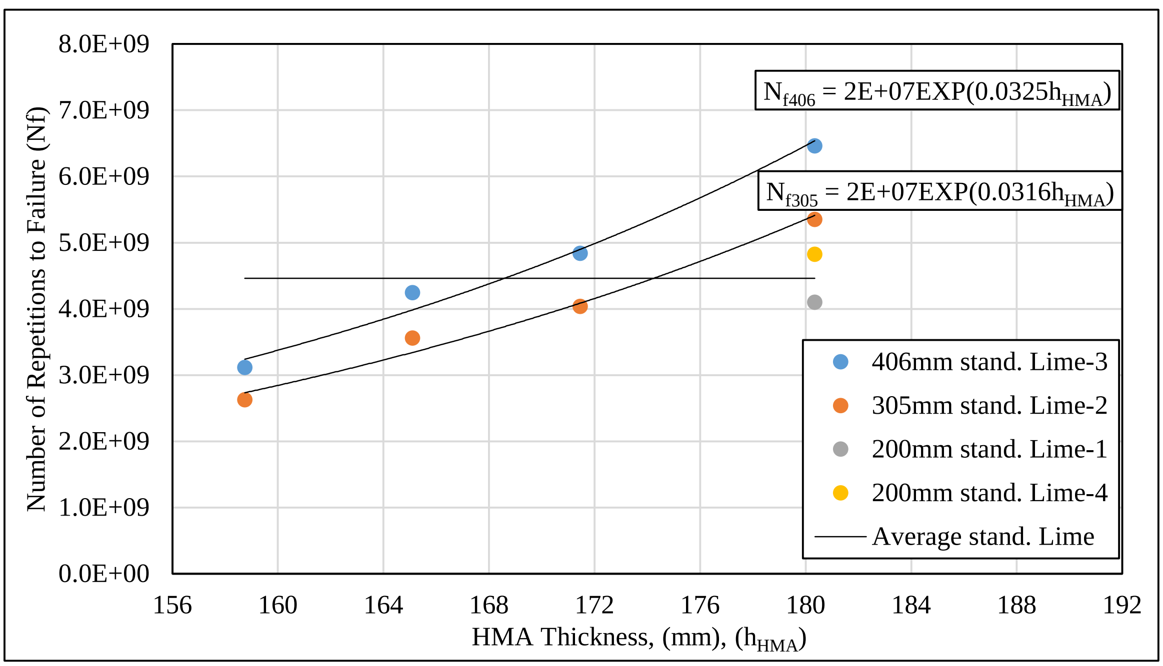

Figure C.3. 2 Load related bottom-up cracking model: lime test section, October 2011 (Based on EVERSTRESS)

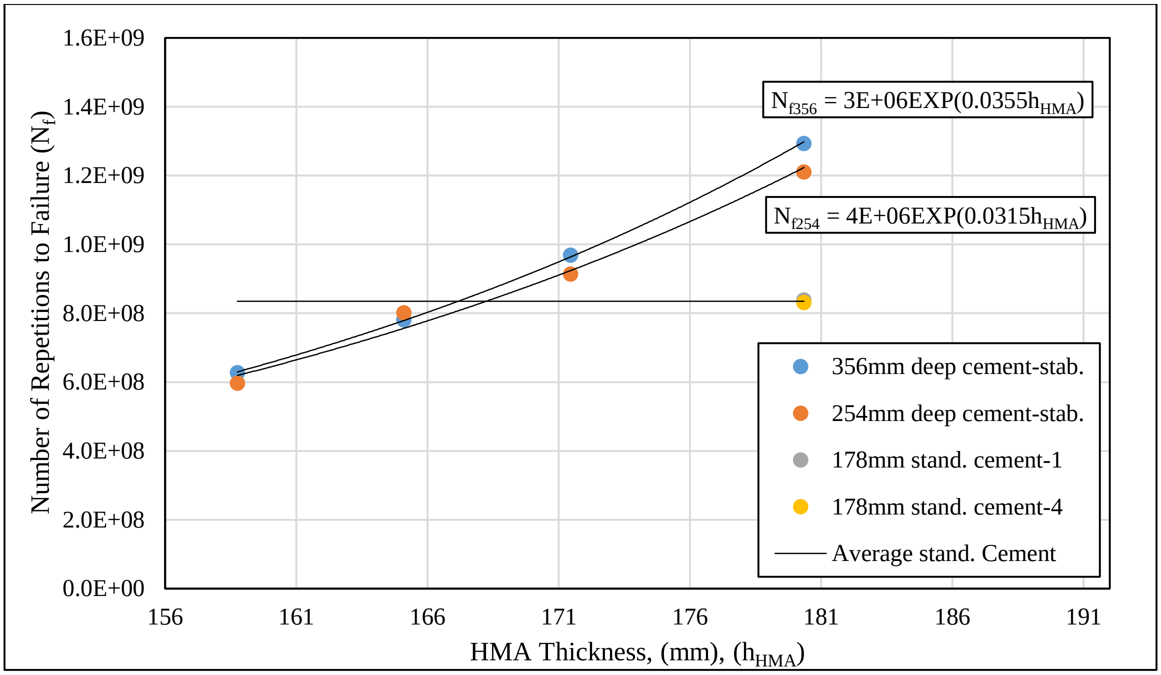

Figure C.2.4 Load related bottom-up cracking model: cement test section, May 2011 (Based on EVERSTRESS)

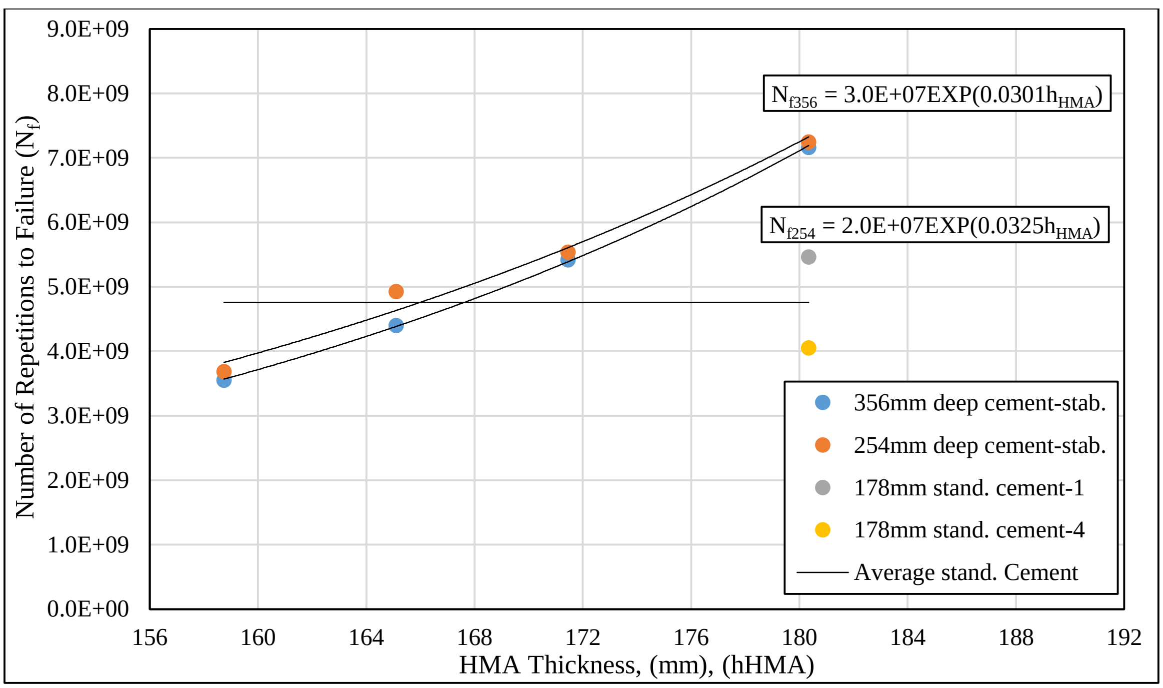

Figure C.2.5 Load related bottom-up cracking model: cement test section, October 2011 (Based on EVERSTRESS)

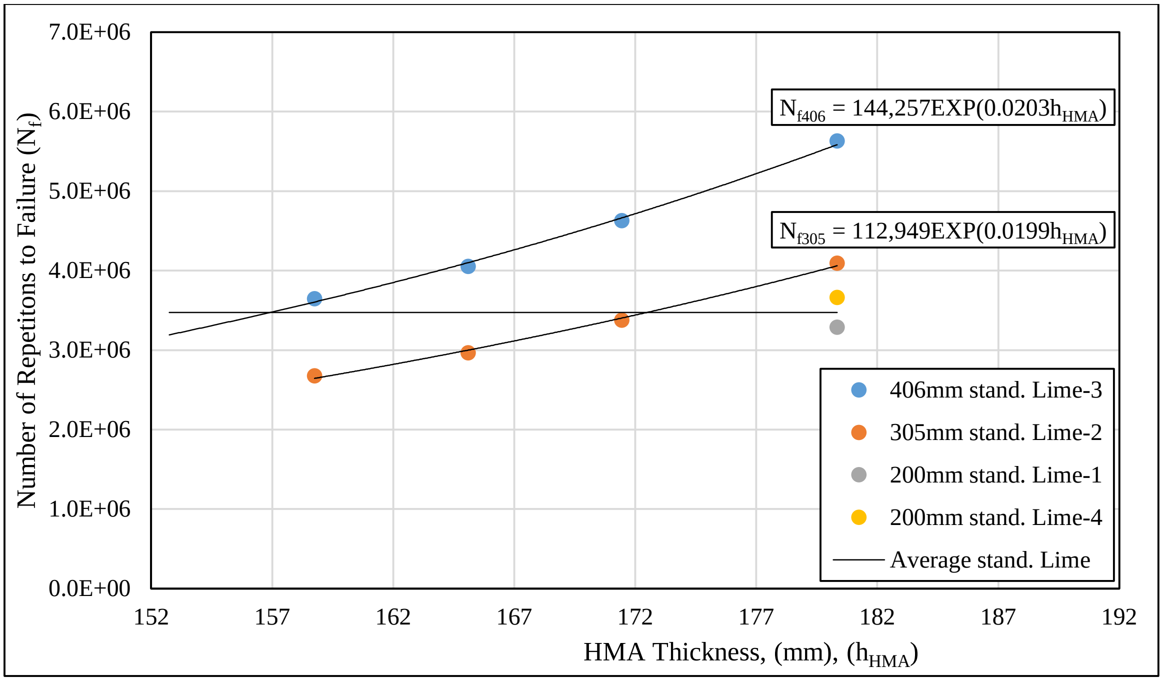

Figure C.2.6 Load related top-down cracking model: lime test section, October 2011 (Based on EVERSTRESS)

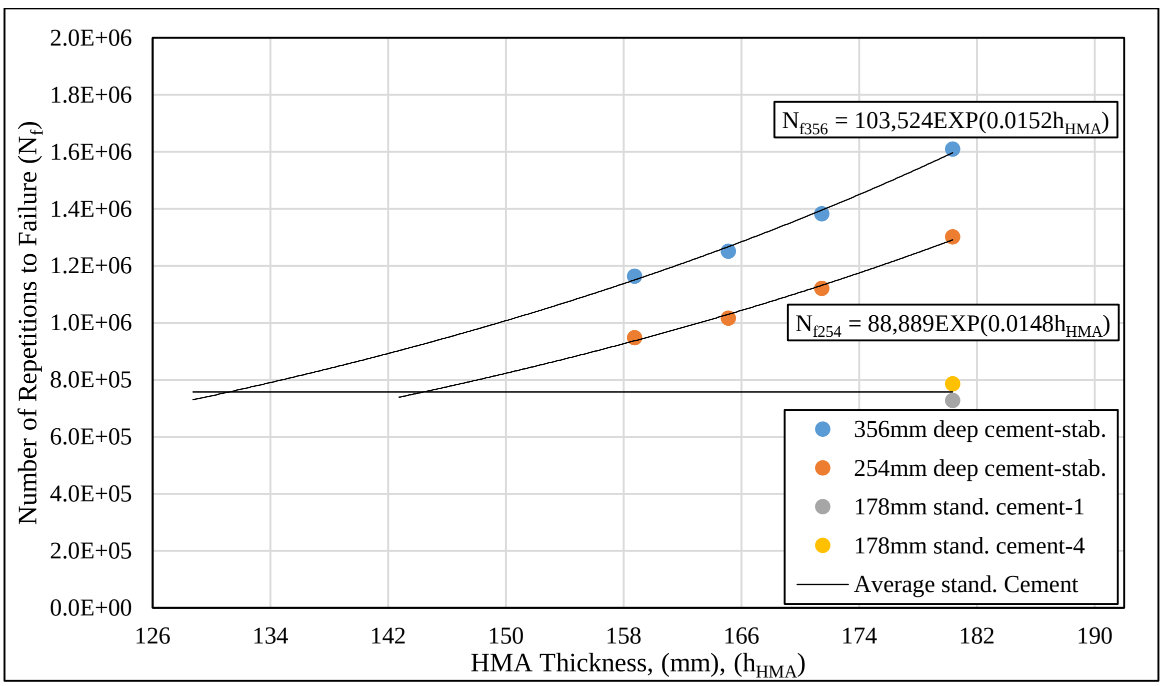

Figure C.2.7 Load related top-down cracking model: cement test section, May 2011 (Based on EVERSTRESS)

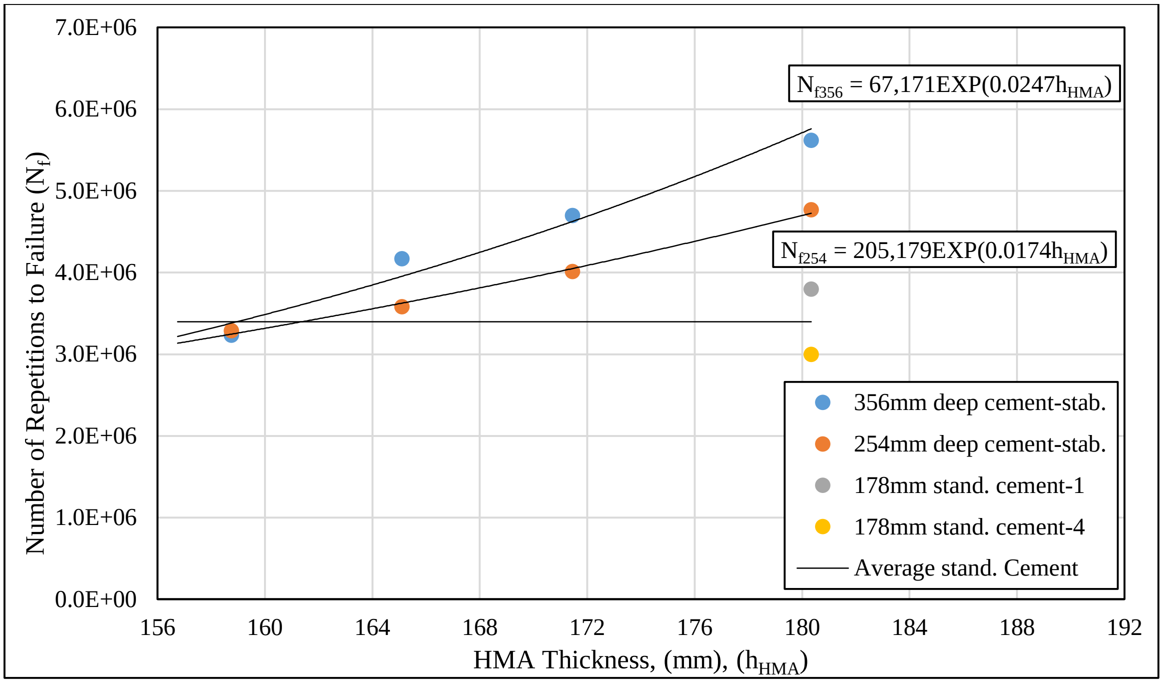

Figure C.2.8 Load related top-down cracking model: cement test section, October 2011 (Based on EVERSTRESS)

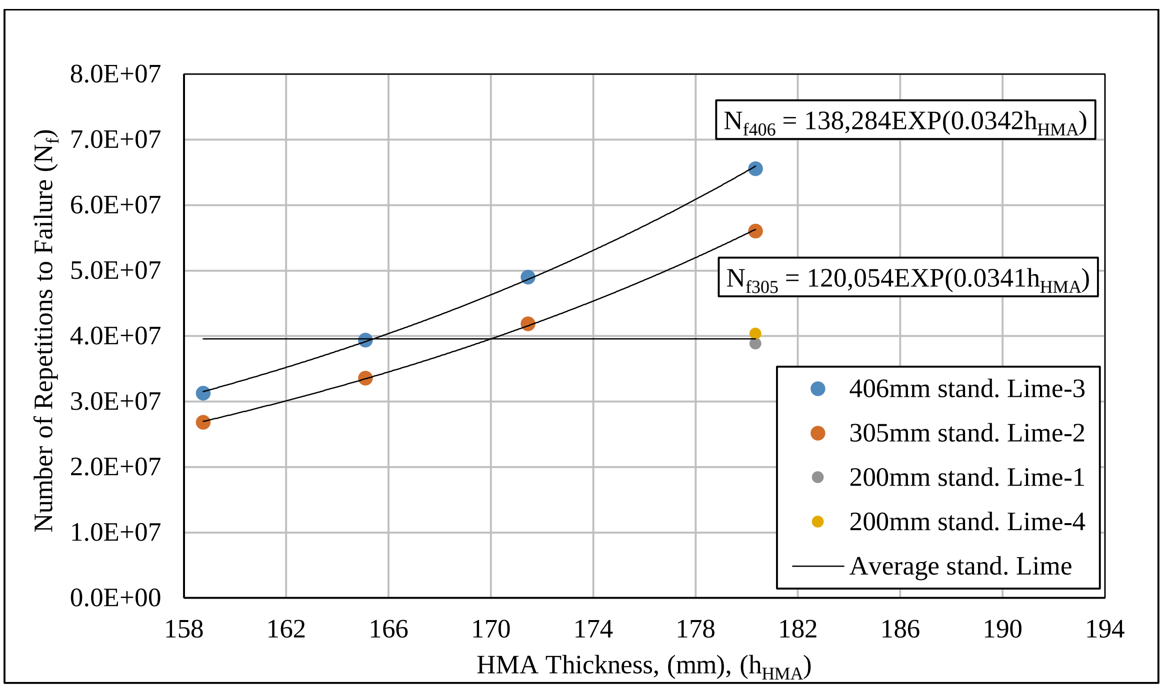

Figure C.2.9 Load related bottom-up cracking model: lime test section, May 2011 (Based on Abaqus)

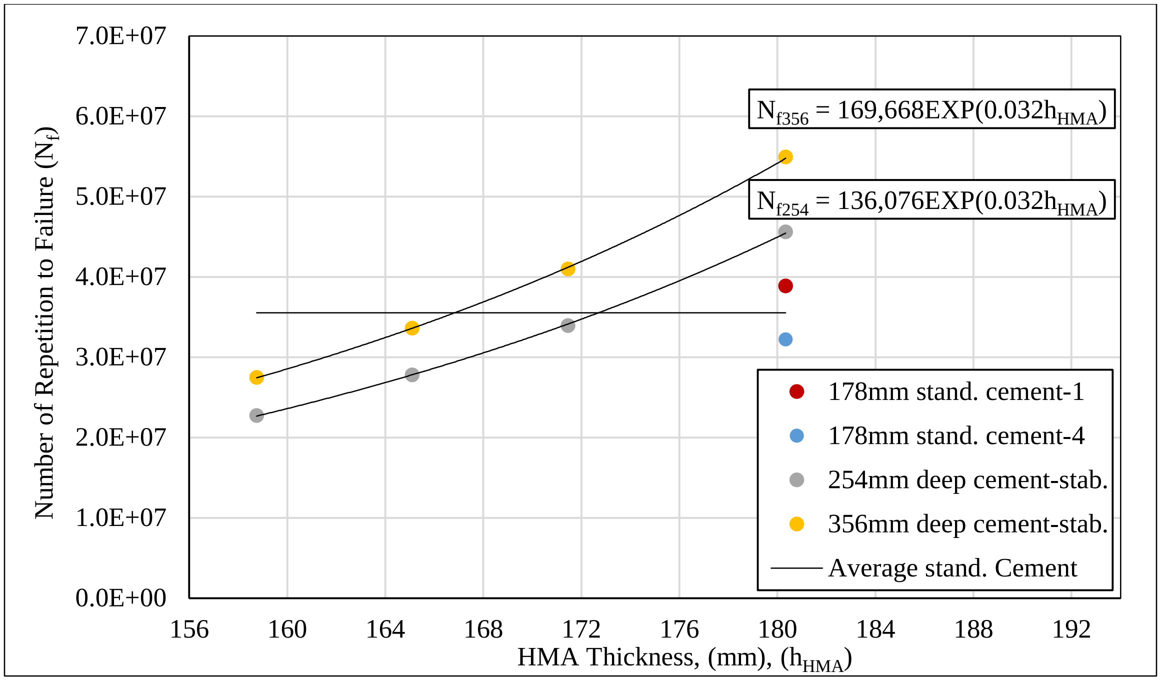

Figure C.2.10 Load related bottom-up cracking model: cement test section, May 2011 (Based on Abaqus)

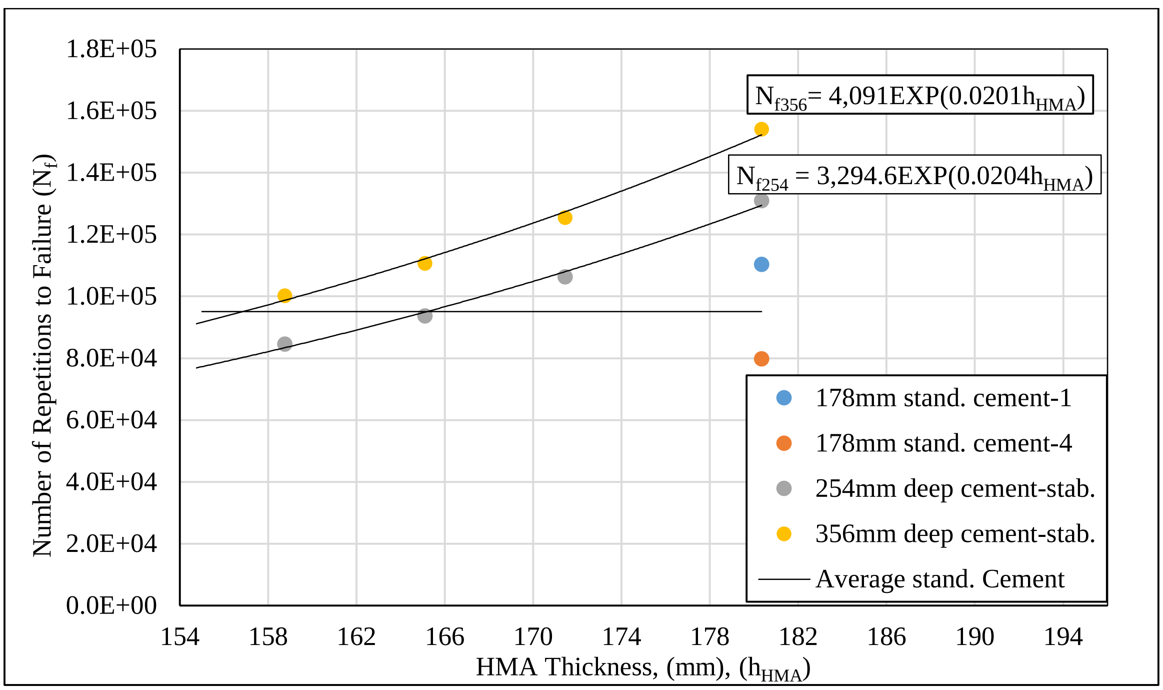

Figure C.2.11 Load related top-down cracking model: cement test section, May 2011 (Based on Abaqus)

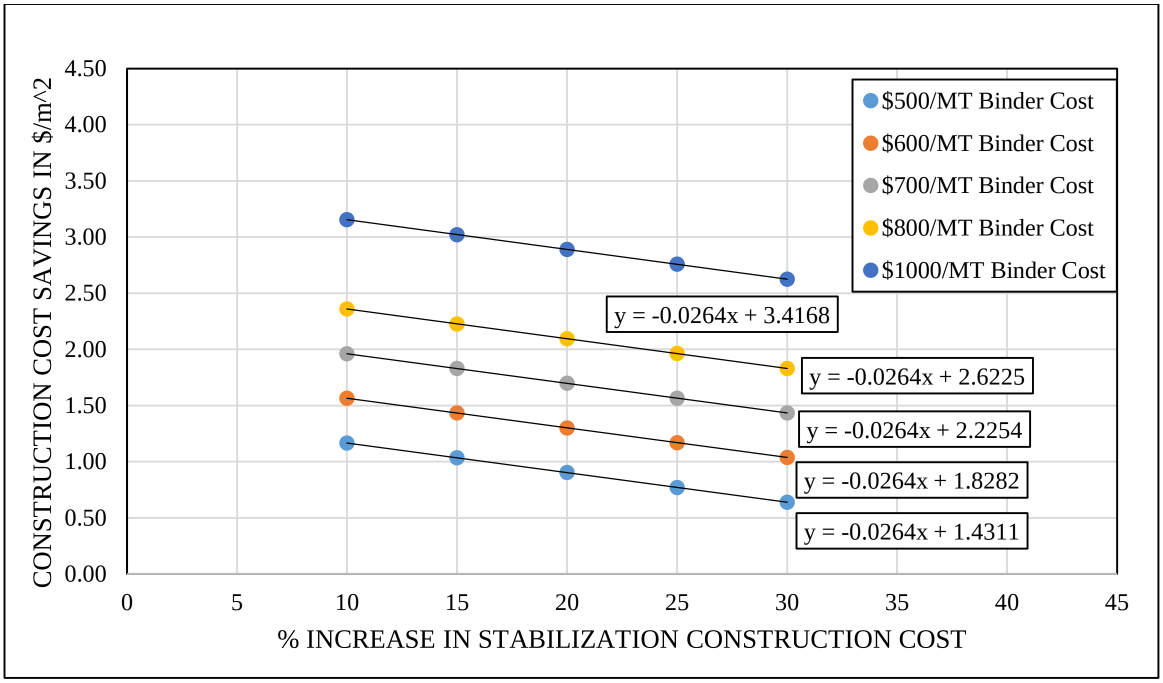

Figure C.2.12 Cost Savings versus % increase in Stabilization Construction Cost for various Binder costs (Lime of 406 mm, S9.5C mix, EVERSTRESS analysis of May 2011 data, top-down)

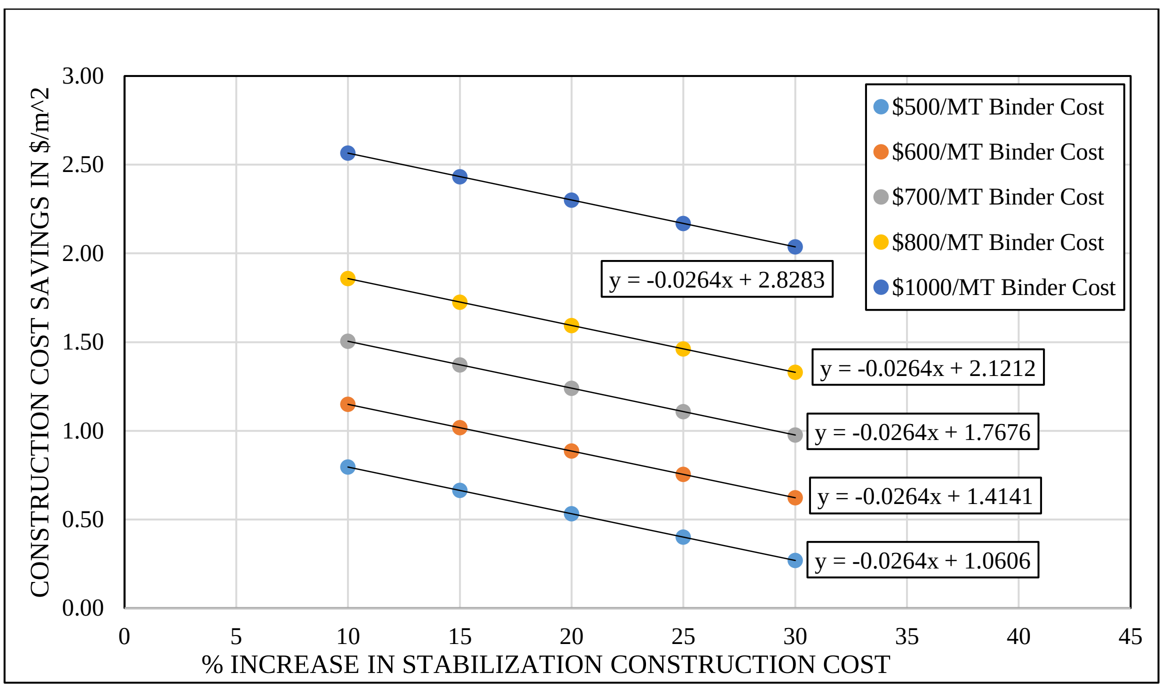

Figure C.2.13 Cost Savings versus % increase in Stabilization Construction Cost for various Binder costs (Lime of 406 mm, I19.0C mix, EVERSTRESS analysis of May 2011 data, top-down)

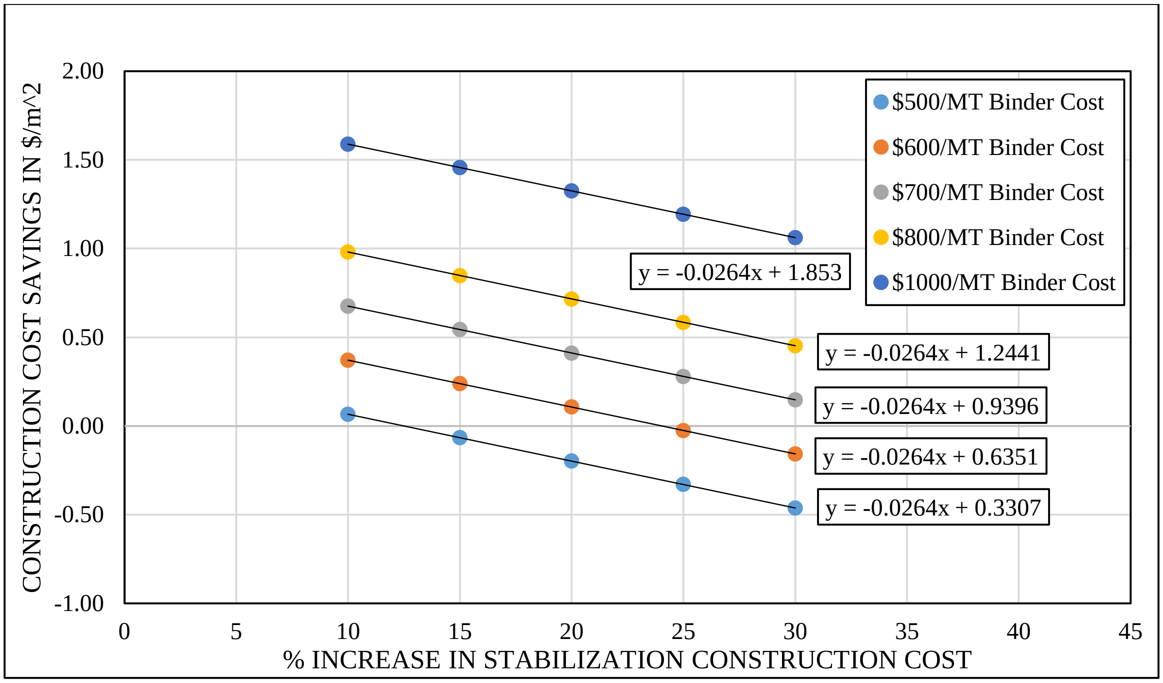

Figure C.2.14 Cost Savings versus % increase in Stabilization Construction Cost for various Binder costs (Lime of 406 mm, S9.5C mix, EVERSTRESS analysis of October 2011 data, top-down)

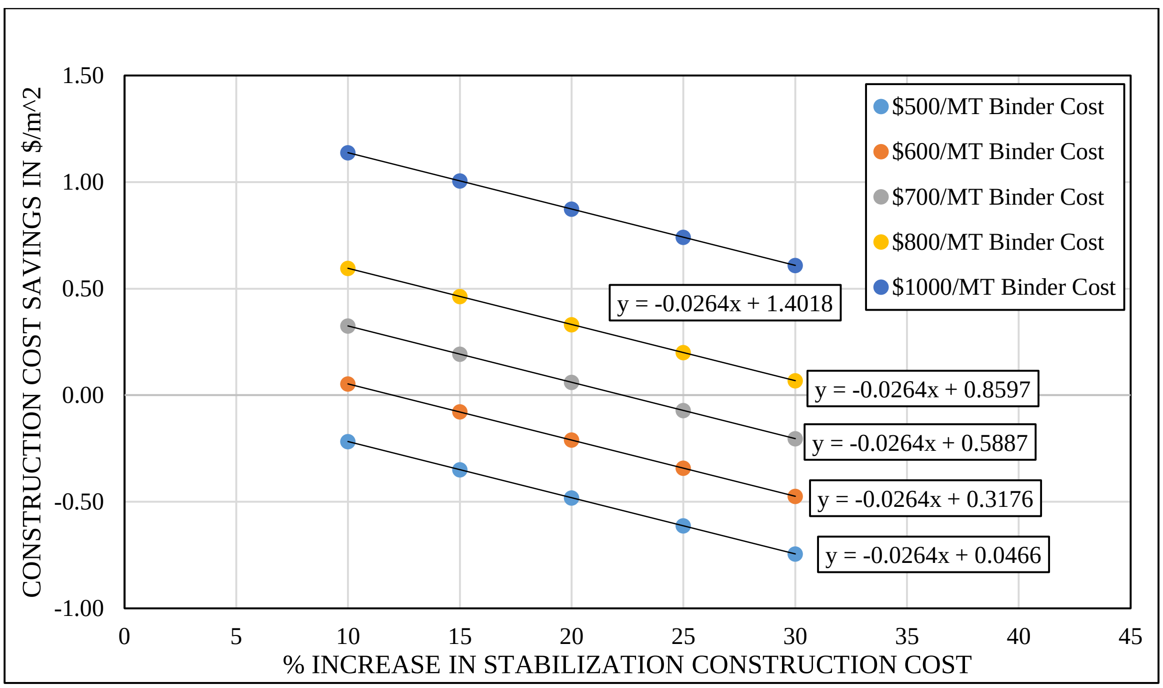

Figure C.2.15 Cost Savings versus % increase in Stabilization Construction Cost for various Binder costs (Lime of 406 mm, I19.0C mix, EVERSTRESS analysis of October 2011 data, top-down)

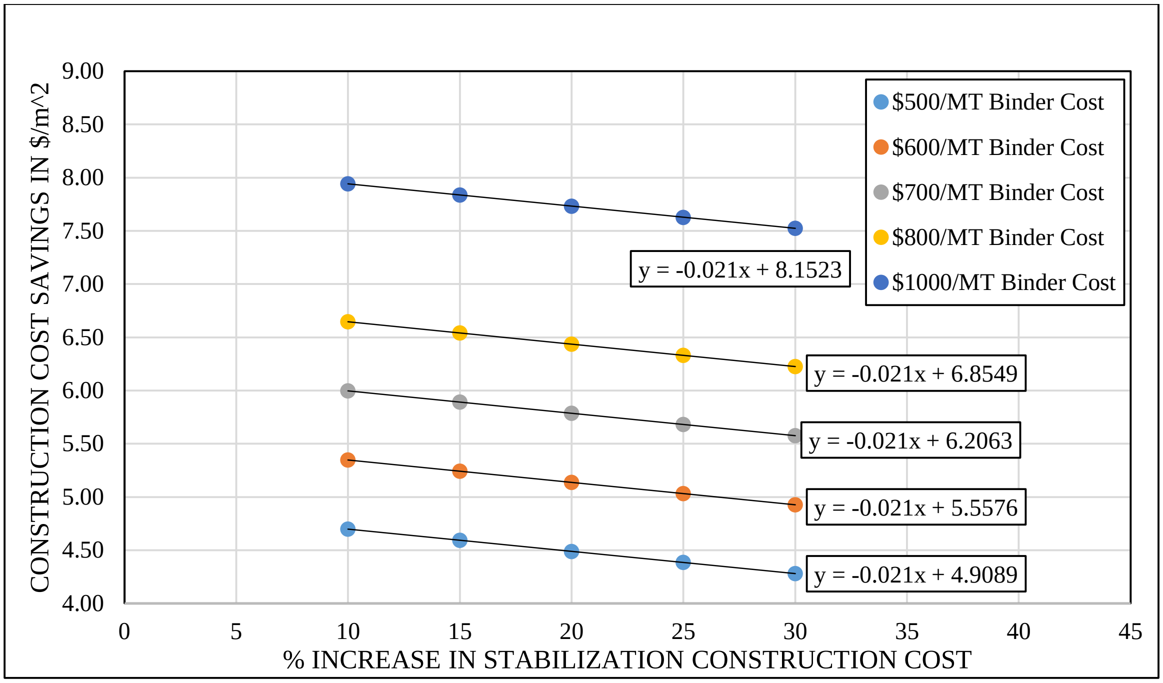

Figure C.2.16 Cost Savings versus % increase in Stabilization Construction Cost for various Binder costs (Cement of 356 mm, S9.5C mix, EVERSTRESS analysis of May 2011 data, top-down)

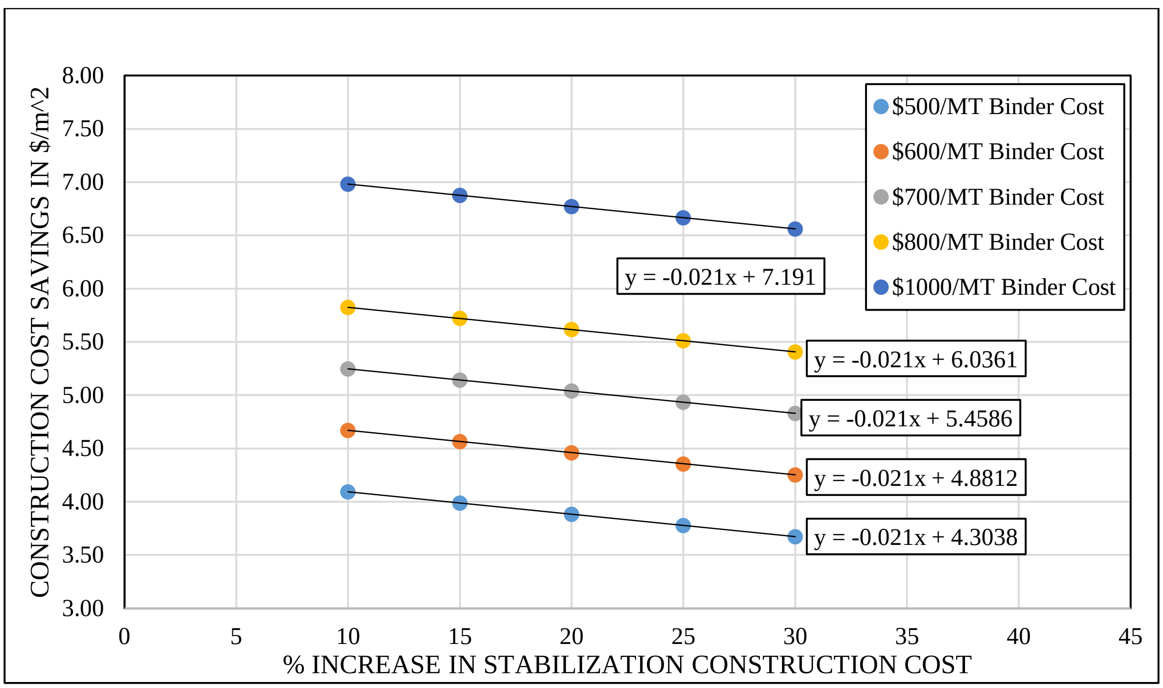

Figure C.2.17 Cost Savings versus % increase in Stabilization Construction Cost for various Binder costs (Cement of 356 mm, I19.0C mix, EVERSTRESS analysis of May 2011 data, top-down)

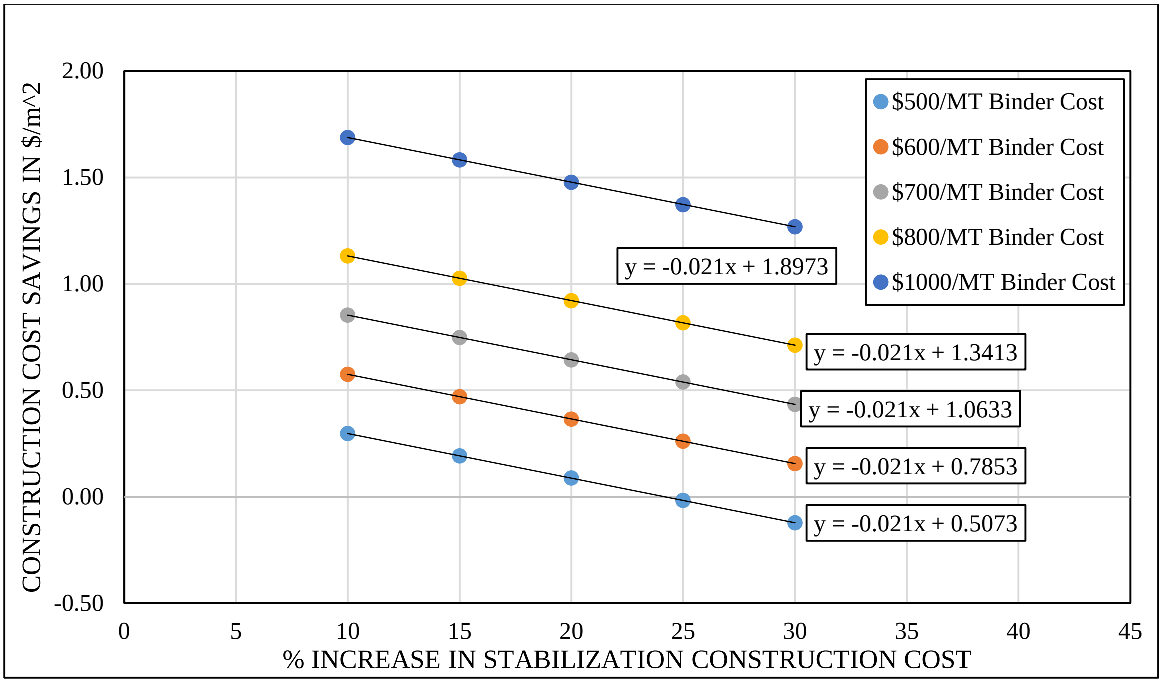

Figure C.2.18 Cost Savings versus % increase in Stabilization Construction Cost for various Binder costs (Cement of 356 mm, S9.5C mix, EVERSTRESS analysis of Oct 2011 data, top-down)

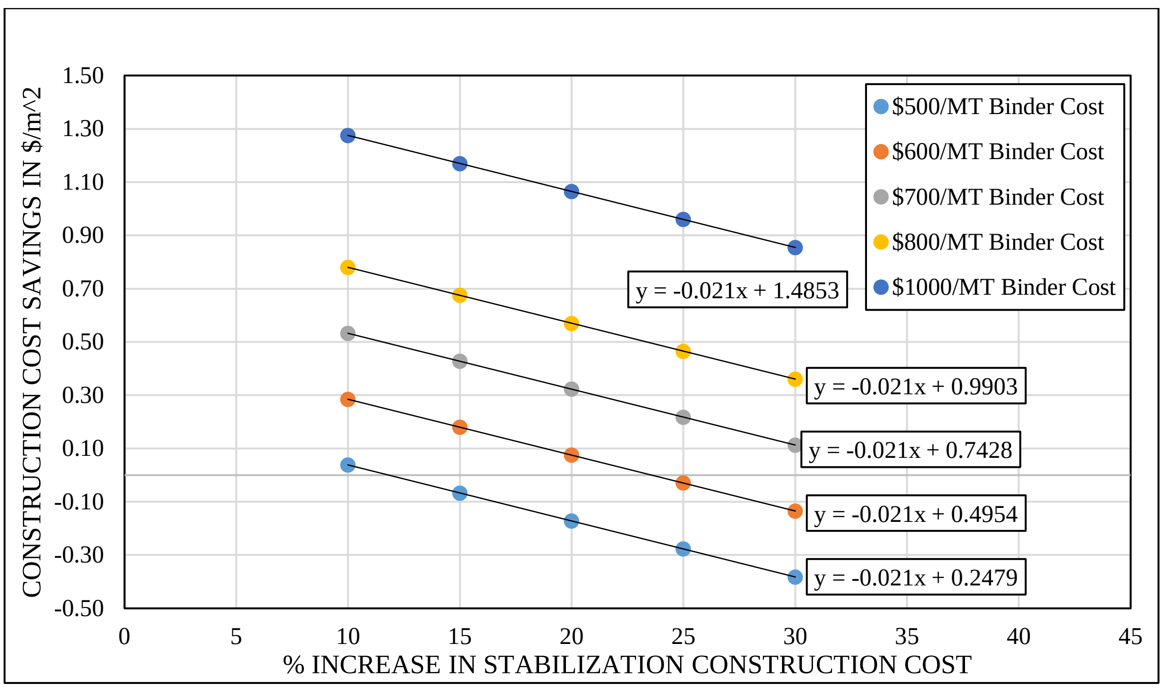

Figure C.2.19 Cost Savings versus % increase in Stabilization Construction Cost for various Binder costs (Cement of 356 mm, I19.0C mix, EVERSTRESS analysis of Oct 2011 data, top-down)

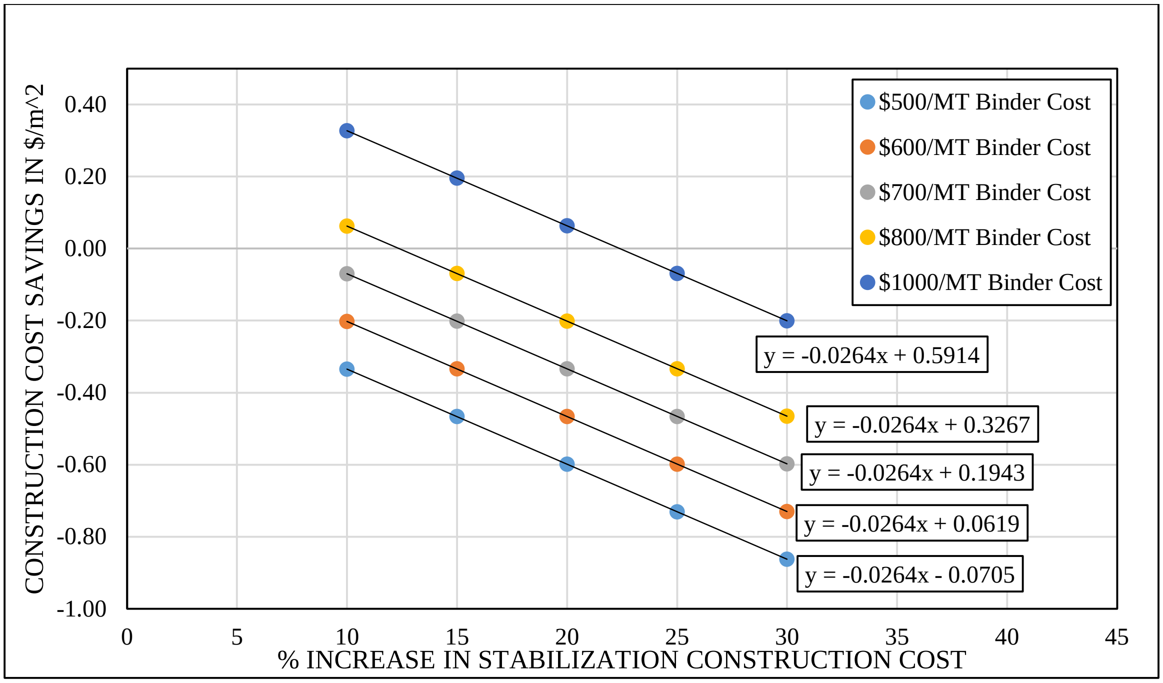

Figure C.2.20 Cost Savings versus % increase in Stabilization Construction Cost for various Binder costs (Lime of 305 mm, S9.5C mix, EVERSTRESS analysis of May 2011 data, top-down)

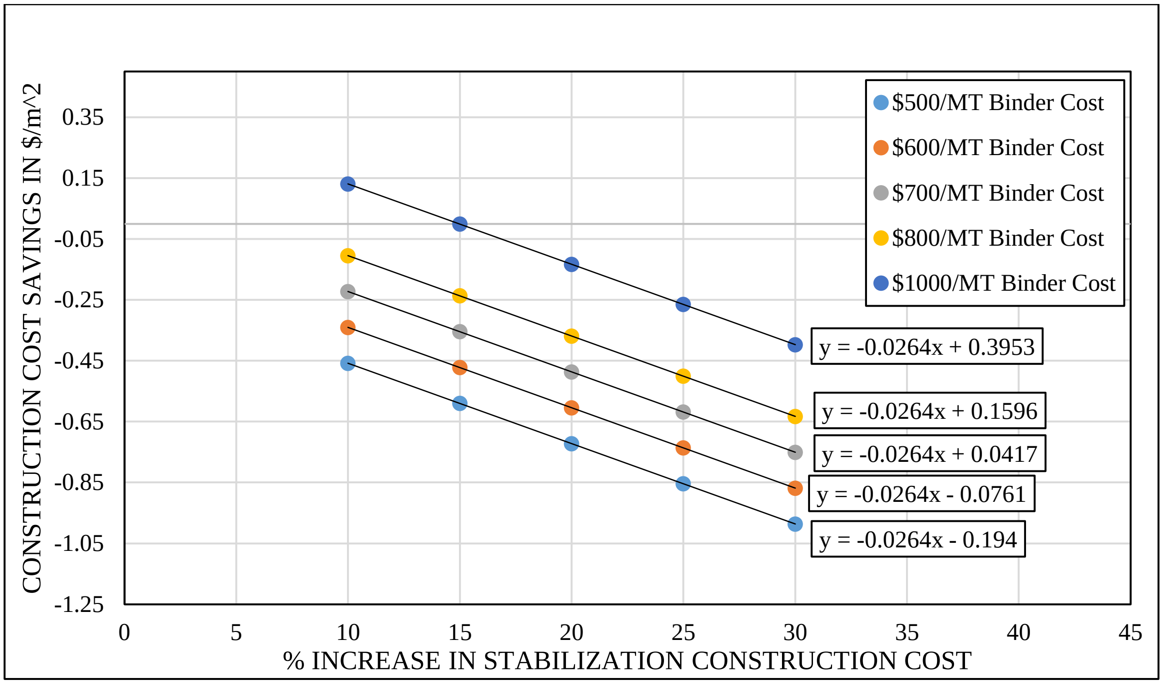

Figure C.2.21 Cost Savings versus % increase in Stabilization Construction Cost for various Binder costs (Lime of 305 mm, I19.0C mix, EVERSTRESS analysis of May 2011 data, top-down)

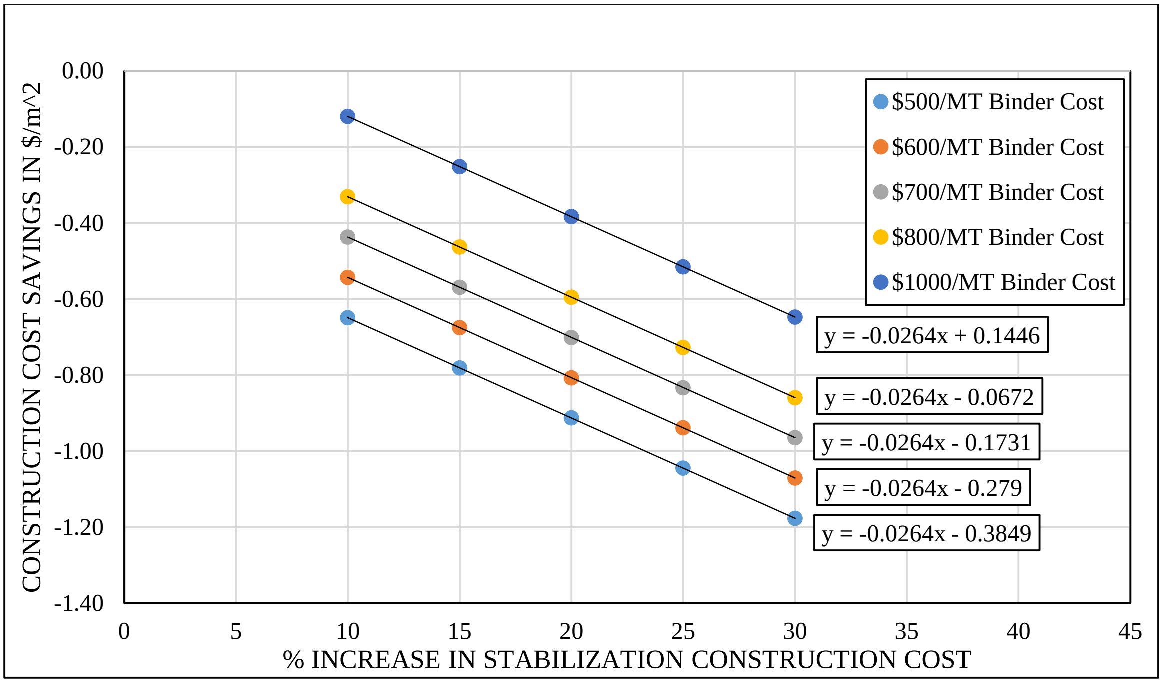

Figure` C.2.22 Cost Savings versus % increase in Stabilization Construction Cost for various Binder costs (Lime of 305 mm, S9.5C, EVERSTRESS analysis of October 2011 data, top-down)

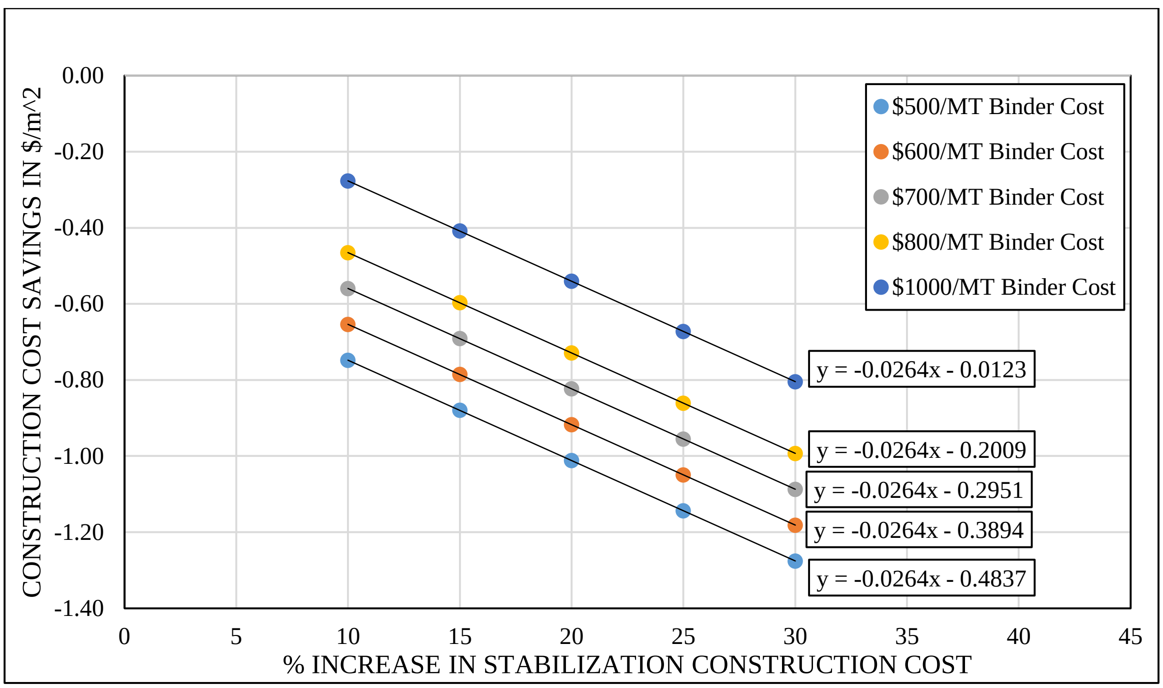

Figure C.2.23 Cost Savings versus % increase in Stabilization Construction Cost for various Binder costs (Lime of 305 mm, I19.0C, EVERSTRESS analysis of October 2011 data, top-down)

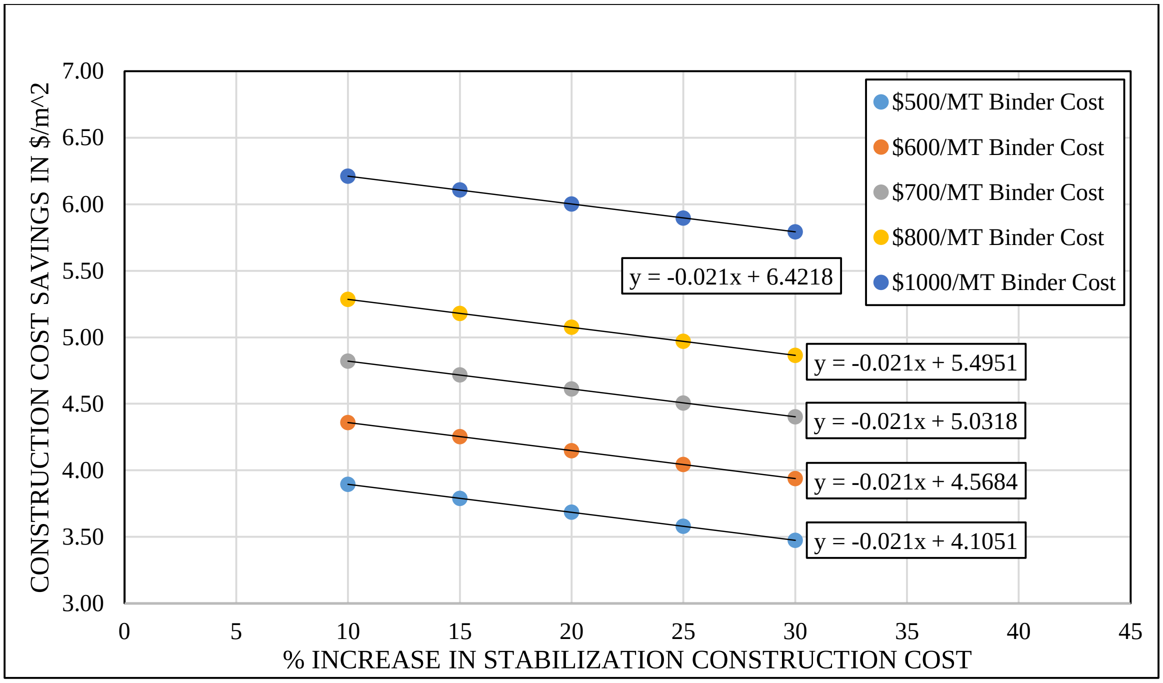

Figure 2.2.24 Cost Savings versus % increase in Stabilization Construction Cost for various Binder costs (Cement of 254 mm, S9.5C, EVERSTRESS analysis of May 2011 data, top-down)

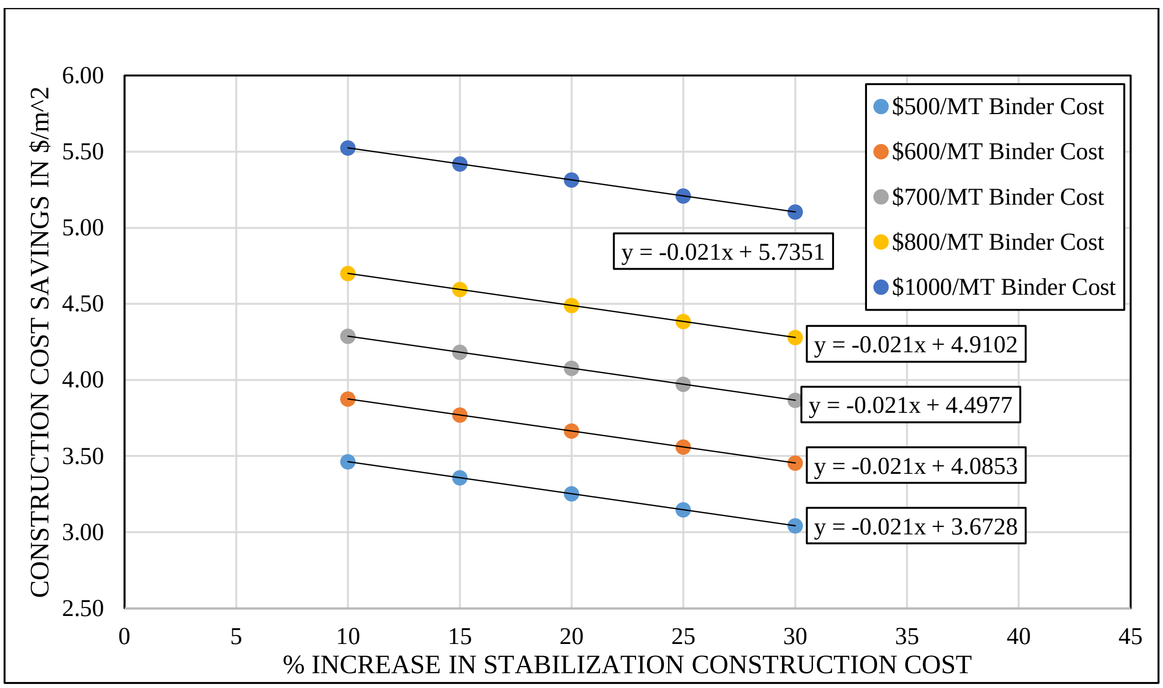

Figure C.2.25 Cost Savings versus % increase in Stabilization Construction Cost for various Binder costs (Cement of 254 mm, I19.0C, EVERSTRESS analysis of May 2011 data, top-down)

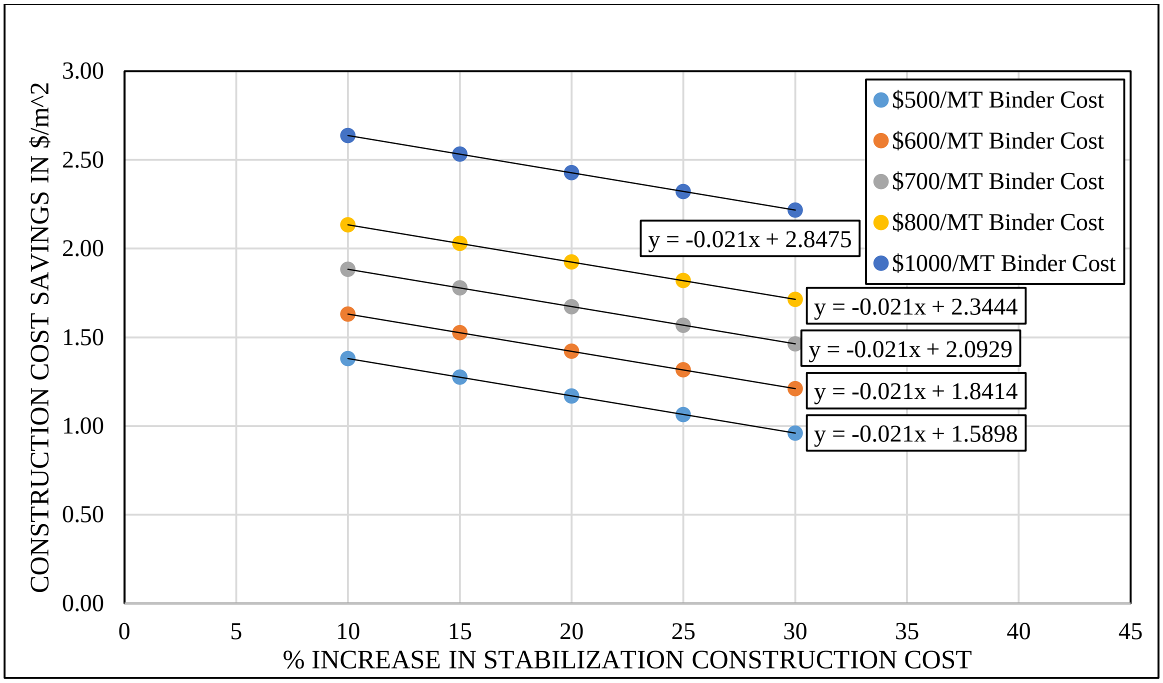

Figure C.2.26 Cost Savings versus % increase in Stabilization Construction Cost for various Binder costs (Cement of 254 mm, S9.5C, EVERSTRESS analysis of October 2011 data, top-down)

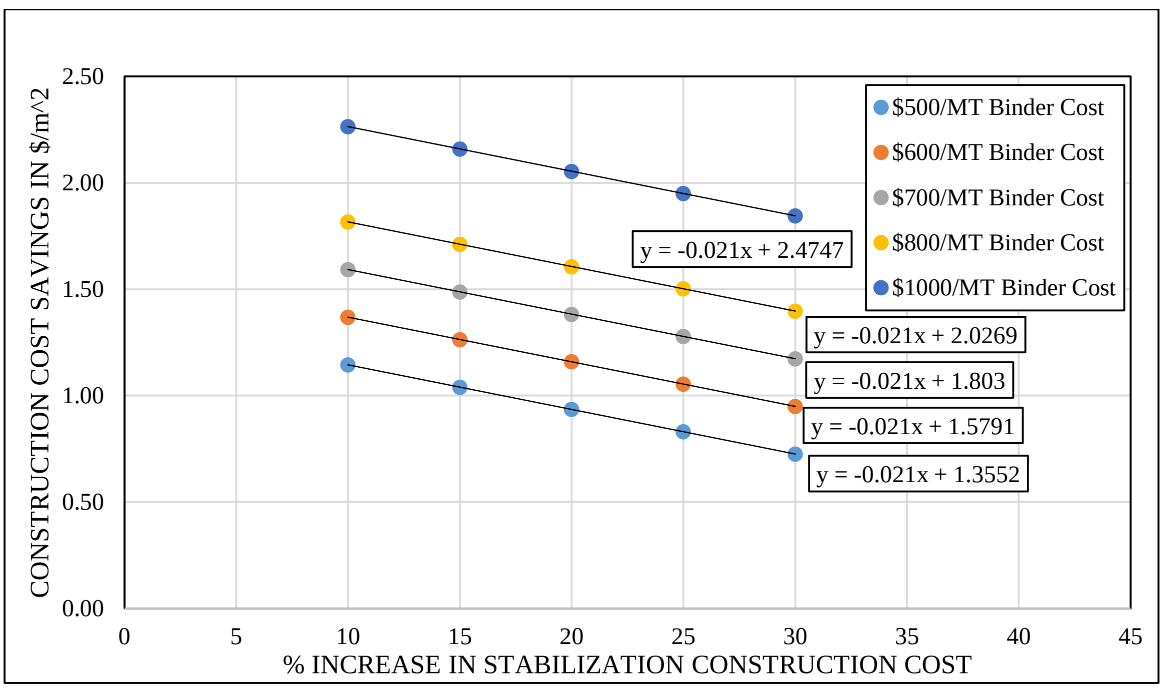

Figure C.2.27 Cost Savings versus % increase in Stabilization Construction Cost for various Binder costs (Cement of 254 mm, I19.0C, EVERSTRESS analysis of October 2011 data, top-down)

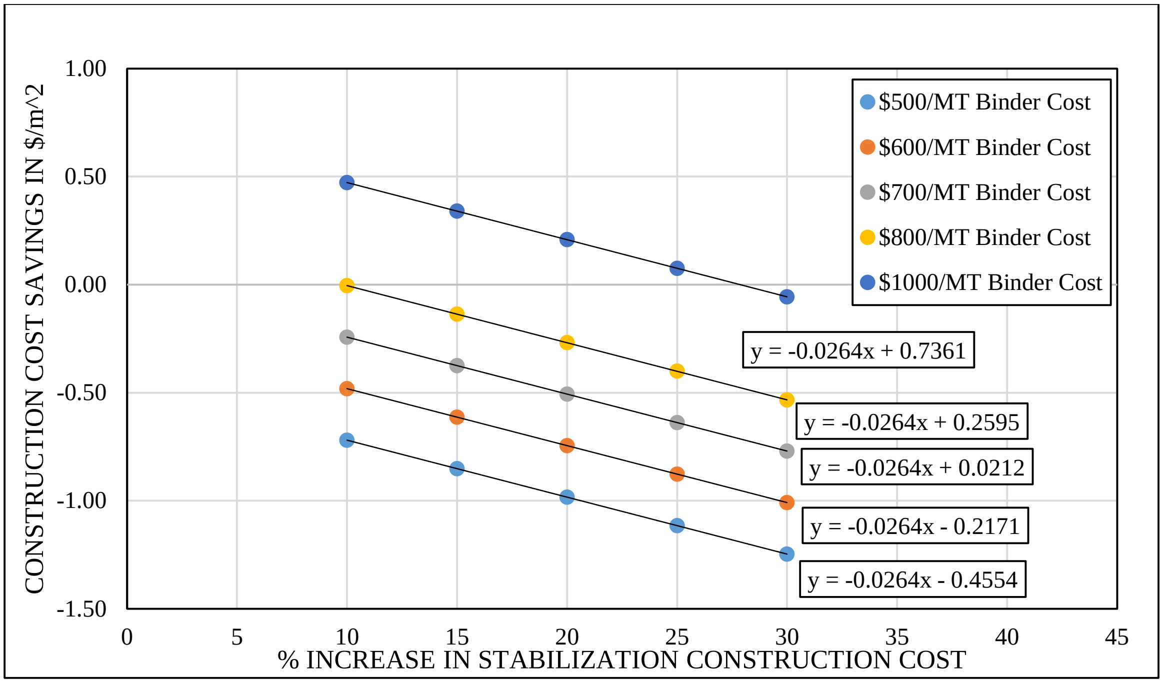

Figure C.2.28 Cost Savings versus % increase in Stabilization Construction Cost for various Binder costs (Lime of 406 mm, S9.5C, EVERSTRESS analysis of May 2011 data, bottom-up)

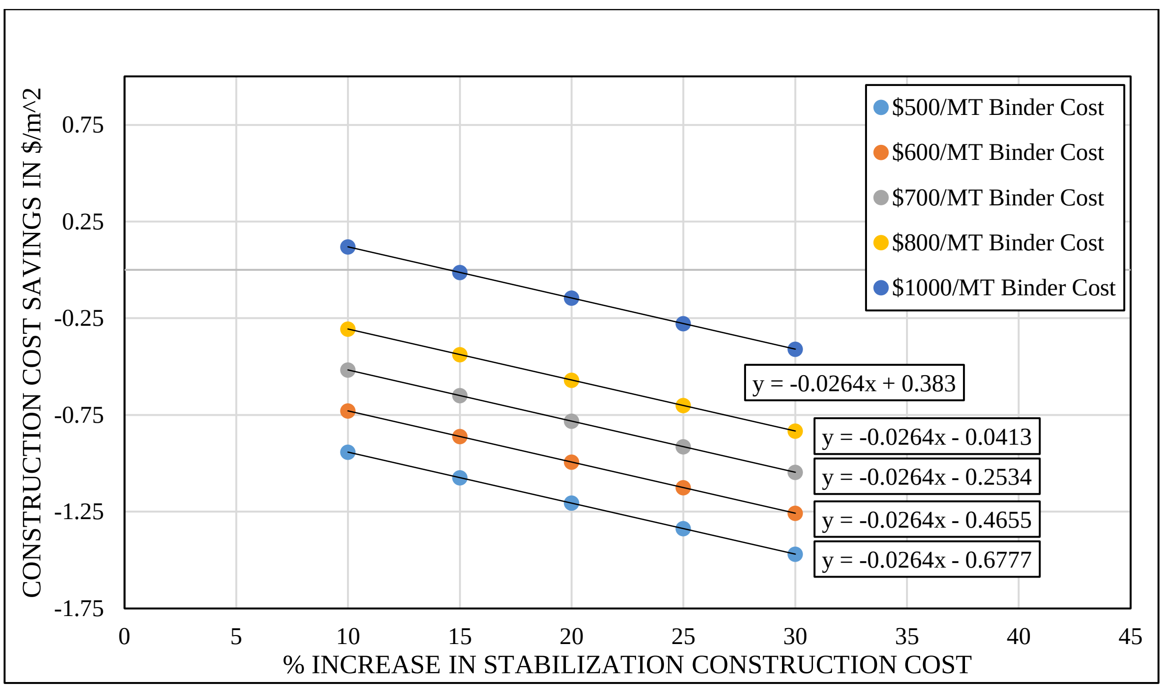

Figure C.2.29 Cost Savings versus % increase in Stabilization Construction Cost for various Binder costs (Lime of 406 mm, I19.0C, EVERSTRESS analysis of May 2011 data, bottom-up)

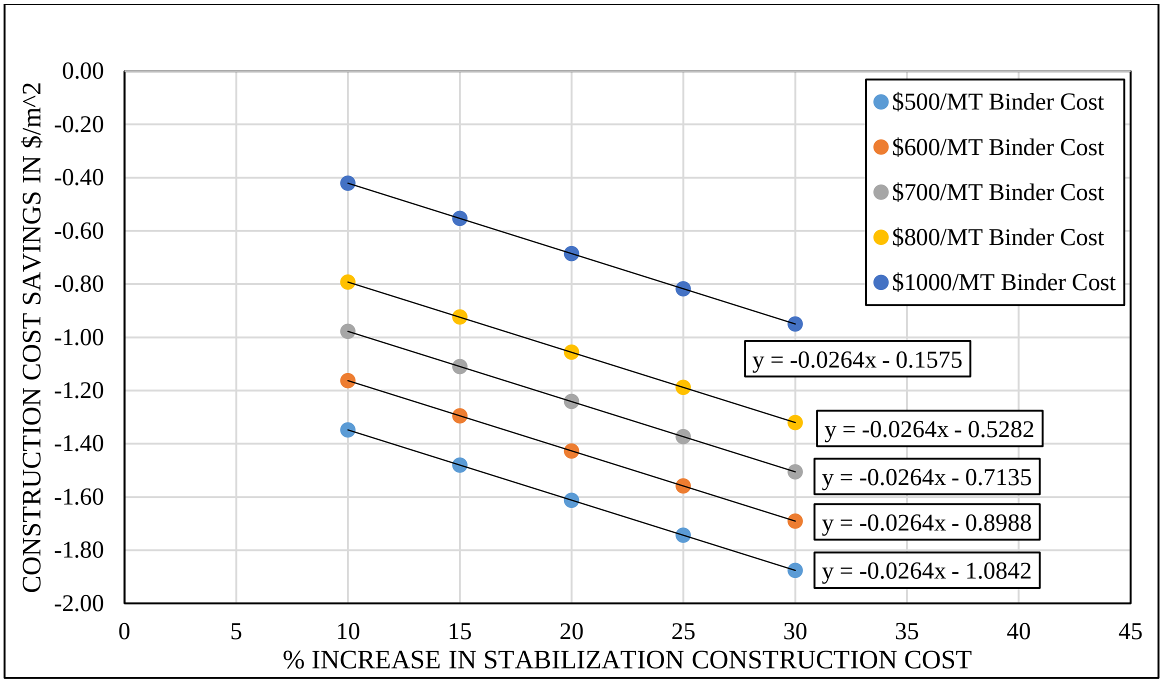

Figure C.2.30 Cost Savings versus % increase in Stabilization Construction Cost for various Binder costs (Lime of 406 mm, S9.5C, EVERSTRESS analysis of October 2011 data, bottom-up)

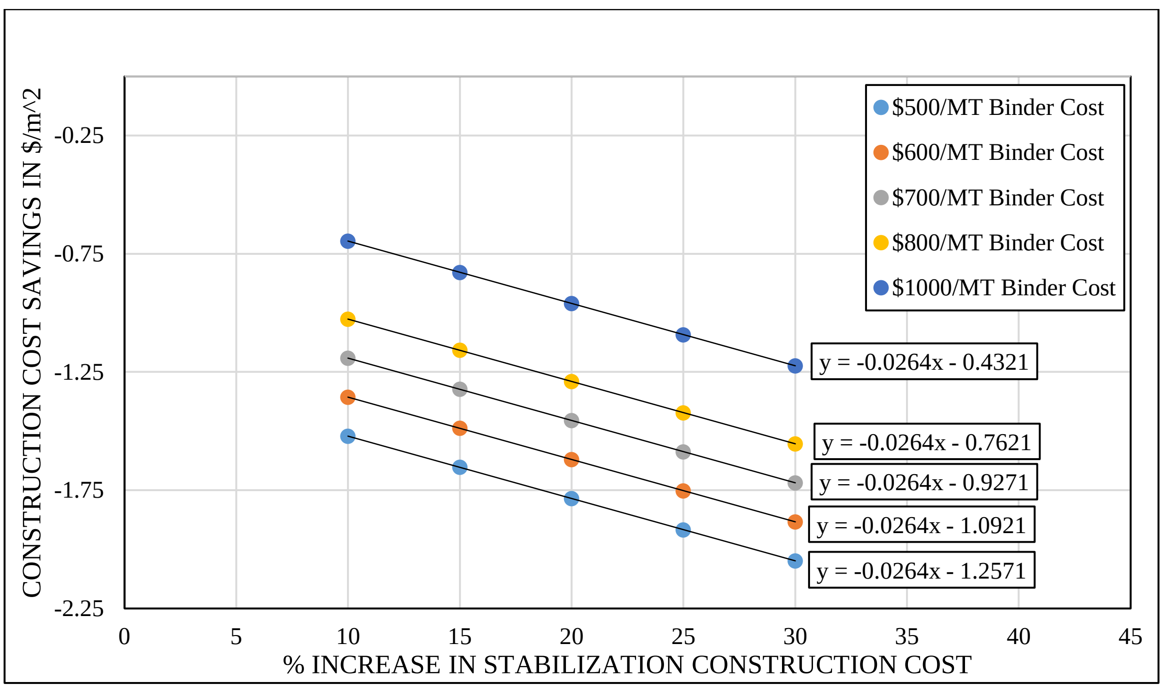

Figure C.2.31 Cost Savings versus % increase in Stabilization Construction Cost for various Binder costs (Lime of 406 mm, I19.0C, EVERSTRESS analysis of October 2011 data, bottom-up)

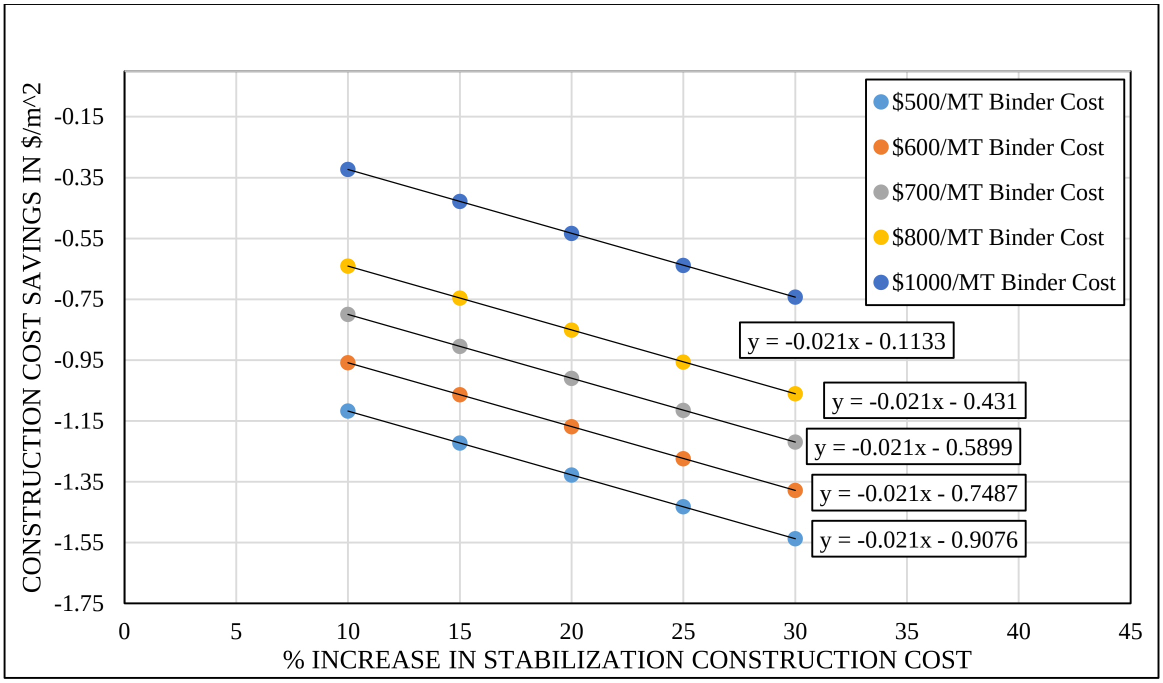

Figure C.2.32 Cost Savings versus % increase in Stabilization Construction Cost for various Binder costs (Cement of 356 mm, S9.5C, EVERSTRESS analysis of May 2011 data, bottom-up)

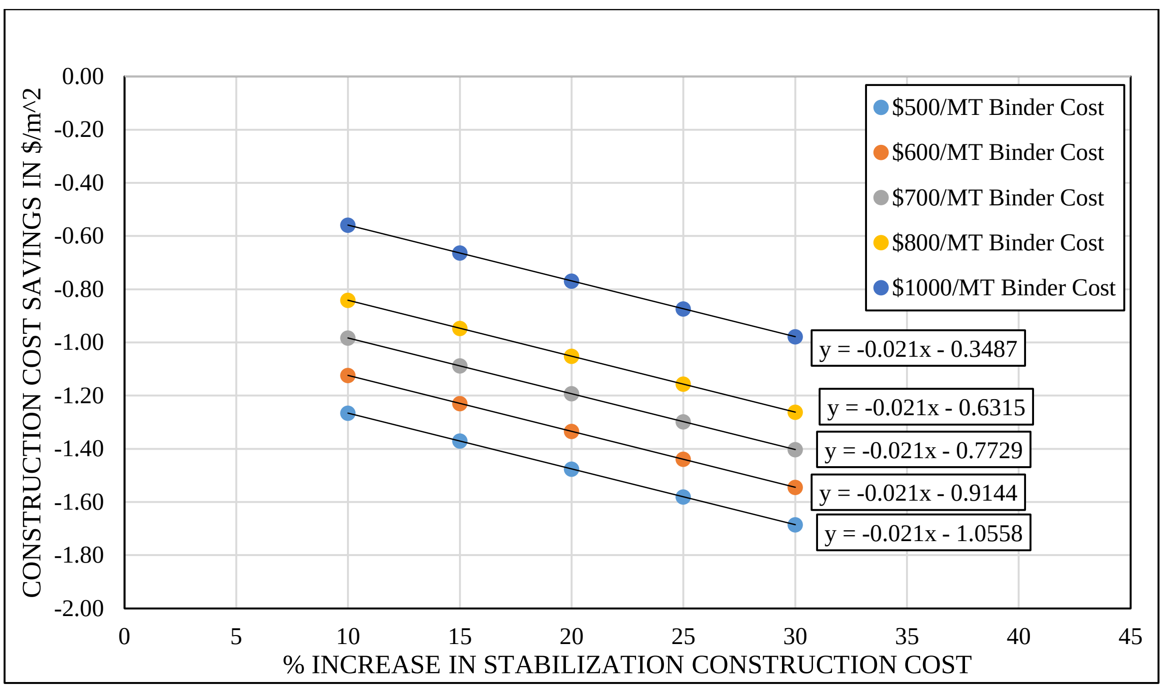

Figure C.2.33 Cost Savings versus % increase in Stabilization Construction Cost for various Binder costs (Cement of 356 mm, I19.0C, EVERSTRESS analysis of May 2011 data, bottom-up)

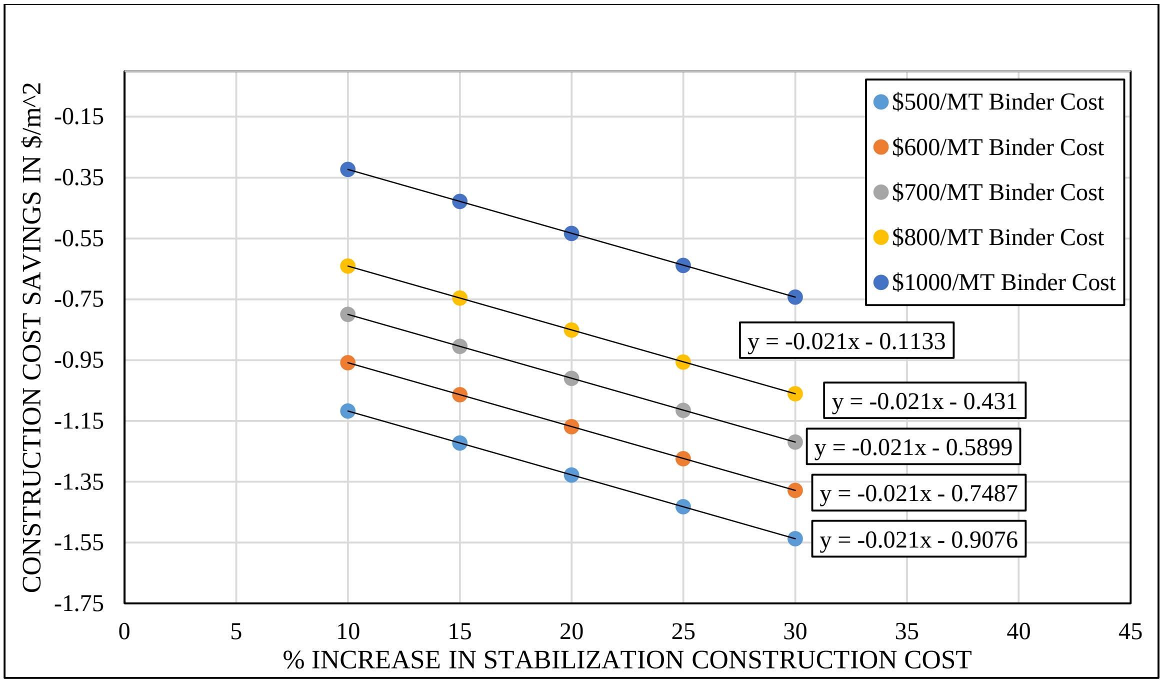

Figure C.2.34 Cost Savings versus % increase in Stabilization Construction Cost for various Binder costs (Cement of 356 mm, S9.5C, EVERSTRESS analysis of October 2011 data, bottom-up)

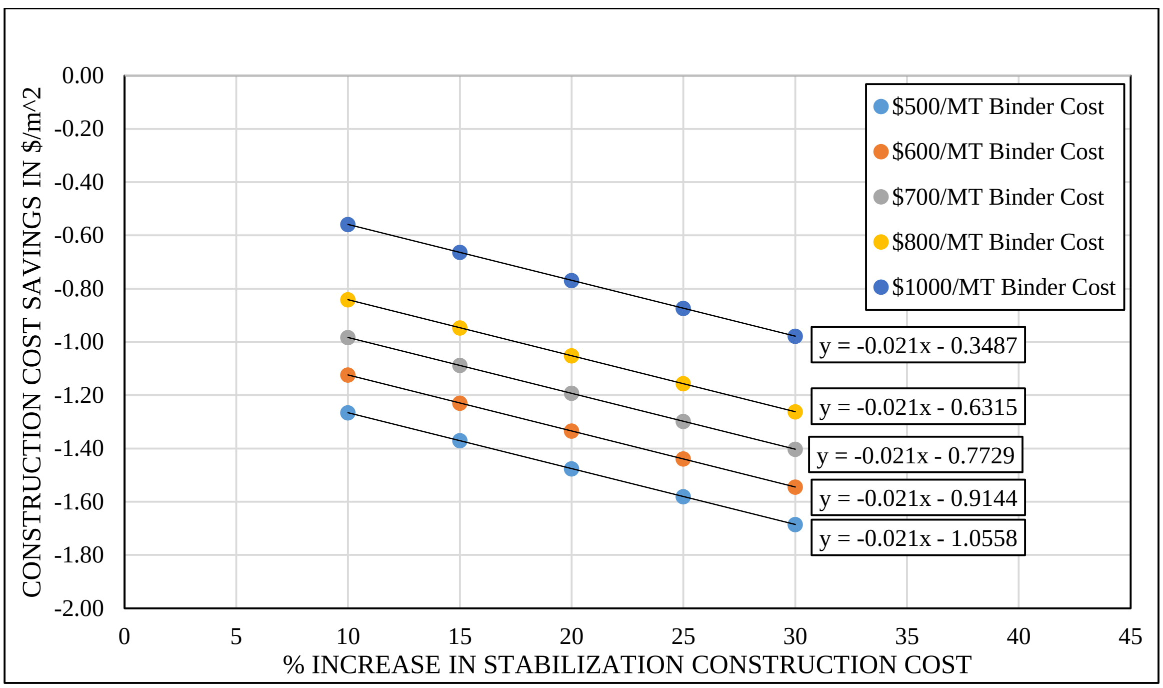

Figure C.2.35 Cost Savings versus % increase in Stabilization Construction Cost for various Binder costs (Cement of 356 mm, I19.0C, EVERSTRESS analysis of October 2011 data, bottom-up)

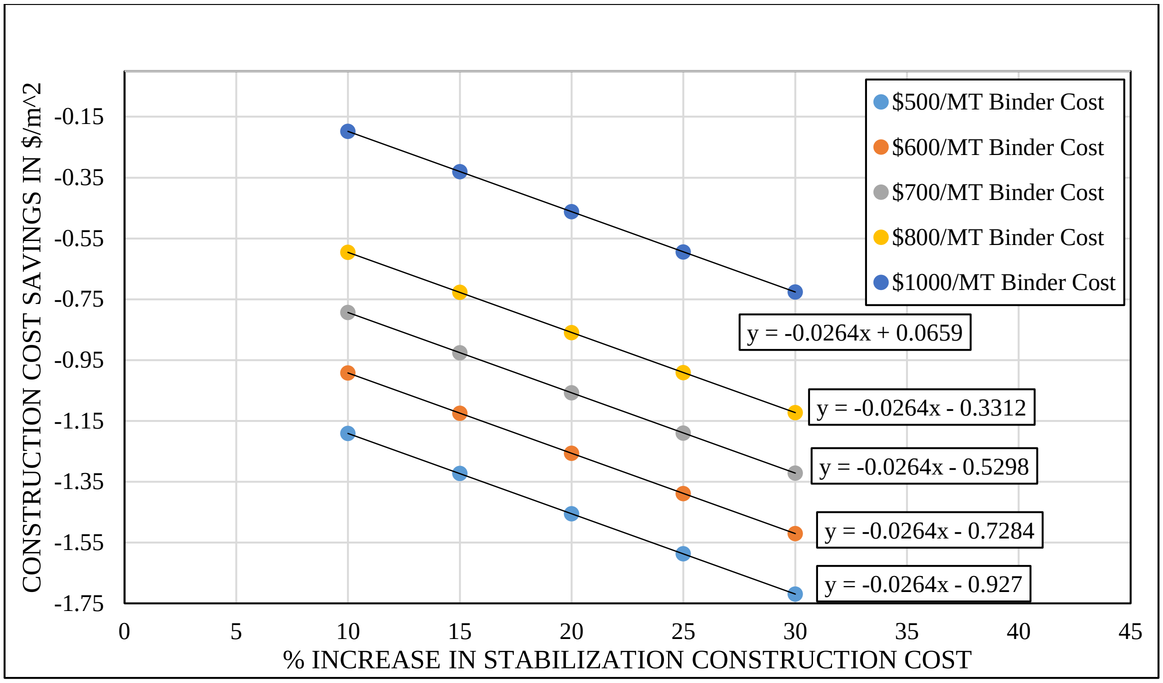

Figure C.2.36 Cost Savings versus % increase in Stabilization Construction Cost for various Binder costs (Lime of 356 mm, S9.5C, Abaqus analysis of May 2011 data, bottom-up)

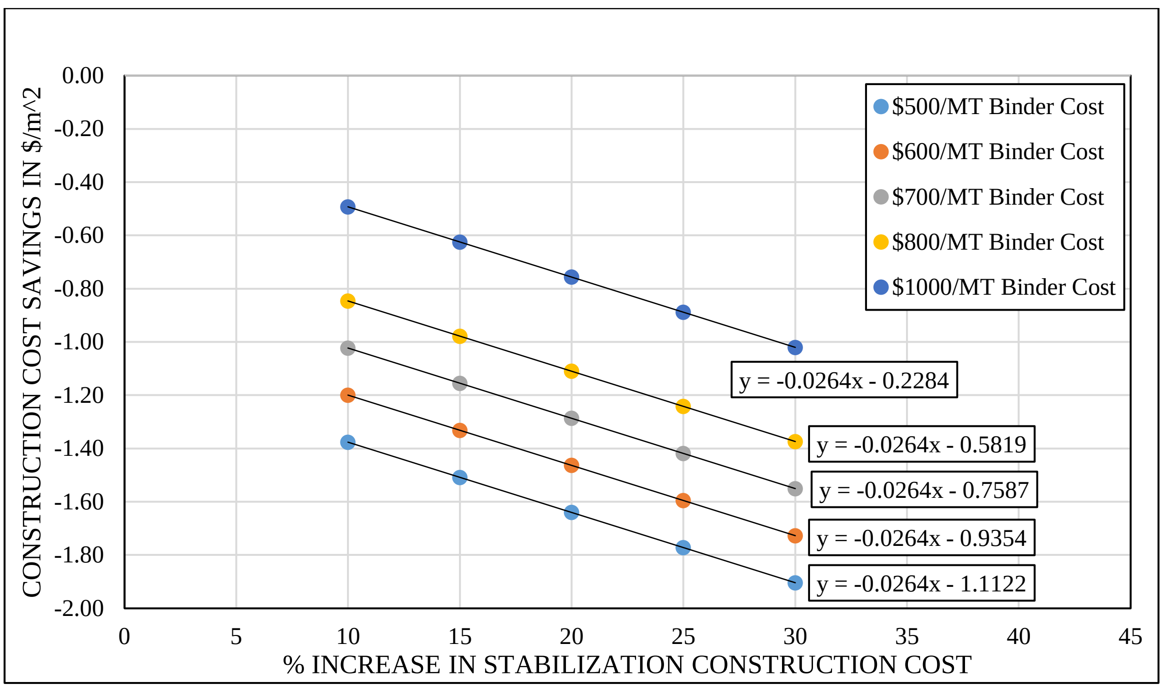

Figure C.2.37 Cost Savings versus % increase in Stabilization Construction Cost for various Binder costs (Lime of 356 mm, I19.0C, Abaqus analysis of May 2011 data, bottom-up)

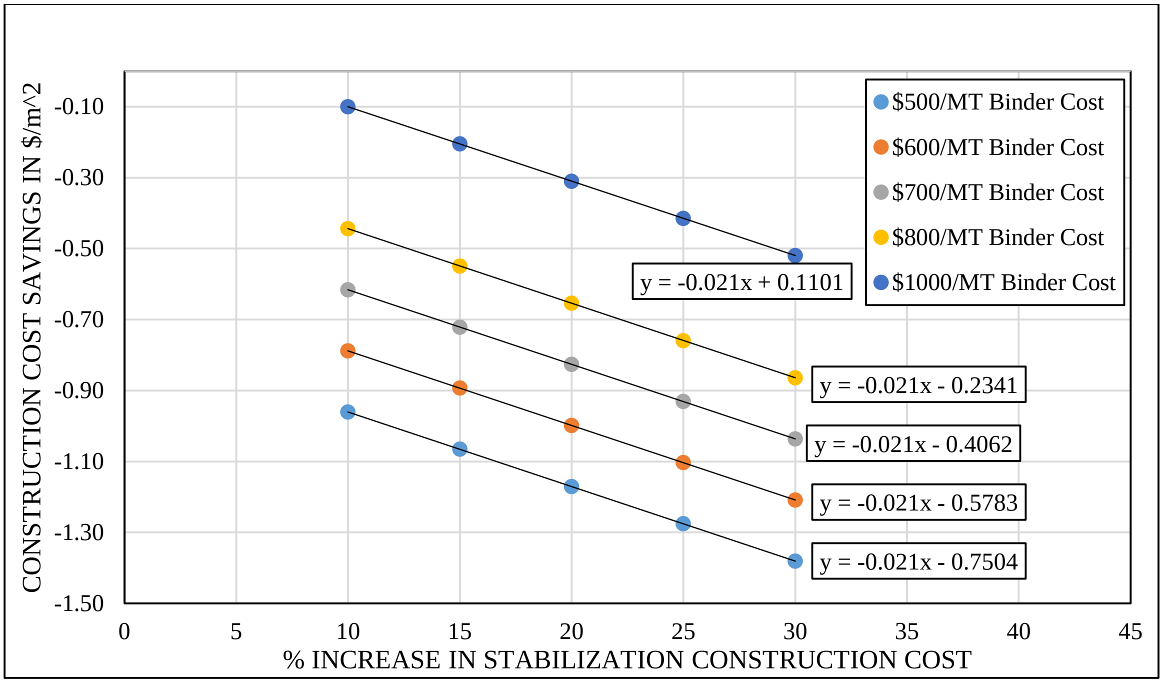

Figure C.2.38 Cost Savings versus % increase in Stabilization Construction Cost for various Binder costs (Cement of 356 mm, S9.5C, Abaqus analysis of May 2011 data, bottom-up)

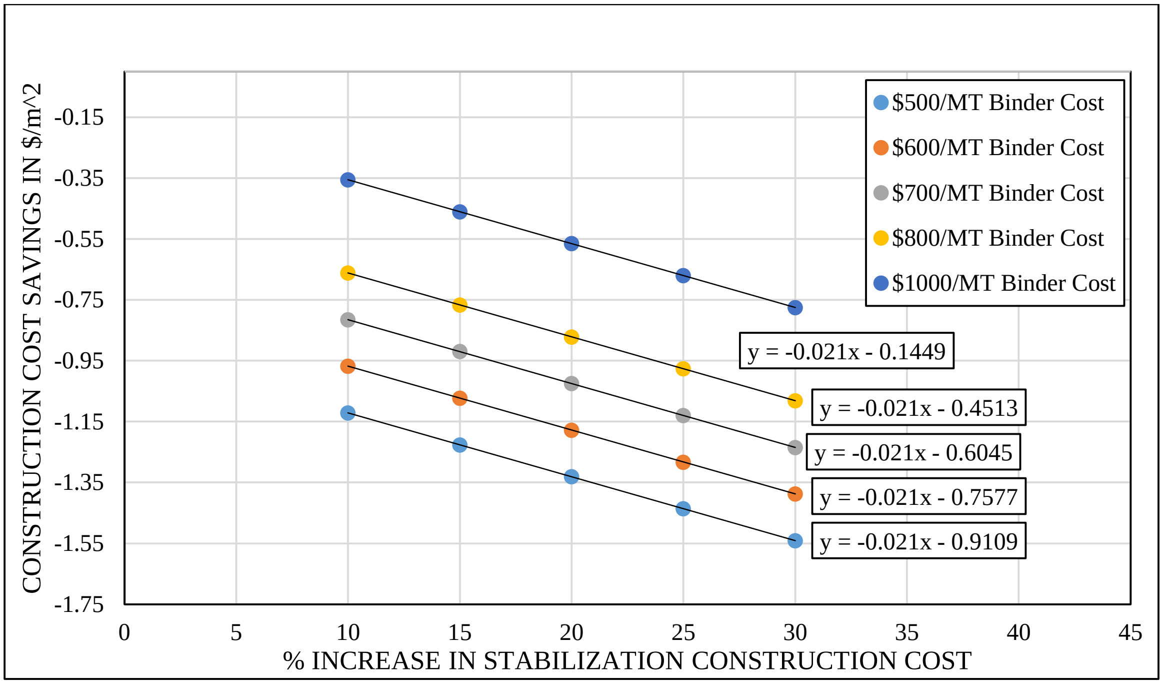

Figure C.2.39 Cost Savings versus % increase in Stabilization Construction Cost for various Binder costs (Cement of 356 mm, I19.0C, Abaqus analysis of May 2011 data, bottom-up)

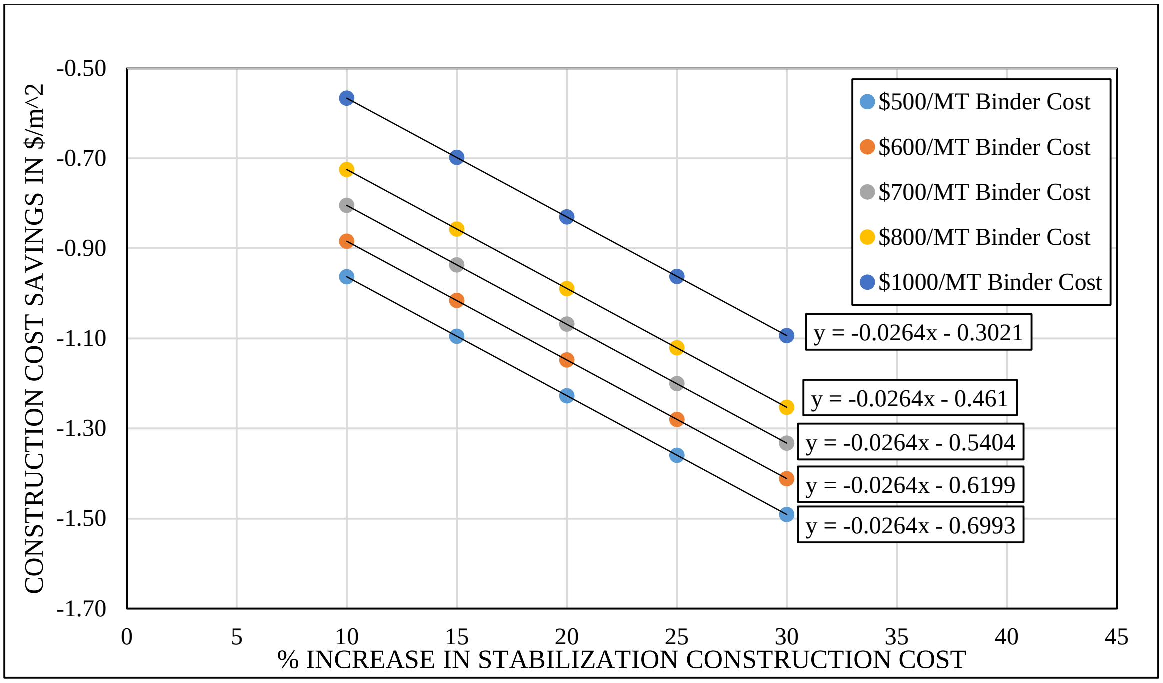

Figure C.2.40 Cost Savings versus % increase in Stabilization Construction Cost for various Binder costs (Lime of 305 mm, S9.5C, EVERSTRESS analysis of May 2011 data, bottom-up)

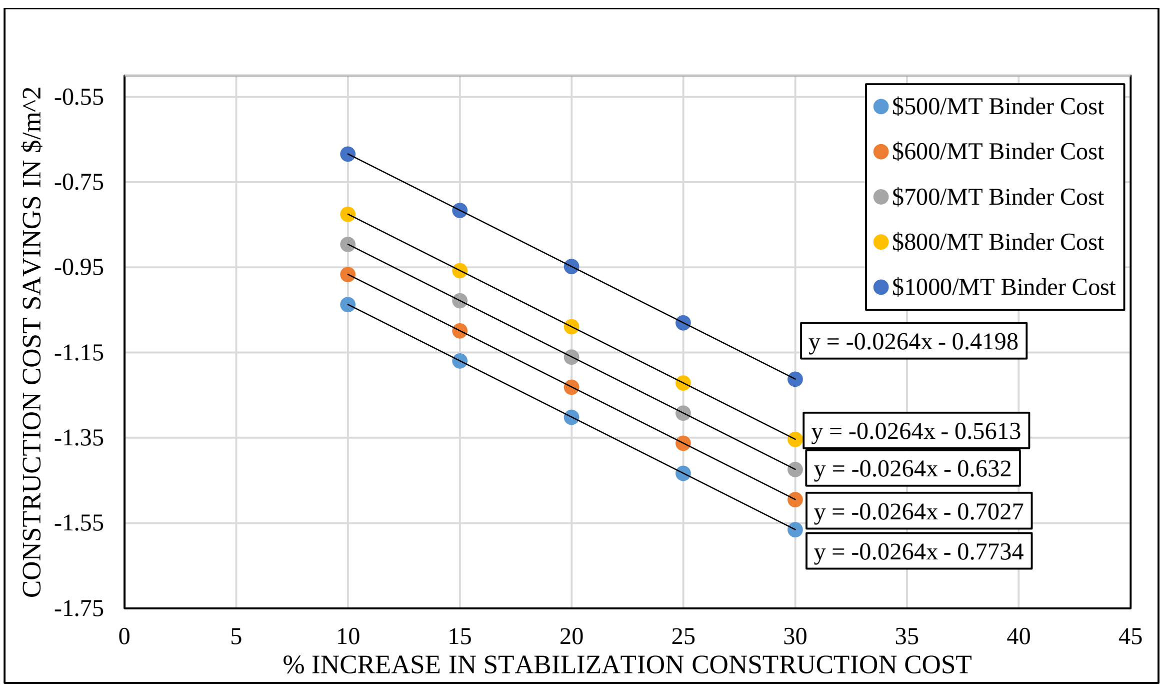

Figure C.2.41 Cost Savings versus % increase in Stabilization Construction Cost for various Binder costs (Lime of 305 mm, I19.0C, EVERSTRESS analysis of May 2011 data, bottom-up)

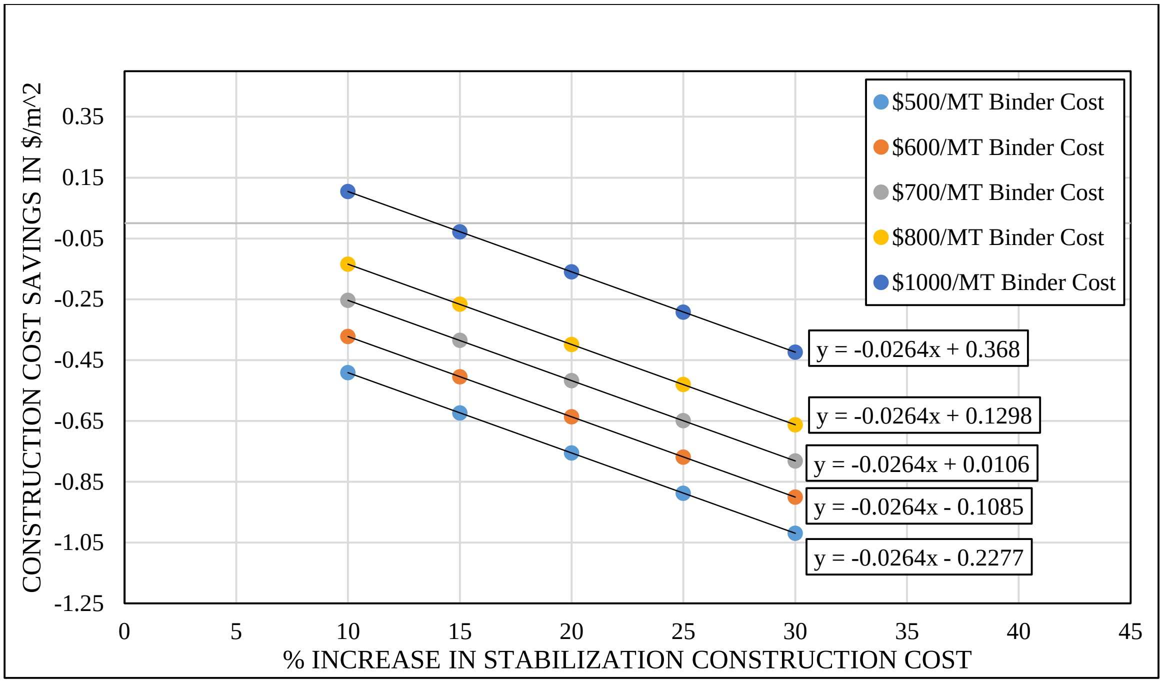

Figure C.2.42 Cost Savings versus % increase in Stabilization Construction Cost for various Binder costs (Lime of 305 mm, S9.5C, EVERSTRESS analysis of October 2011 data, bottom-up)

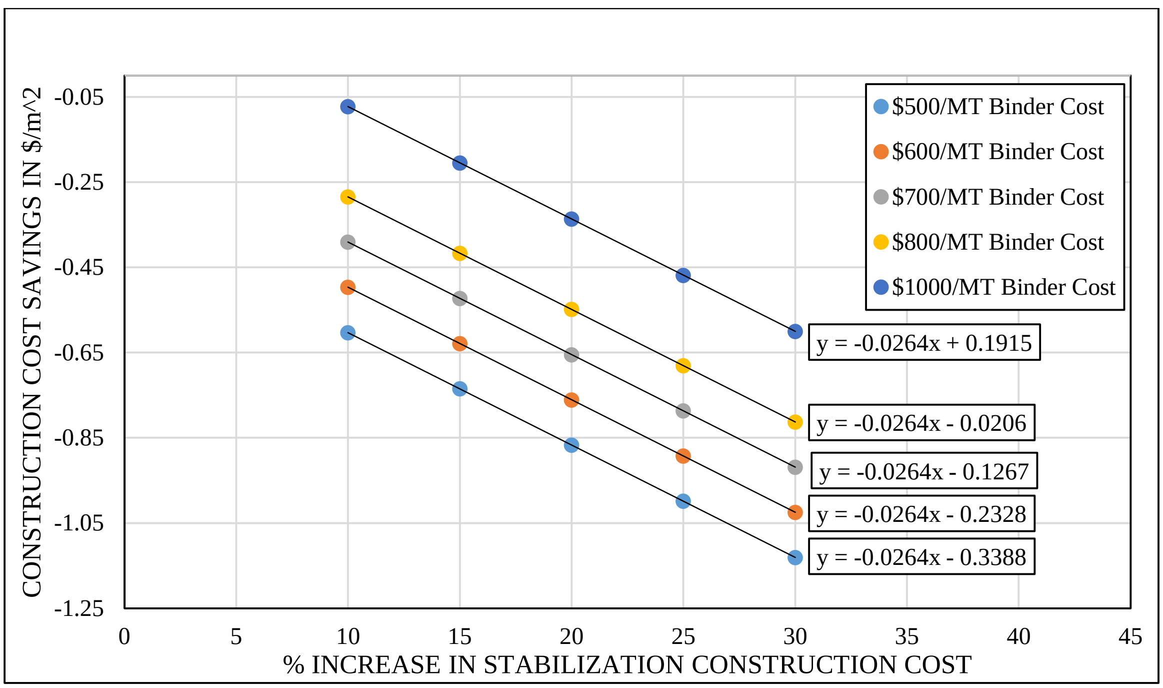

Figure C.2.43 Cost Savings versus % increase in Stabilization Construction Cost for various Binder costs (Lime of 305 mm, I19.0C, EVERSTRESS analysis of October 2011 data, bottom-up)

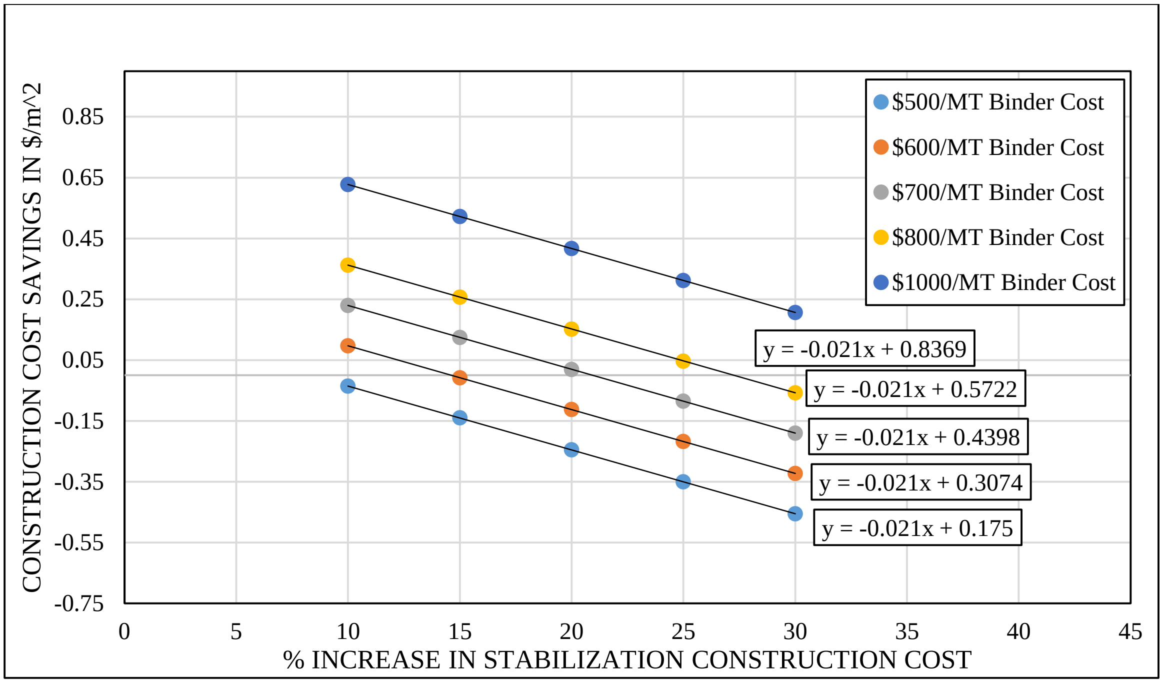

Figure C.2.44 Cost Savings versus % increase in Stabilization Construction Cost for various Binder costs (Cement of 254 mm, S9.5C, EVERSTRESS analysis of May 2011 data, bottom-up)

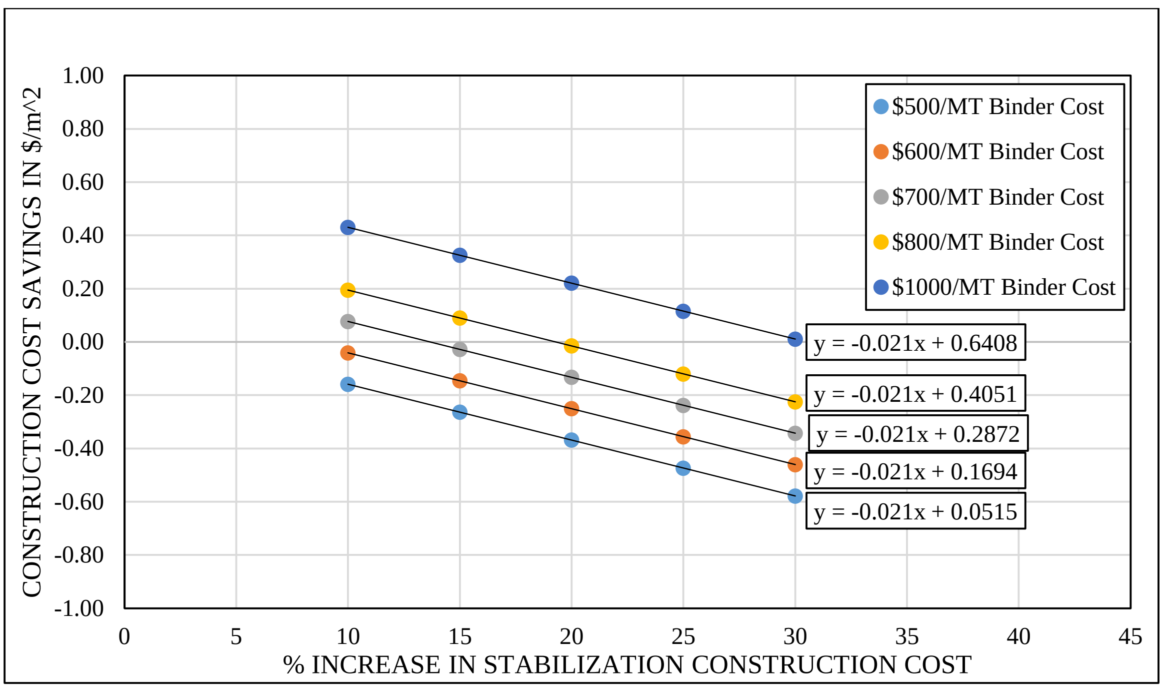

Figure C.2.45 Cost Savings versus % increase in Stabilization Construction Cost for various Binder costs (Cement of 254 mm, I19.0C, EVERSTRESS analysis of May 2011 data, bottom-up)

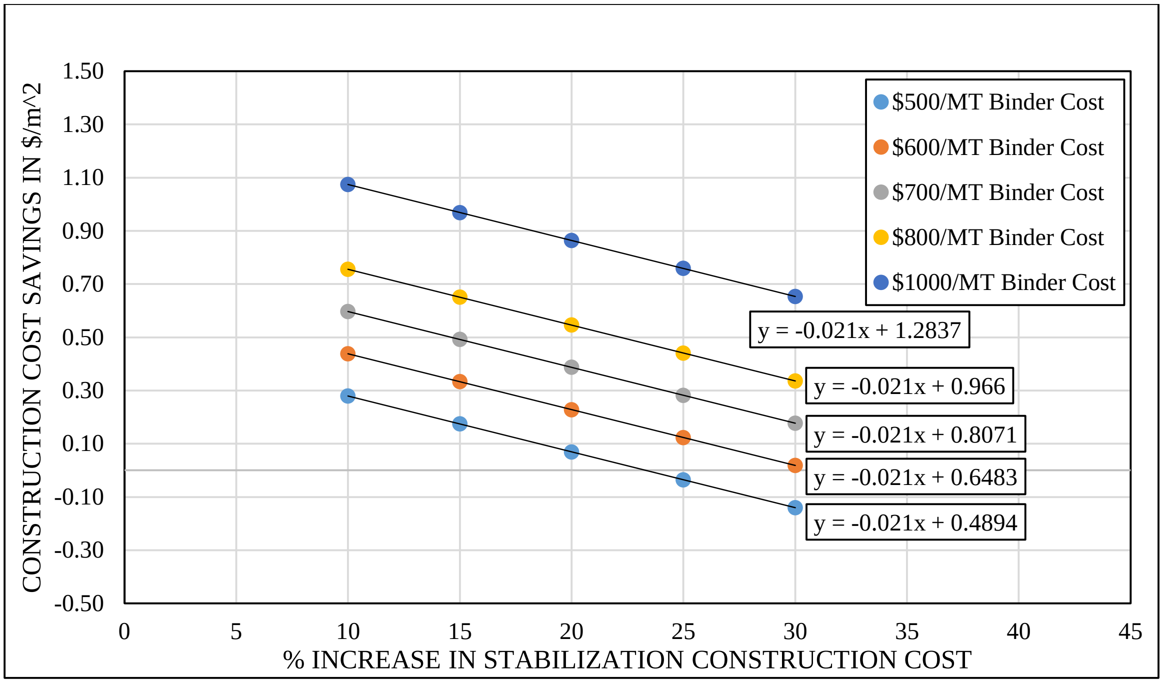

Figure C.2.46 Cost Savings versus % increase in Stabilization Construction Cost for various Binder costs (Cement of 254 mm, S9.5C, EVERSTRESS analysis of October 2011 data, bottom-up)

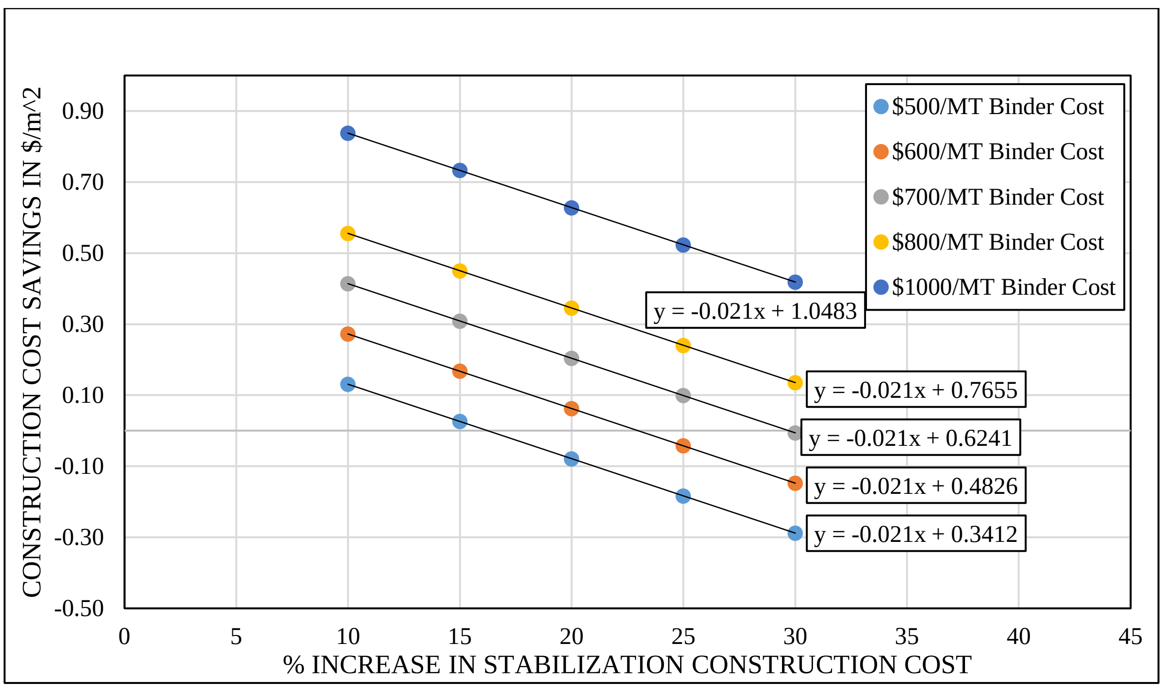

Figure C.2.47 Cost Savings versus % increase in Stabilization Construction Cost for various Binder costs (Cement of 254 mm, I19.0C, EVERSTRESS analysis of October 2011 data, bottom-up)

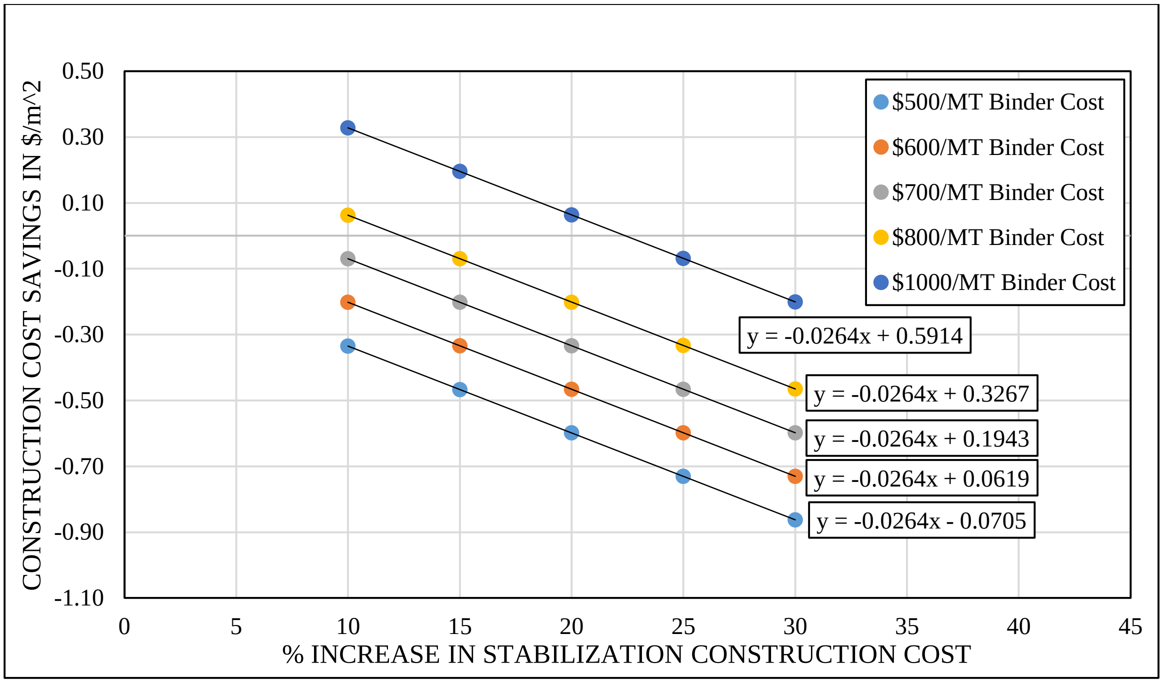

Figure C.2.48 Cost Savings versus % increase in Stabilization Construction Cost for various Binder costs (Lime of 305 mm, S9.5C, Abaqus analysis of May 2011 data, bottom-up)

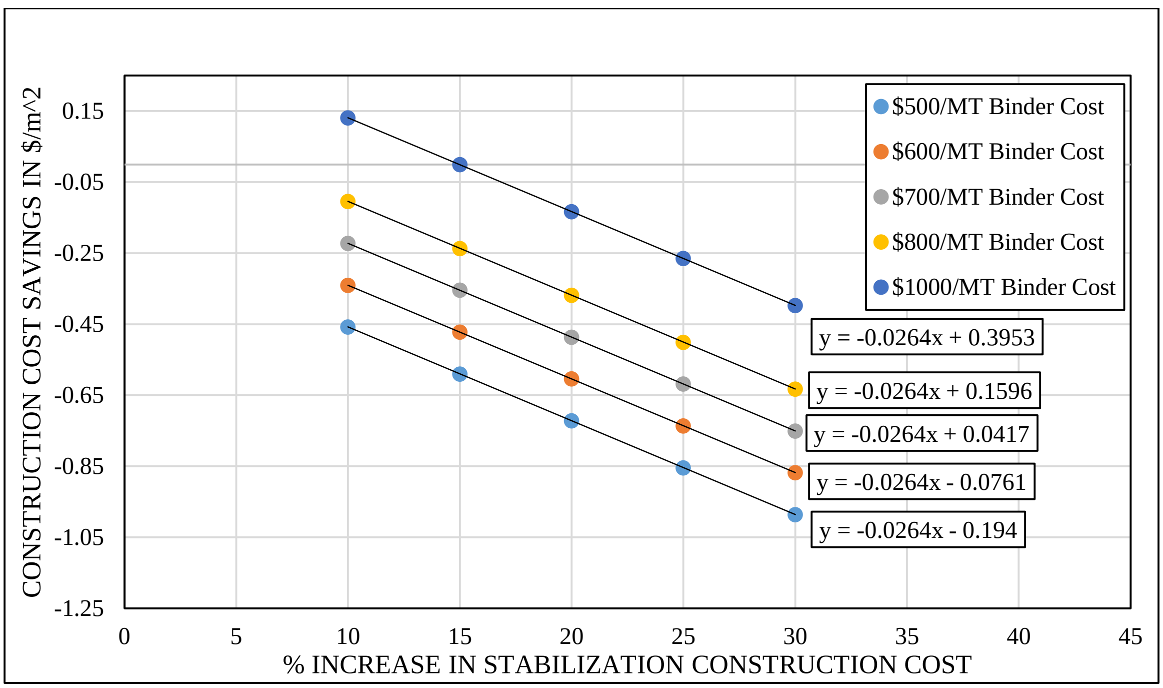

Figure C.2.49 Cost Savings versus % increase in Stabilization Construction Cost for various Binder costs (Lime of 305 mm, I19.0C, Abaqus analysis of May 2011 data, bottom-up)

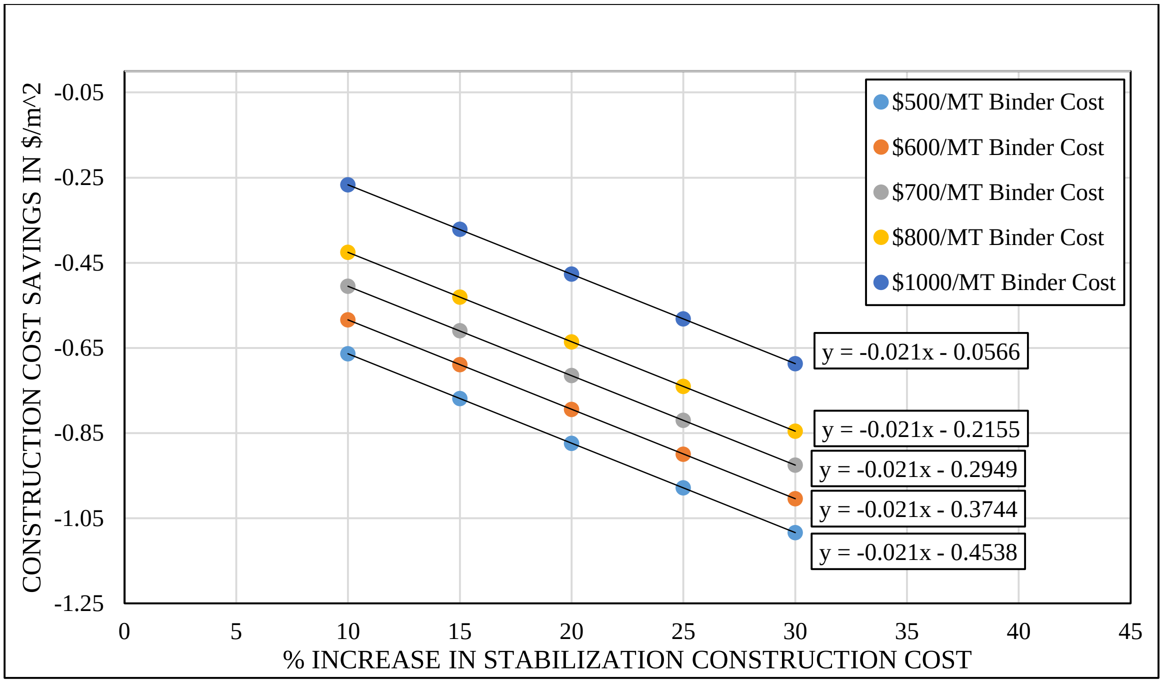

Figure C.2.50 Cost Savings versus % increase in Stabilization Construction Cost for various Binder costs (Cement of 254 mm, S9.5C, Abaqus analysis of May 2011 data, bottom-up)

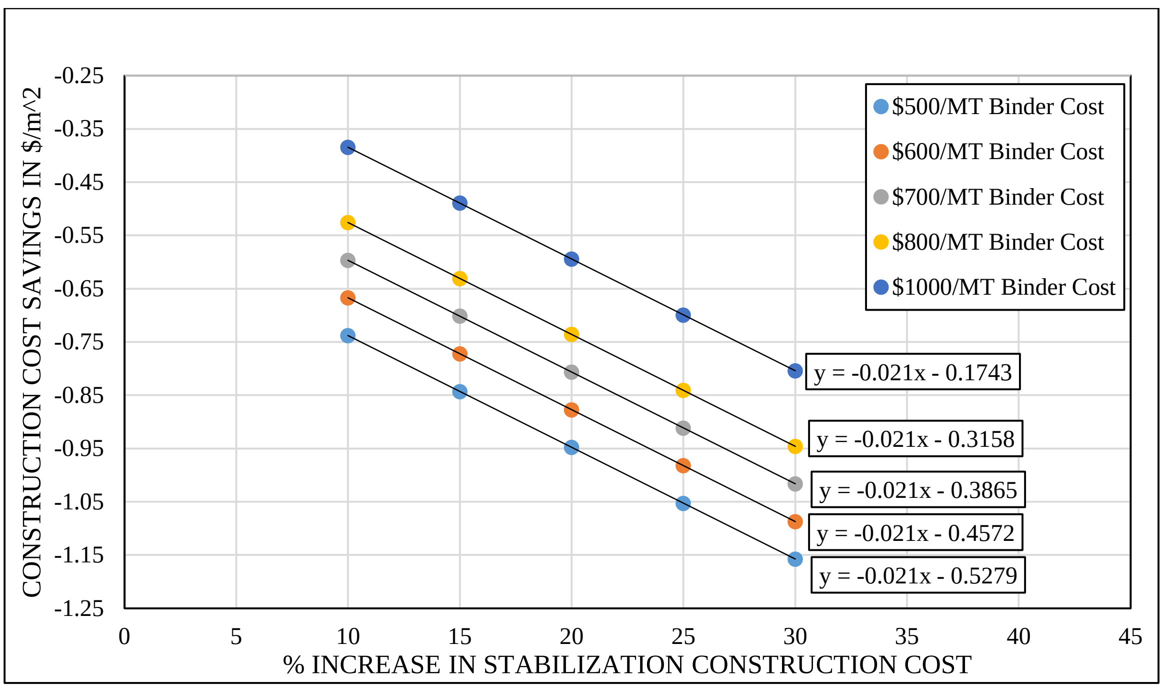

Figure C.2.51 Cost Savings versus % increase in Stabilization Construction Cost for various Binder costs (Cement of 254 mm, I19.0C, Abaqus analysis of May 2011 data, bottom-up)